Topics in Heterocyclic Chemistry 49
Series Editors: Bert Maes · Janine Cossy · Slovenko Polanc

William D. Lubell
Editor

Peptidomimetics II

Springer

49
Topics in Heterocyclic Chemistry

Aims and Scope

The series Topics in Heterocyclic Chemistry presents critical reviews on present and future trends in the research of heterocyclic compounds. Overall the scope is to cover topics dealing with all areas within heterocyclic chemistry, both experimental and theoretical, of interest to the general heterocyclic chemistry community.

The series consists of topic related volumes edited by renowned editors with contributions of experts in the field.

More information about this series at http://www.springer.com/series/7081

William D. Lubell
Editor

Peptidomimetics II

With contributions by

R.S. Ampapathi · P.S. Arora · T.K. Chakraborty ·
M. Chemerovski-Glikman · J.R. Del Valle · U. Ghosh ·
V.V. Komnatnyy · V. Krchňák · A. La-Venia · B.B. Lao ·
T.E. Nielsen · F. Nuti · G. Pacini · S. Pal · A.-M. Papini ·
R.G. Petersen · S. Rahimipour · C. Rentier · M. Richman ·
P. Rovero · C.E. Schafmeister · P. Ventosa-Andrés ·
A.K. Yudin · S. Zaretsky · Q. Zhao

Springer

Editor
William D. Lubell
Université de Montréal
Départemente de Chimie
Montréal, QC
Canada

ISSN 1861-9282 ISSN 1861-9290 (electronic)
Topics in Heterocyclic Chemistry
ISBN 978-3-319-49123-3 ISBN 978-3-319-49124-0 (eBook)
DOI 10.1007/978-3-319-49124-0

Library of Congress Control Number: 2016959972

Printed on acid-free paper

This Springer imprint is published by Springer Nature
The registered company is Springer International Publishing AG
The registered company address is: Gewerbestrasse 11, 6330 Cham, Switzerland

Preface

The second volume of this treatise on heterocycles in peptide mimicry focuses primarily on the replication of the form and function of larger structures. In contrast to Volume I, which examined primarily local constraints and the consequences of heterocyclic amino acids, dipeptides, and five-membered ring systems on global peptide geometry and biological activity, Volume II probes the syntheses and applications of mimics of helices, sheets, and larger folded motifs. In addition, Volume II examines the preparation and applications of macrocyclic peptides, particularly in the areas of chemical biology and medicinal chemistry, as well as the post-translational modification of peptide and protein structures with heterocycles. Maintaining our perspective that peptide mimicry entails the conception of molecular structures, so-called peptidomimetics, that can replicate the elements for the recognition and activity of natural peptides [1–3], a broad variety of examples is discussed to give perspective on the development of the field and future directions.

Various methods have been pursued to create molecules that replicate the shape and activity of natural peptides including de novo designs using small molecules [4–7]. In the context of secondary structures, different strategies have been developed that employ heterocycles to nucleate the formation of intermolecular hydrogen bonds in order to stabilize peptide folds in sheets and helices [8–10]. Alternatively, molecular scaffolds have been developed to orient side chain groups in a geometry that can mimic the topography of a helix [11–13]. Furthermore, cyclic peptides have often been used to create structures with well-ordered conformations [14–16]. On linking multiple residues to create polycyclic peptides, three-dimensional shapes have been created with greater surface areas. In this light, nature has employed disulfide bonds to form links and favor defined folded structures within cyclic peptides such as in the conotoxins [17, 18], sunflower trypsin inhibitor-1 [19], and cyclotides [20, 21]. Inspired by nature, synthetic approaches have been pursued to link together multiple groups along the peptide chain ideally by a single reaction [22 and references 6–11 therein] [23 and references 14–23 therein]. Focusing along this perspective, this volume offers a

sample of such multiple component reactions and their employment to prepare heterocyclic peptidomimetics. The value of cyclic peptides for applications in medicine is also highlighted. Finally, recognizing the importance of post-translational modifications in the normal physiology of peptides and proteins, as well as their relevance in pathology, Volume II examines particular heterocyclic amendments to polyamide structures in nature and in peptide mimicry.

Volume I

Focusing on the applications of heterocycles to control local peptide backbone geometry, Volume I covers a series of methods for restricting motion about the ϕ, ψ, and ω dihedral angles in the sequence. In particular, heterocycles contained within a single amino acid or dipeptide motif are examined. For example, in light of the importance of the natural amino acid proline in peptide folding and function, three chapters of Volume I are dedicated to such modified prolines that alter ring puckering and backbone dihedral angles by way of electronic, steric, and structural interactions. In particular, fluoroproline, silaproline, and methanoproline derivatives are reviewed with focus on their synthesis and application to constrain and alter the properties of peptides in applications spanning chemical biology, medicinal chemistry, materials science, and catalysis. Furthermore, the synthesis and applications of the 6-aza variant of the proline homologue pipecolic acid, piperazic acid [24], are reviewed in a chapter that emphasizes the influences of the hydrazino acid on *N*-terminal amide geometry and local peptide conformation within a variety of natural products with anti-tumor, anti-HIV, antifungal, and antibacterial activities. The synthesis and uses of α-amino lactam dipeptide surrogates, so-called Freidinger–Veber lactams, are presented in two chapters that review recent research on α-amino γ-lactams and their aza variants, *N*-amino-imidazalone and *N*-amino-imidazolidinone dipeptides, as well as α-amino ε-lactams, with attention to their potential for favoring turn conformations and for study of the biologically active conformations of medicinally relevant peptides. Attributes of proline and α-amino lactam motifs are combined in azabicyclo[X.Y.0] alkanone amino acid structures. A chapter focuses on their polyhydroxylated variants, which are compared to sugar-amino acid hybrids. These bicycles are shown to stabilize stand-alone peptide hairpins and to mediate protein–protein interactions. Finally, chapters are respectively dedicated to two important five-membered heterocycle systems for peptide, protein, and peptidomimetic chemistry: thiazoles which are the most common five-membered heterocycle of contemporary pharmaceuticals, and triazoles which are growing in use as amide and disulfide bond mimics, as well as linchpins to cross-link together various biomolecules onto peptide structures.

Volume II

Progressing from the local constraints of heterocyclic amino acids, dipeptides, and five-membered ring systems, Volume II focuses on heterocycles that bias the global folding of larger peptide structures. For example, the opening two chapters focus respectively on helix and sheet mimicry. Presenting their research employing oligomers of oxopiperazines to construct α-helix mimics, Lao and Arora review initially various approaches for mimicry of helical peptides. The synthesis of oxopiperazine oligomers is described, and their suitability for helix mimicry is demonstrated using computational analysis. Finally, oxopiperazine peptidomimetics are shown to be attractive for developing inhibitors of protein–protein interactions and effective as antitumor agents. Reviewing strategies for sheet mimicry, Del Valle probes the requirements for stabilizing extended peptide conformations using heterocyclic peptide surrogates and backbone constraints. Syntheses of β-strand peptidomimetics are discussed with attention to their utility as enzyme inhibitors, receptor ligands, and disruptors of protein–protein interactions. Analyzing applications of 2,5-diketopiperazines (DKPs) as a versatile heterocyclic motif for peptide mimicry, Zhao and Schafmeister illustrate the utility of monomeric and oligomeric DKP analogs to rigidify peptide conformation and to orient hydrogen bonds in α-, β-, and γ-turns, β-hairpins, as well as α- and β-helices. Drawing attention to the integration of DKPs in two-dimensional supramolecular lattices and three-dimensional spiral oligomers with specific shape and functional group orientation, their promise is illustrated for uses in medicine, biomimetic catalysis, and materials science.

The power of reactions employing iminium ions to make peptidomimetics is illustrated in three chapters that demonstrate the value of such chemistry for synthesizing mimics of secondary structure and cyclic peptides. Exploring the potential of the Pictet–Spengler reaction, Petersen, Komnatnyy, and Nielsen examine the broad scope of this condensation of β-arylethylamines with aldehydes or ketones for the construction of peptide turn mimics and rigid molecular scaffolds that display pharmacophores with defined orientations. Studying the iminium ion chemistry of peptide frameworks containing masked aldehydes, La Venia, Andrés, and Krchňák describe a tandem cyclization strategy to furnish multiple ring products for mimicry of various biologically active peptide conformations. Cyclic 6-, 7-, 8-, and 9-membered iminium ion intermediates are generated by unmasking an aldehyde precursor that undergoes intramolecular annulation with various heteroatomic (e.g., alcohols, sulfonamides, thiols) and aromatic nucleophiles to provide diverse fused and bridged heterocyclic peptidomimetics with regio-, chemo-, and stereocontrol. The iminium ion chemistry of aziridine aldehyde is presented by Yudin and Zaretsky with particular focus on multiple component Ugi reactions for the synthesis of a variety of linear, piperazinone, and macrocyclic peptidomimetic structures. In particular, the combination of aziridine aldehyde dimer, isocyanide, and peptides bearing an N-terminal proline residue provides a novel route to cyclic analogs possessing an aziridine moiety that can be

subsequently reacted with nitrogen and sulfur nucleophiles or hydrogenated to give access to diverse cyclic peptides.

In the current climate of interest in peptides for medical and biotechnological applications [25, 26], their cyclic variants have garnered particular attention, due to the potential to exhibit improved drug-like qualities such as reduced polarity, restricted conformation, and stability to proteolysis [27]. Two chapters in Volume II illustrate the importance of cyclic peptides in chemical biology and medicine. Focusing on synthetic methods to develop analogs of the natural cyclic peptide antibiotic gramicidin S, Pal, Ghosh, Ampapathi, and Chakraborty provide a detailed summary of relationships between conformation and biological activity towards the creation of novel therapeutics to treat resistant bacterial strains should the issue of hemolytic activity be overcome. Examining the development of cyclic peptides as disruptors of protein-misfolding diseases, Chemerovski-Glikman, Richman, and Rahimipour review various approaches that use heterocyclic peptides of natural and synthetic origin to perturb the self-assembly of soluble proteins into insoluble extracellular plaques. Towards new therapy for treating the unmet medical predicament of amyloidogenic diseases, cyclic D,L-α-peptides are demonstrated to be promising useful tools for studying structural similarities and cross-interactions between different amyloids, as well as inhibitors of pathogenic structures, because their aggregation into nanotubes provides conformational mimics that mitigate toxic amyloids.

Finally, the importance of the chemistry and biochemistry of the 1,2-dithiolane ring derivative of octanoic acid, so-called lipoic acid, is appraised by Rentier, Pacini, Nuti, Rovero, and Papini, who describe the relevance of this heterocyclic acid as an essential cofactor of several key enzymatic processes involved in cellular oxidative metabolism, including the decarboxylation of pyruvate, acetylation of coenzyme A, decarboxylation of glycine, and amino methylation of tetrahydrofolate. Lipoylation is specifically shown to be an essential post-translational modification for energetic mitochondrial metabolism. Moreover, the therapeutic potential of lipoylated molecules is described for various indications including chelation of heavy metals, diminishing reactive oxygen species, and mediating symptoms of diabetes, multiple sclerosis, and Alzheimer's disease.

Perspectives

Peptide science continues to grow in importance as its roots in natural product isolation, synthesis, and analysis have spread to various other fields with particular impact in medicine [25–28], catalysis [29 and reference 2 therein], materials science [30], and nanotechnology [31, 32]. For example, growing impact in medicine is evidenced by peptide-based drugs, which have exhibited expanded market potential [25, 26] and elevated success rate in clinical trials relative to small molecules [28]. Moreover, the application of peptide chemistry has become more common in the early phases of drug discovery. Paralleling the growth in the field of

peptide science is an inherent interest to gain insight into the mechanism of action and to improve the utility of these polyamide structures. Within the collaborative nature of peptide science, peptide mimicry claims an important spotlight, because of the value of peptidomimetics as tools for studying relationships between conformation and activity to furnish understanding of the interplay of form and function. In this light, the applications of heterocyclic structures have been paramount for presenting the geometry of the peptide backbone and side chains in spatially defined orientations. A bonus of conformational constraint has been improved pharmacokinetics that make peptidomimetics more drug-like than their natural counterparts [33]. I am grateful to the authors of this two-volume treatise and in particular for their impressive efforts to address the various steps in the synthesis, conformational analysis, and assessment of the activity of a broad set of heterocyclic peptidomimetics. Furthermore, they have provided insight into strategies for using the latter in different applications. Although nature has put peptides and their heterocyclic components to work since the origins of life [34], pioneering research in the synthesis and use of heterocyclic peptidomimetics began in earnest less than 40 years ago. In this respect, many of those early pioneers and their students are actively pursuing research today; however, this treatise is intended to welcome and guide the next generation in the field of peptide mimicry as a fertile source for their innovative minds to harvest new tools, probes, and products for advancing scientific research in various disciplines.

Montréal, QC, Canada William D. Lubell

References

1. Marshall GR (1993) A hierarchical approach to peptidomimetic design. Tetrahedron 49:3547–3558
2. Hruby VJ, Cai MY, Insel PA (2013) Design of peptide and peptidomimetic ligands with novel pharmacological activity profiles. Annu Rev Pharmacol Toxicol 53:557–580
3. Ko E, Liu J, Burgess K (2011) Minimalist and universal peptidomimetics. Chem Soc Rev 40:4411–4421
4. Bélanger PC, Dufresne C (1986) Preparation of exo-6-benzyl-exo-2-(m-hydroxyphenyl)-1-dimethylaminomethylbicyclo[2.2.2.]octane. A non-peptide mimic of enkephalins. Can J Chem 64:1514–1520
5. Hirschmann RF, Nicolaou KC, Angeles AR, Chen JS, Smith AB 3rd (2009) The beta-D-glucose scaffold as a beta-turn mimetic. Acc Chem Res 42:1511–1520
6. Dufour-Gallant J, Chatenet D, Lubell WD (2015) De novo conception of small molecule modulators based on endogenous peptide ligands: pyrrolodiazepin-2-one γ-turn mimics that differentially modulate urotensin II receptor-mediated vasoconstriction ex vivo. J Med Chem 58:4624–4637

7. Olson GL, Bolin DR, Bonner MP, Bos M, Cook CM, Fry DC, Graves BJ, Hatada M, Hill DE, Kahn M, Madison VS, Rusiecki VK, Sarabu R, Sepinwall J, Vincent GP, Voss ME (1993) Concepts and progression in the development of peptide mimetics. J Med Chem 36:3039–3049
8. Kemp DS (1990) Peptidomimetics and the template approach to nucleation of beta-sheets and alpha-helices in peptides. Trends Biotechnol 8:249–255
9. Hölzemann G (1991) Peptide conformation mimetics (Part 1). Kontakte (Darmstadt) 3–12
10. Hölzemann G (1991) Peptide conformation mimetics (Part 2). Kontakte (Darmstadt) 56–63
11. Jayatunga MKP, Thompson S, Hamilton AD (2014) α-Helix mimetics: outwards and upwards. Bioorg Med Chem Lett 24:717–724
12. Taylor JW (2002) The synthesis and study of side-chain lactam-bridged peptides. Biopolymers 66:49–75
13. Henchey LK, Jochim AL, Arora PS (2008) Contemporary strategies for the stabilization of peptides in the α-helical conformation. Curr Opin Chem Biol 12:692–697
14. Bockus AT, McEwen CM, Lokey RS (2013) Form and function in cyclic peptide natural products: a pharmacokinetic perspective. Curr Top Med Chem 13:821–836
15. Roxin A, Zheng G (2012) Flexible or fixed: a comparative review of linear and cyclic cancer-targeting peptides. Future Med Chem 4:1601–1618
16. Hill TA, Shepherd NE, Diness F, Fairlie DP (2014) Constraining cyclic peptides to mimic protein structure motifs. Angew Chem Int Ed 53:13020–13041
17. Akondi KB, Muttenthaler M, Dutertre S, Kaas Q, Craik DJ, Lewis RJ, Alewood PF (2014) Discovery, synthesis, and structure–activity relationships of conotoxins. Chem Rev 114:5815–5847
18. Daly NL, Craik DJ (2009) Structural studies of conotoxins. IUBMB Life 61:144–150
19. Colgrave ML, Korsinczky MJ, Clark RJ, Foley F, Craik DJ (2010) Sunflower trypsin inhibitor-1, proteolytic studies on a trypsin inhibitor peptide and its analogs. Biopolymers 94:665–672
20. Burman R, Gunasekera S, Strömstedt AA, Göransson UJ (2014) Chemistry and biology of cyclotides: circular plant peptides outside the box. J Nat Prod 77:724–736
21. Craik DJ, Conibear AC (2011) The chemistry of cyclotides. J Org Chem 76:4805–4817
22. Bashiruddin NK, Nagano M, Suga H (2015) Synthesis of fused tricyclic peptides using a reprogrammed translation system and chemical modification. Bioorg Chem 61:45–50
23. Vinogradov AA, Choo Z-N, Totaro KA, Pentelute BL (2016) Macrocyclization of unprotected peptide isocyanates. Org Lett 18:1226–1229
24. Oelke AJ, France DJ, Hofmann T, Wuitschik G, Ley SV (2011) Piperazic acid-containing natural products: isolation, biological relevance and total synthesis. Nat Prod Rep 28:1445–1471
25. Fosgerau K, Hoffmann T (2015) Peptide therapeutics: current status and future directions. Drug Discov Today 20:122–128
26. Vlieghe P, Lisowski V, Martinez J, Khrestchatisky M (2010) Synthetic therapeutic peptides: science and market. Drug Discov Today 15:40–56
27. Thapa P, Espiritu MJ, Cabalteja C, Bingham J-P (2014) The emergence of cyclic peptides: the potential of bioengineered peptide drugs. Int J Pept Res Ther 20:545–551
28. Otvos L Jr, Wade JD (2014) Current challenges in peptide-based drug discovery. Front Chem 2:62
29. Metrano AJ, Abascal NC, Mercado BQ, Paulson EK, Miller SJ (2016) Structural studies of β-turn-containing peptide catalysts for atroposelective quinazolinone bromination. Chem Commun 52:4816–4819

30. Lefèvre T, Byette F, Marcotte I, Auger M (2014) Protein- and peptide-based materials: a source of inspiration for innovation. In: Gauvin R (ed) Functional materials – for energy, sustainable development and biomedical sciences. De Gruyter, Berlin, pp 415–442
31. Morelli G, Toniolo C, Venanzi M (2014) Peptide materials for biomedicine and nanotechnology. J Pept Sci 20:451–452
32. Lubell WD (2012) Peptide chemistry. Org Lett 14:4297–4302
33. Veber DF, Johnson SR, Cheng HY, Smith BR, Ward KW, Kopple KD (2002) Molecular properties that influence the oral bioavailability of drug candidates. J Med Chem 45:2615–2623
34. Ikehara K (2016) Evolutionary steps in the emergence of life deduced from the bottom-up approach and GADV hypothesis (top-down approach). Life (Basel) 6. pii: E6

Contents

Top Heterocycl Chem (2017) 49: 1–24
DOI: 10.1007/7081_2015_195

Published online: 28 February 2016

Oligooxopiperazines as Topographical Helix Mimetics

Brooke Bullock Lao and Paramjit S. Arora

Abstract Protein–protein interactions are often mediated by amino acid side chain functionality organized on secondary structures. Small molecule scaffolds that reproduce the array of protein-like functionality at interfaces offer an attractive approach to target therapeutically important interactions. Here, we describe the design, synthesis, and the biological potential of small molecule helix mimetics derived from an oxopiperazine scaffold to target protein complexes in which binding is largely dictated by one face of the interfacial helix. The oxopiperazine helix mimetics can be assembled from α-amino acids using standard solid-phase peptide synthesis methodology, enabling rapid diversification of the scaffold and discovery of ligands for protein targets. We have evaluated the biological potential of the oxopiperazine mimetics in cell-free, cell culture, and in vivo models. Our results support the hypothesis that the scaffold offers an attractive platform for the development of novel inhibitors of protein–protein interactions.

Keywords Helix mimic • Peptidomimetic • Protein-protein interaction inhibitor

Contents

B.B. Lao and P.S. Arora (✉)
Department of Chemistry, New York University, New York, NY 10003, USA
e-mail: arora@nyu.edu

1 Introduction

1.1 Helix Mimics

Mimicry of protein α-helical domains has proven to be a successful strategy for the development of synthetic modulators of protein–protein interactions [1–5]. The α-helix is the most abundant secondary structure both within and on the surface of proteins and frequently mediates interactions of proteins with binding partners [6–8]. The helix displays residues on three distinct faces and can utilize one, two, or all three faces for molecular recognition (Fig. 1) [9]. Examination reveals that approximately 60% of helix-mediated protein–protein complexes require only one face for partner recognition implying that a simplified scaffold – peptidic or non-peptidic – imitating the topography of an α-helix could be used to design inhibitors for a target interface [9].

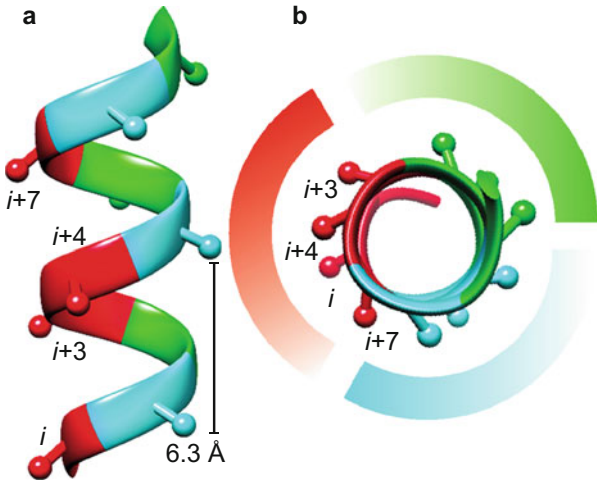

Fig. 1 Canonical α-helix with residues on the same face identified by matching colors in (**a**) side view and (**b**) top view down from C- to N-terminus

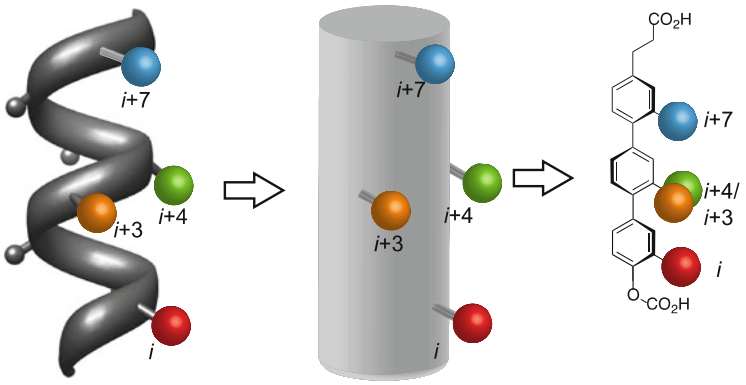

Fig. 2 Topographical helix mimetic. Natural α-helix (*left panel*) represented as a cylinder (*middle panel*). Terphenyl helix mimetic shown in the *right panel* with residues highlighted to match helical projections

1.2 Topographical Mimics

Topographical helix mimics aim to reproduce the side chain projections of protein α-helices on synthetic backbones, based on the hypothesis that the backbone hydrogen-bonding functionality is rarely involved in interactions with binding partners (Fig. 2). Topographical mimics are attractive because they can be synthetically tailored to enhance desired properties such as specificity, affinity, metabolic stability, and solubility [10, 11]. The Hamilton group introduced and pioneered the concept of helix surface mimetics with a scaffold based on tris-substituted 3,2′,2″-terphenyl building blocks [12]. The staggered *ortho* substituents on the terphenyl backbone have been used to imitate the side chain on one helical face at the i, $i+3$ (or $i+4$), and $i+7$ positions (Fig. 2). Terphenyls have been shown to successfully mimic protein helices and to recognize their cognate protein receptors [12–15]. During the past decade, a number of groups have described helix mimetics that build and improve on the earlier designs with regard to solubility, synthesis, and protein targeting potential [1, 2, 16–26]. Some of these derivatives have also shown desired activities in cell culture and animal models [27–31].

2 Oxopiperazine Helix Mimetics

A potential limitation of the aromatic helix mimetics is that they may not effectively discriminate between chiral protein pockets. Although the terphenyls are axial chiral compounds, a majority of aromatic helix mimics do not contain a chiral backbone. We sought to develop topographical helix mimics that could be

assembled from amino acids and retain backbone chirality. The amino acid-derived scaffold would facilitate incorporation of natural and nonnatural side chain functionality for protein mimicry. Critical criteria for our design considerations were to access conformationally defined, non-peptidic scaffolds from amino acids to obtain helix mimics that could be stable toward proteolytic degradation yet rapidly synthesized in a sequence-defined manner.

We began by searching solid-state conformations of amino acid-derived small molecules in the Cambridge Structure Database (CSD). Our search led to oxopiperazine derivatives as potentially attractive building blocks that adhered to the criteria stated above. We were attracted to the piperazine skeleton because it is considered a privileged scaffold for peptidomimetic research and drug discovery [32, 33]. Specifically, the 2-oxopiperazine and the diketopiperazines have a rich history in medicinal chemistry and are considered to be "drug-like" scaffolds [34–36].

We designed several motifs based on the oxopiperazine scaffold and evaluated their ground-state conformations using MacroModel [37, 38]. The results of the MacroModel predictions were corroborated by the crystal structure data on oxopiperazine analogs in the Cambridge Structural Database (CSD). Our molecular modeling studies suggested that oxopiperazine rings linked by α-amino acids would reproduce the array of side chain residues on one face of a canonical α-helix (Fig. 3).

The optimal conformation for helix side chain mimicry requires the ring geometry of the oxopiperazine dimer (Fig. 3b) and the bridging α-amino acid to adopt appropriate ϕ and φ dihedral angles (Fig. 4a). Between the two favored oxopiperazine ring conformations in 1,4-dimethylpiperazin-2-one, the half-chair is ~ 2.9 kcal/mol lower in energy than the boat conformation (Fig. 4b). The central peptide unit of a dimer of oxopiperazines contains three rotatable bonds corresponding to the dihedral angles ϕ, ψ, and ω. The tertiary amide bond may adopt both cis and trans amide conformations similar to proline. Calculations with the MacroModel program suggest that the trans conformation is roughly 1 kcal/mol more stable than the cis conformation in trialanine oxopiperazine (Fig. 4c). A trans amide geometry would place the side chain groups of the dimer to better reproduce the arrangement of i, $i+4$, and $i+7$ residues on an α-helix.

To examine the preferred ϕ and ψ dihedral angles in oxopiperazine dimer **A**, we utilized the "dihedral drive" functionality in MacroModel. The results of these calculations suggested a limited number and narrow range of ϕ and ψ values in the lowest-energy conformers (Table 1). Moreover, the dihedral angles predicted by MacroModel were found in the crystal structures of relevant compounds in CSD (CSD codes: KEMXUV, ZOZTUD, ZARZOH, and FOBFEH) (Table 1). Our calculations indicated that oligooxopiperazines favor ϕ and ψ angles of $-128° \pm 25°$ and $76° \pm 15°$, respectively.

The predicted low-energy structure of the oxopiperazine dimer presents functionality in a way that matches the side chain patterns on a canonical α-helix (Fig. 3). The calculated low-energy conformations exhibited little deviation except for the ring puckers. An ensemble of the 20 lowest-energy conformations of tetraalanine oxopiperazine dimer is shown in Fig. 5 alongside the structures of the first and twentieth lowest-energy conformers. The energy difference between

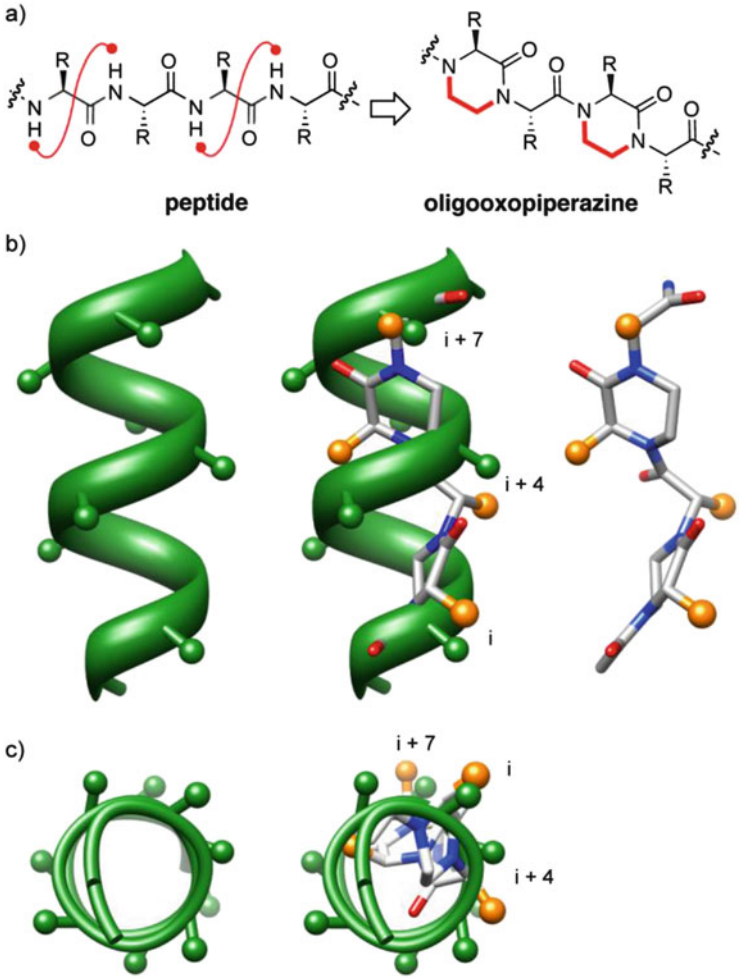

Fig. 3 (**a**) Design of amino acid-derived oligooxopiperazines. (**b**) An 8-mer canonical alpha helix with side chain residues depicted as *green spheres* (*left*). Predicted structure of an oxopiperazine dimer with side chain residues depicted as *orange spheres* (*right*) and overlay of the piperazine dimer and the α-helix (*center*). (**c**) Top-down view of a canonical α-helix (*left*) and overlay of the *i*, $i+4$, and $i+7$ residues of the α-helix and side chain residues of oxopiperazine dimer (*right*) (reprinted with permission from Tošovská and Arora [24] Copyright (2010) Journal of the American Chemical Society)

these two conformations is roughly 0.5 kcal/mol and results from different piperazine half-chair ring pucker geometries. Significantly, the positions of the side chain groups are not perturbed by the ring puckers. The above analyses suggest that the designed oxopiperazine scaffold is well suited for helix mimicry.

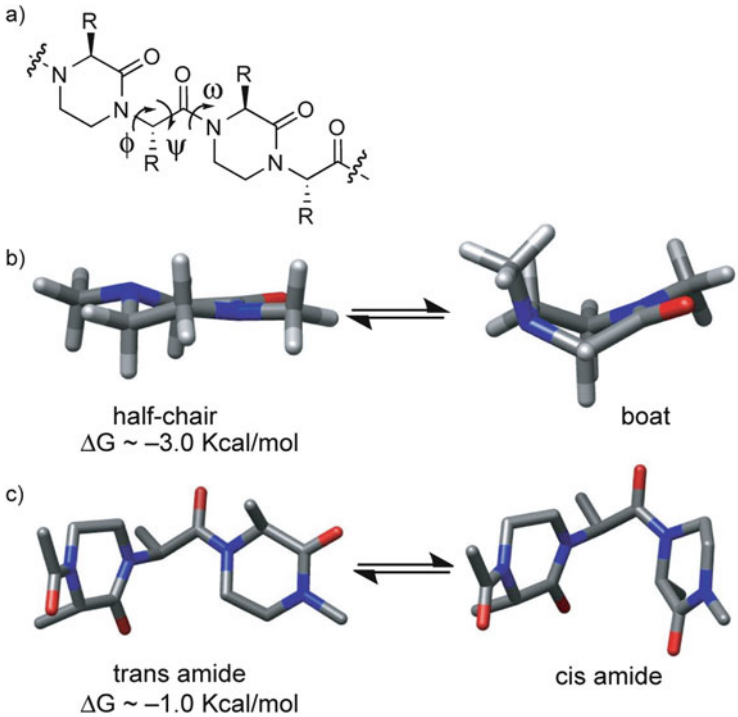

Fig. 4 (**a**) Rotatable bonds in an oxopiperazine dimer. (**b**) Favored chair and boat equilibrium for 1,4-dimethylpiperazin-2-one. (**c**) Favored trans and cis amide equilibrium in an oligoalanine derivative. Values were calculated with MacroModel MMFF force field in chloroform (reprinted with permission from Tošovská and Arora [24] Copyright (2010) Journal of the American Chemical Society)

Table 1 Calculated low-energy ϕ and ψ values for oxopiperazine dimer **A**

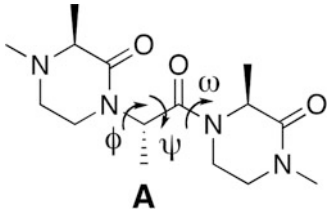

A

	Dihedral angle (°)	Relative energy (kcal/mol)	Cambridge Structure Database Code[a]
ϕ	−150	0.95	–
	−128	0	KEMXUV, ZOZTUD
	−90	1.26	ZARZOH
ψ	60	0.64	–
	76.76	0	ZARZOH
	90	0.34	–
	120	1.87	–

[a]The corresponding dihedral value was found in the indicated CSD structure

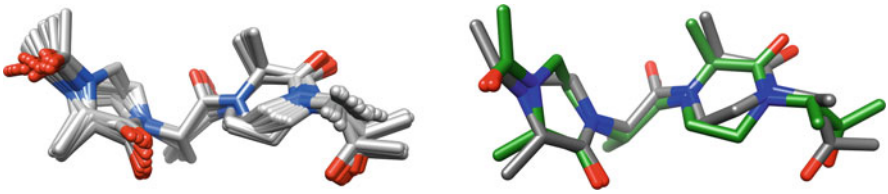

Fig. 5 Ensemble of the 20 lowest-energy structures calculated for tetraalanine oxopiperazine dimer using MacroModel (*left panel*). Overlay of the 1st and the 20th (green skeleton) lowest-energy conformers (*right*)

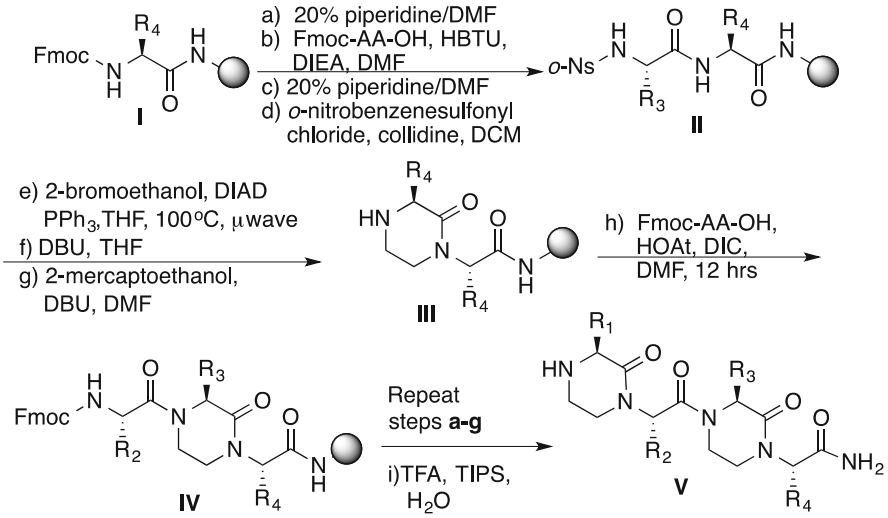

Scheme 1 Solid-phase synthesis of OHM dimer **V**

2.1 Synthesis of Oxopiperazine Helix Mimetics

We have evaluated solution and solid-phase strategies for the synthesis of oxopiperazine helix mimetics (OHMs) [24, 29]. The key step in the synthesis of OHMs is the formation of the six-membered piperazine ring, a formal addition of an ethylene bridge between neighboring amide nitrogens in a peptide chain. Several synthetic routes to piperazines are known, many entailing the use of amino acid building blocks [39–42]. For the solution-phase synthesis, we found the reductive amination route described by Moeller and coworkers to afford short oligomers in respectable yields [24, 42]. The reductive amination approach proved to be cumbersome for the solid-phase method; instead, we turned to alkylation using the Fukuyama–Mitsunobu method (Scheme 1) [29]. The optimized solid-phase strategy utilized standard resins and Fmoc-amino acids and empowered rapid diversification of the side chain functionality.

3 Recognition of Protein Receptors by Oxopiperazine Helix Mimetics

OHMs were designed to target protein receptors in which the residues critical for partner recognition were organized on one or two helical faces. We have developed a dataset of helical interfaces in protein–protein (HIPP) interactions. The dataset catalogs multi-protein complexes mediated by helical domains [6, 7, 9, 43]. The contribution of each helix and the individual helical residues for binding were evaluated using computational alanine-scanning mutagenesis analysis [44]. This dataset reveals protein–protein interactions that may be targeted by topographical helix mimetics and the residues that need to be grafted onto the scaffolds to create suitable mimics.

Equipped with the HIPP database, we set out to determine if OHMs could inhibit helical protein–protein interactions in which the energetically important residues ("hot spot residues") reside on one or two helical faces. We chose the p53/Mdm2 and HIF1α/p300 interactions to test our initial hypotheses.

3.1 p53/Mdm2 as a Model System for Ligand Design

Formation of the p53/Mdm2 complex regulates the balance between cell growth and arrest by leading to the activation of genes essential for cell cycle arrest, apoptosis, and DNA repair [45]. Since its discovery over 30 years ago, p53 has received much attention, because of its crucial role in many physiological processes and because its mutation has been detected in approximately 50% of all human cancers [46]. On binding to Mdm2, an E3-ligase, p53 becomes susceptible to ubiquitination and degradation [47–49]. Under normal conditions, Mdm2 and its homolog, Mdm4 maintains low levels of p53 [50]. In response to stress signals, p53 levels increase, which also increases Mdm2 expression, leading to downregulation of p53. Inhibition of this interface has been demonstrated to trigger programmed cell death by increasing p53 activity [51–54].

The p53 transactivation domain (TAD) binds Mdm2 in a cleft with three main recognition residues organized on one face of a single helix (Fig. 6) [55]. Extensive structural [45, 55] and mutagenesis data [55, 56] as well as the identification of different classes of inhibitors of the p53/Mdm2 complex all have made this interaction a model for the evaluation of helix mimetics [13, 57–64].

The three p53 residues (Phe19, Trp23, and Leu26) that make critical contacts with Mdm2 have been determined both by computational [65] and experimental analyses [55, 66]. The residues occupy the i, $i+4$, and $i+7$ positions in the peptide chain and span two helical turns. Mimicry of the location of the side chains of these hydrophobic residues by the OHM scaffold was at the core of our design of p53 mimics that oriented their R_1, R_2, and R_4 residues to target Mdm2 (Fig. 6 and Table 2).

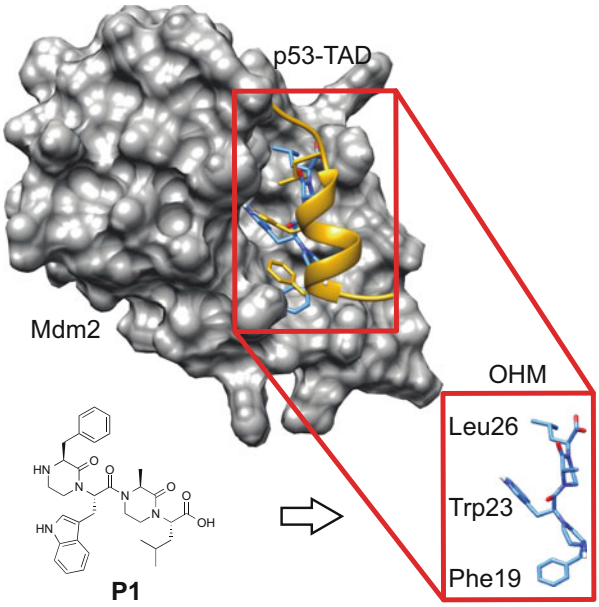

Fig. 6 p53-TAD bound to Mdm2 (PDB code 1YCR). OHM P1 (*blue*) overlaid onto p53 helix (*gold*)

Table 2 Design and Mdm2-binding properties of first-generation p53-OHM mimetics

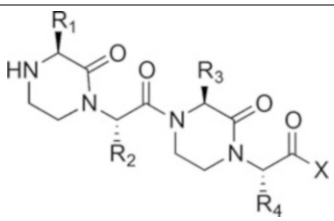

p53-OHM	R_1	R_2	R_3	R_4	X	K_i (μM)[a]
P1	Phe	Trp	Ala	Leu	OH	65.4 ± 0.28
P2	Phe	Trp	Lys	Leu	OH	≥200
P3	Phe	Trp	Leu	Leu	OH	7.90 ± 0.005
P4	Phe	Trp	Phe	Leu	OH	6.90 ± 1.3
P5	Phe	Trp	Phe	Leu	NH_2	2.88 ± 0.012
P6	Phe	Trp	Phe	Lys	NH_2	≥200
P7	Lys	Trp	Phe	Leu	NH_2	≥200
P8	Phe	Ala	Phe	Leu	NH_2	63.9 ± 6.8

[a]Binding affinity for Mdm2 as determined by a competitive fluorescence polarization assay (reprinted with permission from Lao et al. [67] Copyright (2014) Journal of the American Chemical Society)

The first generation of Mdm2 inhibitors focused on variation at the R_3 position, which did not overlay onto a specific residue of a canonical α-helix (Table 2, OHM **P1**–**P4**). Binding affinities were determined using a previously described

competition assay featuring displacement of a fluorescein-labeled p53 peptide to indicate successful occupancy of the p53-binding pocket on Mdm2 by the OHM inhibitor [60, 68]. The formation of an OHM/Mdm2 complex was further supported by an HSQC-NMR titration experiment in which addition of the best candidate to a solution of ^{15}N-labeled Mdm2 revealed peak shifts corresponding to the p53-binding pocket. These initial binding studies revealed that the R_3 position required a hydrophobic residue for high-affinity interactions with Mdm2. In addition, we examined different C-termini and found that both carboxylate and carboxamide functionalities resulted in similar affinities (see results for OHM **P4** and **P5**; Table 2).

Designed negative controls support our hypothesis that the OHMs effectively reproduce the geometry of p53 hot spot residues. Positions R_1, R_2, and R_4 of OHM **P5** bearing Phe, Trp, and Leu side chains occupy the same hydrophobic pockets on Mdm2 as p53 residues Phe19, Trp23, and Leu26, respectively. Individual modification of each residue of OHM **P5** produced OHM derivatives **P6**–**P8**. Each of these mutated controls exhibited reduced affinity for Mdm2.

3.2 In Silico Design of OHMs to Target PPIs

OHM **P5** resulted from direct mimicry of the p53 side chains. Along with the negative controls, OHM **P5** helped us to establish the potential of the scaffold as a helix mimetic. In order to design more potent analogs, we investigated a Rosetta-based computational approach that employed principles of computational protein design [69–71] to study peptidomimetic scaffolds [67, 72]. The hypothesis underlying this effort was that OHMs with nonnatural residues may provide more optimal interactions with the target protein surface, because the trajectories of the side chains emerging from the scaffold were not identical to the $\alpha \rightarrow \beta$ side chain trajectories from the canonical α-helix backbone [73]. Computational design was used to reduce the number of total compounds to be synthesized and to streamline the process to high-affinity binders. Rosetta has proven to be successful in protein design applications, including an experimentally validated protein fold not seen in nature [71], the design of protein–protein and protein–DNA interfaces [44], the hyper-stabilization of proteins [74], and the design of proteins with improved enzymatic activity and ligand affinity [70, 75–81].

The basic design protocol used a fixed backbone template in Rosetta, with the goal of identifying the lowest-energy set of residues and side chain conformations (Fig. 7). To reduce the computational complexity required to model side chain degrees of freedom, the side chains were represented as "rotamers" – discrete side chain conformations located at the centroids of χ angle clusters, which were modeled by analyzing experimental protein structures. Extensions of the Rosetta framework enabled modeling and design of non-canonical backbones on nonnatural scaffolds such as peptoids [82]. Implementation of oxopiperazine design in Rosetta

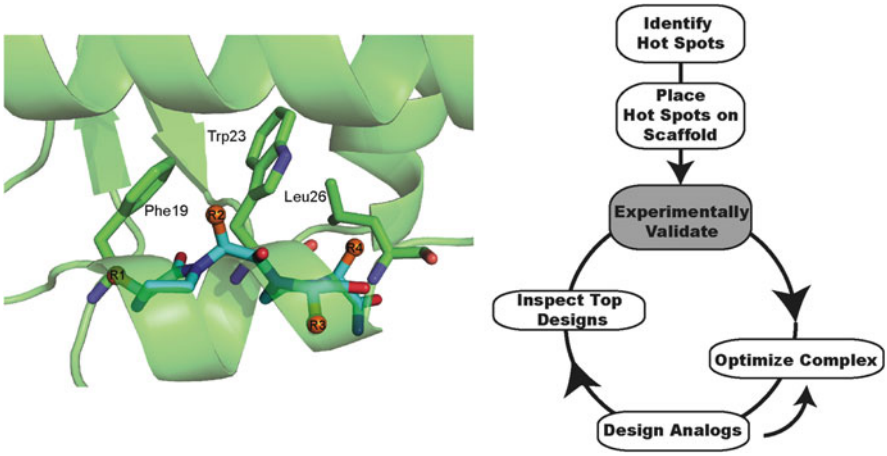

Fig. 7 Docking of the oxopiperazine scaffold in p53-binding pocket of Mdm2 (*left panel*). Figure shows the relative positioning of the oxopiperazine dimer side chains R_1–R_4 and p53 hot spot residues Phe19, Trp23, and Leu26 within the protein pocket. Key steps in the inhibitor design protocol (*right panel*). The protocol was initiated with identification of hot spot residues at the native interface by computational alanine scans. Positions on the scaffold were identified to mimic hot spot residues, and the scaffold featuring the hot spot mimics was experimentally validated. Computational steps including optimization of the conformation of the ligand – protein complex and design of hot spot analogs – were performed using Rosetta. Top designs were inspected for proper binding of the target interface, and proper designs were experimentally validated (adapted with permission from Lao et al. [67]. Copyright (2014) Journal of the American Chemical Society)

has been described, and the protocols are available on the Web (http://rosie.rosettacommons.org) [67, 72, 83].

We began the computational optimization protocol by manually docking a model of OHM **P5** into the p53-binding cleft of Mdm2 with the hot spot residues aligned (Fig. 7a). The OHM docking protocol described by Drew et al. was used to optimize the rigid body conformations [72]. Briefly, the protocol used a fixed backbone protein and flexible ligand so that a set of residues and side chain conformations of low energy could be identified. The rotamer approximation was also applied to the OHM side chains. Extensions in the Rosetta framework expanded the modeling to include non-canonical amino acids and non-peptidic scaffolds [84]. OHM **P5** packed well against Mdm2 and made several energetically favorable contacts at the interface closely resembling the packing of the p53 peptide (Figs. 7 and 8a) [67].

The search for low-energy conformations and sequence optimization involved a two-step protocol encompassing both a Monte Carlo simulation to sample conformations of the rigid oxopiperazine backbone and chain substitution and repacking of the OHM scaffold and target protein. Low-energy designs were scored, and structures based on design predictions were synthesized. Table 3 summarizes the top mimics from Rosetta predictions and their experimental binding affinity values.

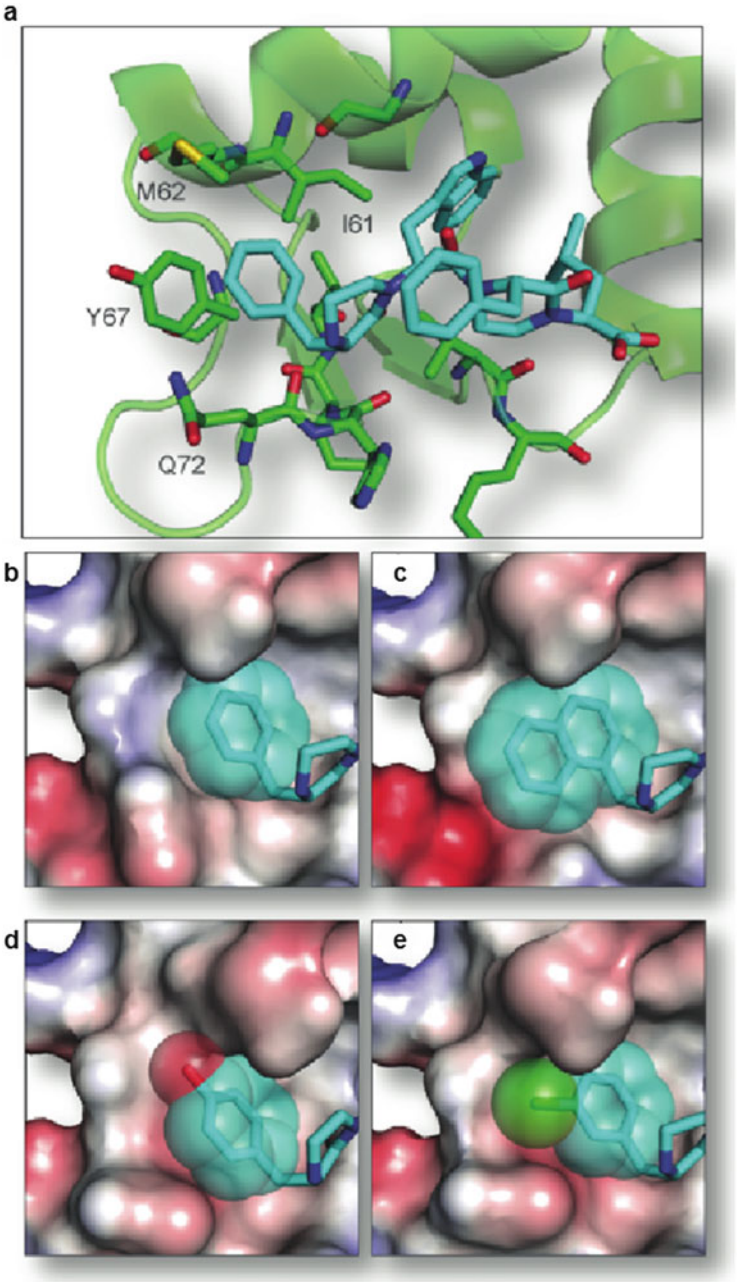

Fig. 8 Examination of the N-terminal residue-binding pocket of Mdm2. (**a**) The phenylalanine residue at the R_1 position of **P5** resides in a flexible pocket consisting of Ile-61, Met62, Tyr67, and Gln72 of Mdm2. (**b**) Predicted orientations of phenylalanine and analogs, (**c**) naphthylalanine, (**d**) tyrosine, and (**e**) 3-chlorophenylalanine. Electrostatic surface of Mdm2 was modeled by PyMOL (reprinted with permission from Lao et al. [67] Copyright (2014) Journal of the American Chemical Society)

Table 3 Computationally predicted oxopiperazine p53 mimics and their potential to target Mdm2

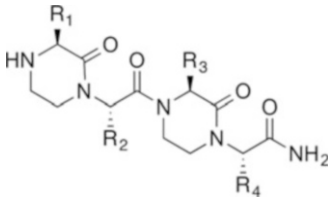

p53-OHM	R_1	R_2	R_3	R_4	K_i (μM)[a]
P9	Phe	Trp	Phe	Nle	2.46 ± 0.520
P10	Phe	Trp	Tyr	Leu	3.10 ± 0.200
P11	Nap	Trp	Phe	Leu	0.850 ± 0.07
P12	Tyr	Trp	Phe	Leu	0.400 ± 0.050
P13	Tyr(O–Me)	Trp	Phe	Leu	0.320 ± 0.010
P14	Phe(3-Cl)	Trp	Phe	Leu	0.330 ± 0.036
P15	Phe(3-Me)	Trp	Phe	Leu	2.60 ± 0.04
P16	Phe(4-Cl)	Trp	Phe	Leu	1.29 ± 0.060

[a]Binding affinity for Mdm2 as determined by a competitive fluorescence polarization assay (reprinted with permission from Lao et al. [67] Copyright (2014) Journal of the American Chemical Society)

Interestingly, we observed that substitutions at the R_4 position were less important for enhanced affinity compared to those at the R_1 position. We chose to further examine substitution effects of the R_1 side chain of the OHM dimer scaffold. Derivatives of phenylalanine, such as tyrosine (e.g., **P12**), and 3-chloro and 3-methyl phenylalanine (e.g., **P13–14**) lead to significantly improved binding relative to OHM **P5**. Analysis suggested that modification of the phenyl ring, especially at the *meta* position, enhanced packing against Mdm2 (Fig. 8).

The computational design effort resulted in ligands with 200-fold enhanced affinity for Mdm2. Central to the present efforts was a combination of rational design (i.e., hot spot mimicry) and a new set of Rosetta functionalities for computational design with non-canonical side chains and backbones.

4 OHMs Targeting the p300/HIF-1α Interaction

We chose Mdm2 as a model protein–protein interaction to evaluate the OHM scaffold and test predictions from the Rosetta analysis. As discussed above, several small molecules and helix mimics that target Mdm2 had already been described. To evaluate the potential of OHMs to target protein–protein interactions that had yet to be blocked by small molecules, we targeted analogs that mimic hypoxia-inducible

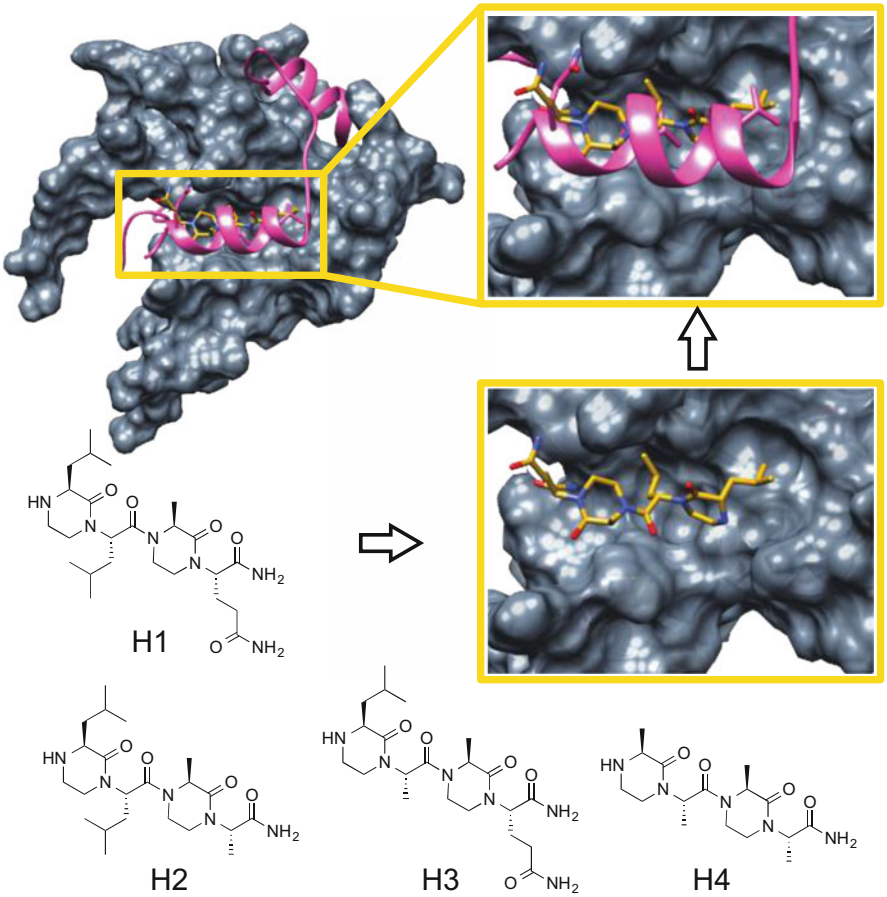

Fig. 9 HIF-1α OHMs. **H1** OHM (*gold*) built from canonical residues docked into p300-CH1 (*gray surface*) and overlaid with HIF-1α helix αB (*pink*); **H2** lacks the $i+6$ glutamine; **H3** has the critical Leu822 mutated to alanine; **H4** is an all alanine OHM dimer with no native residues for partner recognition

factor-1α to inhibit the p300/CBP interactions that regulate hypoxia-inducible genes and tumor progression [85, 86].

The transcription factor hypoxia-inducible factor-1α (HIF-1α) utilizes α-helices to recruit its co-activator partner p300 (or homolog CREB Binding Protein, CBP) in response to low oxygen levels, a nearly universal condition of solid tumors [87]. Upon protein complexation, transcription of numerous cancer survival genes is activated leading to angiogenesis, cell proliferation, metabolism, and metastasis [85, 86, 88–90]. HIF-1α utilizes two α-helices within its C-terminal domain (C-TAD$_{786–827}$) to bind to the CH1 domain of p300 (Fig. 9).

4.1 Development of HIF-1α Mimics

We began our OHM design by grafting residues of the native sequence from the αB helix onto our scaffold. Leucines 818 and 822 were predicted to be critical for partner recognition by computational alanine scanning [44]. These two residues along with Gln824, which may enhance solubility, were mimicked by an oxopiperazine dimer built from the appropriate starting amino acids (OHM H**1**; Fig. 9). Three control analogs of OHM **H1**, featuring alanine residues in place of the native functionality, were synthesized. OHM **H2** and OHM **H3** contain alanine residues in place of Gln824 and Leu822, respectively. Substitution of Gln824 was predicted to have little effect on HIF-1α/p300 complexation. A tetraalanine mutant OHM **H4** was also synthesized as a control.

The potential of the designed OHMs to target p300 was evaluated by an intrinsic tryptophan-binding assay. The cleft of p300-CH1 contains a tryptophan residue, the fluorescence of which is known to change upon HIF-1α binding [91, 92]. We monitored changes in tryptophan fluorescence upon titration with the ligands to obtain binding constants for the designed compounds (Table 4). OHM **H1** was found to target p300-CH1 with a dissociation constant (K_d) of 533 ± 24 nM. OHM **H2**, which contains two critical leucine residues, bound CH1 with a K_d of 623 ± 26 nM. As predicted, the negative controls **H3** and **H4** showed reduced affinity for p300-CH1. The binding site on p300-CH1 for OHM **H1** was confirmed by HSQC-NMR titration experiments with ^{15}N-labeled p300-CH1 [67].

Table 4 Binding affinities and cellular activities of the designed HIF mimetics

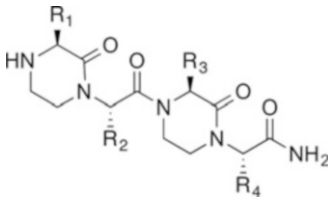

Residue						Decrease in the expression of indicated genes upon treatment with 10 μM OHM as measured by RT-PCR and or luciferase assays[a]			
						Luciferase	RT-PCR		
OHM	R_1	R_2	R_3	R_4	K_d (nM)[b]	HIF1α promoter activity	VEGF	LOX	c-Met
H1	Leu	Leu	Ala	Gln	533 ± 24.0	89%	79%	82%	84%
H2	Leu	Leu	Ala	Ala	623 ± 27.0	56%	89%	91%	83%
H3	Leu	Ala	Ala	Gln	>100,000	ND	ND	ND	ND
H4	Ala	Ala	Ala	Ala	>100,000	0%	1.1%	9.3%	9.1%

ND = not determined

[a]Percent decrease in luciferase activity and mRNA levels under hypoxic conditions maintained using EZ GasPak; data is normalized to the expression of each gene under normoxic conditions

[b]Binding affinities were determined by a tryptophan fluorescence assay

4.2 HIF OHMs Decrease Expression of Downstream Hypoxia-Induced Genes in Cell Culture

HIF-1α OHMs bound directly to p300-CH1 and inhibited transcription downregulating gene expression levels in cell culture. In a luciferase reporter assay, a hypoxia response element (HRE) construct was transfected into a triple negative breast cancer cell line (MDA-MB-231) upstream of the hCMV firefly luciferase promoter [93]. OHMs **H1** and **H2** were found to decrease expression to nearly basal levels at 20 μM concentrations under hypoxic conditions mimicked by a GasPak EZ pouch. At 10 μM concentrations, OHM **H1** reduced luciferase expression by 89% (Table 4). Negative control OHMs were found to be ineffective as inhibitors of the HRE-promoted luciferase expression at concentrations of up to 20 μM.

In addition to evaluating inhibition of transcription using the luciferase construct, we utilized a real-time quantitative PCR assays (qRT-PCR) to assess the expression of specific hypoxia target genes: *VEGF-A*, *LOX*, and *c-Met* genes [94–96]. Tumor growth depends on the regulation of angiogenesis by vascular endothelial growth factor (*VEGF-A*) [97]. The lysyl oxidase *LOX* [95] and the hepatocyte growth factor receptor *c-Met* [98] both are oncoproteins that contribute to tumor metastasis and invasion. The HIF OHMs were examined for effectiveness in hindering hypoxia-inducible signaling (Table 4). At 10 μM concentrations, OHMs **H1** and **H2** were found to downregulate mRNA expression levels of the critical angiogenesis regulator VEGF by 80% and 90%, respectively (Table 4). In comparison, negative controls had no effect on VEGF-A mRNA levels at similar concentrations. Decreased levels were also observed for LOX and c-Met expression using OHMs **H1** and **H2**.

4.3 HIF-1α OHM Suppresses Tumor Growth In Vivo

A long-term goal of OHMs as inhibitors of PPIs is to transition them into novel cancer therapeutics. Two mouse xenograft models were employed to evaluate the efficacy of OHMs in vivo: breast cancer (MDA-MB-231) and renal cell carcinoma (786-O) mouse xenografts. In both models, OHM **H1** was found to reduce tumor growth by ≥50% in comparison to untreated mice (Fig. 10). To our knowledge, OHM **H1** was only the second reported example of a small molecule helix mimetic showing in vivo efficacy [29, 31]. The studies of HIF-1α OHM targeting p300-CH1 revealed their exciting potential to inhibit select protein–protein interactions and to modulate downstream genes both in vitro and in vivo.

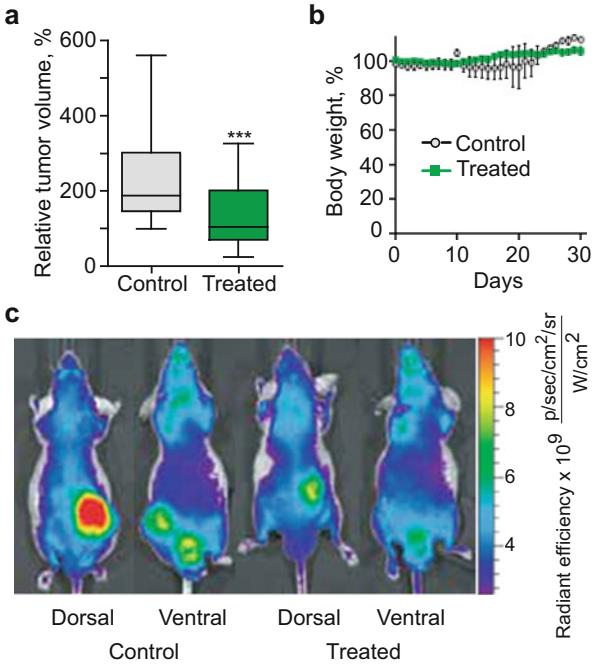

Fig. 10 Influence of OHM **H1** on the tumor growth rate of MDA-MB-231 xenografts. (**a**) Box and Whisker plots of the percentages of tumor volumes measured throughout the duration of the experiment: *boxes* represent the upper and lower quartiles and the median; *error bars* show maximum and minimum tumor volumes. ***$P < 0.001$. (**b**) Weight measurements during the course of the study of control (–O–) and OHM **H1**-treated (–■–) mice with MDA-MB-231 tumor grafts. Error bars are ± SEM of the weight measurements of the mice within each experimental group. (**c**) Localization of the NIR contrast agent IR-783 in the tumors of the control and treated mice. The fluorescence output was processed with Living Image software with one representative sample for each group presented above. Mice from the OHM **H1**-treated group show lower intensity of the signal originating from the tumor-accumulated contrast agent compared with the control group (this figure was originally published in Lao et al. [29])

5 Conclusion

Development of small molecules that target protein–protein interactions has evolved from an academic exercise to a novel means for identifying potential therapeutics [99–101]. Search for protein–protein interaction inhibitors may be broadly divided into three categories: (a) high-throughput screening from small molecule and natural product libraries [4, 102–105]; (b) mimicry of protein domains that are critical for complex formation [3, 106, 107], and (c) fragment-based strategies that build on both structural and high-throughput approaches to identify new sites on the protein surfaces for small molecule intervention [108–112]. Over the last decade our group has developed computational and experimental approaches to identify and mimic protein subdomains to extensively evaluate a

structure-based rational design strategy [6, 7, 9, 93, 113–115]. The success of this approach rests on synthesis of compounds that are metabolically stable, cell permeable, and efficacious in vivo. Several groups have achieved preliminary success toward these goals using both stabilized peptide helices as well as small molecule mimics [5, 29, 31, 93, 116, 117].

In this chapter, we reviewed the motivations for the design of a small molecule topographical helix mimic scaffold based on oligoxopiperazines (OHMs). The design arose from our motivation to develop scaffolds that originate from α-amino acids and retain backbone chirality. OHMs can be effectively synthesized on solid support from α-amino acids. We validated our basic design hypotheses by mimicry of p53 to target Mdm2 but perceived that computational design could be used to optimize mimics, especially with non-canonical side chain residues. Incorporation of the OHM scaffold into Rosetta provided a streamlined platform for the discovery of OHM inhibitors of protein–protein interactions. Computational analysis was employed to perform alanine-scanning mutagenesis to assess the pertinence of side chains for receptor binding. Computer-aided design was also used to optimize the orientation and composition of scaffold-based ligands. We evaluated the computational strategy by developing ligands for Mdm2 as well as p300/CBP [67]. Gratifyingly, the designed HIF-1α OHM ligands proved to be cell permeable, downregulated hypoxia-inducible signaling in cell culture and reduced tumor burden in mouse xenograft models. The initial success of the OHM scaffold in complex cellular and in vivo models supports the hypothesis that mimicry of hot spot residues is a promising approach for the development of small molecule PPI inhibitors [99, 101, 106, 116, 118].

Acknowledgments We thank the National Science Foundation (CHE-1151554) for financial support of this work. The Rosetta computational analyses were performed by Kevin Drew and Richard Bonneau (NYU), while the effects of the designed compounds on the hypoxia-inducible signaling pathway were analyzed in collaboration with Ivan Grishagin and Bogdan Olenyuk (USC). We thank these long-term collaborators for their insights on these projects.

References

1. Azzarito V, Long K, Murphy NS, Wilson AJ (2013) Inhibition of alpha-helix-mediated protein–protein interactions using designed molecules. Nat Chem 5(3):161–173
2. Jayatunga MKP, Thompson S, Hamilton AD (2014) α-Helix mimetics: outwards and upwards. Bioorg Med Chem Lett 24(3):717–724
3. London N, Raveh B, Schueler-Furman O (2013) Druggable protein–protein interactions – from hot spots to hot segments. Curr Opin Chem Biol 17(6):952–959
4. Milroy L-G, Grossmann TN, Hennig S, Brunsveld L, Ottmann C (2014) Modulators of protein–protein interactions. Chem Rev 114(9):4695–4748
5. Walensky LD, Bird GH (2014) Hydrocarbon-stapled peptides: principles, practice, and progress. J Med Chem 57(15):6275–6288
6. Jochim AL, Arora PS (2009) Assessment of helical interfaces in protein–protein interactions. Mol Biosyst 5:924–926

7. Jochim AL, Arora PS (2010) Systematic analysis of helical protein interfaces reveals targets for synthetic inhibitors. ACS Chem Biol 5(10):919–923
8. Jones S, Thornton JM (1996) Principles of protein–protein interactions. Proc Natl Acad Sci U S A 93(1):13–20
9. Bullock BN, Jochim AL, Arora PS (2011) Assessing helical protein interfaces for inhibitor design. J Am Chem Soc 133(36):14220–14223
10. Ko E, Liu J, Burgess K (2011) Minimalist and universal peptidomimetics. Chem Soc Rev 40:4411–4421
11. Ko E, Liu J, Perez LM, Lu G, Schaefer A, Burgess K (2010) Universal peptidomimetics. J Am Chem Soc 133(3):462–477
12. Orner BP, Ernst JT, Hamilton AD (2001) Toward proteomimetics: terphenyl derivatives as structural and functional mimics of extended regions of an alpha-helix. J Am Chem Soc 123 (22):5382–5383
13. Chen L, Yin H, Farooqi B, Sebti S, Hamilton AD, Chen J (2005) p53 alpha-Helix mimetics antagonize p53/MDM2 interaction and activate p53. Mol Cancer Ther 4(6):1019–1025
14. Ernst JT, Kutzki O, Debnath AK, Jiang S, Lu H, Hamilton AD (2002) Design of a protein surface antagonist based on alpha-helix mimicry: inhibition of gp41 assembly and viral fusion. Angew Chem Int Ed Engl 41(2):278–281
15. Kutzki O, Park HS, Ernst JT, Orner BP, Yin H, Hamilton AD (2002) Development of a potent Bcl-x(L) antagonist based on alpha-helix mimicry. J Am Chem Soc 124(40):11838–11839
16. Buhrlage SJ, Bates CA, Rowe SP, Minter AR, Brennan BB, Majmudar CY, Wemmer DE, Al-Hashimi H, Mapp AK (2009) Amphipathic small molecules mimic the binding mode and function of endogenous transcription factors. ACS Chem Biol 4(5):335–344
17. Lee JH, Zhang Q, Jo S, Chai SC, Oh M, Im W, Lu H, Lim HS (2011) Novel pyrrolopyrimidine-based alpha-helix mimetics: cell-permeable inhibitors of protein–protein interactions. J Am Chem Soc 133(4):676–679
18. Maity P, Konig B (2008) Synthesis and structure of 1,4-dipiperazino benzenes: chiral terphenyl-type peptide helix mimetics. Org Lett 10(7):1473–1476
19. Marimganti S, Cheemala MN, Ahn JM (2009) Novel amphiphilic alpha-helix mimetics based on a bis-benzamide scaffold. Org Lett 11(19):4418–4421
20. Plante JP, Burnley T, Malkova B, Webb ME, Warriner SL, Edwards TA, Wilson AJ (2009) Oligobenzamide proteomimetic inhibitors of the p53-hDM2 protein–protein interaction. Chem Commun 34:5091–5093
21. Restorp P, Rebek J Jr (2008) Synthesis of alpha-helix mimetics with four side-chains. Bioorg Med Chem Lett 18(22):5909–5911
22. Rodriguez JM, Nevola L, Ross NT, Lee GI, Hamilton AD (2009) Synthetic inhibitors of extended helix-protein interactions based on a biphenyl 4,4′-dicarboxamide scaffold. Chembiochem 10(5):829–833
23. Shaginian A, Whitby LR, Hong S, Hwang I, Farooqi B, Searcey M, Chen J, Vogt PK, Boger DL (2009) Design, synthesis, and evaluation of an alpha-helix mimetic library targeting protein–protein interactions. J Am Chem Soc 131(15):5564–5572
24. Tosovska P, Arora PS (2010) Oligooxopiperazines as nonpeptidic alpha-helix mimetics. Org Lett 12:1588–1591
25. Yin H, Hamilton AD (2005) Strategies for targeting protein–protein interactions with synthetic agents. Angew Chem Int Ed 44(27):4130–4163
26. Yin H, Lee G-i, Sedey KA, Rodriguez JM, Wang H-G, Sebti SM, Hamilton AD (2005) Terephthalamide derivatives as mimetics of helical peptides: disruption of the Bcl-xL/Bak interaction. J Am Chem Soc 127(15):5463–5468
27. Burslem GM, Kyle HF, Breeze AL, Edwards TA, Nelson A, Warriner SL, Wilson AJ (2014) Small-molecule proteomimetic inhibitors of the HIF-1α–p300 protein–protein interaction. Chembiochem. doi:10.1002/cbic.201400009
28. Cao X, Yap JL, Newell-Rogers MK, Peddaboina C, Jiang W, Papaconstantinou HT, Jupitor D, Rai A, Jung KY, Tubin RP, Yu W, Vanommeslaeghe K, Wilder PT, MacKerell AD Jr, Fletcher S, Smythe RW (2013) The novel BH3 alpha-helix mimetic JY-1-106 induces

apoptosis in a subset of cancer cells (lung cancer, colon cancer and mesothelioma) by disrupting Bcl-xL and Mcl-1 protein–protein interactions with Bak. Mol Cancer 12(1):42
29. Lao BB, Grishagin I, Mesallati H, Brewer TF, Olenyuk BZ, Arora PS (2014) In vivo modulation of hypoxia-inducible signaling by topographical helix mimetics. Proc Natl Acad Sci U S A 111(21):7531–7536
30. Oh M, Lee JH, Wang W, Lee HS, Lee WS, Burlak C, Im W, Hoang QQ, Lim H-S (2014) Potential pharmacological chaperones targeting cancer-associated MCL-1 and Parkinson disease-associated α-synuclein. Proc Natl Acad Sci 111(30):11007–11012
31. Ravindranathan P, Lee TK, Yang L, Centenera MM, Butler L, Tilley WD, Hsieh JT, Ahn JM, Raj GV (2013) Peptidomimetic targeting of critical androgen receptor-coregulator interactions in prostate cancer. Nat Commun 4:1923
32. Gante J (1994) Peptidomimetics – tailored enzyme-inhibitors. Angew Chem Int Ed Engl 33 (17):1699–1720
33. Patchett AA, Nargund RP (2000) Privileged structures - an update. Annu Rep Med Chem 35:289–298
34. Giannis A, Kolter T (1993) Peptidomimetics for receptor ligands discovery, development, and medical perspectives. Angew Chem Int Ed 32(9):1244–1267
35. Hansen TK, Schlienger N, Hansen BS, Andersen PH, Bryce MR (1999) Synthesis of piperazinones and their application in constrained mimetics of the growth hormone secretagogue NN703. Tetrahedron Lett 40(18):3651–3654
36. Tian X, Mishra RK, Switzer AG, Hu XE, Kim N, Mazur AW, Ebetino FH, Wos JA, Crossdoersen D, Pinney BB, Farmer JA, Sheldon RJ (2006) Design and synthesis of potent and selective 1,3,4-trisubstituted-2-oxopiperazine based melanocortin-4 receptor agonists. Bioorg Med Chem Lett 16(17):4668–4673
37. Macromodel (2011) Macromodel. Version 9.9. Schrodinger Inc., New York
38. Mohamadi F, Richards NGJ, Guida WC, Liskamp R, Lipton M, Caufield C, Chang G, Hendrickson T, Still WC (1990) Macromodel - an integrated software system for modeling organic and bioorganic molecules using molecular mechanics. J Comput Chem 11 (4):440–467
39. Bhatt U, Mohamed N, Just G, Roberts E (1997) Derivatized oxopiperazine rings from amino acids. Tetrahedron Lett 38(21):3679–3682
40. Franceschini N, Sonnet P, Guillaume D (2005) Simple, versatile and highly diastereoselective synthesis of 1,3,4-trisubstituted-2-oxopiperazine-containing peptidomimetic precursors. Org Biomol Chem 3(5):787–793
41. Sugihara H, Fukushi H, Miyawaki T, Imai Y, Terashita Z, Kawamura M, Fujisawa Y, Kita S (1998) Novel non-peptide fibrinogen receptor antagonists. 1. Synthesis and glycoprotein IIb-IIIa antagonistic activities of 1,3,4-trisubstituted 2-oxopiperazine derivatives incorporating side-chain functions of the RGDF peptide. J Med Chem 41(4):489–502
42. Tong YS, Fobian YM, Wu MY, Boyd ND, Moeller KD (2000) Conformationally constrained substance P analogues: the total synthesis of a constrained peptidomimetic for the Phe(7)-Phe (8) region. J Org Chem 65(8):2484–2493
43. Bergey CM, Watkins AM, Arora PS (2013) HippDB: a database of readily targeted helical protein–protein interactions. Bioinformatics 29(21):2806–2807
44. Kortemme T, Kim DE, Baker D (2004) Computational alanine scanning of protein–protein interfaces. Sci STKE 2004(219):pl2
45. Joerger AC, Fersht AR (2008) Structural biology of the tumor suppressor p53. Annu Rev Biochem 77:557–582
46. Soussi T, Ishioka C, Claustres M, Beroud C (2006) Locus-specific mutation databases: pitfalls and good practice based on the p53 experience. Nat Rev Cancer 6(1):83–90
47. Haupt Y, Maya R, Kazaz A, Oren M (1997) Mdm2 promotes the rapid degradation of p53. Nature 387(6630):296–299
48. Honda R, Tanaka H, Yasuda H (1997) Oncoprotein MDM2 is a ubiquitin ligase E3 for tumor suppressor p53. FEBS Lett 420(1):25–27

49. Kubbutat MH, Jones SN, Vousden KH (1997) Regulation of p53 stability by Mdm2. Nature 387(6630):299–303
50. Honda R, Yasuda H (1999) Association of p19(ARF) with Mdm2 inhibits ubiquitin ligase activity of Mdm2 for tumor suppressor p53. EMBO J 18(1):22–27
51. Chene P (2003) Inhibiting the p53-MDM2 interaction: an important target for cancer therapy. Nat Rev Cancer 3(2):102–109
52. Cheok CF, Verma CS, Baselga J, Lane DP (2011) Translating p53 into the clinic. Nat Rev Clin Oncol 8(1):25–37
53. Shangary S, Wang S (2008) Targeting the MDM2-p53 interaction for cancer therapy. Clin Cancer Res 14(17):5318–5324
54. Vazquez A, Bond EE, Levine AJ, Bond GL (2008) The genetics of the p53 pathway, apoptosis and cancer therapy. Nat Rev Drug Discov 7(12):979–987
55. Kussie PH, Gorina S, Marechal V, Elenbaas B, Moreau J, Levine AJ, Pavletich NP (1996) Structure of the MDM2 oncoprotein bound to the p53 tumor suppressor transactivation domain. Science 274(5289):948–953
56. Picksley SM, Vojtesek B, Sparks A, Lane DP (1994) Immunochemical analysis of the interaction of p53 with MDM2;--fine mapping of the MDM2 binding site on p53 using synthetic peptides. Oncogene 9(9):2523–2529
57. Bernal F, Tyler AF, Korsmeyer SJ, Walensky LD, Verdine GL (2007) Reactivation of the p53 tumor suppressor pathway by a stapled p53 peptide. J Am Chem Soc 129(9):2456–2457
58. Brown ZZ, Akula K, Arzumanyan A, Alleva J, Jackson M, Bichenkov E, Sheffield JB, Feitelson MA, Schafmeister CE (2012) A spiroligomer α-helix mimic that binds HDM2, penetrates human cells and stabilizes HDM2 in cell culture. PLoS One 7(10):e45948
59. Chang YS, Graves B, Guerlavais V, Tovar C, Packman K, To K-H, Olson KA, Kesavan K, Gangurde P, Mukherjee A, Baker T, Darlak K, Elkin C, Filipovic Z, Qureshi FZ, Cai H, Berry P, Feyfant E, Shi XE, Horstick J, Annis DA, Manning AM, Fotouhi N, Nash H, Vassilev LT, Sawyer TK (2013) Stapled α-helical peptide drug development: a potent dual inhibitor of MDM2 and MDMX for p53-dependent cancer therapy. Proc Natl Acad Sci U S A 110(36):E3445–E3454
60. Henchey LK, Porter JR, Ghosh I, Arora PS (2010) High specificity in protein recognition by hydrogen-bond-surrogate alpha-helices: selective inhibition of the p53/MDM2 complex. Chembiochem 11(15):2104–2107
61. Kritzer JA, Lear JD, Hodsdon ME, Schepartz A (2004) Helical β-peptide inhibitors of the p53-hDM2 interaction. J Am Chem Soc 126(31):9468–9469
62. Murray JK, Gellman SH (2007) Targeting protein–protein interactions: lessons from p53/MDM2. Biopolymers 88(5):657–686
63. Popowicz GM, Dömling A, Holak TA (2011) The structure-based design of Mdm2/Mdmx–p53 inhibitors gets serious. Angew Chem Int Ed 50(12):2680–2688
64. Sakurai K, Chung HS, Kahne D (2004) Use of a retroinverso p53 peptide as an inhibitor of MDM2. J Am Chem Soc 126(50):16288–16289
65. Massova I, Kollman PA (1999) Computational alanine scanning to probe protein–protein interactions: a novel approach to evaluate binding free energies. J Am Chem Soc 121 (36):8133–8143
66. Böttger A, Böttger V, Garcia-Echeverria C, Chène P, Hochkeppel H-K, Sampson W, Ang K, Howard SF, Picksley SM, Lane DP (1997) Molecular characterization of the hdm2-p53 interaction. J Mol Biol 269(5):744–756
67. Lao BB, Drew K, Guarracino DA, Brewer TF, Heindel DW, Bonneau R, Arora PS (2014) Rational design of topographical helix mimics as potent inhibitors of protein–protein interactions. J Am Chem Soc 136(22):7877–7888
68. Knight SM, Umezawa N, Lee HS, Gellman SH, Kay BK (2002) A fluorescence polarization assay for the identification of inhibitors of the p53-DM2 protein–protein interaction. Anal Biochem 300(2):230–236

69. Butterfoss GL, Kuhlman B (2006) Computer-based design of novel protein structures. Ann Rev Biophys Biomol Struct 35:49–65
70. Jiang L, Althoff EA, Clemente FR, Doyle L, Rothlisberger D, Zanghellini A, Gallaher JL, Betker JL, Tanaka F, Barbas CF, Hilvert D, Houk KN, Stoddard BL, Baker D (2008) De novo computational design of retro-aldol enzymes. Science 319(5868):1387–1391
71. Kuhlman B, Dantas G, Ireton GC, Varani G, Stoddard BL, Baker D (2003) Design of a novel globular protein fold with atomic-level accuracy. Science 302(5649):1364–1368
72. Drew K, Renfrew PD, Craven TW, Butterfoss GL, Chou F-C, Lyskov S, Bullock BN, Watkins A, Labonte JW, Pacella M, Kilambi KP, Leaver-Fay A, Kuhlman B, Gray JJ, Bradley P, Kirshenbaum K, Arora PS, Das R, Bonneau R (2013) Adding diverse noncanonical backbones to rosetta: enabling peptidomimetic design. PLoS One 8(7):e67051
73. Xin D, Ko E, Perez LM, Ioerger TR, Burgess K (2013) Evaluating minimalist mimics by exploring key orientations on secondary structures (EKOS). Org Biomol Chem 11 (44):7789–7801
74. Korkegian A, Black ME, Baker D, Stoddard BL (2005) Computational thermostabilization of an enzyme. Science 308(5723):857–860
75. Ashworth J, Havranek JJ, Duarte CM, Sussman D, Monnat RJ, Stoddard BL, Baker D (2006) Computational redesign of endonuclease DNA binding and cleavage specificity. Nature 441 (7093):656–659
76. Dahiyat BI, Mayo SL (1997) De novo protein design: fully automated sequence selection. Science 278(5335):82–87
77. Fleishman SJ, Whitehead TA, Ekiert DC, Dreyfus C, Corn JE, Strauch E-M, Wilson IA, Baker D (2011) Computational design of proteins targeting the conserved stem region of influenza hemagglutinin. Science 332(6031):816–821
78. Harbury PB, Plecs JJ, Tidor B, Alber T, Kim PS (1998) High-resolution protein design with backbone freedom. Science 282(5393):1462–1467
79. Joachimiak LA, Kortemme T, Stoddard BL, Baker D (2006) Computational design of a new hydrogen bond network and at least a 300-fold specificity switch at a protein–protein interface. J Mol Biol 361:195–208
80. Rothlisberger D, Khersonsky O, Wollacott AM, Jiang L, DeChancie J, Betker J, Gallaher JL, Althoff EA, Zanghellini A, Dym O, Albeck S, Houk KN, Tawfik DS, Baker D (2008) Kemp elimination catalysts by computational enzyme design. Nature 453(7192):190–195
81. Shifman JM, Mayo SL (2003) Exploring the origins of binding specificity through the computational redesign of calmodulin. Proc Natl Acad Sci U S A 100(23):13274–13279
82. Butterfoss GL, Renfrew PD, Kuhlman B, Kirshenbaum K, Bonneau R (2009) A preliminary survey of the peptoid folding landscape. J Am Chem Soc 131(46):16798–16807
83. Lyskov S, Chou F-C, Conchúir SÓ, Der BS, Drew K, Kuroda D, Xu J, Weitzner BD, Renfrew PD, Sripakdeevong P, Borgo B, Havranek JJ, Kuhlman B, Kortemme T, Bonneau R, Gray JJ, Das R (2013) Serverification of molecular modeling applications: the Rosetta online server that includes everyone (ROSIE). PLoS One 8(5):e63906
84. Renfrew PD, Choi EJ, Bonneau R, Kuhlman B (2012) Incorporation of noncanonical amino acids into Rosetta and use in computational protein-peptide interface design. PLoS One 7(3): e32637
85. Giaccia A, Siim BG, Johnson RS (2003) HIF-1 as a target for drug development. Nat Rev Drug Discov 2(10):803–811
86. Semenza GL (2003) Targeting HIF-1 for cancer therapy. Nat Rev Cancer 3(10):721–732
87. Schofield CJ, Ratcliffe PJ (2004) Oxygen sensing by HIF hydroxylases. Nat Rev Mol Cell Biol 5(5):343–354
88. Hirota K, Semenza GL (2006) Regulation of angiogenesis by hypoxia-inducible factor 1. Crit Rev Oncol Hematol 59(1):15–26
89. Ivan M, Kondo K, Yang H, Kim W, Valiando J, Ohh M, Salic A, Asara JM, Lane WS, Kaelin WG Jr (2001) HIFalpha targeted for VHL-mediated destruction by proline hydroxylation: implications for O2 sensing. Science 292(5516):464–468

90. Orourke JF, Pugh CW, Bartlett SM, Ratcliffe PJ (1996) Identification of hypoxically inducible mRNAs in HeLa cells using differential-display PCR – role of hypoxia-inducible factor-1. Eur J Biochem 241(2):403–410
91. Dames SA, Martinez-Yamout M, De Guzman RN, Dyson HJ, Wright PE (2002) Structural basis for Hif-1 alpha/CBP recognition in the cellular hypoxic response. Proc Natl Acad Sci U S A 99(8):5271–5276
92. Freedman SJ, Sun ZY, Poy F, Kung AL, Livingston DM, Wagner G, Eck MJ (2002) Structural basis for recruitment of CBP/p300 by hypoxia-inducible factor-1 alpha. Proc Natl Acad Sci U S A 99(8):5367–5372
93. Kushal S, Lao BB, Henchey LK, Dubey R, Mesallati H, Traaseth NJ, Olenyuk BZ, Arora PS (2013) Protein domain mimetics as in vivo modulators of hypoxia-inducible factor signaling. Proc Natl Acad Sci U S A 110(39):15602–15607
94. Chen C, Pore N, Behrooz A, Ismail-Beigi F, Maity A (2001) Regulation of GLUT1 mRNA by hypoxia-inducible factor-1. J Biol Chem 276(12):9519–9525
95. Erler JT, Bennewith KL, Nicolau M, Dornhofer N, Kong C, Le QT, Chi JT, Jeffrey SS, Giaccia AJ (2006) Lysyl oxidase is essential for hypoxia-induced metastasis. Nature 440 (7088):1222–1226
96. Liu Y, Cox SR, Morita T, Kourembanas S (1995) Hypoxia regulates vascular endothelial growth factor gene expression in endothelial cells: identification of a 5′ enhancer. Circ Res 77 (3):638–643
97. Ryan HE, Lo J, Johnson RS (1998) HIF-1 alpha is required for solid tumor formation and embryonic vascularization. EMBO J 17(11):3005–3015
98. Pennacchietti S, Michieli P, Galluzzo M, Mazzone M, Giordano S, Comoglio PM (2003) Hypoxia promotes invasive growth by transcriptional activation of the met protooncogene. Cancer Cell 3(4):347–361
99. Arkin MR, Wells JA (2004) Small-molecule inhibitors of protein–protein interactions: progressing towards the dream. Nat Rev Drug Discov 3(4):301–317
100. Nero TL, Morton CJ, Holien JK, Wielens J, Parker MW (2014) Oncogenic protein interfaces: small molecules, big challenges. Nat Rev Cancer 14(4):248–262
101. Wells JA, McClendon CL (2007) Reaching for high-hanging fruit in drug discovery at protein–protein interfaces. Nature 450(7172):1001–1009
102. Heeres JT, Hergenrother PJ (2011) High-throughput screening for modulators of protein–protein interactions: use of photonic crystal biosensors and complementary technologies. Chem Soc Rev 40(8):4398–4410
103. Stockwell BR (2000) Chemical genetics: ligand-based discovery of gene function. Nat Rev Genet 1(2):116–125
104. Stockwell BR (2004) Exploring biology with small organic molecules. Nature 432 (7019):846–854
105. Tan DS (2005) Diversity-oriented synthesis: exploring the intersections between chemistry and biology. Nat Chem Biol 1(2):74–84
106. Clackson T, Wells JA (1995) A hot-spot of binding-energy in a hormone-receptor interface. Science 267(5196):383–386
107. Raj M, Bullock BN, Arora PS (2013) Plucking the high hanging fruit: a systematic approach for targeting protein–protein interactions. Bioorg Med Chem 21(14):4051–4057
108. Congreve M, Chessari G, Tisi D, Woodhead AJ (2008) Recent developments in fragment-based drug discovery. J Med Chem 51(13):3661–3680
109. Fesik SW (2000) Insights into programmed cell death through structural biology. Cell 103 (2):273–282
110. Hajduk PJ, Greer J (2007) A decade of fragment-based drug design: strategic advances and lessons learned. Nat Rev Drug Discov 6(3):211–219
111. Murray CW, Rees DC (2009) The rise of fragment-based drug discovery. Nat Chem 1 (3):187–192

112. Sun Q, Burke JP, Phan J, Burns MC, Olejniczak ET, Waterson AG, Lee T, Rossanese OW, Fesik SW (2012) Discovery of small molecules that bind to K-Ras and inhibit Sos-mediated activation. Angew Chem Int Ed 51(25):6140–6143
113. Chapman RN, Dimartino G, Arora PS (2004) A highly stable short alpha-helix constrained by a main-chain hydrogen-bond surrogate. J Am Chem Soc 126(39):12252–12253
114. Patgiri A, Jochim AL, Arora PS (2008) A hydrogen bond surrogate approach for stabilization of short peptide sequences in alpha-helical conformation. Acc Chem Res 41(10):1289–1300
115. Patgiri A, Yadav KK, Arora PS, Bar-Sagi D (2011) An orthosteric inhibitor of the Ras-Sos interaction. Nat Chem Biol 7(9):585–587
116. Arkin MR, Tang Y, Wells JA (2014) Small-molecule inhibitors of protein–protein interactions: progressing toward the reality. Chem Biol 21(9):1102–1114
117. Verdine GL, Hilinski GJ (2012) Stapled peptides for intracellular drug targets. Methods Enzymol 503:3–33
118. Arkin MR, Randal M, DeLano WL, Hyde J, Luong TN, Oslob JD, Raphael DR, Taylor L, Wang J, McDowell RS, Wells JA, Braisted AC (2003) Binding of small molecules to an adaptive protein–protein interface. Proc Natl Acad Sci U S A 100(4):1603–1608

Top Heterocycl Chem (2017) 49: 25–50
DOI: 10.1007/7081_2015_163

Published online: 26 August 2015

Heterocyclic Extended Peptide Surrogates for β-Strand Stabilization

Juan R. Del Valle

Abstract Peptidomimetic scaffolds designed to stabilize biologically relevant secondary structures play a key role in ligand-based drug design. Approaches aimed at stabilizing extended peptide conformations hold particular promise for targeting β-strand and β-sheet interactions. An understanding of how specific constraints impact extended backbone conformations is needed to expand their potential utility and to inform the design of novel templates. This chapter describes peptide orthotic and prosthetic approaches toward β-strand stabilization using heterocyclic motifs. Syntheses and conformational analyses are described for selected extended peptide surrogates suitable for incorporation into native sequences.

Keywords β-Sheets • Amino acids • Conformational analysis • Drug design • Peptide synthesis • Peptidomimetics • Protein–protein interactions • Secondary structure

Contents

J.R. Del Valle (✉)
Department of Chemistry, University of South Florida, 4202 E. Fowler Ave. Tampa, FL 33620, USA
e-mail: delvalle@usf.edu

1 Introduction

Biomolecular interactions are largely governed by specific recognition events between protein secondary structures including helices, loops, and sheets. β-Sheets represent the second most common protein structural motif and are comprised of laterally H-bonded extended peptide strands. β-Sheets are known to engage in specific binding events with distinct protein secondary structures as well as with DNA [1, 2]. Edge–edge contacts between β-sheet domains also make up a sizable fraction of the protein interactome [3]. In addition to sheet interactions, a large number of natively disordered peptides adopt extended conformations when bound to proteolytic enzymes, kinases/phosphatases, and transferases [4–8]. Modulating these interactions with peptidomimetics has thus been an area of intense activity – one particularly hampered by the large surface area-to-pharmacophore ratio associated with β-sheet structure. Moreover, the folding and stability of β-sheet peptides are compromised outside the context of surrounding tertiary structures. The ability to predictably stabilize β-sheet-like structure within short host peptides has thus wide-ranging implications for chemical probe development and targeted drug design.

β-Strands within pleated sheets feature an extended or "sawtooth" peptide backbone arrangement that projects residual side chains on either face of the strand in an alternating pattern (Fig. 1). β-Strands lack intramolecular H bonds between backbone elements and readily associate with complementary peptide strands to form β-sheets [9]. The resulting sheets arrange in either a parallel or antiparallel orientation, and their conformations are defined by backbone dihedral angles (ψ, ω, ϕ) that are slightly more acute than those in a fully extended peptide strand [10]. In conjunction with bifacial side chain packing, interstrand H bonds along both edges of the backbone also allow for the higher-order assembly of β-sheets.

Peptidomimetic approaches to stabilize β-strands and β-sheets often involve the restriction of backbone dihedral angles within cyclic motifs (Fig. 2) [11]. This "orthotic" approach retains the composition of the native peptide backbone and introduces constraint through covalent tethering, commonly via cyclization involving side chain or backbone elements. In contrast, the "prosthetic" approach to β-strand stabilization replaces short sections of the backbone with rigid, nonnative scaffolds. Unnatural surrogates and *trans*-amide bond isosteres have proven effective in nucleating β-sheet-like structure [11]. In addition to these two classes of β-strand stabilizers, β-turn peptidomimetic scaffolds have been widely used to stabilize or mimic hairpin structures within peptides [9, 12–18]. However, the requirement of an auxiliary (or scaffolding) strand to support folding renders turn-inducing peptidomimetics unsuitable for the stabilization of isolated β-strands. Within the wider field of β-strand and β-sheet mimicry, a number of groups have also developed artificial secondary structures, composed entirely of non-peptidic oligomers that exhibit topological and chemical properties reminiscent of conformationally extended peptides [19–24].

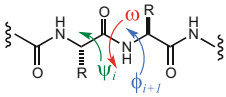

β-strand/sheet	ω	ϕ	ψ
Fully extended strand	180°	180°	180°
Parallel sheet	180°	-119°	113°
Antiparallel sheet	180°	-139°	135°

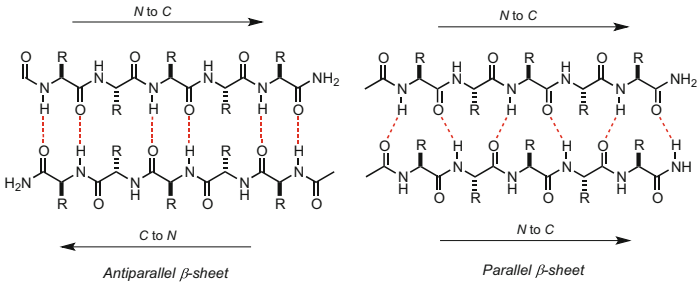

Fig. 1 Conformational characteristics of β-strands and their association into β-sheets

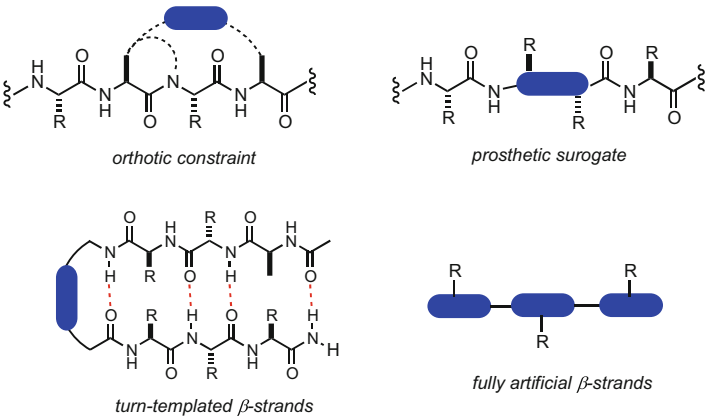

Fig. 2 Approaches toward β-strand stabilization and mimicry

Heterocycles have played a central role in β-strand and β-sheet mimicry owing to their synthetic accessibility and to the importance of hydrogen-bonding elements in β-sheet assembly and recognition. Despite the presence of various heterocyclic β-strand mimics in biologically active compounds, successful applications in drug discovery remain highly context dependent. There is relatively little known regarding the ability of specific peptide orthotics and prosthetics to stabilize extended

peptide conformations (across two or more residues) absent of a biological target. This is in stark contrast to β-turn and α-helix mimicry, for which in-depth conformational studies have led to the widespread application of specific strategies [14, 25–28]. In this chapter, we explore selected heterocyclic peptide surrogates and backbone constraints for β-strand stabilization. Given that chemical approaches to β-strand mimicry have been the subject of various comprehensive reviews [11, 29, 30], we have chosen to focus on peptidomimetics for which some degree of conformational analysis has been reported in an unbound state. Particular attention is paid to the design, synthesis, and structural characterization of β-strand surrogates suitable for incorporation into host peptides. A fundamental understanding of how these scaffolds impact β-strand and β-sheet pre-organization may broaden their potential utility in diverse applications and aid in the design of novel peptidomimetic templates.

2 Native Backbone Orthotics

Covalent tethering of peptide backbone elements is an effective approach toward restricting endocyclic dihedral angles. Coupled with retention of native backbone composition, this mode of constraint can allow for precise mimicry of desired conformations. The section below presents an overview of extended peptide orthotics capable of enforcing β-strand and β-sheet geometries as determined by experimental conformational analysis.

2.1 Lactam Constraints

Side chain-to-backbone lactamization (between $C\alpha_i$ and N_{i+1}) is among the most commonly utilized strategies for peptide conformational constraint. In 1980, Freidinger and coworkers first demonstrated this approach in the pursuit of potent peptidomimetic inhibitors of luteinizing hormone-releasing hormone [31]. In the ensuing years, several research groups have successfully utilized β-, γ-, and δ-lactams, as well as macrocyclic variants, to augment the conformational rigidity, inhibitor potency, and proteolytic stability of bioactive peptides [32–35]. Covalent linkage of $C\alpha_i$ to N_{i+1} effectively locks the amide bond into a *trans* configuration. However, lactam-based dipeptide constraints have been used almost exclusively to enforce turn conformations. This is primarily due to the fact that cyclization of N_{i+1} onto $C\alpha_i$, in which residue *i* possesses an L configuration, constrains generally the ψ_i dihedral angle to values near $-120°$. Coupled with a ϕ_{i+1} torsion that remains flexible, lactam constraints have proven to be particularly effective at stabilizing

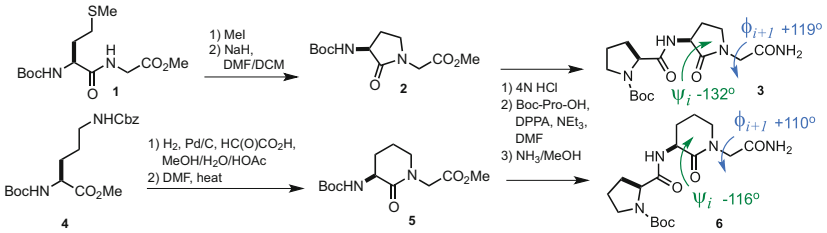

Scheme 1 Synthesis and conformational characteristics (X-ray) of Freidinger–Veber lactam-based β-strand peptidomimetics

type II β-turn conformers within host peptides. Despite this preference, a select few lactam-constrained dipeptides have exhibited extended or β-strand-like conformations that have been characterized by X-ray crystallography and predicted by computational modeling.

Following the general method described previously by Freidinger [32], the groups of Toniolo and Johnson synthesized γ- and δ-lactam-containing tripeptides **3** and **6** and carried out X-ray crystallographic analyses (Scheme 1) [36]. In contrast to the type II β-turn observed in the crystal structure of an unconstrained control peptide (Boc-Pro-Leu-Gly-NH_2), both lactams **3** and **6** adopted extended conformations across the *i* and *i* + 1 residues as evidenced by backbone torsions surrounding the heterocyclic motif. Notably, the ψ_i and ϕ_{i+1} dihedral angles observed in the solid-state structures were of similar magnitude (in the 110° to 132° range) but opposite sign. This alternating pattern is the principle requirement for β-strand and β-sheet structure. The sign of each of these torsions was however opposite to that expected for native β-strands and β-sheets comprised of L residues, because the *i*th residues in **3** and **6** possessed L configuration.

The solid-state conformational preferences of **3** and **6** supported earlier computational studies carried out on peptidomimetic inhibitors of angiotensin-converting enzyme (ACE). Thorsett and coworkers used lactam rings of 5 to 9 members to constrain the ψ_i and ω dihedral angles within a parent tripeptide [37, 38]. Energy-minimized structures of model lactams bearing a D configuration indicated ψ_i torsions in the +135° to +175° range, in good agreement with extended peptides (Fig. 3). Although computational analysis of the ϕ_{i+1} torsion was not carried out, crystal structures of synthetic intermediates also showed an extended conformation across ε-lactam-containing peptidomimetics such as **7**.

Although few conformational studies have examined the stabilization of β-strand structures using $C\alpha_i$–N_{i+1}-linked lactam peptidomimetics, the crystallographic and computational analyses above suggest that D-Met- and D-Lys-derived lactams (at least in the case of Gly_{i+1}-contaning dipeptide subunits) may be effective at promoting extended peptide conformations beyond the constrained

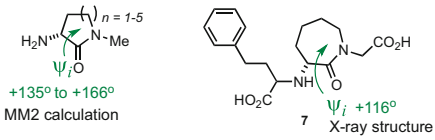

Fig. 3 Calculated and observed ψ dihedral angles within $C\alpha_i$–N_{i+1}-linked lactam peptidomimetics

amide bond. Further studies are required to fully assess the generality of this approach for β-strand stabilization.

2.2 Macrocyclic Tethers

Macrocyclic tethers have been widely utilized for the constraint of bioactive peptides into β-strand conformations [11, 29, 39–41]. Tethering strategies aimed at stabilizing extended backbone conformations involve typically a connection between $C\alpha_i$ and $C\alpha_{i+2}$ by way of side chains residing on the same face of an idealized (all-L configuration) β-strand or β-sheet. The observation that proteases recognize universally extended peptide substrates has prompted extensive use of macrocyclic tethers in drug discovery efforts. Macrocyclic analogs have been described which inhibit HIV proteases, HCV NS3, β-secretase, renin, thrombin, and related targets [4, 42]. In contrast to a wealth of crystallographic data for macrocyclic β-strand peptides bound to protein targets, relatively few efforts have assessed the ability of discrete tethering approaches to promote extended conformations in the absence of macromolecular receptors. By comparison, a variety of peptide "bridging" and "stapling" strategies are known to promote helical and other turn conformations [25–28, 43, 44].

Early investigations on biphenyl ether-linked β-strand macrocycles drew inspiration from the naturally occurring ACE inhibitor K-13 (**8a**, Fig. 4) [45]. Hobbs and Still completed the synthesis of thioether K-13 analog **8b** that exhibited an extended backbone conformation by NMR spectroscopy and molecular modeling [46]. Rich and coworkers subsequently carried out conformational analysis on related 17-membered macrocycles en route to potent inhibitors of HIV protease [47]. Intermediate **9** exhibited large (>11 Hz) ^{1}H NMR NH–CHα coupling constants for both the Ile and Tyr residues, indicating the presence of β-sheet-like ϕ dihedral angles. Moreover, the 2D NOESY spectrum of **9** in $CDCl_3$ revealed strong $CH\alpha_i \rightarrow NH_{i+1}$ correlations typical of an extended conformation. An X-ray crystal structure of a close analog confirmed an extended backbone conformation that overlaid well with the enzyme-bound conformation of the HIV-protease inhibitor JG-365 (**10**). This template was used to prepare biphenyl ether **11**, which inhibited HIV protease in vitro with a K_i of 15 nM.

In 2002, Fairlie and coworkers examined a series of phenyl ether-linked macrocycles possessing 15 to 22 member rings to constrain Val-Tyr derivatives (Scheme 2) [48]. Macrocyclic ethers **14** were readily obtained by intramolecular

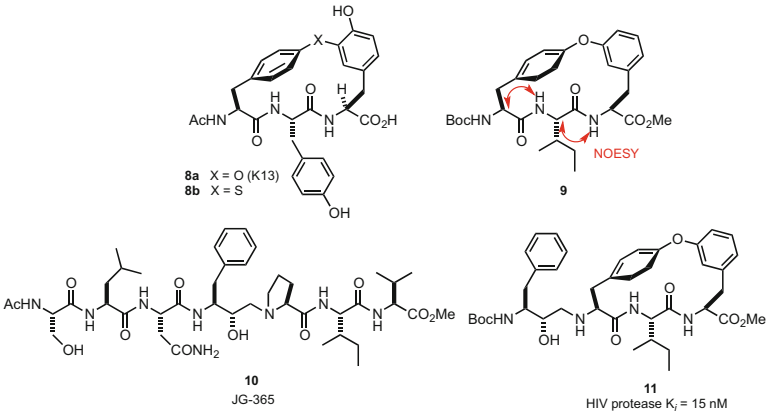

Fig. 4 Biphenyl ether β-strand macrocycles derived from K13

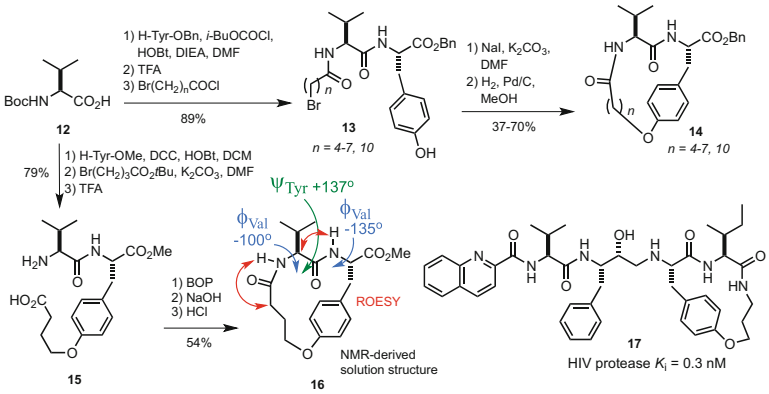

Scheme 2 Synthesis of phenyl ether-linked N- and C-terminal macrocycles and conformational analysis of **16** by NMR spectroscopy

alkylation of the Tyr phenolates derived from bromides **13**. The synthesis of the more constrained derivative **16** required lactam cyclization in the final step. Each of these macrocycles exhibited unusually large NH–CHα coupling constants in the ^{1}H NMR spectra in various solvents, as well as strong $CH\alpha_i \rightarrow NH_{i+1}$ ROESY correlations typical of an extended conformation. In contrast, $NH_i \rightarrow NH_{i+1}$ correlations that are often observed in turn conformations were either weak or absent. Employing distance constraints that were obtained from NMR spectroscopy (in H_2O/D_2O) to calculate 3D structures for **16**, the average backbone dihedral angles were found to be in close agreement with β-sheet values ($\phi_{Val} = -100°$, $\psi_{Val} = 137°$, $\phi_{Tyr} = -135°$). Macrocyclic tethers such as **16** may thus pre-organize short peptides to stabilize β-strand conformations in aqueous solution. A related phenyl ether macrocycle was later employed in the synthesis of potent peptidomimetic HIV-protease inhibitors exemplified by **17** [49, 50].

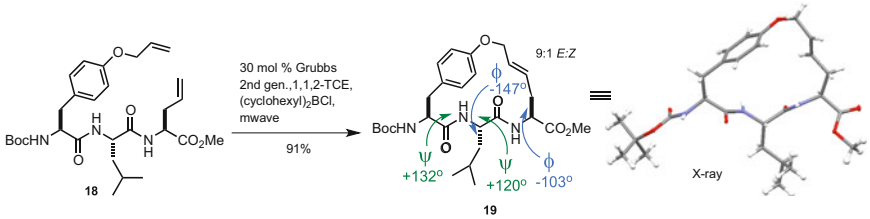

Scheme 3 RCM-based synthesis and X-ray structure of a phenyl allyl ether β-strand macrocycle

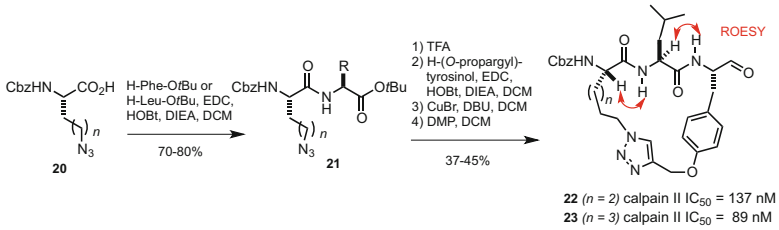

Scheme 4 Synthesis, NMR data, and biological activity of calpain II inhibitors constrained by a phenyl ether triazole linker

Abell and coworkers explored the conformation of β-strand peptides featuring an alkene tether that was introduced through ring-closing metathesis (RCM) [51]. Macrocyclization of substrates such as allyl ether **18** proceeded in excellent yield and *E*:*Z* selectivity in the presence of Grubbs 2nd generation catalyst and a Lewis acid additive (Scheme 3). In the X-ray crystal structure of ether **19**, the peptide backbone dihedral angles were consistent with β-strand geometry.

Novel triazole-containing aryl ether macrocycles were later developed using ω-azido α-amino acids and *O*-propargyl tyrosine as building blocks (Scheme 4) [52]. Employing copper-catalyzed azide alkyne cycloaddition (CuAAC) reactions to form the macrocycles, a series of calpain II inhibitors were prepared in solution. Conformational analysis of potent inhibitors **22** and **23** by ^{1}H NMR spectroscopy in DMSO-d_6 revealed larger NH–CHα coupling constants and stronger $CH\alpha_i \rightarrow NH_{i+1}$ ROESY correlations relative to acyclic and unstructured controls. Variable temperature ^{1}H NMR experiments in DMF-d_7 also showed the NH proton chemical shifts to vary significantly with changes in temperature, indicative of the amides being exposed to solvent and not involved in intramolecular hydrogen bonds typical of turn conformations. Constrained ethers **22** and **23** were more potent inhibitors of calpain II than peptidomimetic analogs that did not adopt stable β-strand conformations in solution [53].

A related set of triazole-tethered macrocycles lacking a phenyl ether bridge was also developed (Scheme 5) [54]. Starting from appropriately protected alkynyl and azido amino acid building blocks, triazoles (e.g., **27**) were synthesized using CuAAC chemistry. The triazole macrocycles were observed to have large NH_i–

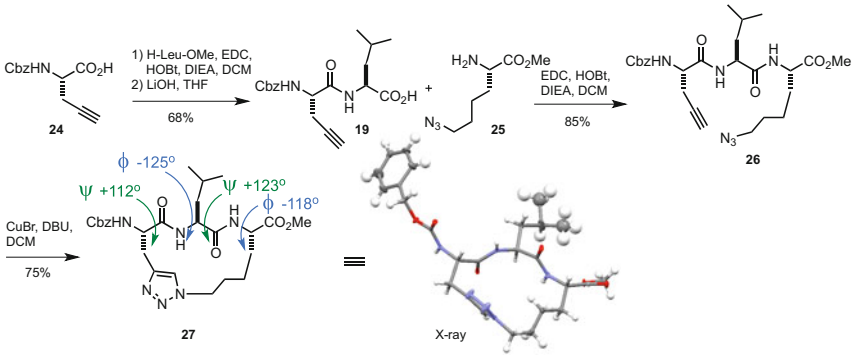

Scheme 5 Synthesis and X-ray structure of 15-member triazole macrocycle **27** exhibiting β-strand conformation

CHα_i ^{1}H NMR coupling constants and strong CH$\alpha_i \rightarrow$ NH$_{i+1}$ ROESY correlations indicative of a β-strand conformation, similar to macrocycles **22** and **23**, albeit their amide NH protons exhibited slow deuterium exchange in DMSO/CD_3OD supporting involvement in strong hydrogen-bond interactions. Crystallographic analysis of triazole **27** revealed β-sheet-like self-association, as well as cylindrical assemblies resulting from macrocycle stacking. The endocyclic ϕ and ψ dihedral angles in the solid-state structure of triazole **27** were in excellent agreement with those typically found in parallel β-sheet structures.

2.3 *Azabicycloalkanes*

Similar to the monocyclic lactams discussed above, azabicycloalkanes have been widely utilized to promote turn conformations. Their synthesis and incorporation into biologically active peptidomimetics has been the subject of numerous reviews [10, 16–18, 55–58]. The use of azabicycloalkane dipeptide surrogates for β-strand stabilization remains uncommon, due in part to a more acute ϕ_{i+1} dihedral angle as depicted in generalized bicycle **28** (Fig. 5). Though few β-strand azabicycloalkane scaffolds have been the subjects of conformational analysis in the absence of an enzyme target, a select number have been proposed as backbone constraints for conformationally extended protease inhibitors. For example, conformational searches carried out by Kahn and coworkers on azabicycloalkane scaffolds **29** and **30** yielded low energy structures that overlaid closely with an idealized antiparallel β-sheet dipeptide [59]. In these cases, mimicry of the β-strand ψ_i torsion was made possible by the D-amino acid-derived stereochemistry at the indicated carbons (Fig. 5).

Recently, Del Valle and coworkers investigated the ability of various novel azabicycloalkanes to mimic extended dipeptide conformations [60]. Their design

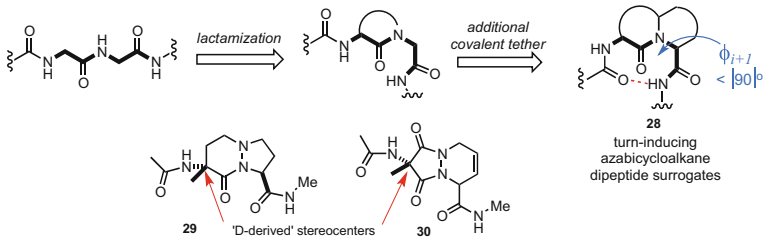

Fig. 5 Design of azabicycloalkane turn mimetics and examples of related β-strand-inducing dipeptide surrogates

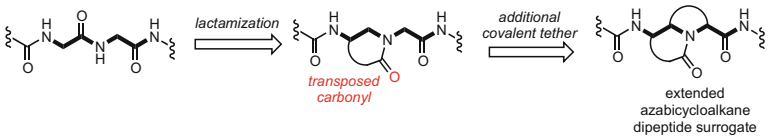

Fig. 6 Design of CO-transposed azabicycloalkanes as conformationally extended dipeptide surrogates

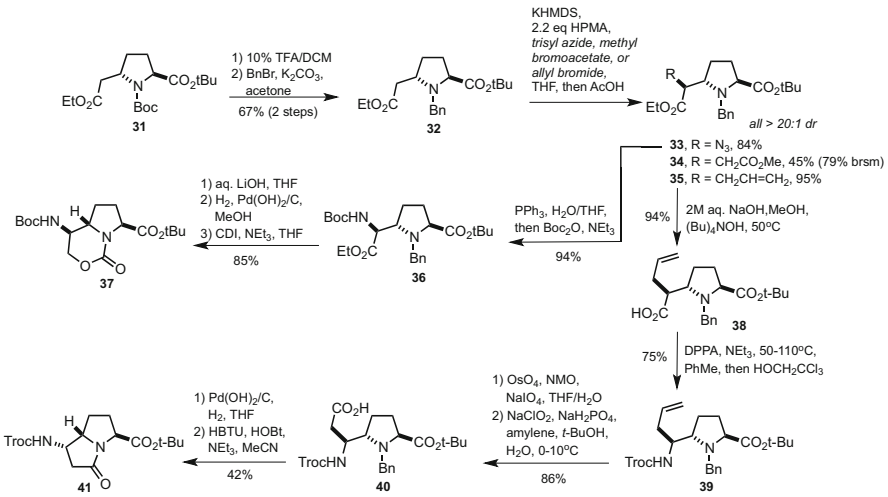

Scheme 6 Diastereoselective synthesis of conformationally extended azabicycloalkane scaffolds

incorporated two covalent backbone tethers and transposition of the carbonyl group to maintain the sp_2 hybridization of the backbone N_{i+1} nitrogen (Fig. 6).

A series of extended dipeptide surrogates including hexahydro-1*H*-pyrrolo [1,2-*c*][1,3]oxazin-1-one **37** and tetrahydro-1*H*-pyrrolizin-3(2*H*)-one **41** were prepared from readily available substituted proline derivative **31** (Scheme 6). In each case, regioselective formation of an ester enolate from **32** was followed by

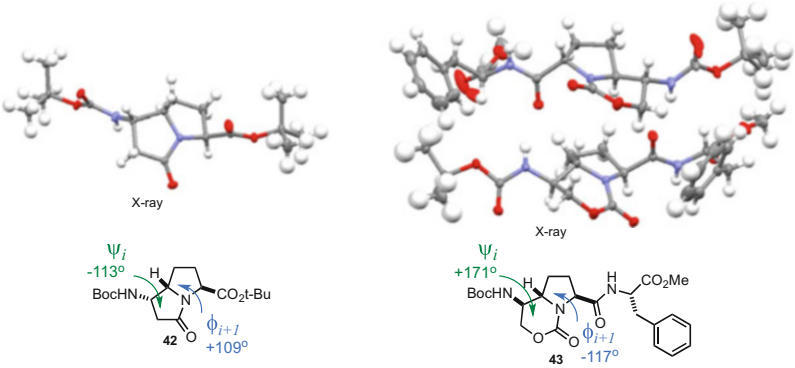

Fig. 7 X-ray crystal structures of tetrahydro-1*H*-pyrrolizin-3(2*H*)-one and hexahydro-1*H*-pyrrolo[1,2-*c*][1,3]oxazin-1-one dipeptide surrogates

diastereoselective alkylation to provide functionalized 5-substituted prolines **33**–**35**. Carbamate **36** was prepared by reduction of azide **33** and Boc protection of the resulting amine. Chemoselective reduction of the ethyl ester, hydrogenolytic cleavage of the *N*-benzyl group, and treatment of the amino alcohol with carbonyldiimidazole afforded cyclic urethane **37** in high yield. Pyrrolizidinone **41** was obtained by oxidative cleavage of alkene **39**, oxidation to the carboxylic acid, and subsequent lactamization.

The ability of scaffolds based on bicycles **37** and **41** to mimic conformationally extended dipeptides was evaluated using X-ray crystallography (Fig. 7). Dihedral angles were labeled in structures **42** and **43** in relation to their corresponding native backbone torsion angles, because of the transposition of the main chain carbonyl groups. The crystal structure of pyrrolizidinone **42** retained the "sawtooth" backbone geometry of a β-strand. Measurement of the putative ψ, ω, and ϕ torsions in the solid state revealed values of −113°, 157°, and 109°, respectively. These values are in good agreement with the ideal values of a parallel β-sheet peptide. The more acute ω angle (157° vs. 180° in an ideal *trans*-amide bond) leads to a slight shortening of the terminal N-to-C dipeptide distance from the 5.9 Å typical of a β-sheet to 5.8 Å in sheet mimic **42**.

Oxazinone **37** was converted into tripeptide mimic **43**, crystallized, and analyzed in the solid state. The observed backbone conformation (ψ_1, ω, and ϕ_2 dihedral angles equal to 171°, 149°, and 117°, respectively) deviated from an ideal β-sheet peptide; however, the bicyclic scaffold adopted an extended conformation in the solid state, featuring a head-to-tail dimer with two intermolecular hydrogen bonds. Moreover, the terminal N-to-C dipeptide distance in **43** (5.9 Å) matched that observed in an ideal extended dipeptide.

The hexahydro-1*H*-pyrrolo[1,2-*c*][1,3]oxazin-1-one scaffold above has been incorporated into peptidomimetic inhibitors of the kinase Akt, the hyperactivation of which is linked strongly to oncogenesis. Replacement of a central dipeptide motif within an Akt peptide substrate led to the discovery of peptidomimetic

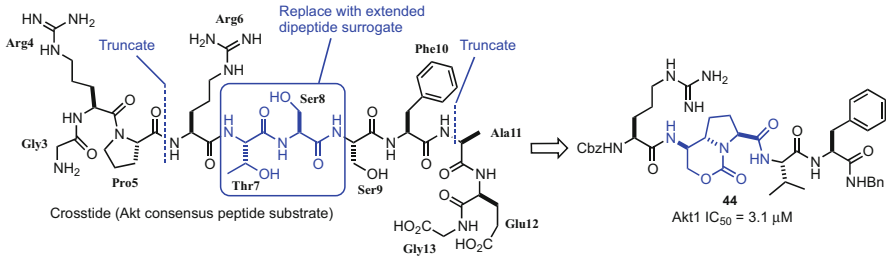

Fig. 8 Development of substrate mimetic inhibitors of Akt1 based on a hexahydro-1*H*-pyrrolo [1,2-*c*][1,3]oxazin-1-one scaffold

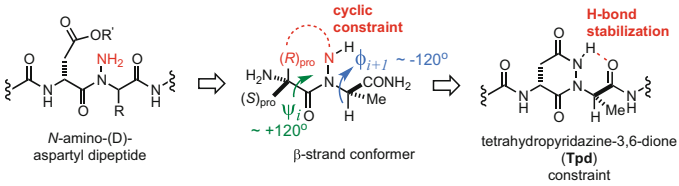

Fig. 9 Design of tetrahydropyridazinedione (Tpd)-constrained peptides as hydrogen bond stabilized β-strand mimics

inhibitors with low micromolar potency (Fig. 8) [61]. The most active analog, substrate mimic **44,** inhibited Akt phosphorylation of a consensus peptide substrate with an IC_{50} value of 3.1 μM in vitro.

2.4 Tetrahydropyridazinediones

In pursuit of minimalist β-strand-stabilizing residues, Del Valle and coworkers designed a readily accessible peptide orthotic that could impart rigidity through both covalent tethering and internal hydrogen bonding [62]. The targeted tetrahydropyridazine-3,6-dione (Tpd) scaffold was derived from a backbone-aminated D-aspartyl dipeptide precursor (Fig. 9). The Tpd scaffold enforces a *trans*-amide configuration and restricts the ψ_i torsion angle value between 120 and 180°, due to $C\alpha_i$–N_{i+1} tethering of the D-Asp *i*-residue. A potential intramolecular hydrogen bond between the azodicarbonyl NH and CO_{i+1} is designed to constrain the ϕ_{i+1} dihedral angle within the β-strand range and sets this scaffold apart from the Freidinger–Veber lactam and related structures, which have been used primarily as β-turn mimics within host peptides (see above).

The synthesis of Tpd peptidomimetics required efficient access to chiral α-hydrazino acid building blocks for incorporation on solid phase (Scheme 7). The requisite acids **47** were prepared starting from α-hydroxy esters **46** that were made by diazotization of the corresponding D-amino acids [63] and esterified.

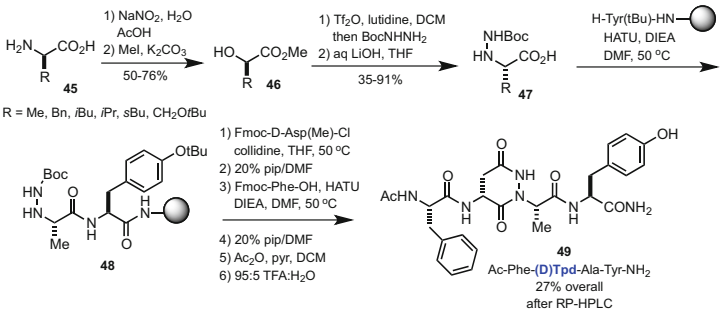

Scheme 7 Solid-phase synthesis of Tpd peptidomimetics from enantiomerically pure α-hydrazino acids

Trifluoromethylsulfonation and displacement of the resulting triflate installed the *t*-butyl carbazate with inversion of stereochemistry. Subsequent saponification gave acids **47**. Building on the observation that the α-amine of *N*-β-(Boc)-α-hydrazino esters was remarkably resistant to acylation under a variety of standard coupling conditions, a chemoselective C-terminal amidation was explored. Acid **47** was coupled to resin-bound amino amides in the presence of HATU to provide immobilized carbazate **48** without any detectable N-terminal acylation. Alanine-derived carbazate **48** was acylated with β-methyl *N*-(Fmoc)aspartate α-acid chloride. The peptide was elongated using standard protocols for solid-phase synthesis with Fmoc amino acids and cleaved from the resin. During cleavage with TFA, the Boc group was removed from the hydrazide, and cyclization occurred to provide Tpd-containing tetrapeptide mimic **49** in good overall yield after HPLC purification.

The scope of this methodology was demonstrated through the assembly of diverse Tpd peptidomimetics on solid support (Fig. 10). The described protocol tolerated both D and L cyclic subunits, and the Tpd ring closure was not adversely affected by the presence of other electrophilic or nucleophilic side chains within the peptides. In addition, hindered α-hydrazino acids such as *N*-amino-Ile, *N*-amino-Val, and *N*-amino-Leu were readily incorporated. Analysis of the crude HPLC traces for various Tpd peptidomimetics revealed good purity with the principle byproduct identified as the acyclic trifluoroacetylated *N*-amino peptides.

Preliminary conformational analysis of D-Tpd peptidomimetics indicated their potential for stabilizing β-strand structure (Fig. 11). Comparison of the ^{1}H NMR spectra for D-Tpd and acyclic control peptides **51** and **50** revealed enhanced resolution of the diastereotopic CHβ methylene ring protons from increased rigidity. Moreover, the Gly CHα protons (external to the Tpd ring) in peptide **51** exhibited a larger difference in chemical shift than those of **50**, indicating pronounced restriction of the ϕ_{i+1} torsion angle likely due to an intramolecular hydrogen bond between the Tpd azidocarbonyl NH and glycine carbonyl. X-ray analysis of crystals of dipeptide mimic **52** confirmed the presence of this predicted hydrogen bond in the solid state, despite crystallization from a known hydrogen-bonding solvent.

sequence	isolated yield (%)
Ac-Phe-**(D)Tpd**-Gly-Tyr-NH_2	23
Ac-Phe-**(D)Tpd**-Ala-Tyr-NH_2	27
Ac-Leu-**(D)Tpd**-Ala-Phe-NH_2	21
Ac-Leu-**(L)Tpd**-Ala-Phe-NH_2	34
Ac-Leu-**(D)Tpd**-Phe-Phe-NH_2	18
Ac-Leu-**(D)Tpd**-Ile-Phe-NH_2	26
Ac-Leu-**(D)Tpd**-Leu-Phe-NH_2	42
Ac-Leu-**(D)Tpd**-Val-Phe-NH_2	30
Ac-Leu-**(D)Tpd**-Ser-Phe-NH_2	3
Ac-Ser-Leu-**(D)Tpd**-Ala-Tyr-NH_2	21
Ac-Ile-**(D)Tpd**-Ala-Ser-Phe-NH_2	16
H-Gly-Leu-**(D)Tpd**-Ala-Ser-Phe-NH_2	18
H-Gly-Leu-**(D)Tpd**-Phe-Ser-Ala-NH_2	13
H-Gly-Leu-**(L)Tpd**-Phe-Ser-Ala-NH_2	13
Ac-Val-Lys-Asn-Pro-Asp-Gly-**(D)Tpd**-Ala-Thr-NH_2	22

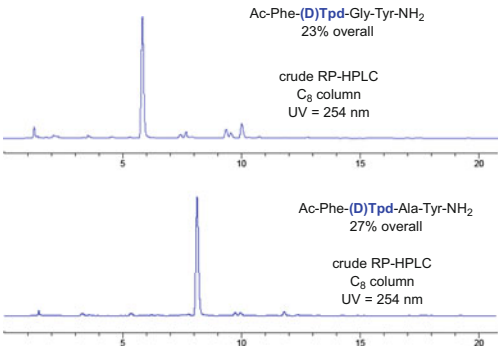

Fig. 10 Tpd peptides prepared on solid support and crude purities for selected examples

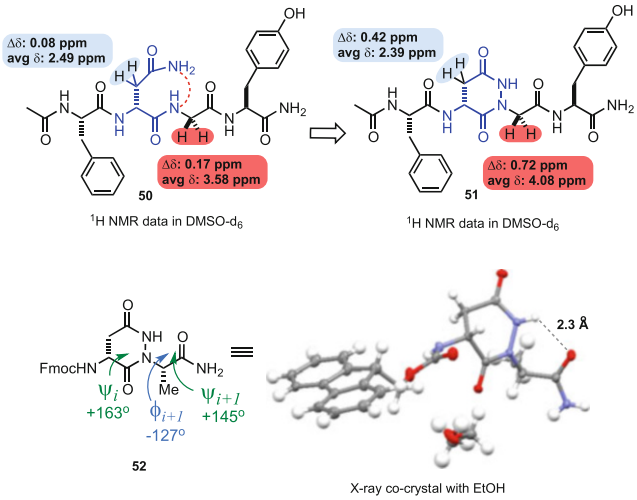

Fig. 11 Effect of Tpd constraint on diastereotopic chemical shifts and X-ray structure of dipeptide mimic **52** exhibiting NβH-CO_{Ala} hydrogen bond

3 Heterocyclic Backbone Prosthetics

Prosthetic scaffolds deviate generally from native backbone conformations owing to their non-peptidic structures. Several conformationally extended scaffolds that effectively promote β-sheet-like folding have however been achieved through careful design considerations for the incorporation of hydrogen-bond donor and acceptor elements, the mimicry of side chains, and the isosteric replacement of

backbone amides. Below are selected examples of heterocyclic motifs suitable for incorporation into host peptides. Their ability to enforce extended peptide conformations external to the scaffold itself has been investigated in model systems using both NMR spectroscopy and X-ray crystallography.

3.1 Pyrrolinones

In 1992, the laboratories of Hirschmann and Smith reported the development of a new class of β-strand mimic based on an oligomeric pyrrolinone scaffold (Fig. 12) [64, 65]. This marked the first comprehensive effort to mimic peptide β-strand and β-sheet structure using an entirely non-peptidic backbone. A 3,5-linked pyrrolinone motif harboring transposed backbone nitrogen was designed to retain key backbone hydrogen-bonding elements and to display side-chain functionalities in the desired three-dimensional arrangement. The putative ϕ dihedral angles within these rigidified structures were further constrained by intramolecular hydrogen bonds that were predicted using Monte Carlo conformational searches. Detailed crystallographic analysis of polypyrrolinones exemplified by **53** indicated solid-state conformations that closely overlaid with β-sheet peptides [19]. A number of these oligomeric structures exhibited β-sheet-like self-association in which the displaced backbone NH was engaged in H-bonding interactions with adjacent strands [65].

Diverse 3,5-linked polypyrrolinones have found broad utility in the study of self-assembling superstructures and in the development of non-peptide inhibitors of HIV protease, somatostatin receptors, and major histocompatibility complex proteins [66–73]. Although these oligomeric motifs were originally developed as fully artificial secondary structure mimics (foldameric repeats of unnatural subunits), their use as heterocyclic surrogates within β-strand host peptides was demonstrated in the pursuit of potent ligands of the major histocompatibility complex, class II, HLA-DR1 [67, 68]. The targeted peptidomimetics were composed of a central bis-pyrrolinone subunit as a tetrapeptide replacement. The synthesis of this unnatural backbone prosthetic employed quaternary amino acid derivative **54** as a

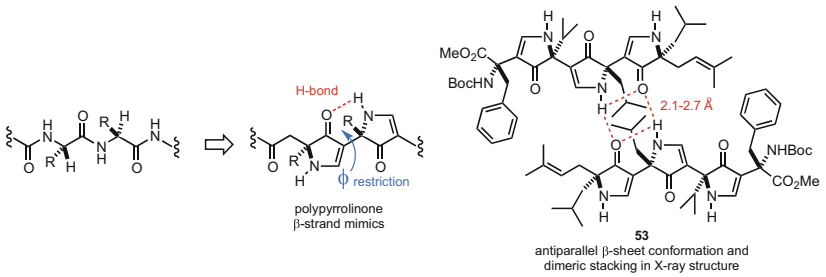

Fig. 12 Design of pyrrolinone-based β-strand mimics and self-association of tetrapeptide mimic **53** confirmed by X-ray analysis

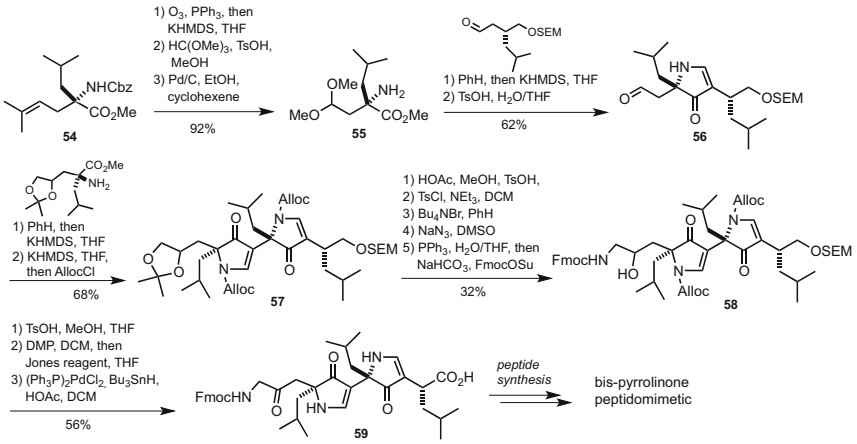

Scheme 8 Synthesis and application of bis-pyrrolinone tetrapeptide mimic **59**

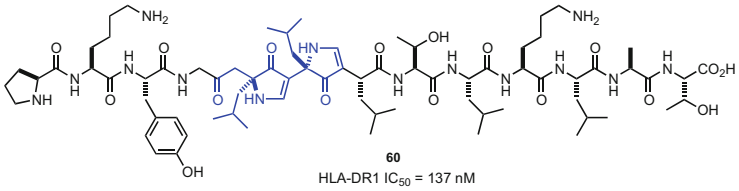

Fig. 13 Bis-pyrrolinone **60** exhibited potent activity against the class II major histocompatibility protein HLA-DR1

starting material (Scheme 8). Ozonolysis and acetal protection was then followed by hydrogenolytic removal of the Cbz protection to give amino acetal **55**. Schiff base formation with a chiral aldehyde synthon, base-promoted cyclization, and acetal hydrolysis gave pyrrolinone aldehyde **56**, which was employed in a second pyrrolinone formation sequence to afford bis-pyrrolinone **57** after Alloc protection. An N-terminal amine was introduced as an azide, which was reduced and protected to *N*-(Fmoc)amino alcohol **58**. Finally, SEM deprotection, oxidation of the alcohols, and removal of the Alloc groups provided keto acid **59** as a building block suitable for incorporation into host peptides.

Bis-pyrrolinone **60** (Fig. 13), a tridecapeptide mimic corresponding to a parent HLA-DR1 ligand, was assembled from **59** by conventional solid-phase peptide synthesis on Wang resin and displayed an in vitro IC_{50} of 137 nM against HLA-DR1 in a competitive displacement assay [67, 68]. The observed activity was comparable to the parent tridecapeptide ligand, which is known to bind HLA-DR1 in a β-strand-like conformation.

3.2 Dihydropyridinones and Dihydropyrazinones

Dihydropyridinone subunits have been shown to stabilize β-sheet association and folding using a combination of NMR and circular dichroism (CD) spectroscopy by Bartlett and coworkers [74–76]. The dihydropyridinone residue ("Ach") was designed as an amino acid replacement that restricts ψ and ϕ torsion angles within a cyclic enamide structure (Fig. 14). Transposition of the backbone carbonyl group results in a strand that retains hydrogen-bonding capacity on one edge but is incapable of forming complementary hydrogen bonds on the modified edge. Similar to the macrocycle, lactam, and tetrahydropyridazinedione designs described above, the dihydropyridinone peptides (known as @-tides) offer promise as β-sheet "breakers" capable of interrupting β-sheet propagation.

An optimized solution-phase synthesis of @-tides relied on the Lewis acid-promoted addition–elimination of α-amino esters onto 5-hydroxydihydropyridinone **62** (Scheme 9) [77]. Removal of the Alloc group and coupling of the dihydropyridinone nitrogen to an Alloc-protected amino acid set the stage for further iterations, as illustrated in the preparation of tetrapeptide mimic **64**. Moreover, the protocol was successfully adapted to the solid-phase synthesis of @-tides such as pentapeptide mimic **65** on Merrifield resin.

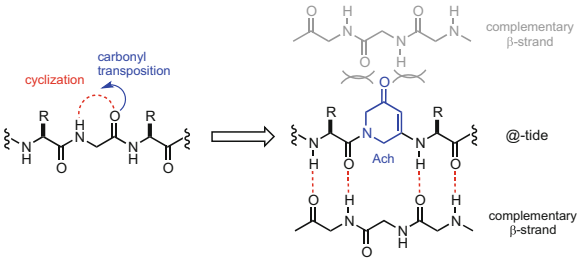

Fig. 14 Design of @-tides which exhibit self-limiting β-strand dimerization

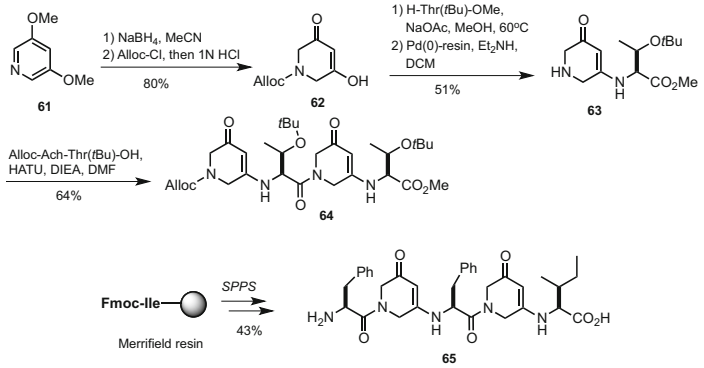

Scheme 9 Solution and solid-phase synthesis of @-tide β-strand mimics

The propensity for @-tides to form self-limiting dimers was examined, because they possess hydrogen-bond donor and acceptor groups on only one backbone edge (Fig. 15) [74]. In solution, model @-tides such as amide **66** exhibited a greater concentration dependence of their backbone amine proton NMR chemical shifts relative to acyclic control peptides. This concentration dependence was used to derive dissociation constants that correlated with increased constraint in the oligomeric Ach-containing peptidomimetics. The presence of extensive interstrand as well as sequential $CH\alpha_i \rightarrow NH_{i+1}$ NOE correlations in 1% $CD_3OD/CDCl_3$ further supported the self-association of @-tide strands into dimeric antiparallel β-sheet-like structures. Incorporation of a single Ach residue into a short β-hairpin model system likewise stabilized β-sheet folding relative to control peptides as evidenced by NMR and circular dichroism (CD) spectroscopy in $CD_3OD/CDCl_3$ of @-tides such as hairpin mimic **67** [76]. The distinct CD signatures of the vinylogous amide within the @-tide Ach residue was sensitive to solution conformation and degree of β-sheet-like association [75] and served as a diagnostic of the folding propensity of various @-tide β-hairpin mimics [77].

In an effort to maintain side-chain functionality on both faces of the @-tide strand, Bartlett and coworkers later developed a novel dihydropyrazinone scaffold that was derived synthetically from amino acid precursors [78]. An example of this modified "aza"-@-tide subunit was prepared via intramolecular cyclization of leucine thioamide **69** (Scheme 10). Methylation activated **69** as the corresponding thioimidate, which underwent an addition–elimination reaction with H-Val-O*t*Bu and cyclization to furnish aza-@-tide subunit **70**. Elongation under standard peptide synthesis conditions provided access to longer aza-@-tides.

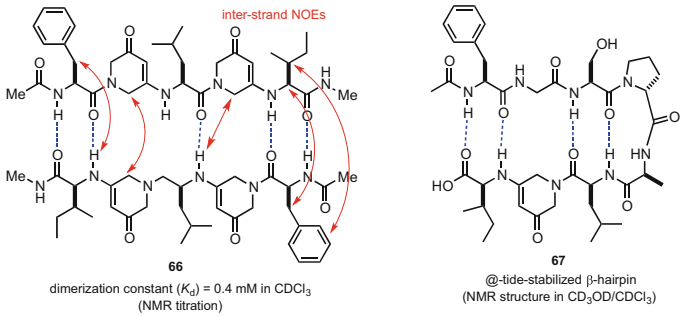

Fig. 15 β-Sheet-like association and folding of @-tides observed by NMR spectroscopy

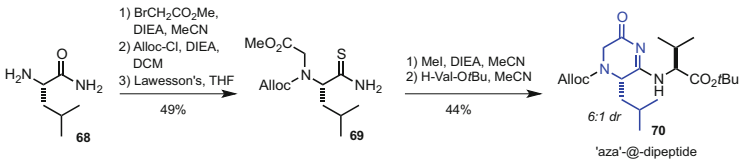

Scheme 10 Synthesis of aza-@-tide **70** from α-amino amide **68**

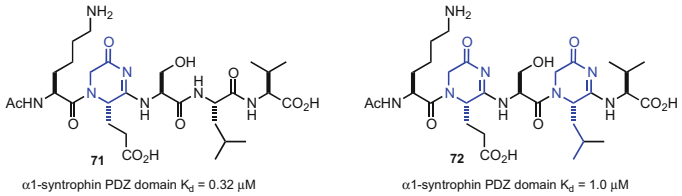

Fig. 16 Aza-@-tide β-strand mimics as inhibitors of the α1-syntrophin PDZ domain

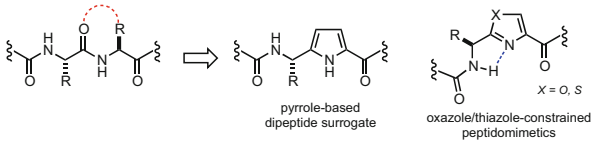

Fig. 17 Pyrrole surrogate of extended peptide backbone and oxazole/thiazole peptidomimetics predisposed to form intramolecular hydrogen bonds

Aza-@-tides **71** and **72** were used to disrupt protein–protein interactions as constrained peptide substrates of PDZ domains [78]. A pentapeptide inhibitor of the PDZ domain from α1-syntrophin (Ac-KESLV-OH) was used as the parent structure for aza-@-tide subunit scanning, because it was known to bind in an extended conformation (Fig. 16). The constrained β-strand mimics **71** and **72** bound the PDZ domain target with higher in vitro affinities than the parent peptide.

3.3 Pyrroles

The use of pyrroles as β-strand inducers was initially reported for the design of artificial β-sheet receptors [79–81]. A guanidinocarbonylpyrrole residue was found to promote β-strand association with selected natural substrates when attached to the peptide C-terminus. 5-Aminomethyl pyrrole-2-carboxylates were synthesized and employed as dipeptide surrogates to stabilize β-hairpin model peptides [82]. In contrast to more commonly utilized oxazole and thiazole isosteres that tend to be hydrogen-bond acceptors predisposed to adopt peptide backbone turn conformations [83], pyrrole derivatives possess a hydrogen-bond donor that may mimic the amide NH to favor β-strand geometry (Fig. 17).

For use as an extended dipeptide surrogate, methoxypyrrole amino acid (MOPA) **75** was synthesized from 3-hydroxy-pyrrole-2-carboxylate **73** by *O*-methylation and Vilsmeier–Haack formylation, followed by a two-step reductive amination (Scheme 11). Hydrolysis of ester **75** and carboxylate activation gave hydroxybenzotriazole ester **76**, which was incorporated as a dipeptide surrogate into a short turn-promoting sequence using standard solution-phase peptide synthesis. In spite

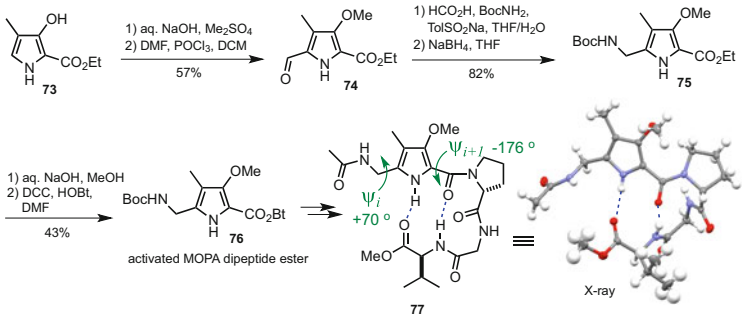

Scheme 11 Synthesis and X-ray crystal structure of MOPA-based β-hairpin peptidomimetic **77**

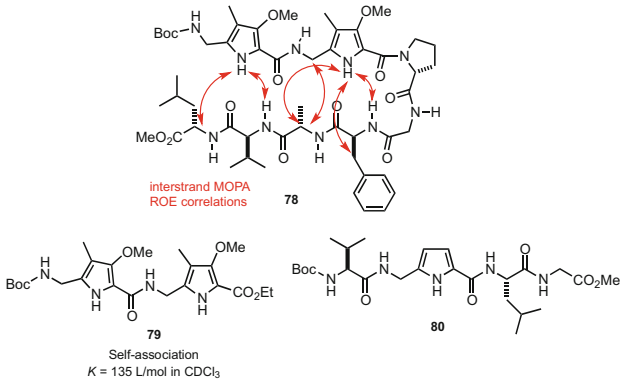

Fig. 18 β-Sheet folding and self-association of 5-aminomethylpyrrole-2-carboxylate peptidomimetics

of its small size, tetrapeptide mimic **77** adopted a β-hairpin fold that was observed by X-ray crystallographic analysis. Although the ψ_i, (70°) and ϕ_{i+1} (−176°) torsion angles deviated from ideal β-sheet peptide values, the MOPA residue pyrrole NH engaged in complementary interstrand hydrogen bonds in the solid state.

The combination of two sequential MOPA subunits and a D-Pro-Gly turn motif in model decapeptide **78** was found to stabilize a β-hairpin fold exhibiting various interstrand ROESY correlations in $CDCl_3$ (Fig. 18). Moreover, MOPA tetrapeptide mimic **79** self-associated in $CDCl_3$ with a binding constant of 135 L/mol, as determined by NMR spectroscopy during dilution experiments. Similarly, Chakraborty and coworkers synthesized 5-aminomethylpyrrole-2-carboxylates that were used as Gly-Ala mimics in short peptides (e.g., **80**), which were observed by 2D NOE experiments to adopt an extended conformation in DMSO-d_6 [84].

3.4 Imidazopyridines

Imidazo[1,2-*a*]pyridines (IP) have been investigated as heteroaromatic replacements in conformationally extended dipeptides by Del Valle and coworkers [85]. The IP subunit was designed to display a native side-chain pharmacophore and to retain hydrogen-bonding capacity on one edge of the putative backbone (Fig. 19). Overlap of the backbone hydrogen-bond acceptor groups was observed in the overlay of MM2 energy-minimized IP tetrapeptidomimetic and the antiparallel β-sheet conformer of tetra-alanine. Similar to other aromatic prosthetics, the IP surrogate possesses a planar structure that offers better mimicry of the fully extended β-strand.

Diverse substituted β-keto esters **81** were condensed with (*N*-Cbz)-diamino pyridine to provide access to protected IP subunits **82** bearing native residue side chains (Scheme 12). The acid and amine moieties of unprotected IP intermediate **83** were chemoselectively coupled, respectively, to protected amino acids to provide tetrapeptide mimic **84**. Moreover, oligomeric IP structures, such as **86**, were prepared using *N*-Cbz IP units.

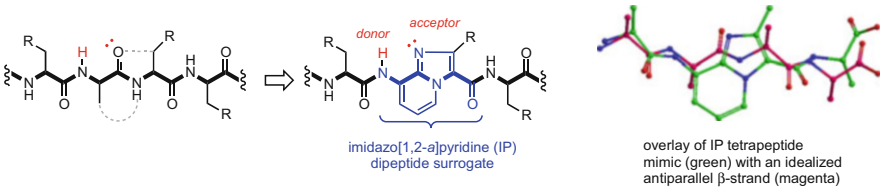

Fig. 19 Substituted imidazopyridines as conformationally extended dipeptide surrogates

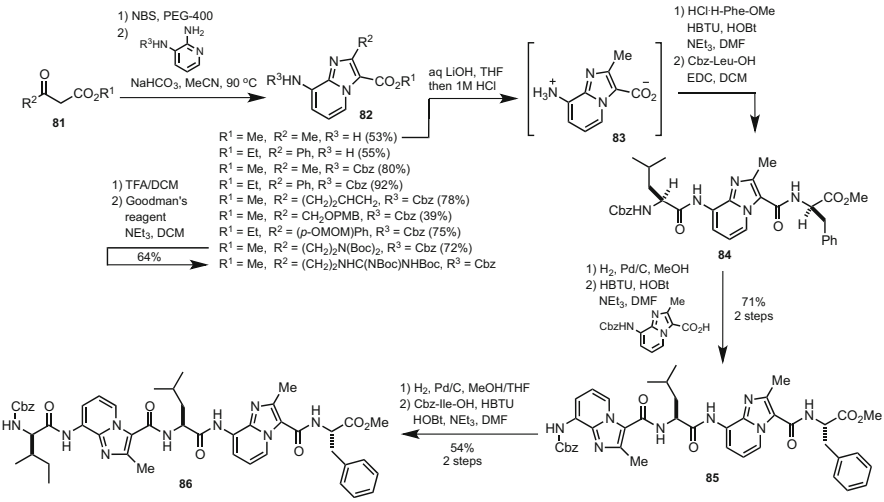

Scheme 12 Synthesis of IP β-strand mimics

The conformational preferences of IP peptides were evaluated by a variety of NMR methods, which demonstrated the absence of rotational isomers (Fig. 20). For example, in the ^{1}H NMR spectrum of IP heptapeptide **86**, the CHα proton chemical shifts for the natural residues (Ile, Leu, and Phe) were indicative of extended β-strand structure and 0.4–0.8 ppm downfield of their expected values in a random coil peptide. The backbone ϕ torsion angles derived from NH_i–$CH\alpha_i$ coupling constants within **86** were in agreement with a β-strand conformer. In addition, ROESY correlations between the IP methyl and neighboring backbone NH protons indicated the presence of amide *trans* isomers throughout the peptidomimetic. Prominent $CH\alpha_i \rightarrow NH_{i+1}$ ROESY correlations were also observed that were typical of an extended peptide conformer.

Similar to the hexahydro-1*H*-pyrrolo[1,2-*c*][1,3]oxazin-1-one scaffold described above, the IP subunit was incorporated into Akt1 inhibitors in an effort to mimic the extended conformation of the native substrate (Fig. 21) [86]. A structure-activity-relationship campaign led to the identification of IP mimic **87**, which inhibited the activity of Akt isoforms 1–3 with in vitro IC_{50} values of 0.64, 0.76, and 0.13 μM, respectively. Computational analysis of **87** and comparison with the crystal structure of a GSK3β peptide substrate bound to Akt1 revealed good overlap with the side chain geometries in the native ligand.

proton	δ (obs)	δ (random coil)
$Ile_{CH\alpha}$	4.34 ppm	3.95 ppm
$Leu_{CH\alpha}$	5.00 ppm	4.17 ppm
$Phe_{CH\alpha}$	5.10 ppm	4.66 ppm

proton	*J* value	ϕ angle (calc)	δΔ/δT
Ile_{NH}	8.9 Hz	-100°/-140°	5.6 ppb/K
Leu_{NH}	8.1 Hz	-92°/-148°	4.4 ppb/K
Phe_{NH}	7.3 Hz	-85°/-155°	7.2 ppb/K
$IP1_{NH}$	-	-	6.2 ppb/K
$IP2_{NH}$	-	-	6.4 ppb/K

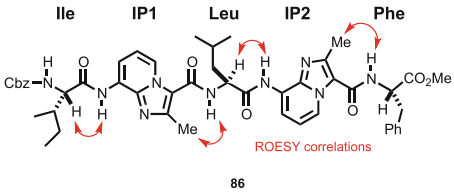

Fig. 20 Conformational analysis of a di-IP β-strand mimic **86** by NMR spectroscopy

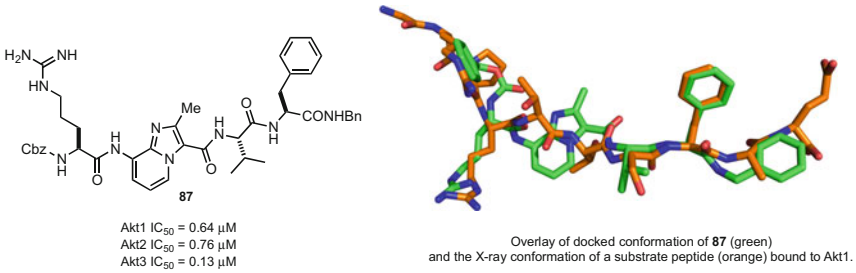

Fig. 21 A conformationally extended IP-based substrate mimetic inhibitor of Akt1-3

4 Conclusions

The importance of β-strand and β-sheet structures in recognition events of biological processes has prompted the development of various approaches toward their mimicry. Successful designs of mimics that interact with specific target proteins have motivated further studies of the conformational impact of specific peptide modifications. The examples presented here are representative of heterocyclic peptide surrogates capable of pre-organizing host structures into extended conformations. Building on preliminary conformational analyses, these motifs offer promise as promoters of β-sheet structure and as bioactive protein mimics. To complement the existing array of peptide surrogates, structurally well-characterized and broadly useful approaches are still needed for β-strand stabilization. Application of small extended peptide surrogates as "minimalist" β-strand mimics may be particularly useful for drug discovery efforts to target protein–protein interfaces. In-depth conformational and biological studies necessitate development of efficient synthetic routes toward β-strand constraints amenable to peptide scanning applications. Heterocyclic mimics of β-strand interactions will thus continue to play a central role in probing relevant structures for applications in peptide science, chemical biology, and medicinal chemistry.

References

1. Watkins AM, Arora PS (2014) ACS Chem Biol 9:1747
2. Tateno M, Yamasaki K, Amano N, Kakinuma J, Koike H, Allen MD, Suzuki M (1997) Biopolymers 44:335
3. Dou Y, Baisnee P-F, Pollastri G, Pecout Y, Nowick J, Baldi P (2004) Bioinformatics 20:2767
4. Tyndall JDA, Nall T, Fairlie DP (2005) Chem Rev 105:973
5. Yang J, Cron P, Good VM, Thompson V, Hemmings BA, Barford D (2002) Nat Struct Mol Biol 9:940
6. Sawyer TK, Bohacek RS, Dalgarno DC, Eyermann CJ, Kawahata N, Metcalf CA, Shakespeare WC, Sundaramoorthi R, Wang Y, Yang MG (2002) Mini Rev Med Chem 2:475
7. Townsend A, Bodmer H (1989) Annu Rev Immunol 7:601
8. Qian Y, Blaskovich MA, Saleem M, Seong CM, Wathen SP, Hamilton AD, Sebti SM (1994) J Biol Chem 269:12410
9. Venkatraman J, Shankaramma SC, Balaram P (2001) Chem Rev 101:3131
10. Gillespie P, Cicariello J, Olson GL (1997) Pept Sci 43:191
11. Loughlin WA, Tyndall JDA, Glenn MP, Fairlie DP (2004) Chem Rev 104:6085
12. Smith CK, Regan L (1997) Acc Chem Res 30:153
13. Gellman SH (1998) Curr Opin Chem Biol 2:717
14. Fuller AA, Du D, Liu F, Davoren JE, Bhabha G, Kroon G, Case DA, Dyson HJ, Powers ET, Wipf P, Gruebele M, Kelly JW (2009) Proc Natl Acad Sci 106:11067
15. Robinson JA (2008) Acc Chem Res 41:1278
16. Cluzeau J, Lubell WD (2005) Pept Sci 80:98
17. Halab L, Gosselin F, Lubell WD (2000) Pept Sci 55:101
18. Hanessian S, McNaughtonSmith G, Lombart HG, Lubell WD (1997) Tetrahedron 53:12789

19. Smith AB, Guzman MC, Sprengeler PA, Keenan TP, Holcomb RC, Wood JL, Carroll PJ, Hirschmann R (1994) J Am Chem Soc 116:9947
20. Angelo NG, Arora PS (2005) J Am Chem Soc 127:17134
21. Wyrembak PN, Hamilton AD (2009) J Am Chem Soc 131:4566
22. Jamieson AG, Russell D, Hamilton AD (2012) Chem Commun 48:3709
23. Ko E, Liu J, Perez LM, Lu G, Schaefer A, Burgess K (2010) J Am Chem Soc 133:462
24. Raghuraman A, Ko E, Perez LM, Ioerger TR, Burgess K (2011) J Am Chem Soc 133:12350
25. Schafmeister CE, Po J, Verdine GL (2000) J Am Chem Soc 122:5891
26. Chapman RN, Dimartino G, Arora PS (2004) J Am Chem Soc 126:12252
27. Henchey LK, Jochim AL, Arora PS (2008) Curr Opin Chem Biol 12:692
28. de Araujo AD, Hoang HN, Kok WM, Diness F, Gupta P, Hill TA, Driver RW, Price DA, Liras S, Fairlie DP (2014) Angew Chem Int Ed Engl 53:6965
29. Glenn MP, Fairlie DP (2002) Mini Rev Med Chem 2:433
30. Hill TA, Shepherd NE, Diness F, Fairlie DP (2014) Angew Chem Int Ed Engl 53:13020–13041
31. Freidinger RM, Veber DF, Perlow DS, Brooks JR, Saperstein R (1980) Science 210:656
32. Freidinger RM, Perlow DS, Veber DF (1982) J Org Chem 47:104
33. Perdih A, Kikelj D (2006) Curr Med Chem 13:1525
34. Freidinger RM (2003) J Med Chem 46:5553
35. Aube J (1997) Adv Amino Acid Mimetics Peptidomimetics 1:193
36. Valle G, Crisma M, Toniolo C, Yu K-L, Johnson RL (1989) J Chem Soc Perkin Trans 2:83
37. Thorsett ED, Harris EE, Aster SD, Peterson ER, Snyder JP, Springer JP, Hirshfield J, Tristram EW, Patchett AA, Ulm EH et al (1986) J Med Chem 29:251
38. Thorsett ED, Harris EE, Aster S, Peterson ER, Taub D, Patchett AA, Ulm EH, Vassil TC (1983) Biochem Biophys Res Commun 111:166
39. Marsault E, Peterson ML (2011) J Med Chem 54:1961
40. Gilon C, Halle D, Chorev M, Selincer Z, Byk G (1991) Biopolymers 31:745
41. Tyndall JD, Fairlie DP (2001) Curr Med Chem 8:893
42. Pehere A, Abell A (2013) Macrocyclic protease inhibitors constrained into a beta-strand geometry. In: Chakraborti S, Dhalla NS (eds) Proteases in health and disease, vol 7. Springer, New York, pp 181–192
43. Cabezas E, Satterthwait AC (1999) J Am Chem Soc 121:3862
44. Felix AM, Heimer EP, Wang CT, Lambros TJ, Fournier A, Mowles TF, Maines S, Campbell RM, Wegrzynski BB, Toome V et al (1988) Int J Pept Protein Res 32:441
45. Kase H, Kaneko M, Yamada K (1987) J Antibiot (Tokyo) 40:450
46. Hobbs DW, Clark Still W (1989) Tetrahedron Lett 30:5405
47. Janetka JW, Raman P, Satyshur K, Flentke GR, Rich DH (1997) J Am Chem Soc 119:441
48. Reid RC, Kelso MJ, Scanlon MJ, Fairlie DP (2002) J Am Chem Soc 124:5673
49. Reid RC, Pattenden LK, Tyndall JD, Martin JL, Walsh T, Fairlie DP (2004) J Med Chem 47:1641
50. Glenn MP, Pattenden LK, Reid RC, Tyssen DP, Tyndall JD, Birch CJ, Fairlie DP (2002) J Med Chem 45:371
51. Abell AD, Alexander NA, Aitken SG, Chen H, Coxon JM, Jones MA, McNabb SB, Muscroft-Taylor A (2009) J Org Chem 74:4354
52. Pehere AD, Abell AD (2012) Org Lett 14:1330
53. Pehere AD, Pietsch M, Gutschow M, Neilsen PM, Pedersen DS, Nguyen S, Zvarec O, Sykes MJ, Callen DF, Abell AD (2013) Chemistry 19:7975
54. Pehere AD, Sumby CJ, Abell AD (2013) Org Biomol Chem 11:425
55. Belvisi L, Colombo L, Manzoni L, Potenza D, Scolastico C (2004) Synlett 1449
56. Khashper A, Lubell WD (2014) Org Biomol Chem 12:5052
57. Maison W, Prenzel AHGP (2005) Synthesis 1031
58. Souers AJ, Ellman JA (2001) Tetrahedron 57:7431

59. Ogbu CO, Qabar MN, Boatman PD, Urban J, Meara JP, Ferguson MD, Tulinsky J, Lum C, Babu S, Blaskovich MA, Nakanishi H, Ruan F, Cao B, Minarik R, Little T, Nelson S, Nguyen M, Gall A, Kahn M (1998) Bioorg Med Chem Lett 8:2321
60. Ranatunga S, Liyanage W, Del Valle JR (2010) J Org Chem 75:5113
61. Ranatunga S, Del Valle JR (2011) Bioorgan Med Chem Lett 21:7166
62. Kang CW, Ranatunga S, Sarnowski MP, Del Valle JR (2014) Org Lett 16:5434
63. Deechongkit S, You S-L, Kelly JW (2004) Org Lett 6:497
64. Smith AB III, Keenan TP, Holcomb RC, Sprengeler PA, Guzman MC, Wood JL, Carroll PJ, Hirschmann R (1992) J Am Chem Soc 114:10672
65. Smith AB 3rd, Charnley AK, Hirschmann R (2011) Acc Chem Res 44:180
66. Smith AB III, Hirschmann R, Pasternak A, Yao W, Sprengeler PA, Holloway MK, Kuo LC, Chen Z, Darke PL, Schleif WA (1997) J Med Chem 40:2440
67. Smith AB III, Benowitz AB, Guzman MC, Sprengeler PA, Hirschmann R, Schweiger EJ, Bolin DR, Nagy Z, Campbell RM, Cox DC, Olson GL (1998) J Am Chem Soc 120:12704
68. Smith AB III, Benowitz AB, Sprengeler PA, Barbosa J, Guzman MC, Hirschmann R, Schweiger EJ, Bolin DR, Nagy Z, Campbell RM, Cox DC, Olson GL (1999) J Am Chem Soc 121:9286
69. Smith AB III, Nittoli T, Sprengeler PA, Duan JJW, Liu R-Q, Hirschmann RF (2000) Org Lett 2:3809
70. Smith AB III, Cantin L-D, Pasternak A, Guise-Zawacki L, Yao W, Charnley AK, Barbosa J, Sprengeler PA, Hirschmann R, Munshi S, Olsen DB, Schleif WA, Kuo LC (2003) J Med Chem 46:1831
71. Smith AB III, Charnley AK, Mesaros EF, Kikuchi O, Wang W, Benowitz A, Chu C-L, Feng J-J, Chen K-H, Lin A, Cheng F-C, Taylor L, Hirschmann R (2005) Org Lett 7:399
72. Smith AB III, Wang W, Charnley AK, Carroll PJ, Kenesky CS, Hirschmann R (2010) Org Lett 12:2990
73. Smith AB III, Xiong H, Charnley AK, Brenner M, Mesaros EF, Kenesky CS, Di Costanzo L, Christianson DW, Hirschmann R (2010) Org Lett 12:2994
74. Phillips ST, Rezac M, Abel U, Kossenjans M, Bartlett PA (2002) J Am Chem Soc 124:58
75. Phillips ST, Blasdel LK, Bartlett PA (2005) J Am Chem Soc 127:4193
76. Phillips ST, Blasdel LK, Bartlett PA (2005) J Org Chem 70:1865
77. Phillips ST, Piersanti G, Bartlett PA (2005) Proc Natl Acad Sci U S A 102:13737
78. Hammond MC, Harris BZ, Lim WA, Bartlett PA (2006) Chem Biol 13:1247
79. Schmuck C, Heil M (2003) Chembiochem 4:1232
80. Schmuck C, Heil M (2003) Org Biomol Chem 1:633
81. Schmuck C, Bickert V (2003) Org Lett 5:4579
82. Bonauer C, Zabel M, Konig B (2004) Org Lett 6:1349
83. Siodlak D, Stas M, Broda MA, Bujak M, Lis T (2014) J Phys Chem B 118:2340
84. Chakraborty TK, Mohan BK, Kumar SK, Kunwar AC (2002) Tetrahedron Lett 43:2589
85. Kang CW, Sun Y, Del Valle JR (2012) Org Lett 14:6162
86. Kim YB, Kang CW, Ranatunga S, Yang H, Sebti SM, Del Valle JR (2014) Bioorg Med Chem Lett 24:4650

Top Heterocycl Chem (2017) 49: 51–80
DOI: 10.1007/7081_2015_165

Published online: 21 November 2015

Diketopiperazine-Based Peptide Mimic Scaffolds

Qingquan Zhao and Christian E. Schafmeister

Abstract 2,5-Diketopiperazines (2,5-DKPs) are heterocyclic molecules cyclized from two alpha amino acids. Their ease of synthesis, ability to display up to six functional groups, and pre-organization all led 2,5-DKPs to be utilized in drug discovery, catalysis, and material science. This review focuses on recent developments and applications of the diketopiperazine motif as a rigid scaffold in peptide science to mimic protein secondary structures and in crystal engineering to organize functional groups in three-dimensional space, as well as in molecular recognition and catalysis.

Keywords 2,5-Diketopiperazine · Peptidomimetics · Spiroligomers · α-Helical mimics · β-Hairpin · β-Turn

Contents

Q. Zhao and C.E. Schafmeister (✉)
Department of Chemistry, Temple University, 1901 North 13th Street, Philadelphia, PA 19122, USA
e-mail: meister@temple.edu

Abbreviations

Boc	*tert*-Butoxycarbonyl
Cbz	Carboxybenzyl
CD Spectroscopy	Circular dichroism spectroscopy
CD_3OH	Deuterated methanol
$CDCl_3$	Deuterated chloroform
CuAAC	Cu(I)-catalyzed alkyne–azide cycloaddition
d^6-DMSO	Deuterated dimethyl sulfoxide
DIC	Diisopropylcarbodiimide
DIPEA	*N*,*N*-Diisopropylethylamine
DKP	Diketopiperazine
Fmoc	9-Fluorenylmethoxycarbonyl
HATU	O-(7-azabenzotriazol-1-yl)-*N*,*N*,*N*′,*N*′-tetramethyluronium hexafluorophosphate
HBr	Hydrobromic acid
HOAt	Hydroxyazabenzotriazole
HUVEC	Human umbilical vein endothelial cells
MARK	Mitogen-activated protein kinase
MC/SD simulations	Monte Carlo/stochastic dynamics simulations
MeIm	Methylimidazole
MMFF	Merck molecular force field
MSNT	1-(Mesitylene-2-sulfonyl)-3-nitro-1,2,4-triazole
NOE	Nuclear overhauser effect
NOESY	Nuclear overhauser effect spectroscopy
ROESY	Rotating frame nuclear overhauser effect spectroscopy
TFA	Trifluoroacetic acid
THBC	Tetrahydro-β-carboline
Trk	Tropomyosin receptor kinase

1 Introduction

The remarkable biological functions of peptides and proteins are achieved by adopting structures with well-defined conformations by virtue of a variety of non-covalent forces, including hydrophobic interactions, the formation of intramolecular hydrogen bonds, and van der Waals forces [1]. This folding process positions chemical groups, both reactive and unreactive, precisely in three-dimensional space either inward, in the case of enzymes, to catalyze chemical reactions or outward to create recognition elements to bind proteins and other macromolecules. Applications of synthetic peptides are limited due to the difficulty involved in controlling the three-dimensional structure of peptides due to their highly dynamic

Fig. 1 The general structure of a 2,5-diketopiperazine (DKP)

behavior in solution, their susceptibility to proteolytic cleavage, and the tenuous nature of the forces that govern folding [2]. Therefore, peptidomimetic compounds have been widely developed to mimic secondary structures of peptides and proteins. Toward this goal, the application of scaffolds that constrain peptide conformation has received much attention given their ability to order molecules into well-defined structures for presenting essential functionalities in orientations necessary to achieve binding and catalytic functions [2].

2,5-Diketopiperazines (Fig. 1, DKPs) have been identified in many natural products [3]. Diketopiperazines are the smallest constrained cyclic peptide. They have been incorporated into linear peptides to induce and to stabilize secondary structure, and they have been assembled into oligomers with discrete conformationally ordered folds in solution to mimic specific protein structures. Recent reviews of the synthesis and bioactivities of DKP-containing compounds have been written [3–7]. There are also recent reviews on the synthesis and utilization of DKP motifs in receptors for molecular recognition and peptidomimetics authored by Ressurreição et al. in 2011 [8] and Borthwick in 2012 [3]. This review covers recent developments and applications of the DKP motif with focus on its use as a rigid scaffold in peptide science to mimic protein secondary structures, crystal engineering to organize functional groups in three-dimensional space, and molecular recognition to create functional molecules and catalysts.

2 Diketopiperazines as Rigid Units in Flexible Molecules

2.1 β-Turn Mimics

One of three major elements of secondary structure in bioactive peptides and proteins, the β-turn reverses the direction of a polypeptide (Fig. 2). Defined as a peptide conformation that places the Cα atoms of the *i* and *i* + *3* residues within a distance of less than 7 Å, the β-turn may form a ten-member ring by way of an intramolecular hydrogen bond between the amide carbonyl and NH of these two opposing residues. At least 14 different types of β-turn structures have been described in the literature [8, 9].

To date, a great deal of attention has been directed toward β-turn mimicry. Among the designs, considerable success has been achieved by the synthesis of conformationally restricted β-turn peptidomimetics featuring DKP structures. The diketopiperazine ring has served in three categories (Fig. 2): (a) internal β-turn mimics, in which a DKP is part of the rigid scaffold that mimics the β-turn structure;

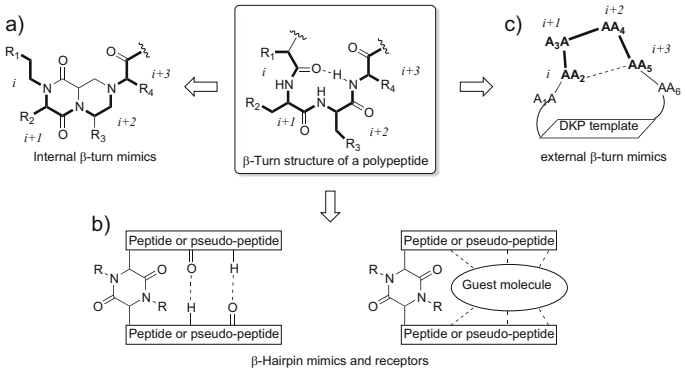

Fig. 2 β-turn structure in polypeptides and three categories of β-turn mimics (*bold*) based on diketopiperazines. (**a**) internal β-turn mimics; (**b**) β-hairpin mimics and receptors; (**c**) external β-turn mimics

(b) β-hairpin mimics and receptors, in which the DKP is incorporated into a peptide or pseudo-peptide chain to induce a U-shaped turn conformation; and (c) external β-turn mimics, in which DKPs act as templates in a cyclic peptide to stabilize a specific β-turn secondary structure.

2.1.1 Internal β-Turns

Early examples of DKP-based internal β-turn mimics have been prepared by Kahn and co-workers using solution-phase synthesis [10], as well as by Golebiowski et al. who made two generations of 6,6-fused ring systems using solid-phase synthesis [11–13]. A highlight of Kahn's synthesis is formation of the diketopiperazine-fused ring system **5** in one step on treatment of ketone **2** with TFA, followed by bicarbonate workup. Failure to reduce the imine intermediate **3** with $ZnCl_2/NaBH_3CN$ was presumed to be due to rapid isomerization to enamine **4**. Although the absolute stereochemistry of the diastereomers was not assigned, the synthesis successfully introduced three substituents (R_1, R_3, and R_4) onto the DKP bicycle **6** to mimic the side chains of the β-turn structure (Fig. 3a).

Two high-throughput solid-phase syntheses were developed by Golebiowski and co-workers for introducing substituents onto a similar bicyclic fused ring scaffold containing a diketopiperazine (Fig. 3b, c) [11–13]. Synthesis of the first generation of analogs started from the supported piperazine-2-carboxylic acid **7**. A Petasis reaction was used to introduce the R_4 group, and a subsequent peptide coupling added R_5 to provide amide **8**. After Fmoc removal from **8**, a variety of α-amino acids were coupled to introduce the R_1 and R_2 substituents (Fig. 3b) [12]. Using this synthetic pathway, the authors found that the R_4 group was restricted to aromatic and conjugated systems. A second-generation synthesis was developed to overcome this drawback and to introduce the R_3 group (Fig. 3c) [11, 13]. In this modified pathway, the R_3, R_4, and R_5 groups were introduced in one step through a

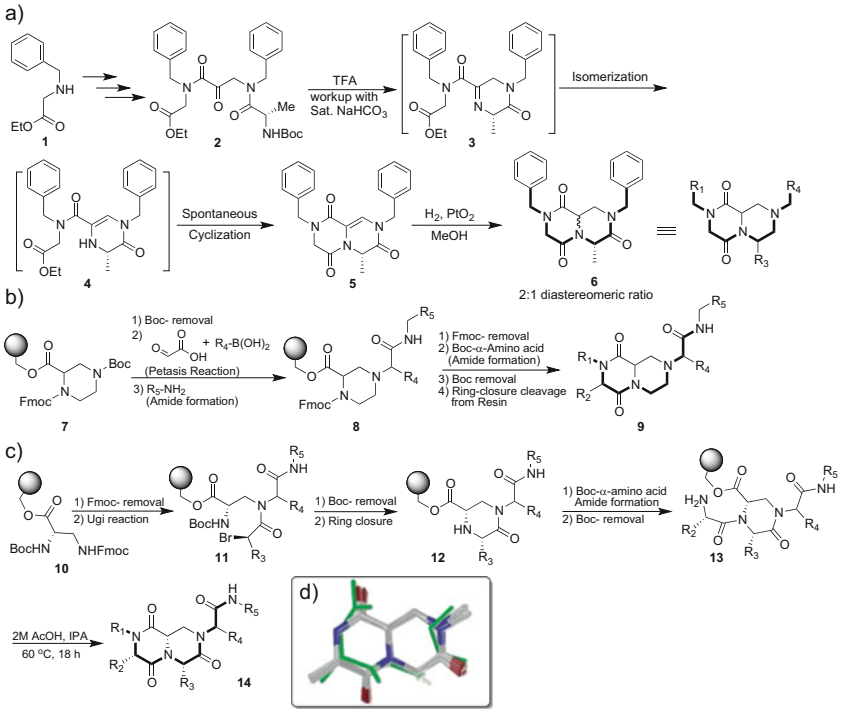

Fig. 3 Examples of internal β-turn mimic syntheses. (**a**) Solution-phase synthesis by Kahn and co-workers; (**b**) and (**c**) first and second-generation solid-phase syntheses by Golebiowski et al.; (**d**) Mimic **14** (*S*-epimer) superimposed onto an ideal type I β-turn conformation

multicomponent Ugi reaction, allowing for the rapid generation of diverse analogs. The bicyclic fused ring scaffold was shown to overlap closely with a type I β-turn using simulated annealing calculations and the SYBYL 6.7.2 (Tripos Inc., St. Louis, MO) program with the MMFF (Fig. 3d) [11].

In 2010, Burgess and co-workers reported an antagonist of the tropomyosin receptor kinase C (TrkC) receptor composed of two DKP internal β-turn mimics (Fig. 4) [14]. The interaction of the TrkC receptor and neurotrophin-3 (NT-3) mediates neurotrophic factor effects such as neuronal differentiation and has been targeted for therapeutics of pathologies including cancer and neurodegeneration. In the design hypothesis, close distances between the Cβ atoms of the R_2 and R_3 groups were considered critical for biologically active β-turns (Fig. 4a). Compared with the longer distance (5.5 Å) between the Cβ atoms in type B mimics **16**, the separation between the two Cβ atoms is about 5.15 Å in type A mimics **15** and close to the 5.2 Å distance displayed in natural peptide β-turns. A library consisting of a variety of substituted diketopiperazines was synthesized and attached in different ways onto a 4,6-dichloro-1,3,5-triazinylamino-biotin core with either short or long linkers (Fig. 4b). The resulting compounds were tested in binding assays, biological assays, and biochemical signal transduction assays. Mimic **17** antagonized

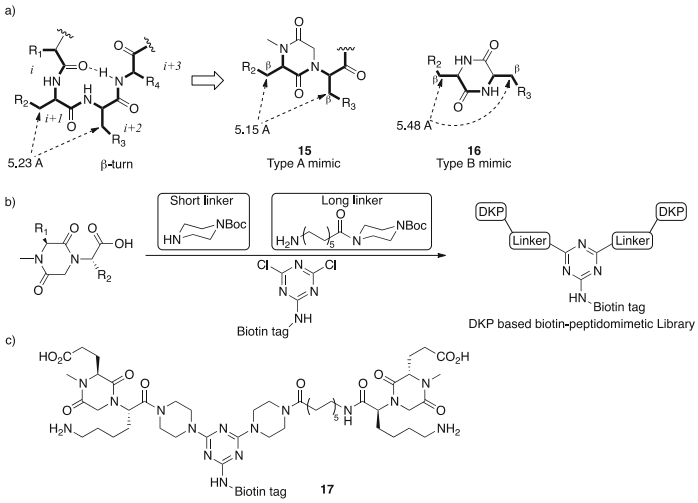

Fig. 4 Conception of DKP-based bivalent tropomysin receptor kinase C (TrkC) antagonist **17**: (**a**) design of internal β-turn mimics based on the distance between two Cβ atoms; (**b**) library generation by linking two DKP motifs and a biotin tag using different length linkers; (**c**) inhibitor **17**

selectively TrkC–NT-3 activity without influencing TrkA and blocked mitogen-activated protein kinase (MARK) activation of signal transduction (Fig. 4c).

2.1.2 β-Hairpin Peptidomimetics and Receptors

β-Hairpins are peptide turn units that typically induce antiparallel β-sheet formation (Fig. 5a). Diketopiperazines functionalized with amine and carboxylic acid groups have been designed for incorporation into peptide and pseudo-peptide chains to nucleate β-hairpin formation. Contingent on its substitution, the DKP turn unit may stabilize parallel or antiparallel β-sheet formation.

The concept of a DKP structure in a β-sheet inducer was contributed by Davies and co-workers [15]. who employed computational modeling to show that *cis*-carbamato ester **18** could serve as a β-turn structure suitable for hairpin nucleation (Fig. 5b). Although the racemic DKP was synthesized, no further DKP as β-sheet mimic was reported.

The bifunctional DKP scaffold **23** bearing orthogonally protected carboxylic acid and amine functionalities was reported by Gennari and Piarulli and co-workers (Fig. 6) [16]. Protected aspartic acid was coupled to *N*-benzyl serine methyl ester **19** by way of an *O*- to *N*-acyl migration of ester intermediate **20** [17]. The resulting primary alcohol **22** was converted to *N*-(Boc)aminomethyl DKP **23** by a sequence featuring a Mitsunobu reaction with hydrazoic acid and a one-pot Staudinger reaction/Boc protection. Selective removal of the Boc- and allyl-protecting groups permitted functionalization of the DKP core with two separate peptide sequences to

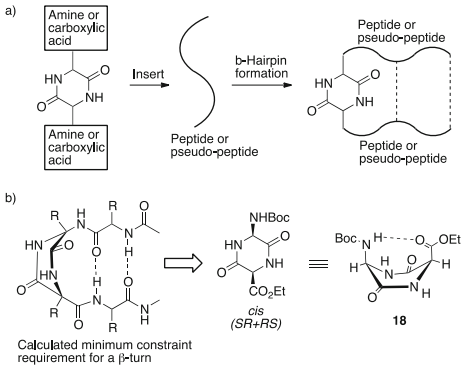

Fig. 5 (**a**) Diketopiperazine with amine and carboxylic acid functional groups inserted in peptide/pseudo-peptides to form β-hairpin conformations; (**b**) calculation of the minimum constraint requirement for a β-turn structure by Davies and co-workers resulted in *cis*-DKP unit **18**

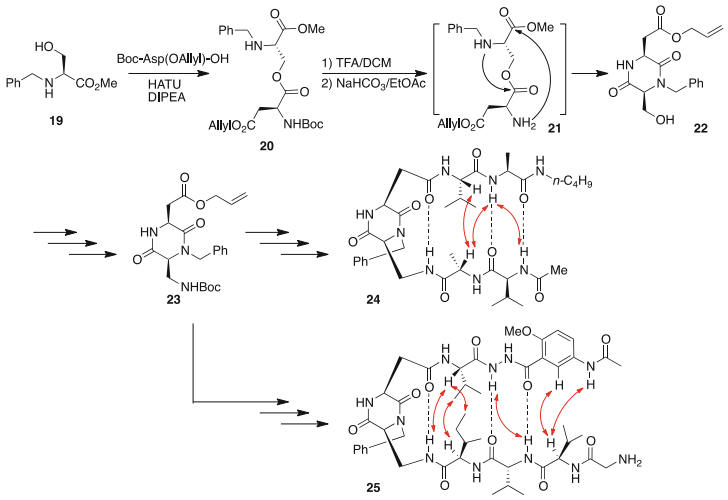

Fig. 6 Synthesis and application of DKP scaffold **23** in β-hairpin analogs **24** and **25** (*red arrows* indicate observed NOE/ROE correlations)

form hairpin mimic **24**. Conformational studies on **24** were carried out using a combination of one-dimensional/two-dimensional NMR, IR, and CD spectroscopy and compared with results from molecular modeling. In the ROESY spectrum of **24** in d^6-DMSO, interstrand NOE cross-peaks were observed between the opposing α-carbon and amide nitrogen protons (Fig. 6, red arrows). Furthermore, downfield chemical shifts of the amide protons in the ^{1}H NMR spectrum in 5% CD_3OH-$CDCl_3$ supported the presence of intramolecular hydrogen bonds between the opposing peptide chains. The β-hairpin conformation of **24** was also predicted from an unconstrained Monte Carlo/energy minimization (MC/EM)

conformational search. A second DKP β-hairpin **25** was later reported to be stabilized using 5-amino-2-methoxybenzhydrazide [18], which had previously proven effective for favoring intermolecular β-sheets preventing dimerization and proteolysis [19–21]. Evidence for β-hairpin **25** came from the observation of a number of long-range ROEs between the two strands, albeit the chemical shifts of the amide protons on both strands showed higher temperature dependence than expected. These two examples demonstrated that DKP scaffold **23** was an efficient β-turn mimic for inducing β-hairpins toward β-sheet mimicry.

In addition to bifunctionalized DKP peptidomimetics, multifunctionalized DKP units have been developed. For example, diamino carboxylate DKPs **29**-**31** were synthesized by Gellerman et al. from glyoxylic acid and orthogonally protected lysine using a reductive amination/peptide coupling/lactam formation sequence (Fig. 7a) [22, 23]. The coupling step gave only moderate yield, presumably due to the weak nucleophilicity and steric hindrance of secondary amine **27**

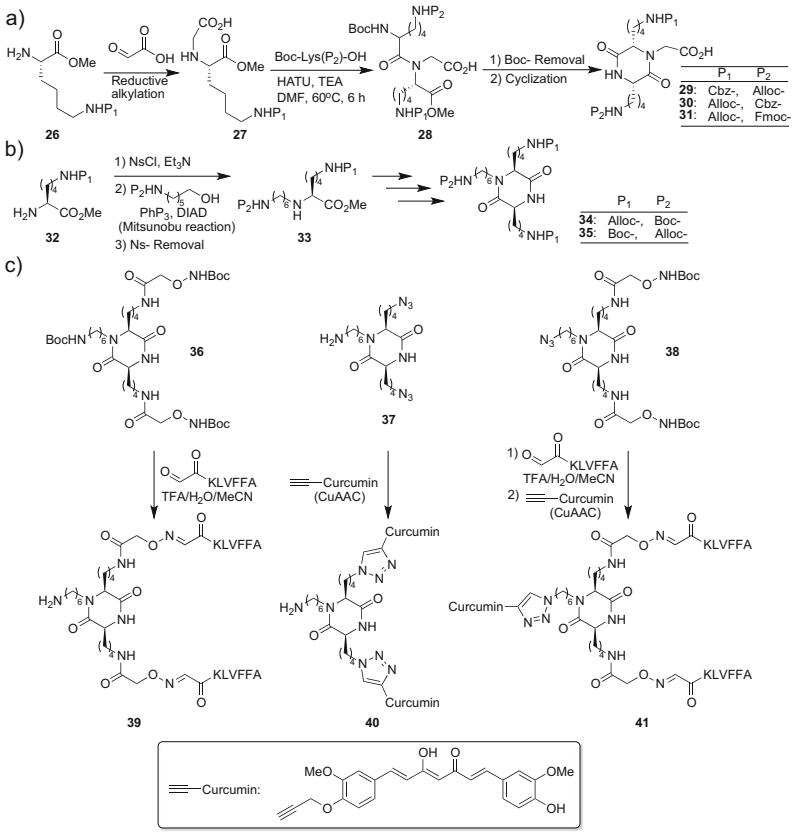

Fig. 7 Synthesis and application of multifunctionalized DKPs: (**a**) diamino carboxylate DKPs developed by Gellerman and co-workers; (**b**) triamino DKPs developed by Chierici and co-workers; (**c**) examples of triazole-functionalized DKPs designed as Aβ aggregation inhibitors

[24]. Triamino DKPs **34** and **35** were synthesized by Chierici and co-workers using a similar strategy in which the *N*-aminoalkyl group was installed by a Mitsunobu reaction to give secondary amine **33** (Fig. 7b) [25]. Orthogonally protected triamino DKPs were converted to a set of precursors **36–38** bearing glyoxyloyl, aminooxy, alkynyl, or azido functionalities for subsequent ligation to the peptide KLVFFA and curcumin by way of oxime formation and copper-catalyzed azide–alkyne cyclization (CuAAC) reactions to make DKPs **39–41** (Fig. 7c). With the interest of diminishing amyloid plaques found in the brains of Alzheimer patients, the ability of **39–41** to inhibit amyloid-β40 fibril formation was evaluated in thioflavin T fluorescence assays. Among the three analogs, DKP **39** gave the best activity reducing florescence to 80% at 1 μM concentration, and at 10 μM, was shown by atomic force microscopy to reduce the number and length of fibrils in a sample of amyloid β40.

4-Aminoproline-derived DKPs have been used to induce turn structures in peptide sequences (Fig. 8a) [26–30]. Compared with the DKPs discussed above, the tricyclic 4-aminoproline-derived DKPs are more rigid and possess a longer end-to-end distance. Wennemers and co-workers reported the synthesis of a set of receptors **42** employing such a tricyclic DKP to display two flexible tripeptide chains, each possessing a red azo dye attached to the phenolic hydroxy group of a tyrosine residue. Receptors **42** were employed in on-bead screening against libraries prepared on polystyrene resin using encoded split-and-mix methods and containing a maximum of $29^3 = 24{,}389$ different acylated tripeptides with unprotected and protected side chains [26, 27]. Different receptors **42** bound selectively different peptides from the side chain-free and protected libraries. In the case of the side chain-protected peptide library, adding one single additional methylene group to the receptor (from asparagine to glutamine) eliminated receptor binding affinity indicating that subtle changes in structure can significantly alter receptor properties [27]. The importance of the central DKP scaffold for creating a cleft to hold two side arms apart from each other was highlighted by its replacement with flexible and shorter diamine linkers **43–46**, which abolished all interactions between receptor and substrates, presumably due to aggregation of the opposing peptide chains through hydrogen bonding in the receptor (Fig. 8b) [31]. The four-position stereochemistry of the aminoprolines in the DKP scaffold was also shown to be crucial for activity, which was lost employing the *cis,cis*-diketopiperazine. X-ray analysis of the *trans,trans*- and the *cis,cis*-DKPs **47** and **48** revealed that they adopted respectively turn and linear conformations with distances between the terminal amines of 7.8 and 8.7 Å (Fig. 8c). Employing NMR spectroscopic analysis, *cis,cis*-DKP scaffold **48** was shown to be relatively more flexible than *trans,trans*-DKP **47**. Joining the terminal ends of receptors **42** with different linker lengths gave macrocycles **49**, which exhibited reduced binding affinities for the original peptide substrates, as well as alternative selectivity (Fig. 8d) [32], highlighting the importance of DKP core pre-organization and peptide side arm flexibility.

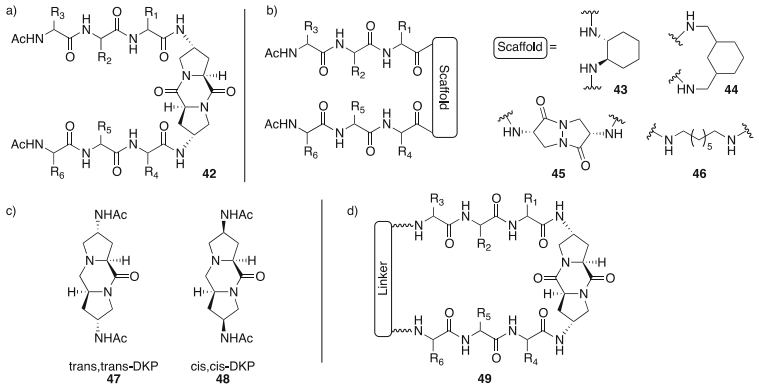

Fig. 8 DKP-based receptors with two-peptide side arms reported by Wennemers and co-workers: (**a**) general receptor structure; (**b**) unsuccessful linker strategies; (**c**) *trans,trans*- and *cis,cis*-DKPs **47** and **48**; (**d**) macrocycle receptor **49**

2.1.3 External β-Turn (Peptide Loops)

External β-turn mimics refer to DKPs that act as templates to stabilize β-turn and β-hairpin structures inside cyclic peptide analogs, as pioneered by the groups of Robinson [33–40] and Albericio [41].

Bicyclic and tricyclic DKPs **52–55** have been inserted into peptide sequences containing Asn-Pro-Asn-Ala (e.g., NPNA, **50**) and Arg-Gly-Asp (e.g., RGD, **51**, Fig. 9a) [33–40]. Moreover, a monocyclic DKP has been introduced into cyclic RGD peptides **57–59** by a solid-phase synthetic approach employing a backbone amide linker (BAL) resin [41]. Toward the development of a vaccine against malaria, constrained cyclic peptides **50** have elicited sporozoite cross-reactive antibodies under conditions in which the linear peptide sequence failed to induce a detectable cross-reactive immune response. Studying the binding of DKPs **51** and **57–59** to the $\alpha_v\beta_3$ integrin receptor, which is important for tumor angiogenesis, greater conformational constraint was considered as a means for improving affinity.

Further research on cyclic RGD mimics **60–67** employed *N*-benzyl and *N*,*N*-dibenzyl DKP scaffolds of different configurations (Fig. 10) [42, 43]. In the construction of the DKP core, *O*- to *N*-acyl migration (Fig. 6) [16, 17], and employment of symmetric anhydride coupling conditions surmounted the difficulties in the acylation to the secondary amine. For macrocycle **66**, two different atropisomers **66A** and **66B** were isolated due to the large energy barrier required to flip the DKP by rotating the *N*-benzyl groups through the inside of the macrocycle ring (Fig. 10c). Macrocyclic RGD peptidomimetics **60–67** were tested in competition with biotinylated vitronectin for binding to immobilized $\alpha_v\beta_3$ and $\alpha_v\beta_5$ integrin receptors (Fig. 10b). Although micromolar affinity toward the $\alpha_v\beta_3$ integrin was exhibited by analogs bearing the *cis*-DKP, examination of a *trans*-DKP core in the RGD macrocycles gave nanomolar affinities, as well as 10–500-fold greater

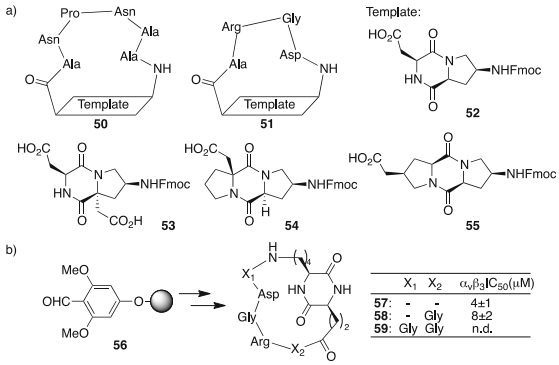

Fig. 9 External β-turn mimics: (**a**) DKP templates in Asn-Pro-Asn-Ala (NPNA) and Arg-Gly-Asp (RGD) sequences reported by Robinson and co-workers; (**b**) solid-phase synthesis of DKP cyclic RGD mimic reported by Albericio and co-workers

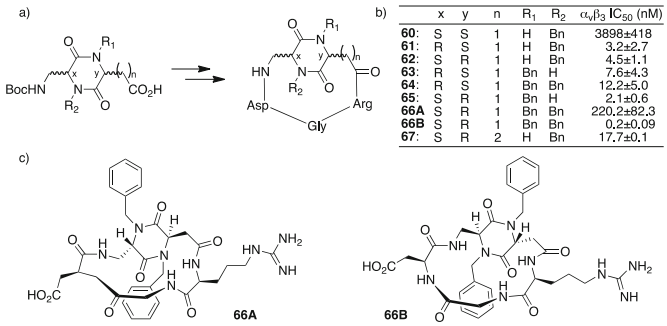

Fig. 10 (**a**) Cyclic RGD analogs containing *N*-benzyl and *N*,*N*-dibenzyl DKPs; (**b**) their IC_{50} values; (**c**) atropisomers **66A** and **66B** [42, 43]

selective for $\alpha_v\beta_3$ over $\alpha_v\beta_5$ receptors compared to the reference compounds, such as *c*(RGDfV) and ST1646.

Conformational analysis of **60–67** using variable temperature NMR and NOESY spectroscopy supported by Monte Carlo/stochastic dynamics simulations and molecular docking calculations identified five preferred intramolecular hydrogen-bonding patterns (Fig. 11) [43]. Peptidomimetics showing high bioactivity adopted well-defined conformations with a turn motif within the RGD sequence. For example, analogs **61**, **62**, and **64** with good affinity showed only one relevant long-range coupling in their NOESY spectra between the amide protons of the Gly and Arg residues, indicating a turn motif centered on the DKP and Arg residues (type III conformer). High-affinity analog **63** and the tightest-binding analog **66B** adopted a β-turn motif centered at the Gly–Asp sequence (type I hydrogen-bonding pattern) as determined by the low temperature coefficient of the DKP–NH, which exhibited a cross peak with the Asp–NH in the NOESY spectra. Relatively lower

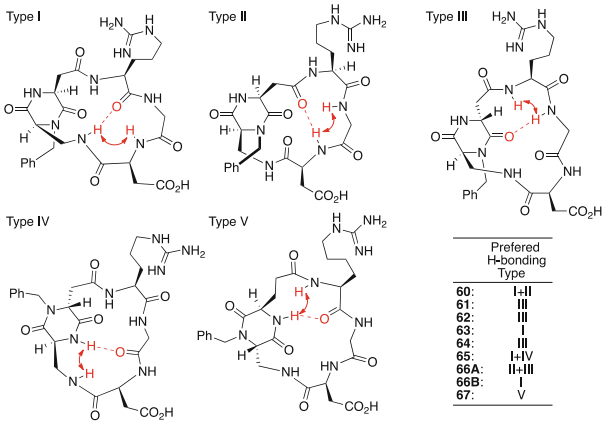

Fig. 11 Conformational analysis of hydrogen-bonding patterns of cyclic RGD mimics containing DKP-related high bioactivity with well-defined turn motifs about the peptide sequence

affinity analog **67** preferred a turn centered on the Arg–DKP residues evidenced by a strong long-range NOE correlation between their corresponding NH protons (type V conformer). On the other hand, weak-affinity compounds **60** and **66A** existed in equilibrium between two different conformations. In docking studies, the highest affinity analog **66B** superimposed well with the bound conformation of the reference peptide and former clinical candidate cilengitide, *c*[RGDf(NMe)V], in the crystal structure of the extracellular domain of $\alpha_v\beta_3$ integrin. Without affecting cell viability and proliferation, peptidomimetic **62** inhibited angiogenesis in human umbilical vein endothelial cells by a mechanism involving reduced phosphorylation of protein kinase B (Akt) and disruption of integrin-mediated adhesion [44].

2.2 α- and γ-Turn Mimics

In addition to the β-turn structure discussed previously, other protein secondary structures are classified as α-, γ-, δ-, and π-turns according to their number of residues (Fig. 12).

An important motif in many proteins [45], the α-helix is composed of 13-member ring hydrogen bonds between the carbonyl group of residue *i* and the amide NH group of residue $i+4$ [46]. These so-called α-turn units repeat with consistent backbone dihedral angles ($\phi = -58°$, $\psi = -47°$) resulting in an ideal right-handed α-helix. These consecutive angles deviate however in proteins due to backbone sequence, side chain orientations, and helical pitch [47, 48]. Compared with β-turn peptidomimetics, few examples of DKPs stabilizing α-turn structures have been reported [47, 48].

A fused tetrahydro-β-carboline (THBC)–DKP scaffold was synthesized by Silvani and co-workers to mimic the α-turn conformation (Fig. 13) [49]. A Pictet–Spengler reaction between L-tryptophan methyl ester (**68**) and *N*-(Cbz)glycinal dimethyl acetal (**69**) provided tetrahydro-β-carboline **70** in good yield and a 7:3

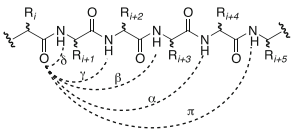

Fig. 12 Classifications of turn structures in proteins based on hydrogen-bonding patterns

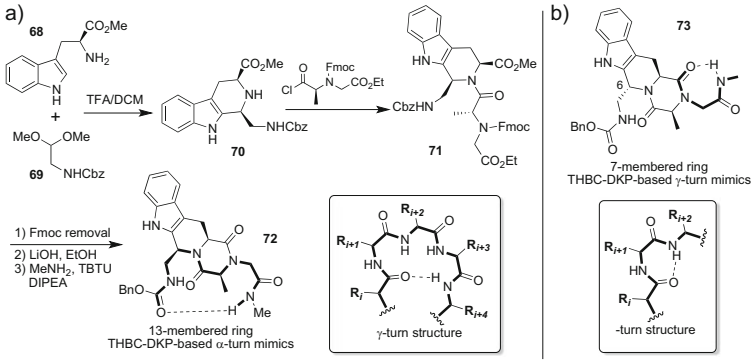

Fig. 13 (**a**) Synthesis of THBC–DKP α-turn mimics; (**b**) inversion of C6-stereochemistry resulted in a γ-turn-like seven-member intramolecular hydrogen-bonding pattern

diastereomeric ratio. Amino acylation of the major diastereomer and cyclization gave DKP **72**, which was suggested to adopt an α-turn conformation based on ^{1}H NMR experiments and computational analysis using Monte Carlo searches with molecular mechanics. Although unconfirmed by NMR studies, computational analysis suggested that diastereomer **73** from the minor Pictet–Spengler product, which has the opposite stereochemistry at C6, would adopt a low energy seven-member intramolecular hydrogen-bonded γ-turn conformation (Fig. 13b).

2.3 Peptoid Peptidomimetics Containing Diketopiperazines

Peptoids are *N*-substituted glycine oligomers that may fold without hydrogen bond stabilization. They may also exhibit resistance to proteolysis. Introduced into the literature by Zuckermann and co-workers [50], peptoids have been used to mimic peptide and protein structures in a variety of applications. In contrast to peptides that usually possess secondary amides which prefer *trans* conformations, the tertiary amides of peptides may exist in equilibrium between *trans* and *cis* isomers [51], such that the steric interactions and electrostatic repulsion of side chains [52–54], as well as backbone cyclization [55–57], have been used to pre-organize peptoid conformation to mimic natural secondary structures (e.g., helices).

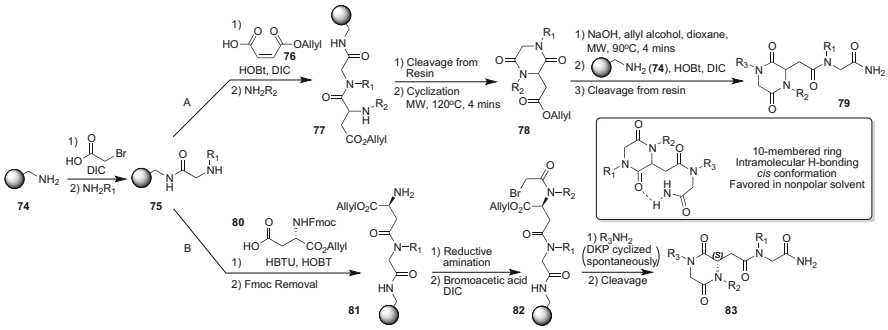

Fig. 14 Solid-phase synthesis of peptoids with DKPs that rigidify the chain: (**a**) racemic synthesis by aza-Michael reactions; (**b**) enantiomerically pure synthesis

To reduce peptoid conformational diversity, Messeguer and co-workers incorporated DKPs that changed amide *trans*/*cis* isomer ratios and stabilized secondary structure (Fig. 14) [58]. The synthesis started by acylation of Rink amide polystyrene resin **74** using bromoacetic acid and DIC, followed by bromide displacement with a primary amine to form secondary amine **75**. Acylation of amine **75** with allyl maleate **76** was performed with HOBt and DIC. Michael addition of a primary amine gave regioselectively aspartamide **77**, which on microwave heating underwent cyclization with resin cleavage to give DKP **78** (Fig. 14, route A). Removal of the allyl protection gave the carboxylic acid that was loaded onto resin **74** and cleaved to give racemic DKP peptoid amide **79**. Analysis of tertiary amide **79** by NMR spectroscopy revealed a predominant *cis* isomer in $CDCl_3$ and a 50:50 *trans*/*cis* isomer ratio in d^6-DMSO. Moreover, the signal for the terminal amide protons of **79** underwent a significant change in chemical shift on addition of d^6-DMSO into the $CDCl_3$ solution, suggesting that an intramolecular hydrogen bond between the terminal amide NH and the DKP carbonyl stabilized the *cis* isomer in the nonpolar solvent. As solvent polarity increased, the hydrogen bond was disrupted, and the amide *cis* isomer population decreased. Enantiomerically pure **83** was subsequently synthesized, respectively, using D- and L-aspartate **80** in the acylation of secondary amine **75** (Fig. 14, route B) [59]. Respective evaluations of both enantiomers of DKP peptoids **83** demonstrated no significant difference in their potency as apoptosis inhibitors in vitro, indicating that the chiral center was not crucial for this biological activity.

Solid-phase syntheses of peptoids bearing DKPs as main chain (e.g., **89**), side chain (e.g., **90**), and terminating (e.g., **91**) units were developed by Kodadek and co-workers using Rink amide resin (Fig. 15) [60]. In these approaches, α-amino esters **85** displaced bromoacetamides **84** to install half of the DKP unit. The resulting secondary amine **86** was acylated with bromoacetic acid, the bromide was displaced with another amine, and the resulting amino ester **87** was heated overnight to induce cyclization. Resin cleavage provided DKP peptoids **88**. This synthetic route was adopted to split-and-mix strategies to prepare DKP peptoid

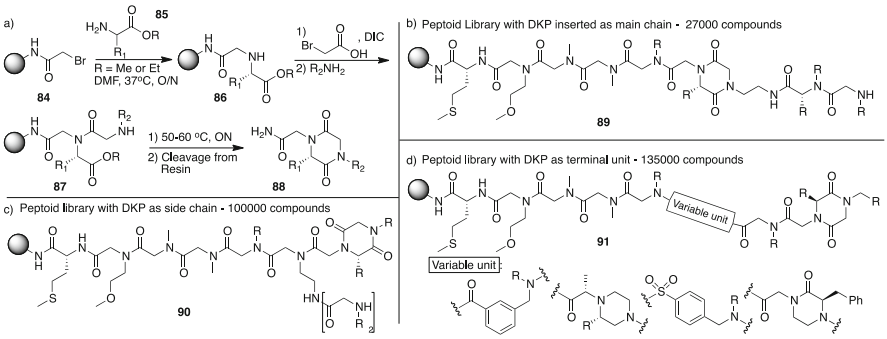

Fig. 15 (**a**) Solid-phase synthesis of DKP peptoids by Kodadeck and co-workers; libraries prepared by split-and-mix strategies with DKP as (**b**) side chain, (**c**) main chain, and (**d**) terminal element

libraries **89–91**, as confirmed by MALDI MS and MS/MS analysis of randomly selected beads. Screening of these libraries may identify new bioactive compounds.

3 Diketopiperazines as Monomers in Macromolecules

3.1 Diketopiperazines Assembled via Non-covalent Bonds (Crystal Engineering)

The conformations of DKPs possessing up to four substituents have been studied [61–67] and reviewed [3, 68]. Although constrained, DKPs are not completely rigid, because of the similar energies of their planar and boat conformations, in the solid state, intermolecular hydrogen bonding between two amides permits formation of supermolecular structures. Linear tape orientations of DKPs without N-substituents have been observed to exist in hydrogen-bonded cyclic eight-membered rings. Substituted DKPs may adopt layer structures contingent on ring substitution. One-dimensional hydrogen-bonded tapes and dimers are generally observed for mono-N-substituted DKPs.

By virtue of its rigidity, synthetic accessibility, structural diversity, and resistance to proteolytic enzymes, the DKP moiety has been extensively studied as a building block in supramolecular chemistry. Symmetrical DKPs **92** with cycloalkyl substituents were shown to form tapes by Whitesides and Palmore (Fig. 16a) [69–71]. Mash and co-workers postulated that three geometrically and chemically independent elements may be used to make ordered three-dimensional organic crystals: amide-to-amide hydrogen bonding between DKPs along the *z*-axis; van der Waals forces shared by R_1, R_4, R_5, and R_8 substituents along the *y*-axis; and other interactions between the R_2, R_3, R_6, and R_7 groups in the *x*-axis (Fig. 16b). A series of studies toward such designs have been reported [72–76] and reviewed [77].

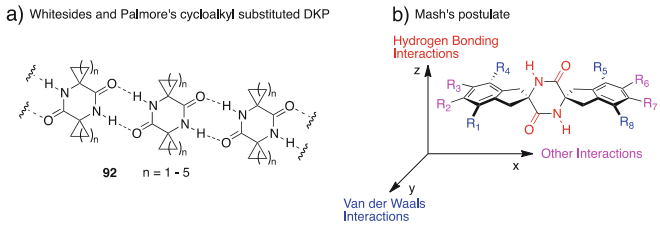

Fig. 16 (**a**) Assembly of symmetric cycloalkyl-substituted DKP reported by Whitesides and Palmore; (**b**) Mash's postulate that three independent sets of interactions between groups displayed on diketopiperazine containing compounds can generate three-dimensional networks and control crystal formation

Emphasizing the importance of aromatic side chain substituents in DKP ensembles, Verma and co-workers chose four different model systems **93–96** to form two-dimensional extended structures employing π−π interactions from the aromatic groups to create intermolecular interactions orthogonal to the hydrogen bonding between amides (Fig. 17a) [78]. Employing similar π−π interaction in the self-assembly of DKPs **97** and **98**, Govindaraju and co-workers prepared two-dimensional nano- and mesosheets (Fig. 17b) [79]. These networks that combine π−π interactions and hydrogen bonding have been characterized by NMR spectroscopy and X-ray diffraction. Similarly, low-molecular-weight gelator soft materials were formed by sequential heating and cooling DKPs **99** (Fig. 17c) [80]. Chemical shift values in NMR analyses at various concentrations and temperatures revealed the formation of intermolecular ladders through hydrogen bonds, respectively, between DKP amides and side chain carbamates. In addition, aromatic π−π interactions were crucial for the self-assembly process. Similarly, gelation of DKP **100** was observed in a number of solvents including water using agitation with ultrasound (Fig. 17d) [81]. These organic hydrogels may be applied as entrapping agents, drug delivery systems, and thermo-responsive soft materials.

Helical chirality, which is ubiquitous in proteins, was adopted by naphthalene-diimide (NDI)–DKP supramolecular assemblies designed by Govindaraju and co-workers (Fig. 18) [82]. For example, the monosignate negative CD signal of NDI–DKP **101** in hexafluoroisopropanol (HFIP) indicated a left-handed *M*-helical assembly, which on titration with DMSO underwent a reversible transition from *M*- to *P*-helicity leading to a bisignate positive Cotton signal. On the other hand, NDI–DKP diastereomer **102** exhibited no preference to adopt helical geometry in mixture of DMSO and HFIP.

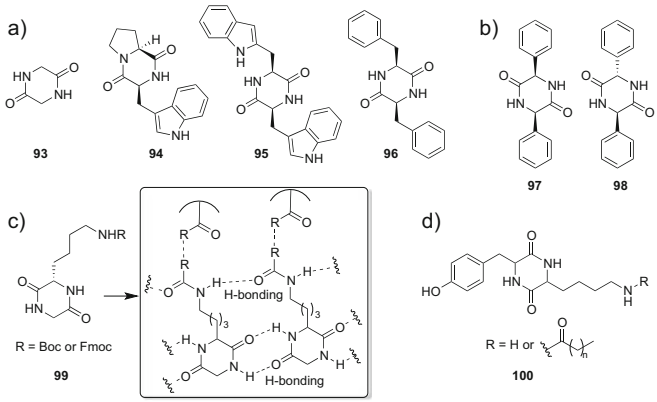

Fig. 17 Substituted DKPs used in crystal engineering

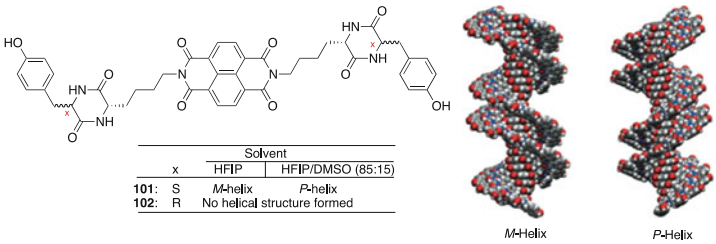

Fig. 18 Solvent and stereochemistry-dependent helical conformations formed from NDI–DKP

3.2 Foldamers Containing Multiple Diketopiperazines

"Foldamers," oligomers that adopt a well-defined secondary structure stabilized by non-covalent interactions, were developed to mimic the conformations and abilities of proteins and nucleic acids. Foldamers are often assembled chemically by coupling unnatural monomers into sequence-specific oligomers. Various applications have been reported using different foldamers: β-peptides [83, 84], peptoids [85, 86], aryl-based oligomers [87–89], and others [90–93]. Several foldamers containing DKPs have been reported to mimic protein secondary structure.

3.2.1 β-Bend Ribbon Mimics

β-bend ribbon is normally considered a subtype of the peptide 3_{10} helix featuring a succession of repeating β-turn conformations, in which the carbonyl group of residue *i* is hydrogen bonded to the NH of the *i* + *3* residue [94]. Peptides containing repeating units composed of proline or α-aminoisobutyric acid (Aib) often adopt this secondary structure [95, 96]. In 2010, Piarulli and co-workers reported β-bend

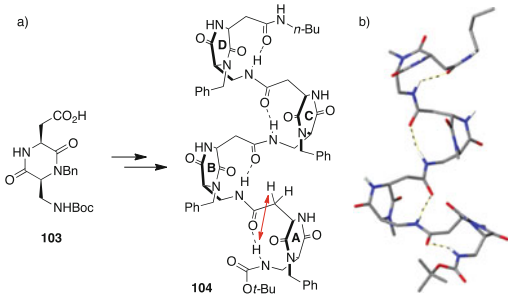

Fig. 19 (**a**) β-Bend ribbon **104** composed of amino acid DKPs **103**; (**b**) SD simulation of tetramer **104**

ribbon **104** formed by linking four-amino acid DKP monomers **103** through amide bonds (Fig. 19a) [97].

Tetramer **104** exhibited characteristics of a β-bend ribbon in NMR and CD spectroscopic experiments and stochastic dynamic (SD) simulations. For example, titration of **104** with deuterated methanol in d^6-DMSO revealed intramolecular hydrogen bonds between exocyclic amide protons, which exchanged at slower rates compared to the DKP N–H protons. Moreover, the exocyclic amide and methylene protons exhibited NOE correlations (red arrows in Fig. 19a). The CD spectrum of tetramer **104** displayed a typical Cotton effect with strong and weak negative maximum, respectively, at 200 and 215 nm, similar to oligopeptides that are known to adopt ten-member hydrogen-bonded conformations. The spectroscopic evidence and SD simulations, all indicated that the DKP scaffolds pre-organized tetramer **104** to adopt a conformer featuring repeating ten-member hydrogen bonds (Fig. 19b).

3.2.2 Spiroligomers, Ladder Molecules Containing Multiple Diketopiperazines

The α-helical structure in proteins is a common secondary structure consisting of repeating α-turns every 3.4 amino acid residues with the side chains of the *i*, *i* + *4* and *i* + *7* residues aligned roughly on the same face (Fig. 20). About 30% of all known protein structures are composed of helical peptide segments [47], and 62% of the protein–protein interaction interfaces observed in the Protein Data Bank (PDB) contain an α-helix [98, 99]. Many foldamers have been designed to mimic helical structures including β-peptides [84, 100], peptoids [101, 102], *N*,*N*′-linked oligo-ureas [92], aromatic amino acid oligomers [103, 104], and others [105–108].

Seeking to develop disruptors of protein–protein interactions, our group made *pro4*-DKPs to mimic α-helix structure (Fig. 21a) [109, 110]. Hypothesizing that shape-persistent and programmable backbones may be rationally designed using pre-organized arrays of functional groups to selectively bind protein surfaces, a collection of cyclic, enantiomerically pure diamino acid monomers have been coupled to form spiral-ladder oligomers named "spiroligomers" (Fig. 21a, b) [111, 112]. Featuring fused ring systems having well-defined three-dimensional

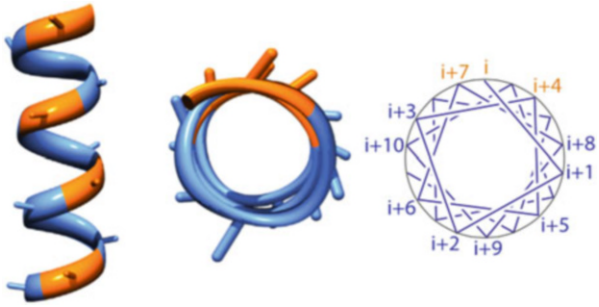

Fig. 20 Depictions of the α-helix show residue side chain alignments

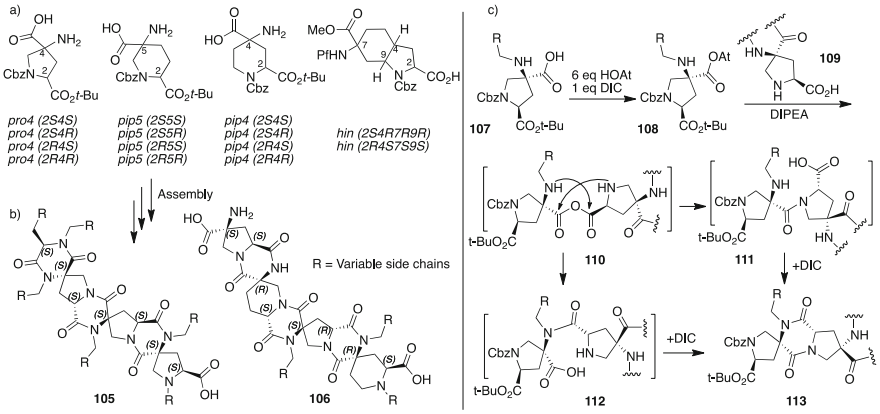

Fig. 21 The diamino acid-based approach to form spiroligomer scaffolds; (**a**) bis-amino acid monomers include *pro4*, *pip5*, *pip4*, *hin* categories; (**b**) two representative spiroligomers **105** from *pro4 (2S4S)* monomer and **106** from a variety of diamino acids with different stereochemistry and ring structure; (**c**) functionalized DKP formation by way of mixed anhydride **110**

structures, spiroligomers do not fold like flexible peptides and proteins [113–115]. A variety of diamino acids have been synthesized and assembled into spiroligomers having different sizes and shapes [116–121]. In addition, an effective method for DKP assembly was developed featuring formation of amino acid-mixed anhydrides (e.g., **110**) and acyl transfer. Spiroligomers made from such DKPs are highly functionalized, shape-programmable ladder molecules, on which functional group presentation is controlled by the sequence and stereochemistry of the component monomers.

The synthesis of α-helix peptidomimetics based on the *pro4*-DKP approach is analogous to peptide synthesis and may be extended to incorporate as many monomers as desired (Fig. 22a). For example, diamino acid **114** was combined with activated ester **115** and stirred at room temperature overnight to furnish two products observed by HPLC/MS to be consistent with amide and DKP intermediates (e.g., **111**–**113**, Fig. 21c). On addition of another equivalent of DIC to the

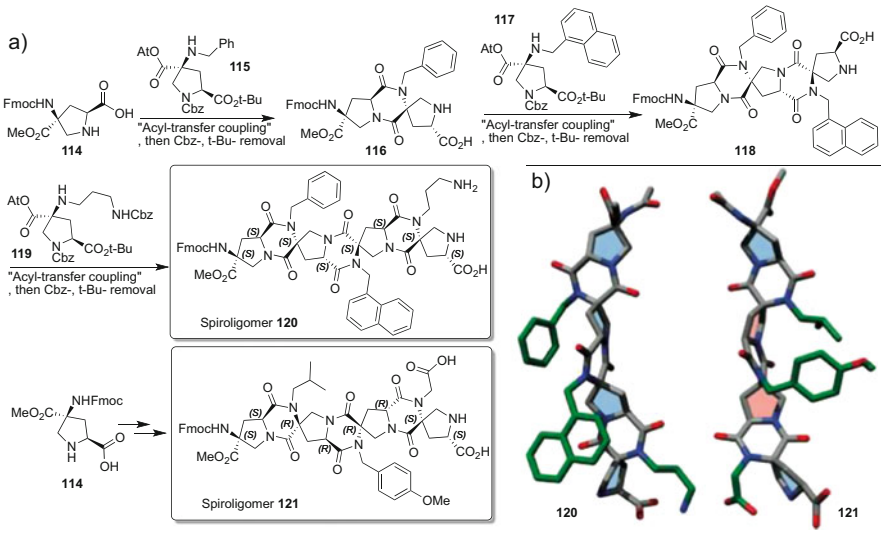

Fig. 22 (**a**) Solution-phase synthesis of spiroligomers **120** and **121**; (**b**) lowest energy conformers of **120** (*left*) and **121** (*right*) on which side chains project, respectively, in left- and right-handed helical orientations

reaction mixture, the amide was converted to DKP, which on removal of the Cbz- and *tert*-butyl protecting groups with HBr in acetic acid, gave amino acid **116** after purification by reverse-phase chromatography. Multiple repetitions of this DKP synthesis protocol afforded spiroligomers **120** and **121**.

The lowest energy conformers of spiroligomers **120** and **121** were analyzed by computation using the AMBER94 force field (Fig. 22b). Spiroligomer **120**, which was composed of all *pro4* monomers with *S*-stereochemistry, arranged to mimic a left-handed helical alignment with the side chains of residues i, $i+3$, and $i+6$ superimposed on the same helical face with a distance between each successive pair of functionalized amide nitrogen of 5.6 Å. By inverting the stereochemistry of the middle two *pro4* monomers in spiroligomer **121**, a right-handed helical structure was mimicked with the side chains of residues i, $i+4$, and $i+8$ superimposed on the same α-helical face.

The solid-phase synthesis of spiroligomers **133** and **134** was conducted on acid-stable HMBA resin (Fig. 23). Attachment of *Pro4* monomer **122** onto the resin featured esterification using MSNT and methylimidazole as base. Removal of the Boc and *tert*-butyl groups with 95% TFA in the presence of scavenger gave amino acid **123**, that was elongated by the general DKP synthesis procedure as described in solution. Acylation with activated ester (e.g., **124**) in the presence of DIPEA, followed by treatment with DIC/HOAt for 4 h gave the DKP, from which removal of the Cbz- and *tert*-butyl ester groups liberated the next amino acid for acyl-transfer coupling to diamino acid **125**. The chain was terminated by DKP formation with Boc-homophenylalanine **126** to give spiroligomer **127**. Formation of a final

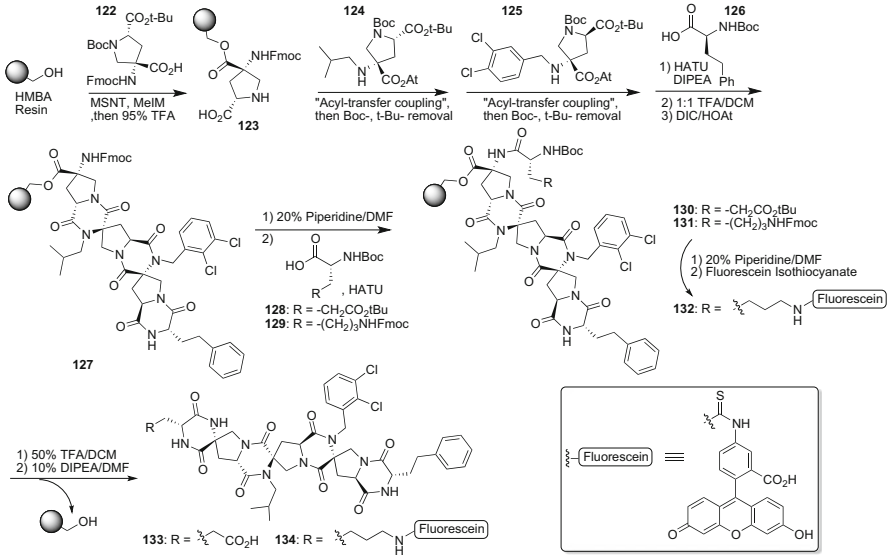

Fig. 23 Solid-phase synthesis of spiroligomers **133** and **134**

DKP residue with resin cleavage was then used to deliver the desired spiroligomers. After Fmoc removal using piperidine, the resin was split into two portions, that were respectively acylated with *tert*-butyl *N*-(Boc)glutamate **128** and ε-*N*-(Fmoc)-lysine **129** to produce resin-bound oligomers **130** and **131**. Removal of Fmoc group from **131** and treatment with fluorescein isothiocyanate yielded resin-bound oligomer **132**. Treatment of the resins **130** and **132** with TFA removed the Boc group, and DKP formation by nucleophilic resin cleavage in the presence of DIPEA gave respectively spiroligomers **133** and **134**.

Spiroligomers **133** and **134** were designed to disrupt the p53/hdm2 protein–protein interaction by mimicking the hydrophobic face of the α-helix of p53. A direct binding fluorescence polarization assay was used to measure the binding affinity to HDM2. Spiroligomers **134** exhibited a K_d of 0.4 μM and bound more tightly than the fluorescein derivative of natural p53 (0.62 μM). Notably, both the spiroligomer side chain composition and configuration influenced binding affinity. For example, changing the stereocenter of the terminal lysine residue, to which the fluorophore was attached, caused a 17-fold increase in affinity. Spiroligomer **134** was demonstrated to penetrate human cells by passive diffusion and stabilized HDM2 in a p53 mutant cell line culture. In spite of their size, spiroligomers with pre-organized conformation can thus penetrate cells, bind protein surfaces, and invoke biological responses.

4 Diketopiperazines Involved in Mimicking Enzyme Active Sites

2,5-Diketopiperazines are attractive platforms for orienting catalytic groups to mimic enzyme active sites as reviewed [3, 122–124]. In particular, DKPs have been used to catalyze cyanohydrin formation [125–129], Strecker [130, 131], Reformatsky [132] Michael addition [133], and Diels–Alder reactions [134]. Catalysis has also been explored using *pro4*-DKPs in spiroligomer scaffolds.

4.1 Scaffolds Containing One DKP

In 2012, our group developed a series of modified proline catalysts including a *pro4*-DKP fused catalyst that promoted the aldol reaction in water with high activity (down to 0.5 mol% catalyst loading) and selectivity (up to 98% *ee*) (Fig. 24a) [135]. The DKP-based catalyst **138** showed similar activity and selectivity as hydantoin catalyst **139**, which had been demonstrated to function by a specific hydrophobic interaction in water between an aromatic ring on the catalyst and the aldehyde substrate **136**. Catalysts (e.g., **138** and **139**) that favored this interaction were ~43 times faster than those (e.g., **140**) unable to make such contacts. Hydrophobic effects have been proposed to enhance the rate of the aldol reaction in water by other proline catalysts [136]. Quantum chemical calculations indicated a hydrophobic edge-to-face interaction stabilized transition state **139** relative to **140** by 2.6 kcal/mol, in excellent agreement with experimentally observed $\Delta\Delta G^{\neq}$ of 2.3 kcal/mol (Fig. 24b).

Mimicry of the enzyme ketosteroid isomerase by a catalytic *pro4*-DKP system was demonstrated by the acceleration of the Claisen rearrangement of ally ether **141** to phenol **142** (Fig. 25) [137]. In the catalyst design, a carboxylic acid and a phenol alcohol were positioned close to each other to donate hydrogen bonds to the substrate ether oxygen and stabilize the developing negative charge in the transition state. First-generation catalyst DKP **143** accelerated the reaction 11-fold relative to background. Rate acceleration dropped to twofold above background (similar to the

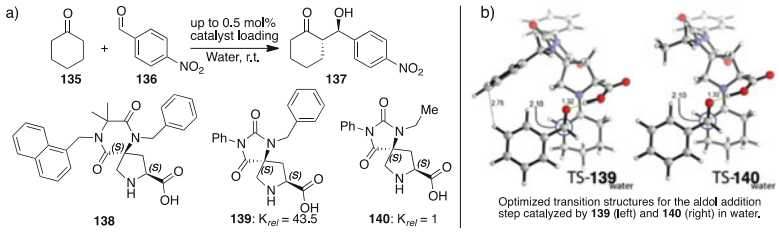

Fig. 24 (**a**) Aldol reaction catalyzed by DKP and hydantoin proline motifs in water; (**b**) quantum chemical calculations support a specific hydrophobic interaction for successful catalyst design

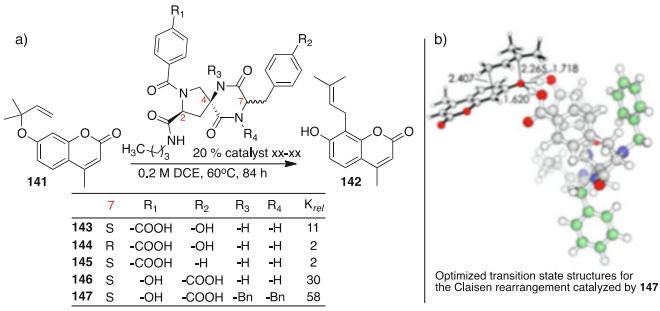

	7	R_1	R_2	R_3	R_4	K_{rel}
143	S	-COOH	-OH	-H	-H	11
144	R	-COOH	-OH	-H	-H	2
145	S	-COOH	-H	-H	-H	2
146	S	-OH	-COOH	-H	-H	30
147	S	-OH	-COOH	-Bn	-Bn	58

Fig. 25 (**a**) Claisen rearrangement accelerated by *pro4*-DKP catalysts; (**b**) optimized transition state with catalyst **147**

activity of benzoic acid alone) on inverting the seven-position stereocenter in DKP **144** and by removing the phenol alcohol in **145**, suggesting a dual activation process from accurate positioning of the catalytic groups in the transition state. Improved alignment of the alcohol and the carboxylic acid based on the theoretical design gave **146**, which increased the relative reaction rate to 30-fold over background. Considering that the carboxylic acid and phenol alcohol may simultaneously donate hydrogen bonds to the ether oxygen, we made a second generation of *N*-benzyl-DKP catalysts that exhibited increased activity. The combined quantum mechanical and molecular dynamic computational study of these systems suggested that the acceleration was due to an optimal disposition of the phenol and benzoic acid moieties in both the TS and the reactant complex. Among the *N*-benzyl-DKP catalysts, *N*,*N*-dibenzyl-DKP catalyst **147** exhibited the best activity giving a 58-fold acceleration relative to the background reaction, due in part to a lower activation barrier from pre-organization of both hydrogen donors in close proximity: ca. 94% of the time during the 1 μs MD simulation. In contrast to common N–H hydrogen bond donor catalysts composed of urea, thiourea, and guanidinium moieties, DKP catalysts such as **147** represent the first examples in which O–H hydrogen bond donors are used outside of biological systems, such as ketosteroid isomerase.

4.2 Scaffolds Containing Several DKPs

Spiroligomers **148**–**154** were studied in a design to arrange multiple functional groups to catalyze a transesterification reaction [138]. In enzymology, the catalytic Ser-His-Asp triad enhances the nucleophilicity of the hydroxyl group of the serine residue to attack acylating agents [139]. The histidine residue is proposed to act as a general base, facilitate deprotonation, and enhance nucleophilicity of the serine hydroxyl group. The so-called charge relay system is terminated by neutralization of the resulting charge on the imidazole by the aspartate residue (Fig. 26a) [139].

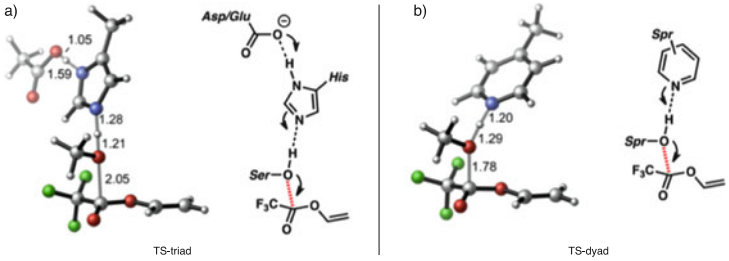

Fig. 26 Transition states for nucleophilic addition to vinyl trifluoroacetate by a model Ser-His-Asp/Glu triad (**a**) and pyridine–alcohol dyad (**b**)

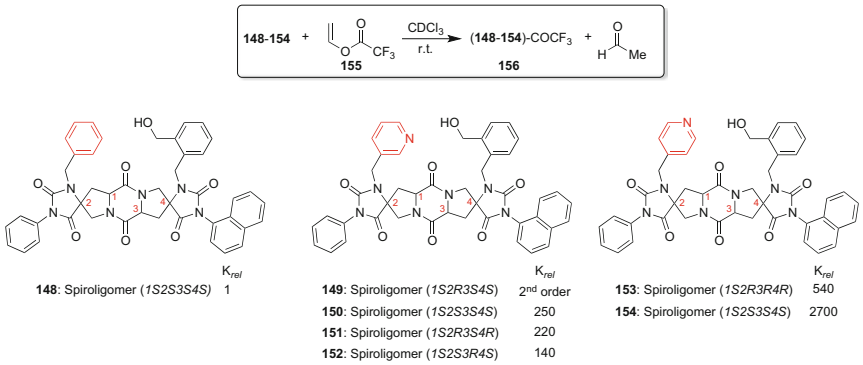

Fig. 27 Nucleophilic enhancement of the alcohol on spiroligomers **148–154**

X-ray analysis of the triad in proteases, such as subtilisin, has revealed that an oxy-anion hole in the active site stabilizes the resulting negative charge formed on the substrate ester carbonyl oxygen in the tetrahedral intermediate [140]. Quantum mechanical calculations have suggested that the carboxylate–imidazole pair in the triad may be replaced with a simpler pyridine to lower the activation barrier of the acyl transfer reaction in the catalytic mechanism (Fig. 26b) [138].

In spiroligomers **148–154**, enhancement of the nucleophilicity was explored by placing an alcohol proximal to a pyridine group as a general base (Fig. 27). Esterification of vinyl trifluoroacetate **155** was monitored in kinetic experiments using ^{19}F NMR spectroscopy in the presence of spiroligomers **148–154**. Large differences in the activity of the alcohol were observed to be contingent on the spiroligomer stereochemistry and the point of attachment of the pyridine moiety. The orientation of the pyridine base to the alcohol nucleophile in **154** favored ten times faster acylation compared to **150** with a k_{rel} value of 2,700 over the background reaction.

With spiroligomer **154** as a catalyst, transesterification of vinyl trifluoroacetate was attempted in methanol, but only a slight rate enhancement was observed over background suggesting that an "oxy-anion hole" was necessary to stabilize the

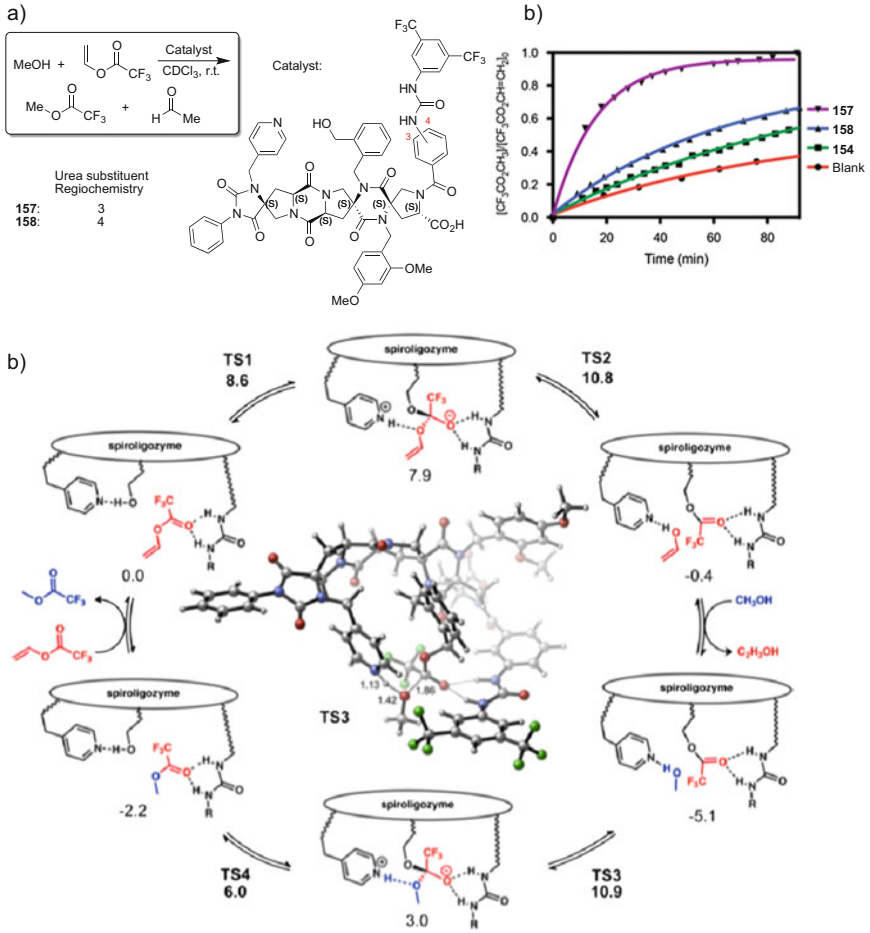

Fig. 28 (**a**) Spiroligozymes **157** and **158**; (**b**) kinetic experiments of transesterification catalyzed by **154**, **157**, and **158**; (**c**) energy profile for transesterification of vinyl trifluoroacetate catalyzed by **158**

transition state of the methanolysis reaction (Fig. 28a). Trifunctional spiroligomers **157** and **158** were thus synthesized using a third *pro4* building block to display a urea as a potential hydrogen bond donor (Fig. 28a).

Both catalysts **157** and **158** accelerated transesterification relative to the reaction catalyzed by spiroligomer **154** and the background reaction (Fig. 28a). Calculation of second-order rate constants revealed a 2200-fold rate enhancement for k_1 (acylation of spiroligomer) and 130-fold acceleration of k_2 (deacylation of trifluoroacyl–spiroligomer complex) compared to the background reaction. The calculated energy of each stationary point along the transesterification pathway demonstrated that spiroligomers were able to position catalytic arrays for effective catalysis. Pre-organization and reorganization of the conformation of the catalytic groups

maintained optimal transition-state stabilization along the reaction pathway in a way that mimicked the active sites of natural esterases (Fig. 28b).

5 Conclusion

2,5-Diketopiperazines have served effectively to rigidify peptide conformation and orient hydrogen bonds in various scaffolds that mimic particular secondary structures: α-, β-, and γ-turns and β-hairpins. The non-covalent interactions of DKPs have also been used to assemble well-ordered supramolecular structures. The linkage of multiple DKP analogs has been applied to stabilize larger secondary structures such as β-helices. Moreover, the integration of DKPs in spiroligomers has provided effective means for arranging functional groups in specific orientations on shape-persistent and programmable backbones. Assembled like peptides by iterative methods that have been adopted to solid-phase chemistry, the spiroligomers represent a promising motif for the construction of larger protein-like surfaces for versatile applications. For example, spiroligomer mimics of α-helices that exhibit membrane permeability have demonstrated promising utility for inhibiting protein–protein interactions in cells. Catalytic DKPs have demonstrated utility for accelerating various reactions. Moreover, the introduction of spiroligomers bearing multiple reactive groups has illustrated their promise for enzyme active site mimicry. Considering advances in synthetic methodology for their construction by both solution- and solid-phase methods, the future employment of DKPs in the mimicry of peptides and proteins, as well as in applications in two-dimensional supramolecular structures, offers promise for novel innovations in various fields including medicine, catalysis, and material science.

References

1. Creighton T (1993) In: Proteins structures and molecular properties. W.H. Freeman, New York
2. Trabocchi A, Guarna A (2014) In: Peptidomimetics in organic and medicinal chemistry: the art of transforming peptides in drugs. Wiley, Hoboken
3. Borthwick AD (2012) Chem Rev 112:3641–3716
4. Cornacchia C, Cacciatore I, Baldassarre L, Mollica A, Feliciani F, Pinnen F (2012) Mini-Rev Med Chem 12:2–12
5. Martins MB, Carvalho I (2007) Tetrahedron 63:9923–9932
6. De Carvalho MP, Abraham W-R (2012) Curr Med Chem 19:3564–3577
7. Koopmanschap G, Ruijter E, Orru RVA (2014) Beilstein J Org Chem 10:544–598
8. Ressurreição ASM, Delatouche R, Gennari C, Piarulli U (2011) Eur J Org Chem 2011:217–228
9. Rose GD, Gierasch LM, Smith JA (1985) In: Advances in protein chemistry. Academic, Orlando
10. Kim H-O, Nakanishi H, Lee MS, Kahn M (2000) Org Lett 2:301–302

11. Golebiowski A, Jozwik J, Klopfenstein SR, Colson A-O, Grieb AL, Russell AF, Rastogi VL, Diven CF, Portlock DE, Chen JJ (2002) J Comb Chem 4:584–590
12. Golebiowski A, Klopfenstein SR, Chen JJ, Shao X (2000) Tetrahedron Lett 41:4841–4844
13. Golebiowski A, Klopfenstein SR, Shao X, Chen JJ, Colson A-O, Grieb AL, Russell AF (2000) Org Lett 2:2615–2617
14. Liu J, Brahimi F, Saragovi HU, Burgess K (2010) J Med Chem 53:5044–5048
15. Davies JS, Stelmach-Diddams M, Fromentin R, Howells A, Cotton R (2000) J Chem Soc Perkin Trans 1:239–243
16. Ressurreição ASM, Bordessa A, Civera M, Belvisi L, Gennari C, Piarulli U (2007) J Org Chem 73:652–660
17. Marchini M, Mingozzi M, Colombo R, Gennari C, Durini M, Piarulli U (2010) Tetrahedron 66:9528–9531
18. Vahdati L, Fanelli R, Bernadat G, Correia I, Lequin O, Ongeri S, Piarulli U (2015) Synthesis and conformational studies of a stable peptidomimetic β-hairpin based on a bifunctional diketopiperazine turn inducer. New J Chem 39:3250–3258. doi:10.1039/C4NJ01437E
19. Bannwarth L, Kessler A, Pèthe S, Collinet B, Merabet N, Boggetto N, Sicsic S, Reboud-Ravaux M, Ongeri S (2006) J Med Chem 49:4657–4664
20. Nowick JS, Chung DM, Maitra K, Maitra S, Stigers KD, Sun Y (2000) J Am Chem Soc 122:7654–7661
21. Vidu A, Dufau L, Bannwarth L, Soulier J-L, Sicsic S, Piarulli U, Reboud-Ravaux M, Ongeri S (2010) ChemMedChem 5:1899–1906
22. Gellerman G, Hazan E, Brider T, Traube T, Albeck A, Shatzmiler S (2008) Int J Pept Res Ther 14:183–192
23. Gellerman G, Hazan E, Kovaliov M, Albeck A, Shatzmiler S (2009) Tetrahedron 65:1389–1396
24. Brown ZZ, Schafmeister CE (2008) J Am Chem Soc 130:14382–14383
25. Dufour E, Moni L, Bonnat L, Chierici S, Garcia J (2014) Org Biomol Chem 12:4964–4974
26. Wennemers H, Conza M, Nold M, Krattiger P (2001) Chem Eur J 7:3342–3347
27. Conza M, Wennemers H (2002) J Org Chem 67:2696–2698
28. Krattiger P, Wennemers H (2005) Synlett 2005:706–708
29. Loergen JW, Kreutz C, Bargon J, Krattiger P, Wennemers H (2005) Sens Actuators B 107:366–371
30. Faul CFJ, Krattiger P, Smarsly BM, Wennemers H (2008) J Mater Chem 18:2962–2967
31. Wennemers H, Nold MC, Conza MM, Kulicke KJ, Neuburger M (2003) Chem Eur J 9:442–448
32. Bernard J, Wennemers H (2007) Org Lett 9:4283–4286
33. Beeli R, Steger M, Linden A, Robinson JA (1996) Helv Chim Acta 79:2235–2248
34. Bisang C, Jiang L, Freund E, Emery F, Bauch C, Matile H, Pluschke G, Robinson JA (1998) J Am Chem Soc 120:7439–7449
35. Bisang C, Weber C, Robinson JA (1996) Helv Chim Acta 79:1825–1842
36. Pfeifer ME, Robinson JA (1998) Chem Commun 1998:1977–1978
37. Emery F, Bisang C, Favre M, Jiang L, Robinson JA (1996) Chem Commun 2155–2156
38. Moreno R, Jiang L, Moehle K, Zurbriggen R, Glück R, Robinson JA, Pluschke G (2001) ChemBioChem 2:838–843
39. Pfeifer ME, Linden A, Robinson JA (1997) Helv Chim Acta 80:1513–1527
40. Pfeifer ME, Moehle K, Linden A, Robinson JA (2000) Helv Chim Acta 83:444–464
41. Royo M, Van Den Nest W, del Fresno M, Frieden A, Yahalom D, Rosenblatt M, Chorev M, Albericio F (2001) Tetrahedron Lett 42:7387–7391
42. da Ressurreição ASM, Vidu A, Civera M, Belvisi L, Potenza D, Manzoni L, Ongeri S, Gennari C, Piarulli U (2009) Chem Eur J 15:12184–12188
43. Marchini M, Mingozzi M, Colombo R, Guzzetti I, Belvisi L, Vasile F, Potenza D, Piarulli U, Arosio D, Gennari C (2012) Chem Eur J 18:6195–6207

44. Fanelli R, Schembri L, Piarulli U, Pinoli M, Rasini E, Paolillo M, Galiazzo M, Cosentino M, Marino F (2014) Vascular Cell 6:11
45. Artymiuk PJ, Blake CCF (1981) J Mol Biol 152:737–762
46. Nataraj DV, Srinivasan N, Sowdhamini R, Ramakrishnan C (1995) Curr Sci 69:434–446
47. Hoang HN, Driver RW, Beyer RL, Malde AK, Le GT, Abbenante G, Mark AE, Fairlie DP (2011) Angew Chem Int Ed 50:11107–11111
48. Krishna Y, Sharma S, Ampapathi RS, Koley D (2014) Org Lett 16:2084–2087
49. Airaghi F, Fiorati A, Lesma G, Musolino M, Sacchetti A, Silvani A (2013) Beilstein J Org Chem 9:147–154
50. Simon RJ, Kania RS, Zuckermann RN, Huebner VD, Jewell DA, Banville S, Ng S, Wang L, Rosenberg S, Marlowe CK (1992) Proc Natl Acad Sci U S A 89:9367–9371
51. Sui Q, Borchardt D, Rabenstein DL (2007) J Am Chem Soc 129:12042–12048
52. Kirshenbaum K, Barron AE, Goldsmith RA, Armand P, Bradley EK, Truong KTV, Dill KA, Cohen FE, Zuckermann RN (1998) Proc Natl Acad Sci U S A 95:4303–4308
53. Wu CW, Sanborn TJ, Zuckermann RN, Barron AE (2001) J Am Chem Soc 123:2958–2963
54. Gorske BC, Bastian BL, Geske GD, Blackwell HE (2007) J Am Chem Soc 129:8928–8929
55. Holub JM, Jang H, Kirshenbaum K (2007) Org Lett 9:3275–3278
56. Shin SBY, Yoo B, Todaro LJ, Kirshenbaum K (2007) J Am Chem Soc 129:3218–3225
57. Vercillo OE, Andrade CKZ, Wessjohann LA (2007) Org Lett 10:205–208
58. Moure A, Sanclimens G, Bujons J, Masip I, Alvarez-Larena A, Pérez-Payá E, Alfonso I, Messeguer A (2011) Chem Eur J 17:7927–7939
59. Moure A, Orzáez M, Sancho M, Messeguer A (2012) Bioorg Med Chem Lett 22:7097–7099
60. Suwal S, Kodadek T (2014) Org Biomol Chem 12:5831–5834
61. Zhu Y, Tang M, Shi X, Zhao Y (2007) Int J Quantum Chem 107:745–753
62. Bettens FL, Bettens RPA, Brown RD, Godfrey PD (2000) J Am Chem Soc 122:5856–5860
63. Hirst JD, Persson BJ, Phys J (1998) Chem A 102:7519–7524
64. Mendham AP, Dines TJ, Snowden MJ, Chowdhry BZ, Withnall R (2009) J Raman Spectrosc 40:1478–1497
65. Mendham AP, Dines TJ, Snowden MJ, Withnall R, Chowdhry BZ (2009) J Raman Spectrosc 40:1508–1520
66. Mendham AP, Palmer RA, Potter BS, Dines TJ, Snowden MJ, Withnall R, Chowdhry BZ (2010) J Raman Spectrosc 41:288–302
67. Mendham AP, Potter BS, Palmer RA, Dines TJ, Mitchell JC, Withnall R, Chowdhry BZ (2010) J Raman Spectrosc 41:148–159
68. MacDonald JC, Whitesides GM (1994) Chem Rev 94:2383–2420
69. de Meijere A, Kozhushkov SI, Schill H (2006) Chem Rev 106:4926–4996
70. Brackmann F, de Meijere A (2007) Chem Rev 107:4493–4537
71. Burrows A (2004) In: Mingos DM (ed) Crystal engineering using multiple hydrogen bonds, vol 108. Springer, Berlin Heidelberg, pp 55–96
72. Williams LJ, Jagadish B, Lansdown MG, Carducci MD, Mash EA (1999) Tetrahedron 55:14301–14322
73. Williams LJ, Jagadish B, Lyon SR, Kloster RA, Carducci MD, Mash EA (1999) Tetrahedron 55:14281–14300
74. Weatherhead-Kloster RA, Selby HD, Miller WB, Mash EA (2005) J Org Chem 70:8693–8702
75. Ntirampebura D, Jagadish B, Nichol GS, Carducci MD, Dawson A, Rajapakshe A, Oliver AG, Clegg W, Harrington RW, Layne L, Margolis JI, Mash EA (2008) Cryst Growth Des 8:3257–3270
76. Wells KE, Weatherhead RA, Murigi FN, Nichol GS, Carducci MD, Selby HD, Mash EA (2012) Cryst Growth Des 12:5056–5068
77. Mash EA (2014) CrystEngComm 16:8620–8637
78. Joshi KB, Verma S (2008) Tetrahedron Lett 49:4231–4234

79. Govindaraju T, Pandeeswar M, Jayaramulu K, Jaipuria G, Atreya HS (2011) Supramol Chem 23:487–492
80. Manchineella S, Govindaraju T (2012) RSC Adv 2:5539–5542
81. Xie Z, Zhang A, Ye L, Feng Z-g (2009) Soft Matter 5:1474–1482
82. Manchineella S, Prathyusha V, Priyakumar UD, Govindaraju T (2013) Chem Eur J 19:16615–16624
83. Appella DH, Christianson LA, Karle IL, Powell DR, Gellman SH (1996) J Am Chem Soc 118:13071–13072
84. Cheng RP, Gellman SH, DeGrado WF (2001) Chem Rev 101:3219–3232
85. Zuckermann RN, Kerr JM, Kent SBH, Moos WH (1992) J Am Chem Soc 114:10646–10647
86. Carsten B, Robert G, Hans-Jörg H (2006) Phys Biol 3:S1
87. Orner BP, Ernst JT, Hamilton AD (2001) J Am Chem Soc 123:5382–5383
88. Hamuro Y, Geib SJ, Hamilton AD (1996) J Am Chem Soc 118:7529–7541
89. Hamuro Y, Geib SJ, Hamilton AD (1997) J Am Chem Soc 119:10587–10593
90. Seebach D, Beck AK, Bierbaum DJ (2004) Chem Biodiv 1:1111–1239
91. Löser R, Frizler M, Schilling K, Gütschow M (2008) Angew Chem Int Ed 47:4331–4334
92. Violette A, Averlant-Petit MC, Semetey V, Hemmerlin C, Casimir R, Graff R, Marraud M, Briand J-P, Rognan D, Guichard G (2005) J Am Chem Soc 127:2156–2164
93. Fischer L, Didierjean C, Jolibois F, Semetey V, Manuel Lozano J, Briand J-P, Marraud M, Poteau R, Guichard G (2008) Org Biomol Chem 6:2596–2610
94. Di Blasio B, Pavone V, Saviano M, Lombardi A, Nastri F, Pedone C, Benedetti E, Crisma M, Anzolin M, Toniolo C (1992) J Am Chem Soc 114:6273–6278
95. Ségalas I, Prigent Y, Davoust D, Bodo B, Rebuffat S (1999) Biopolymers 50:71–85
96. Karle IL, Flippen-Anderson J, Sukumar M, Balaram P (1987) Proc Natl Acad Sci U S A 84:5087–5091
97. Delatouche R, Durini M, Civera M, Belvisi L, Piarulli U (2010) Tetrahedron Lett 51:4278–4280
98. Jayatunga MKP, Thompson S, Hamilton AD (2014) Bioorg Med Chem Lett 24:717–724
99. Bullock BN, Jochim AL, Arora PS (2011) J Am Chem Soc 133:14220–14223
100. Murray JK, Farooqi B, Sadowsky JD, Scalf M, Freund WA, Smith LM, Chen J, Gellman SH (2005) J Am Chem Soc 127:13271–13280
101. Hara T, Durell SR, Myers MC, Appella DH (2006) J Am Chem Soc 128:1995–2004
102. Wu CW, Kirshenbaum K, Sanborn TJ, Patch JA, Huang K, Dill KA, Zuckermann RN, Barron AE (2003) J Am Chem Soc 125:13525–13530
103. Yin H, Lee G-i, Park HS, Payne GA, Rodriguez JM, Sebti SM, Hamilton AD (2005) Angew Chem Int Ed 44:2704–2707
104. Kolomiets E, Berl V, Lehn J-M (2007) Chem Eur J 13:5466–5479
105. Hill DJ, Mio MJ, Prince RB, Hughes TS, Moore JS (2001) Chem Rev 101:3893–4012
106. Crisma M, Formaggio F, Moretto A, Toniolo C (2006) Pept Sci 84:3–12
107. Bao C, Kauffmann B, Gan Q, Srinivas K, Jiang H, Huc I (2008) Angew Chem Int Ed 47:4153–4156
108. Wolffs M, Delsuc N, Veldman D, Anh NV, Williams RM, Meskers SCJ, Janssen RAJ, Huc I, Schenning APHJ (2009) J Am Chem Soc 131:4819–4829
109. Brown ZZ, Schafmeister CE (2010) Org Lett 12:1436–1439
110. Brown ZZ, Akula K, Arzumanyan A, Alleva J, Jackson M, Bichenkov E, Sheffield JB, Feitelson MA, Schafmeister CE (2012) PLoS One 7, e45948
111. Schafmeister CE, Brown ZZ, Gupta S (2008) Acc Chem Res 41:1387–1398
112. Levins CG, Schafmeister CE (2005) J Org Chem 70:9002–9008
113. Pornsuwan S, Bird G, Schafmeister CE, Saxena S (2006) J Am Chem Soc 128:3876–3877
114. Pornsuwan S, Schafmeister CE, Saxena S, Phys J (2008) Chem C 112:1377–1384
115. Bird GH, Pornsuwan S, Saxena S, Schafmeister CE (2008) ACS Nano 2:1857–1864
116. Levins CG, Schafmeister CE (2003) J Am Chem Soc 125:4702–4703
117. Gupta S, Das BC, Schafmeister CE (2005) Org Lett 7:2861–2864

118. Habay SA, Schafmeister CE (2004) Org Lett 6:3369–3371
119. Levins CG, Brown ZZ, Schafmeister CE (2006) Org Lett 8:2807–2810
120. Gupta S, Macala M, Schafmeister CE (2006) J Org Chem 71:8691–8695
121. Gupta S, Schafmeister CE (2009) J Org Chem 74:3652–3658
122. Davie EAC, Mennen SM, Xu Y, Miller SJ (2007) Chem Rev 107:5759–5812
123. Giacalone F, Gruttadauria M, Agrigento P, Noto R (2012) Chem Soc Rev 41:2406–2447
124. Jarvo ER, Miller SJ (2002) Tetrahedron 58:2481–2495
125. Schoenebeck F, Houk KN (2009) J Org Chem 74:1464–1472
126. Oku J-I, Inoue S (1981) J Chem Soc Chem Comm 229–230
127. Shvo Y, Gal M, Becker Y, Elgavi A (1996) Tetrahedron Asymmetry 7:911–924
128. Tanaka K, Mori A, Inoue S (1990) J Org Chem 55:181–185
129. Danda H (1991) Synlett 1991:263–264
130. Becker C, Hoben C, Schollmeyer D, Scherr G, Kunz H (2005) Eur J Org Chem 2005:1497–1499
131. Iyer MS, Gigstad KM, Namdev ND, Lipton M (1996) J Am Chem Soc 118:4910–4911
132. Wang Z, Shen J, Jiang C, You T (2000) Chin Chem Lett 11:659
133. Durini M, Sahr FA, Kuhn M, Civera M, Gennari C, Piarulli U (2011) Eur J Org Chem 2011:5599–5607
134. Furutani M, Sakamoto S, Kudo K (2009) Heterocycles 78:1171–1176
135. Zhao Q, Lam Y-h, Kheirabadi M, Xu C, Houk KN, Schafmeister CE (2012) J Org Chem 77:4784–4792
136. Giacalone F, Gruttadauria M, Agrigento P, Lo Meo P, Noto R (2010) Eur J Org Chem 2010:5696–5704
137. Parker MFL, Osuna S, Bollot G, Vaddypally S, Zdilla MJ, Houk KN, Schafmeister CE (2014) J Am Chem Soc 136:3817–3827
138. Kheirabadi M, Çelebi-Ölçüm N, Parker MFL, Zhao Q, Kiss G, Houk KN, Schafmeister CE (2012) J Am Chem Soc 134:18345–18353
139. Hedstrom L (2002) Chem Rev 102:4501–4524
140. Katona G, Wilmouth RC, Wright PA, Berglund GI, Hajdu J, Neutze R, Schofield CJ (2002) J Biol Chem 277:21962–21970

Top Heterocycl Chem (2017) 49: 81–104
DOI: 10.1007/7081_2015_190

Published online: 12 January 2016

Synthesis of Constrained Peptidomimetics via the Pictet-Spengler Reaction

Rico G. Petersen, Vitaly V. Komnatnyy, and Thomas E. Nielsen

Abstract Peptidomimetics offers a solution to the poor pharmacokinetic properties displayed by natural peptides, by providing pharmaceutically useful chemical structures with the ability to mimic the endogenous polyamide structure. This chapter gives an overview of the past decade's developments in the field of Pictet-Spengler reactions for the synthesis of peptidomimetics, with an emphasis on the applications of constrained heterocycles in mimicry of peptide geometry and biology.

Keywords Drug discovery • Peptidomimetics • Pictet-Spengler reaction

Contents

R.G. Petersen and V.V. Komnatnyy
Department of Chemistry, Technical University of Denmark, Kemitorvet, Building 207, 2800 Kgs. Lyngby, Denmark

T.E. Nielsen (✉)
Protein and Peptide Chemistry, Novo Nordisk A/S, Novo Nordisk Park, 2760 Maaloev, Denmark
e-mail: tedn@novonordisk.com

1 Introduction

1.1 Peptidomimetics

Proteins and peptides exert a plethora of important functions in living organisms. For example, protein scaffolds (e.g., histones) and catalysts (e.g., RNA polymerase) are key components involved in the preservation, transcription, and translation of genetic material [1–3]. The healing of damaged tissue involves complex interplay of enzyme activation and protein-protein interactions toward the formation of fibrin clots to stop bleeding [4]. The actions of dynamic proteins, such as G-protein-coupled receptors [5] and ion channels [6], are responsible for cellular interactions with the environment. The relatively smaller peptides function as agonists, antagonists, substrates, inhibitors, and hormones (e.g., somatostatin, substance P, and angiotensin) and play many roles in numerous physiological processes (e.g., neurotransmission and neuromodulation), including those tightly associated with disease [7].

Peptide sequences embedded in larger proteins adopt typically ordered secondary structures, the most important being α-helices, β-sheets, and β-turns. Secondary structures, such as β-turns, are further categorized according to subtle differences in their backbone ϕ, ψ, and ω dihedral angles [8]. Although the α-helix is the most abundant secondary structure [9], β- and γ-turns are particularly attractive targets for peptide mimicry, because they appear frequently as recognition motifs in biochemical processes [10].

Structurally diverse and physiologically safe peptides are routinely developed by means of iterative rounds of solid-phase synthesis and biological testing to characterize structure-activity relationships for modulating pharmacologically relevant targets. Peptides are thus attractive molecular scaffolds in the hunt for new drugs. Peptides display however properties, such as poor bioavailability and low metabolic stability due to the nature of the polymeric amino acid structure [11]. Amphiphilic, high-molecular-weight peptides are often poorly absorbed through the intestinal mucosa and easily excreted through the liver and kidneys. Furthermore, peptide bonds are targets for proteases in the gastrointestinal tract and in serum. These factors render the biological half-life of peptides in the human body relatively short. In addition, small peptides do not typically fold into rigid secondary structures but remain more flexible. Small peptides may thus serve as ligands for multiple receptors and enzymes, because they adopt numerous conformations. Their lack of selectivity against a given target may translate into adverse side effects in a therapeutic context. Synthetically tractable peptidomimetics that contain modified amino acids or completely lack the polymeric amino acid structure may be superior molecules for the development of therapeutic agents, because of their capacity to retain the biological activity of the native peptide without the drawbacks of metabolic instability and poor bioavailability [12–15].

Structural knowledge of the peptide or protein and its target is valuable in the rational design of peptidomimetics and may be obtained from X-ray and NMR

spectroscopic analysis. Alternatively, knowledge obtained from the amino acid sequence of the endogenous peptide may be used to develop a mimic. For example, investigation of the lead peptide may begin by performing an "alanine" scan in which solid-phase peptide synthesis is systematically performed to replace discrete amino acid residues sequentially with alanine [16]. The importance of side chains for activity may then be ascertained by analysis of the bioactivity of the resulting alanine analogs. Moreover, the relevance of side-chain functional groups and orientation for bioactivity may be assessed by systematic substitutions of amino acid residues with surrogates possessing alternative charge, hydrophobicity, stereochemistry, and ability to form non-covalent interactions [17]. The minimal sequence required for biological activity may similarly be accessed using analogs from abridgment of the different ends of the peptide chain. With the active sequence in hand, steps toward peptidomimetic design entail usually the determination of the active conformation employing amino acids that restrain the backbone geometry, such as substituted prolines, aminolactams, azabicycloalkanone amino acids, α,α-dialkylglycines, *N*-alkyl, and α,β-unsaturated amino acids [18, 19]. Examination of the orientation of the side chain with respect to the backbone has also been accomplished using amino acids possessing β-substituents that restrict the χ-dihedral angle [20, 21]. Metabolically labile amides may be replaced with isosteric groups, such as hydroxyethylene ($CH(OH)CH_2$), *E*-alkene (CH=CH), and reduced amide (CH_2NH) moieties [22]. Alternatively, strategies involving β-amino acid [23], *N*-alkylglycine (peptoid) [24], and retro-inverso analogs [25] may be employed to confer increased resistance toward protease activity. In sum, a variety of methods have been used to convert peptide leads into peptidomimetics.

Natural products represent an alternative source of molecules that exhibit peptidomimetic activity. The drug morphine, which was isolated from the poppy over two centuries ago, may be considered the grandfather of peptidomimetics, because of its capacity to exhibit analgesic activity similar to the natural peptide enkephalin by binding and exhibiting agonist potency ($ED_{50} = 3.0$ nM) at the μ opioid receptor subtype [26, 27]. The antibiotic penicillin may likely mimic the D-Ala-D-Ala dipeptide when inhibiting the cross-linking of peptidoglycan by transpeptidase enzymes during bacterial cell wall synthesis [28, 29]. Furthermore, the immunosuppressant Rapamycin mimics proline-containing peptide substrates when inhibiting the peptidyl-prolyl *cis-trans*-isomerase, FKB12 protein [30, 31]. In addition, natural products that mimic peptides may display improved pharmacokinetic properties, including enhanced oral bioavailability and metabolic stability.

1.2 The Pictet-Spengler Reaction

The synthesis of tetrahydroisoquinoline analogs by condensation of 2-phenylethylamine derivatives (e.g., **1**) and dimethoxymethane on heating in concentrated aqueous hydrochloric acid was first reported by Amé Pictet and Theodor Spengler in 1911 (Scheme 1) [32].

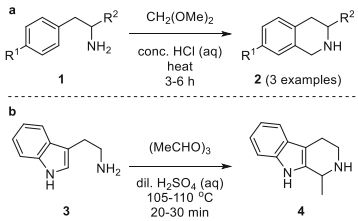

Scheme 1 Representative early examples of Pictet-Spengler reactions: (**a**) 2-phenylethylamine derivatives with dimethoxymethane was reported by Pictet and Spengler [32]; (**b**) tryptamine with paraldehyde by Tatsui [34]

The reaction is believed to proceed by a 6-*endo-trig* cyclization featuring intramolecular electrophilic aromatic substitution of an iminium ion intermediate [33]. In the original report, Pictet and Spengler employed three different substrates (2-phenylethylamine, Phe, and Tyr) obtaining tetrahydroisoquinolines **2** with higher yields for the amino acids. Subsequently in 1928, Goro Tatsui reacted tryptamine (**3**) with paraldehyde (the trimer of acetaldehyde) in dilute aqueous sulfuric acid to obtain tetrahydro-β-carboline **4** [34]. The mechanism of the Pictet-Spengler reaction with tryptamine is commonly assumed to occur by way of attack of the indole 3-position onto the iminium ion to provide a spirocyclic intermediate that undergoes 1,2-rearrangement and ring expansion to the fused ring system [35]. Electron-rich aromatic systems were soon found to give product under milder conditions. For example, tryptophan condensed with formaldehyde under physiological conditions to give after 4 days 1,2,3,4-tetrahydroisoquinoline-3-carboxylic acid (Tic) [36, 37]. Moreover, the enzyme strictosidine synthase (STR) has been characterized as the first Pictet-Spenglerase and shown to catalyze the Pictet-Spengler reaction of tryptamine with secologanin to give 3α(*S*)-strictosidine, a central intermediate in the biosynthesis of many indole alkaloids, such as vindoline [38–42]. In contrast to STR, which is specific for tryptamine substrates [43, 44], the Pictet-Spenglerase norcoclaurine synthase (NCS) requires the 3-hydroxy substituent on the aromatic ring of dopamine to catalyze condensations, such as that with 4-hydroxyphenylacetaldehyde to give (*S*)-norcoclaurine, a precursor for the biosynthesis of (*S*)-reticulin and morphine [45–51]. Complementing the plant-derived enzymes, a fungal Pictet-Spenglerase (FPS) was found to catalyze the reaction of 1-methyl-Trp with flavipin [52].

Pictet-Spengler reactions with aldehydes other than formaldehyde afford a new chiral center, which may be introduced stereoselectively with enzymes and other chiral catalysts [53, 54]. In 2004, Taylor and Jacobsen described the first enantioselective catalytic Pictet-Spengler reaction [55], employing *N*-acyliminium ions to increase reactivity during thiourea catalysis (Scheme 2a). Tryptamines (e.g., **5**) were treated with aldehyde to form the corresponding imines, activated by acylation with acetyl chloride, and reacted in the presence of thiourea catalyst **6** to produce tetrahydro-β-carbolines **7** in good yields and 86–95% enantiomeric purity.

Subsequently, enantioselectivity (32–92% ee) without acyl iminium ion formation was achieved using aromatic aldehydes, which were first condensed with

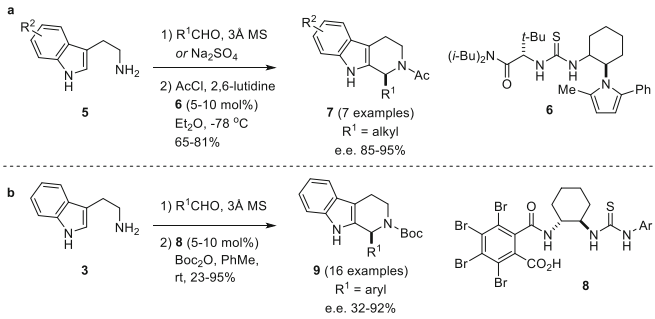

Scheme 2 Representative catalytic enantioselective Pictet–Spengler reactions: (**a**) chiral thiourea catalyzed *N*-acyliminium reaction by Taylor and Jacobsen [55]; (**b**) chiral Brønsted acid catalyzed iminium reaction [56]. *MS* molecular sieves, *Boc tert*-butoxycarbonyl

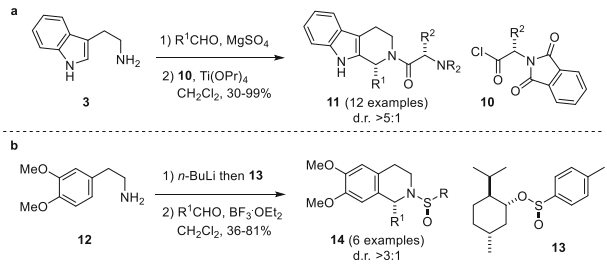

Scheme 3 Representative examples of Pictet–Spengler reactions using chiral auxiliaries: (**a**) reaction of *N*,*N*-phthaloyl-protected amino acid derivatives [57, 58]; (**b**) reaction of *N*-sulfinylated derivatives [59]

amine to form imine, and then reacted with Brønsted acid catalyst **8** with trapping of the fused piperidine product in situ with di-*tert*-butyl dicarbonate to afford tetrahydro-β-carbolines **9** in 23–95% yields (Scheme 2b) [56].

Chiral auxiliaries have been employed in diastereoselective Pictet-Spengler reactions. For example, preformed imines were activated with *N*,*N*-phthaloyl-protected amino acid chlorides (e.g., **10**) and catalytic titanium isopropoxide to provide tetrahydro-β-carbolines **11** with >5:1 diastereoselectivity (Scheme 3a) [57, 58]. The valine-derived chiral auxiliary was later removed reductively on treatment with lithium aluminum hydride. Sulfinylation with (1*R*,2*S*,5*R*)-menthyl-(*S*)-*p*-toluenesulfinate installed the sulfinyl chiral auxiliary on dopamine **12**, which underwent Pictet-Spengler reactions with aldehydes in the presence of boron trifluoride to provide tetrahydroisoquinolines **14** in 36–86% yields with >3:1 diastereoselectivity (Scheme 3b) [59]. The chiral auxiliary was removed by solvolysis with acid. The sulfinyl auxiliary has also been employed in the diastereoselective conversion of tryptamine into tetrahydro-β-carbolines [60].

Diastereoselective Pictet-Spengler reactions of α-amino acid derivatives proceed with varying degrees of chiral induction. For example, tryptophan-derived β-amino nitrile **15** reacted with different aldehydes to give tetrahydro-β-carbolines

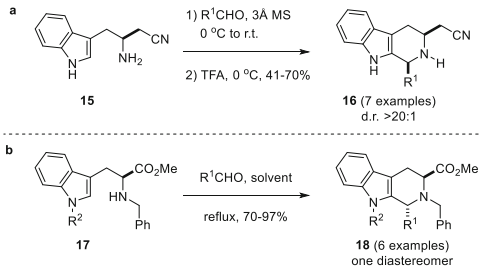

Scheme 4 Representative examples of diastereoselective Pictet–Spengler reactions: (**a**) reaction of beta-amino nitrile tryptophan derivatives [61]; (**b**) reaction of *N*-benzyl tryptophan derivatives [62, 63]. *MS* molecular sieves, *TFA* trifluoroacetic acid

16 with >20:1 diastereoselectivity in favor of the *cis*-diastereomer (Scheme 4a) [61]. *N*-Benzyl tryptophan methyl ester reacted with aldehydes in Pictet-Spengler reactions to exclusively give the *trans*-isomer of tetrahydro-β-carbolines **18** in >70% yields [62, 63]. The *N*-benzyl group was subsequently removed by catalytic hydrogenation.

2 Synthesis of Peptidomimetics via the Pictet-Spengler Reaction

2.1 Bi- and Tricyclic Peptidomimetics

The Pictet-Spengler reaction is well suited for the preparation of peptidomimetics, because constrained aromatic amino acids can be readily synthesized from their natural counterparts with stereocontrol: 1,2,3,4-tetrahydroisoquinoline-3-carboxylic acid (Tic) from Phe [64]; 7-hydroxy-1,2,3,4-tetrahydroisoquinoline-3-carboxylic acid (Htc) from Tyr [65]; 1,2,3,4-tetrahydro-β-carboline-3-carboxylic acid (Tcc) from Trp [66]; and spinacine (Spi) from His [67]. These conformationally rigid amino acids have been synthesized as discrete building blocks and incorporated into the peptide chains, as well as assembled directly on the peptide. They are useful for the development of peptidomimetics, because of their potential to: (1) improve metabolic stability by *N*-alkylation, (2) increase oral bioavailability by increasing lipophilicity, and (3) constrain the peptide into the active conformation. For example, the constrained phenylalanine derivative 1,2,3,4-tetrahydroisoquinoline-3-carboxylic acid (Tic, **19**) and its enantiomer have successfully been applied in the design of subtype (μ, δ) selective opioid receptor antagonists (Fig. 1). In particular, the μ-selective ($\mu/\delta = 7{,}770$) antagonist TCTP (**21**) was prepared from the potent ($IC_{50} = 3.7$ nM) μ-antagonist CTP (**20**) by replacement of the terminal D-Phe with D-Tic [68, 69]. The δ-selective ($\delta/\mu = 1{,}410$) antagonist TIPP (**23**) was prepared from the μ-selective ($\mu/\delta = 38$) agonist Tyr-D-Phe-$(Phe)_2$-NH_2 (**22**) by

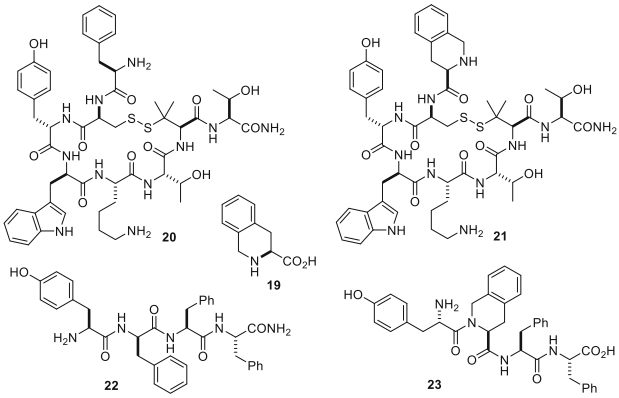

Fig. 1 Representative examples of peptides possessing 1,2,3,4-tetrahydroisoquinoline-3-carboxylic acid (Tic, **19**) residues

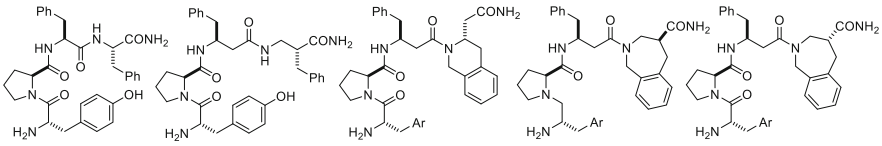

	EM 2	24	25	26*S*	26*R*
K_δ/K_μ	639	245	83	13	33
K_i (μ, nM)	5.3 ± 0.4	5.5 ± 0.18	20 ± 1.9	21 ± 1.4	14 ± 1.2

Fig. 2 Opioid μ-receptor selectivity (K_δ/K_μ) and affinity (K_i) of EM2, β^3hPhe/β^2hPhe analog **24**, and constrained analogs **25**, **26*R***, and **26*S*** [71]

exchanging D-Phe and the terminal carboxamide with Tic and carboxylate, respectively [70].

Pictet-Spengler reactions of formaldehyde with *N*-Cbz-β^2- and β^3-homophenylalanine methyl esters followed by hydrogenolytic cleavage of the carbamate protection have provided respectively methyl 2-(1,2,3,4-tetrahydroisoquinolin-3-yl)acetate (Tia) and methyl 2,3,4,5-tetrahydro-1*H*-benzo[c]azepine-4-carboxylate (Tbac), which were introduced into constrained analogs of endomorphin-2 (EM-2, Tyr-Pro-Phe-Phe-NH_2, Fig. 2) [71]. The parent peptide EM-2 exhibits high affinity and selectivity for the μ-relative to the δ- and κ-opioid receptor subtypes, but lacks oral availability and a long duration of action.

Constrained EM-2 analogs were synthesized containing the tetrahydroisoquinoline (e.g., **25**) and tetrahydrobenzo[c]azepine (e.g., **26*S*** and **26*R***) heterocycles and tested for affinity and selectivity toward opioid receptors expressed in Chinese hamster ovary cells, respectively, against [^{3}H]DPDPE (cyclo[D-Pen^2,D-Pen^5]-enkephalin and [^{3}H]DAMGO ([D-Ala^2,*N*-MePhe^4,Gly-ol^5]-enkephalin) as μ- and δ-subtype selective radio ligands. All three constrained analogs (**25**, **26*S***, and **26*R***) exhibited lower affinity and a loss of μ/δ selectivity relative to EM-2 and its non-constrained β-Phe counterpart **24** [71].

The Pictet-Spengler reaction has also been used in the synthesis of analogs of bioactive natural products that may be regarded as peptidomimetics, such as the

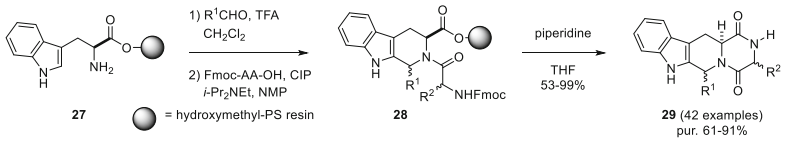

Scheme 5 Utilization of Pictet-Spengler reaction in the solid-phase synthesis of fumitremorgin-type diketopiperazines [65, 66]. *AA* amino acid, *CIP* 2-chloro-4,5-dihydro-1,3-dimethylimidazolium hexafluorophosphate, *NMP N*-methyl-2-pyrrolidone

fumitremorgin-type diketopiperazines [72, 73]. Employing a solid-phase approach, a 42-membered library of diastereomeric mixtures of fumitremorgin-type diketopiperazines was prepared from tryptophan resin **27**. Six different aldehydes were condensed with **27** to produce tetrahydro-β-carbolines (Scheme 5), each of which was coupled to seven different amino acids to provide dipeptides **28**. After Fmoc removal, cyclization of **28** to diketopiperazines with concomitant cleavage gave fumitremorgin analogs **29** in moderate to excellent overall yields and purity. After screening the library, several members were identified as selective inhibitors of breast cancer resistance protein that were devoid of the undesired effects exhibited by fumitremorgin C [74].

Turn mimics have been prepared by Pictet-Spengler reactions between various amino aldehydes and amino acids with aromatic side chains (e.g., Phe, Tyr, Trp, and His). The resulting heterocyclic amino acids may mimic the central residues of β-turn motifs in longer peptides to enhance biological activity and improve metabolic stability. Furthermore, the tetrahydroisoquinoline bicyclic framework is a common pharmacophore [75] and thus an intriguing motif for enhancing peptide properties.

β-Turn mimics **34*R*,*S*** and **37*R*,*S*** with capability of stabilizing a ten-membered hydrogen-bonded ring structure were, respectively, synthesized by Pictet-Spengler reactions of the phenylalanine derivatives **31** and **35** with *N*-Cbz-alaninal and 5% TFA in dichloromethane (Scheme 6) [76]. Conformational analysis of the individual diastereomers of **34** and **37** by computation, as well as NMR and IR spectroscopy, indicated that all of the four isomers were capable of adopting preferred turn conformations featuring ten-membered hydrogen bonds. Moreover, tetrahydroisoquinoline **37*S*** with the 1- and 3-position ring substituents in the *trans*-configuration was found to stabilize a second 14-membered hydrogen bond in a β-hairpin conformation (Scheme 6).

Type II′ β-turn mimics possessing pyrroloisoquinoline structures were synthesized by a route featuring the Pictet-Spengler reaction of L-DOPA **38** with aspartate β-aldehyde **39** using 5% TFA in dichloromethane (Scheme 7) [77]. Tetrahydroisoquinolines **40** were isolated as a 1:1 mixture of diastereomers, which on heating in toluene at reflux provided lactams **41** that were separated by chromatography on silica gel. After the exchange of the Cbz protection for an acetyl group, diastereomers **42*S*** and **42*R*** were, respectively, isolated in 31% and 30% overall yield from **38**.

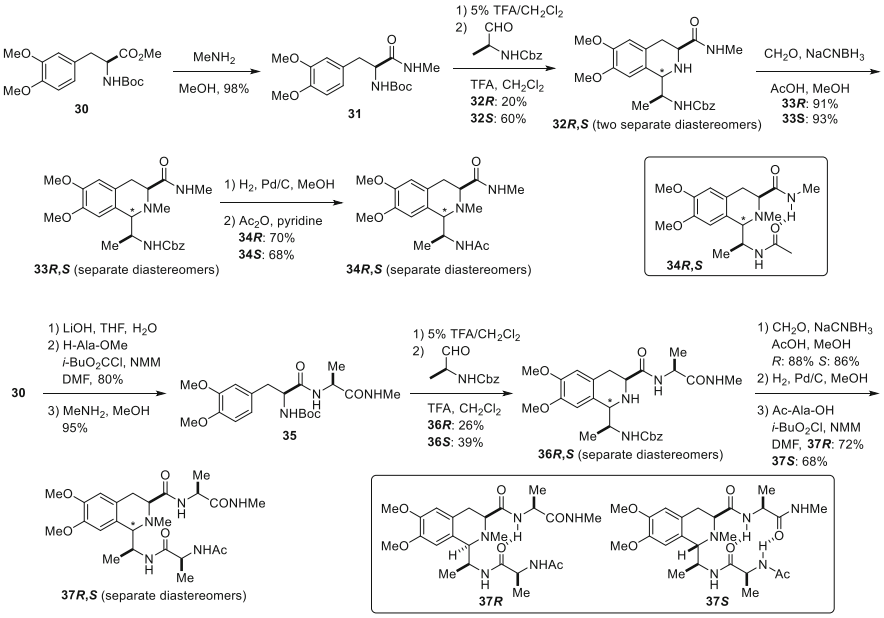

Scheme 6 Synthesis of tetrahydroisoquinoline turn mimetics [76]. *THF* tetrahydrofuran, *NMM* *N*-methylmorpholine, *DMF N*,*N*-dimethylformamide

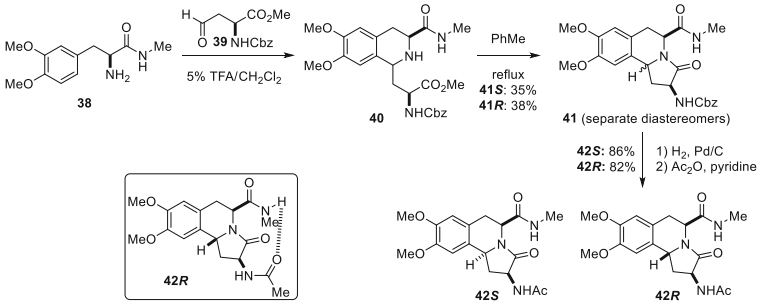

Scheme 7 Synthesis of pyrroloisoquinoline peptidomimetics **42*R*** and **42*S*** and hydrogen bonding of **42*R*** [77]. *Cbz* carboxybenzyl

Conformational analysis of pyrroloisoquinolines **42** using computation as well as NMR and IR spectroscopy indicated the convex isomer **42*R*** favored a type II′ β-turn. On the other hand, the convex isomer **42*S*** was suggested to prefer an inverse γ-turn structure. The lowest energy conformer of **42*R*** obtained by Monte-Carlo calculations was shown to adopt torsion angles and a ten-membered hydrogen-bonded ring characteristic of a type II′ β-turn conformation [77]. Involvement of the methylamide NH in an intramolecular hydrogen bonding was supported by the limited influence of increasing temperature on its chemical shift during NMR experiments, as well as observation of a lower-energy stretching vibration in the

NH region of the IR spectra. Pyrroloisoquinolines may thus serve as turn inducers for mimicry of Tyr-Ala motifs in the central core of β- and γ-turn secondary structures [77].

Toward γ-turn mimicry, pyrrolo[3,2-e][1,4]diazepin-2-ones have been prepared by a route featuring Pictet-Spengler reaction and their conformation studied by X-ray crystallographic analysis [78]. In the solid state, the amino acid component of pyrrolo[3,2-e][1,4]diazepin-2-one **45** ($R^1 = s$-Bu, $R^2 = Ph$) exhibited dihedral angles ($\psi = 72°$ and $\phi = -93$) comparable to those of the central residue in an ideal reverse γ-turn ($\psi = 60–70°$ and $\phi = -70°$ to $-85°$).

In a solution-phase approach, methyl (*S*)-4-oxo-1-(9-phenyl-9*H*-fluoren-9-yl) prolinate (**43**) was treated with different amines in the presence of *p*-TsOH to furnish 4-*N*-substituted-aminopyrrole-2-carboxylates that were coupled with different *N*-Fmoc-amino acids to give amides **44**. Following Fmoc deprotection and formation of the HCl salt, the resulting amino pyrroles underwent intramolecular Pictet-Spengler-type reactions to provide pyrrolo[3,2-e][1,4]diazepin-2-ones **45**, predominantly as the *cis*-isomer (Scheme 8). The preference for the *cis*-isomer was suggested to be due to the amino acid side chain adopting an equatorial orientation in a transition state featuring *endo*-attack on the *E*-iminium ion. To facilitate diversity-oriented synthesis of pyrrolodiazepinone libraries, alternative strategies were later studied using Merrifield and Wang resins [79], as well as tetraarylphosphonium (TAP) soluble support [80]. Compounds containing the pyrrolo[3,2-e][1,4]diazepin-2-one scaffold (**45**), designed as mimetics of the Bip-Lys-Tyr sequence of urocontrin, were found to differentially modulate urotensin II-mediated vasoconstriction ex vivo [81].

The Pictet-Spengler reaction with [^{11}C]formaldehyde has been used to successfully introduce a radiolabel into the integrin receptor ligand cyclo[Arg-Gly-Asp-D-Tyr-Lys] [82]. After installation of a Trp residue on the ε-amine of the Lys residue in peptide **46**, both manual and remote-controlled syntheses were used to perform the Pictet-Spengler reactions and isolate the labeled Tcc analog **47** in $5.9 \pm 1.9\%$ radiochemical yield ($n = 4$), with a total synthesis time of about 35 min (Scheme 9).

Exploiting the bio-orthogonal reaction of aldehydes and alkoxyamines to form oxyiminium ion intermediates, a Pictet-Spengler reaction between aldehyde-functionalized proteins **48** and a modified (e.g., fluorescently labeled) indole **49** at pH 4–6 was developed to label proteins, such as glyoxal-myoglobin and FGly-α-HER2 (a formylglycine variant of a therapeutic antibody) with hydrolytically stable oxacarbolines **51** (Scheme 10) [83]. Employing the hydrazine counterpart, *N*-labeled 2-((1,2-dimethylhydrazinyl)methyl)indole **50** in the related Pictet-

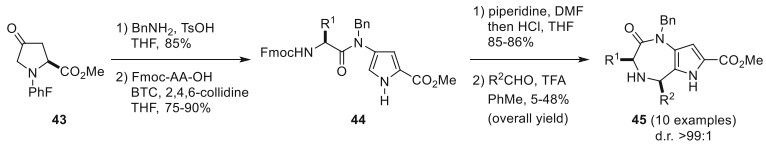

Scheme 8 Synthesis of pyrrolo[3,2-e][1,4]diazepin-2-ones **45** [78]. *BTC* bis(trichloromethyl) carbonate, *PhF* 9-phenylfluoren-9-yl

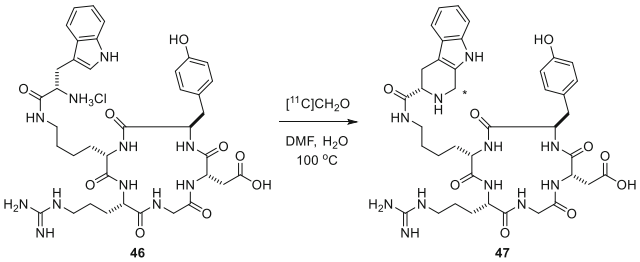

Scheme 9 Radiochemical labeling (^{11}C) of the RGD peptide using a Pictet-Spengler reaction [82]

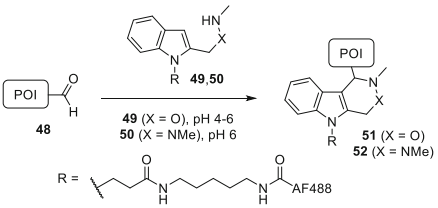

Scheme 10 Biocompatible hydroxylamino-Pictet-Spengler ligation of aldehyde proteins **48** [83, 84]. *POI* protein of interest, *AF488* Alexa Fluor 488 (fluorescent dye)

Spengler reaction, the corresponding azacarboline **52** conjugates were prepared and shown to be stable in human plasma for over 5 days, a period during which the related hydrazone and oxime analogs were usually hydrolytically labile [84].

2.2 Polycyclic Peptidomimetics

Heterocycles containing multiple rings have been synthesized using strategies featuring the Pictet-Spengler reaction [85, 86]. Extra rings may increase conformational rigidity and lipophilic character with consequences of improved metabolic stability and oral bioavailability.

Four novel tetrahydro-β-carboline peptidomimetic scaffolds were prepared starting from the Pictet-Spengler reaction of Trp methyl ester (**53**) with different α-amino aldehydes: Ala-H, Val-H, Leu-H, Phe-H, Ile-H, and Nle-H [87]. The relative stereochemistry of tetrahydro-β-carboline **54** was contingent on the configuration of the starting materials, such that L-Trp reacted with D- and L-α-amino aldehydes to provide stereoselectively the *cis*- and *trans*-ring systems, respectively [88]. Subsequent cyclizations on the different diastereomers gave skeletally diverse imidazolidin-2-one, imidazolidine, and piperazin-2-one peptidomimetic products **55**–**58** (Scheme 11). The conformation of the methylamide derivatives of esters **55**, **57**, and **58** were examined by computational and NMR spectroscopic methods, which indicated a preference for extended backbone geometry. In contrast to β-turn

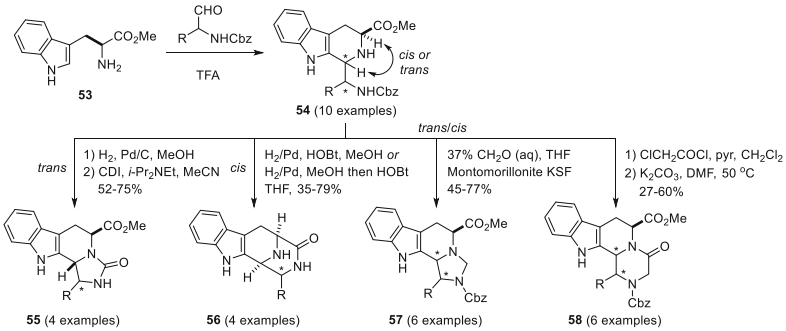

Scheme 11 Synthesis of tetracyclic tetrahydro-β-carboline peptidomimetics from Trp [87]. *CDI* *N*,*N′*-carbonyldiimidazole, *HOBt* hydroxybenzotriazole

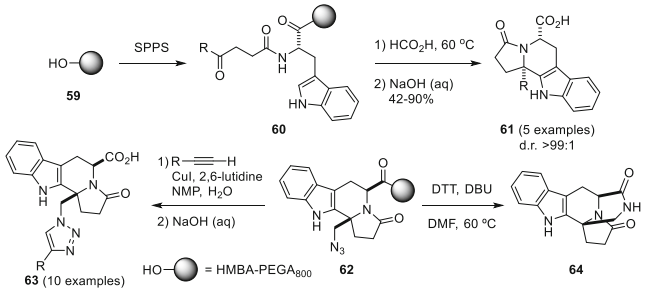

Scheme 12 Solid-phase *N*-acyliminium synthesis of **61**, **63**, and **64** [89]. *SPPS* solid-phase peptide synthesis, *HMBA* 4-hydroxymethylbenzoic acid, *DTT* dithioerythritol, *DBU* 1,8-diazabicyclo[5.4.0]undec-7-ene

inducing scaffolds (e.g., **34**) which display χ^1 *gauche*-(−) conformation, the additional ring of analogs of **55**, **57**, and **58** creates allylic strain that forces the carboxylate axial and changes the χ^1 conformation to *gauche*-(+) orienting extended structure [76].

Levulinamides derived from amino acids bearing electron-rich aromatic (e.g., 3,4-dimethoxyphenyl) and heteroaromatic (e.g., furyl, thienyl, benzothienyl, and indolyl) side chains (e.g., **60**) were employed as precursors to *N*-acyliminium ion intermediates in a diastereoselective solid-phase Pictet-Spengler reaction strategy (Scheme 12) to synthesize various peptidomimetic heterocyclic systems (17 examples, e.g., **61**) [89]. Elaboration of 5-azido-levulinamide **60** in the sequence gave *cis*-tetrahydro-β-carboline **62**, which was subsequently reacted with different acetylenes using the Cu^I-catalyzed azide-alkyne cycloaddition reaction to provide triazoles **63**. Alternatively, reduction of azide **62** and lactam formation gave bridged ketopiperazine **64**.

The combination of multicomponent reactions with the Pictet-Spengler cyclization has proven an effective approach for assembling polycyclic peptidomimetics

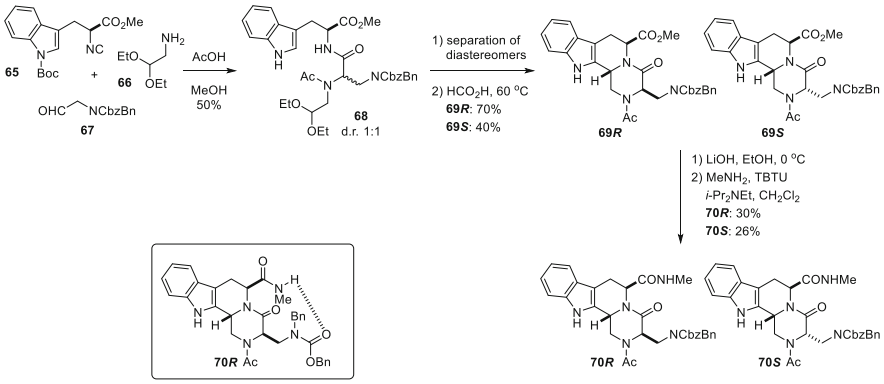

Scheme 13 An Ugi/Pictet-Spengler reaction sequence to β-turn mimic **70*R*** [94]. *TBTU N*-[(1*H*-benzotriazol-1-yl)(dimethylamino)methylene]-*N*-methylmethanaminium tetrafluoroborate *N*-oxide

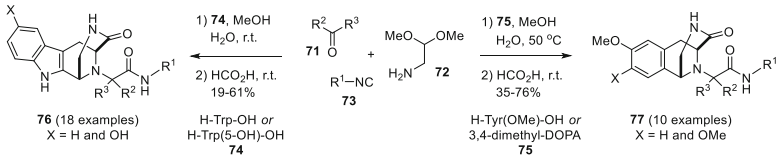

Scheme 14 One-pot Ugi/Pictet-Spengler reaction to bridged ketopiperazine-tetrahydro-β-carbolines **76** and tetrahydroisoquinolines **77** [95]

[90–93]. For example, the combination of Ugi and Pictet-Spengler reactions has been used to assemble β-turn mimic **70** (Scheme 13) [94].

The Ugi reaction of tryptophan-derived isocyanide **65** with glycine-derived amine **66** and aldehyde **67** and acetic acid in methanol gave a 1:1 mixture of diastereomers **68** in 50% yield. After separation by chromatography, each diastereomer of **68** was respectively exposed to formic acid at elevated temperature to provide ketopiperazines **69*R*** and **69*S***. Ester hydrolysis and amidation gave methylamides **70*R*** and **70*S*** possessing, respectively, the amino methyl residue on the same or opposite face of the bicycle as the carboxamide. Only the *R*-diastereomer (**70*R***) was observed to adopt a β-turn-like conformer based on computational analysis and NMR experiments, in which the exchange of the amide NH protons with deuterium and changes of amide NH chemical shifts with temperature and solvent composition were studied [94].

Bridged ketopiperazine-tetrahydro-β-carbolines **76** and tetrahydroisoquinolines **77** were prepared by a similar Ugi/Pictet-Spengler approach using, respectively, tryptophan, 5-hydroxytryptophan, *O*-methyl tyrosine, and *O*,*O*-dimethyl DOPA as the carboxylate component (Scheme 14) [95]. Sets of ketones **71** and isocyanides **73** were reacted with aminoacetaldehyde dimethyl acetal (**72**) and the amino acid (**74** or **75**) in a one-pot Ugi reaction in methanol to give the corresponding amido amide

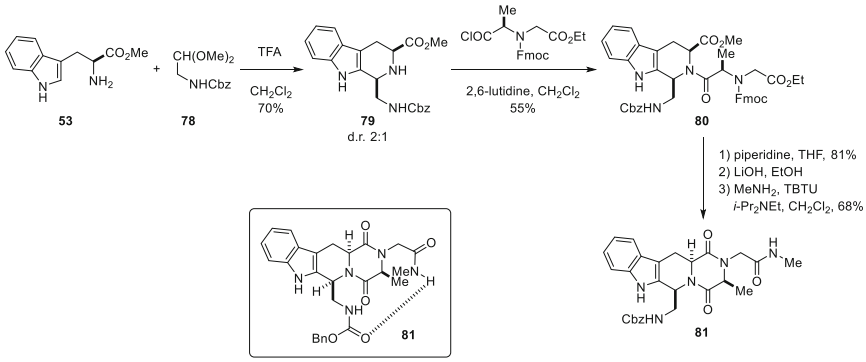

Scheme 15 Synthesis of fused tetrahydro-β-carboline-diketopiperazine α-turn mimic [97]

products, which after evaporation of the volatiles were dissolved in formic acid to affect the Pictet-Spengler reaction. After purification, the bridged ketopiperazines **76** and **77** were obtained as single diastereomers without detectable loss of the amino acid configuration, in modest to good yield. Along similar lines, a one-pot sequential Ugi/Pictet-Spengler/reductive methylation protocol was used to synthesize piperazinohydroisoquinolines related to alkaloid natural products [96].

Diketopiperazines are cyclic dipeptides that may exhibit hydrogen bonding and non-covalent side-chain interactions but are relatively metabolically stable compared to linear peptides, in part because they are not recognized by proteases. Diketopiperazines have thus been employed as core units in the design of different peptidomimetics for drug discovery.

For example, α-turn mimic **81** was prepared by a combination of the tetrahydro-β-carboline and diketopiperazine skeletons (Scheme 15) [97]. Segments of regular α-helical peptides featuring a hydrogen bond between the carbonyl oxygen of the *i* and the amide NH of the $i+4$ residues, α-turn peptide analogs have exhibited bacteriolytic, antiviral, and anti-HIV activities. Tetrahydro-β-carboline **79** was synthesized as a 2:1 mixture of *cis-trans*-diastereomers in 70% yield by the Pictet-Spengler reaction of tryptophan methyl ester and *N*-Cbz-aminoacetaldehyde dimethyl acetal using TFA in dichloromethane. Annulation of the diketopiperazine onto *cis*-isomer **79** and conversion of the ethyl ester to its *N*-methylamide counterpart gave **81**, which was predicted to adopt the 13-membered hydrogen-bonded α-turn structure using computer-aided conformational analysis. Subsequently, the α-turn was supported by NMR spectroscopic studies, in which the chemical shift of the amide NH signal was relatively unaffected compared to the carbamate NH signal during modifications of temperature and environment.

Two solid-phase approaches were developed to combine the tetrahydroisoquinoline and diketopiperazine skeletons in peptidomimetics **84** and **86–88** (Scheme 16) [98]. In the first, solid-phase peptide synthesis was used to prepare linear peptide precursor **83** featuring serine and an electron-rich phenylalanine derivative at the first and third residues in the sequence. Oxidative cleavage of the serine residue with sodium periodate generated the *N*-terminal glyoxylic amide,

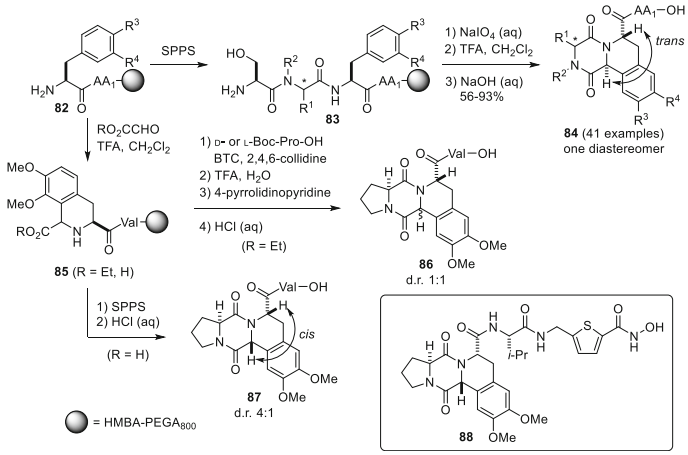

Scheme 16 The stereoselective synthesis of fused tetrahydro-β-carboline and diketopiperazine skeletons [98]

which underwent Pictet-Spengler reaction on treatment with acid and was cleaved from the support by basic hydrolysis to give the fused *trans*-tetrahydroisoquinoline-diketopiperazine ring systems **84**. The cyclic *N*-acyliminium ion intermediate was readily formed with a variety of amino acids at the second residue in the sequence, including cyclic and linear amino acids with aromatic and aliphatic side chains, and reacted with complete diastereoselectivity. In the second strategy, glyoxylic acid was reacted with the *N*-terminal *O*,*O*-dimethyl DOPA residue of the resin-bound peptide to provide a preference of the *cis*-tetrahydroisoquinoline diastereomer, which was coupled to proline and cyclized to diketopiperazine **87**. The utility of the strategy was validated by the synthesis of hydroxamates (e.g., **88**) that exhibited inhibitory activity for class IIb histone deacetylases (HDACs) with selectivity for the HDAC 6 over the HDAC 10 isoform.

2.3 Spirocyclic Peptidomimetics

Spirocyclic heterocycles are common components of natural products, such as gelsemine and spirotryprostatins. In peptidomimetics, spirocycles have been employed to restrict backbone geometry as well as to orient pharmacophores in spatially defined scaffolds. A series of spirocyclic β-turn mimics have been prepared employing sequences featuring Pictet-Spengler reactions on α-benzyl and α-indolylmethyl α-amino γ-lactams derived from **90** and **94** (Scheme 17) [99–101]. The respective tetrahydroisoquinoline and tetrahydro-β-carboline spirocyclic γ-lactam derivatives (e.g., **92** and **96**) have been demonstrated to adopt β-turn conformations and have been employed to study biologically active peptides (vide infra) [99, 100].

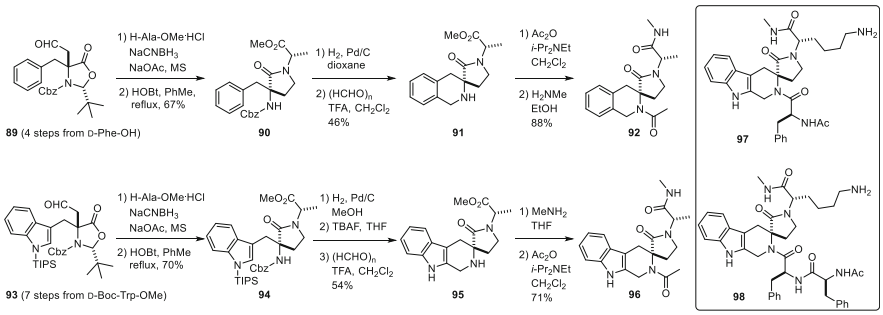

Scheme 17 Synthesis of tetrahydroisoquinoline and tetrahydro-β-carboline spirocyclic γ-lactams, somatostatin mimics **97** and **98** [99, 100]. *TBAF tetra-n*-butylammonium fluoride

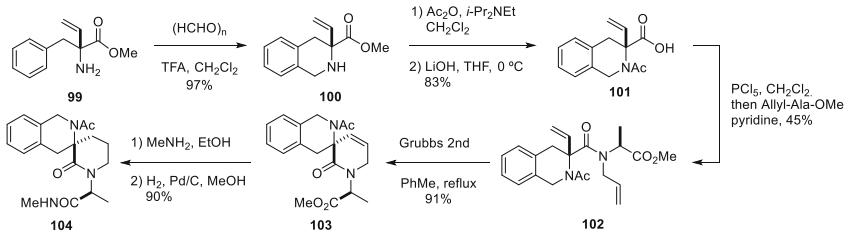

Scheme 18 Synthesis of tetrahydroisoquinoline spirocyclic δ-lactams [101]

Table 1 Dihedral angles for spirocyclic lactams **92**, **96**, and **104** (solid state) and for an ideal β-turn [99–101]

Compound	φ ($i+1$)	ψ ($i+1$)	φ ($i+2$)	ψ ($i+2$)
92	48.9°	−133.7°	−89.4°	10.8°
96	51.0°	−134.0°	−105.0°	31.0°
104	49.4°	−135.5°	−110.1°	40.7°
Ideal β-turn	60°	−120°	−80°	0°

Tetrahydroisoquinoline spirocyclic δ-lactam **104** was synthesized from α-benzyl vinylglycine **99** by a related approach featuring a Pictet-Spengler reaction followed by ring-closing metathesis (Scheme 18). After aminolysis of ester **103**, hydrogenation of the double bond gave δ-lactam **104**.

The β-turn conformation of the spirocyclic mimics was predicted using molecular mechanic calculations, which suggested the presence of a ten-membered hydrogen bond. This observation was further supported by NMR and IR spectroscopic studies. Moreover, the X-ray crystal structure of **92**, **96**, and **104** demonstrated that they adopted the hydrogen bond and dihedral angle values similar to that of an ideal type II′ β-turn (Table 1) [99–101].

In an attempt to illustrate their potential as peptidomimetics, tetrahydro-β-carboline spirocyclic γ-lactams were introduced into analogs **97** and **98** to mimic the β-turn fragment of the biologically active peptide somatostatin (Scheme 17), albeit without significant detectable receptor affinity [100].

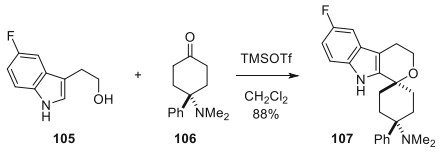

Scheme 19 Synthesis of cebranopadol **107** via an oxo-Pictet-Spengler reaction [103, 104]. *TMS* trimethylsilyl, *Tf* trifluoromethanesulfonyl

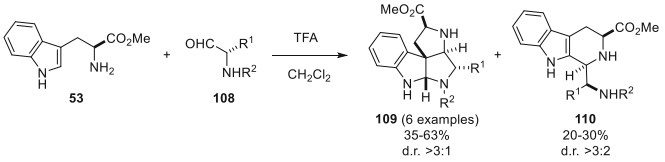

Scheme 20 Novel octahydropyrrolo[3′,2′:3,4]pyrrolo[2,3-b]indoles from condensation of α-amino aldehydes with Trp-OMe [105]

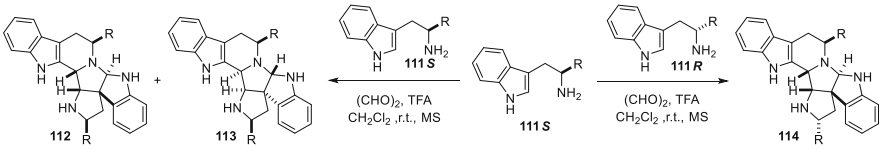

Scheme 21 Pictet-Spengler reactions with glyoxal and Trp derivatives to provide diastereomeric heptacycles **112–114** [106]

The oxa-Pictet-Spengler reaction was used to synthesize cebranopadol **107** (Scheme 19) [102]. A novel analgesic, cebranopadol **107**, has been found to activate all four opioid receptor subtypes and to exhibit efficacy in a mouse model of acute pain with potency comparable to fentanyl [103, 104].

Employing one equivalent of TFA in dichloromethane, octahydropyrrolo [3′,2′:3,4]pyrrolo[2,3-b]indoles **109** were isolated as the major product in 35–63% yields along with 20–30% of the expected tetrahydro-β-carbolines **110** from Pictet-Spengler reactions of Trp methyl ester (**53**) and a variety of enantiopure α-amino aldehydes **108**: Fmoc-Gyl-H, Fmoc-Ala-H, Fmoc-Phe-H, Boc-Phe-H, Fmoc-Asp (tBu)-H, and Fmoc-Lys(Boc)-H (Scheme 20) [105]. Scaffold **109** arises from trapping the spiro-iminium intermediate (vide supra) with the appended amino functionality and offers promise for peptidomimetic development.

Ring systems related to octahydropyrrolo[3′,2′:3,4]pyrrolo[2,3-b]indoles **109** were prepared by employing glyoxal to react on two Trp derivatives **111** (Scheme 21) [106]. Initially, Pictet-Spengler reaction of L-Trp derivative **111*S***, glyoxal, and catalytic TFA provided a tetrahydro-β-carboline aldehyde intermediate that reacted subsequently with a second L- or D-Trp derivative **111*S*** or **111*R*** to provide diastereomeric heptacycles **112–114**. Although the combination of two L-Trp derivatives **111*S*** gave a diastereomeric mixture of **112** and **113**, the mixture of L- and D-Trp derivatives **111*S*** and **111*R*** with glyoxal produced a racemic mixture of **114**.

3 Perspectives

Peptides are attractive natural leads for drug discovery, and they can be elaborated to modulate many pharmacological targets. Unfortunately, native peptides often display unfavorable pharmacokinetic properties, including poor bioavailability, low metabolic stability, and lack of receptor selectivity. Peptidomimetics ideally combine the ability to bind targets with high affinity with improved pharmacokinetic properties. The Pictet-Spengler reaction has played a major role in the development of such peptidomimetics, reflecting its unique synthetic potential for the construction of structurally diverse molecular architectures. Applications of enantioselective catalysis, diversity-oriented synthesis, and solid-phase combinatorial chemistry have facilitated the assembly of peptidomimetics by the Pictet-Spengler reaction for studies in peptide science and chemical biology. In particular, the Pictet-Spengler reaction has proven effective for the construction of peptide turn mimics and rigid molecular scaffolds for displaying pharmacophores with defined orientations. Moreover, the Pictet-Spengler reaction has also proven valuable for labeling and tagging peptide and protein structures by way of metabolically stable linkers. Considering the diverse range of applications and utility of the Pictet-Spengler reaction, there is little doubt that this reaction will retain its popularity in the hunt for bioactive molecules in the future.

References

1. Luger K, Mäder AW, Richmond RK, Sargent DF, Richmond TJ (1997) Crystal structure of the nucleosome core particle at 2.8 Å resolution. Nature 389:251–260
2. Jenuwein T, Allis CD (2001) Translating the histone code. Science 293:1074–1080
3. Hurwitz J (2005) The discovery of RNA polymerase. J Biol Chem 280:42477–42485
4. Furie B, Furie BC (1988) The molecular basis of blood coagulation. Cell 53:505–518
5. Takeda S, Kadowaki S, Haga T, Takaesu H, Mitaku S (2002) Identification of G protein-coupled receptor genes from the human genome sequence. FEBS Lett 520:97–101
6. Doyle DA, Cabral JM, Pfuetzner RA, Kuo A, Gulbis JM, Cohen SL, Chait BT, MacKinnon R (1988) The structure of the potassium channel: molecular basis of K^+ conduction and selectivity. Science 280:69–77
7. Adessi C, Soto C (2002) Converting a peptide into a drug: strategies to improve stability and bioavailability. Curr Med Chem 9:963–978
8. Chatterjee S, Roy RS, Balaram P (2007) Expanding the polypeptide backbone: hydrogen-bonded conformations in hybrid polypeptides containing the higher homologues of α-amino acids. J R Soc Interface 4:587–606
9. Kabsch W, Sander C (1983) Dictionary of protein secondary structure: pattern recognition of hydrogen-bonded and geometrical features. Biopolymers 22:2577–2637
10. Liskamp RMJ (1994) Conformationally restricted amino acids and dipeptides, (non) peptidomimetics and secondary structure mimetics. Recl Trav Chim Pays-Bas 113:1–19
11. Powell MF, Grey H, Gaeta F, Sette A, Colón S (1992) Peptide stability in drug development: a comparison of peptide reactivity in different biological media. J Pharm Sci 81:731–735
12. Bursavich MG, Rich DH (2002) Designing non-peptide peptidomimetics in the 21st century: inhibitors targeting conformational ensembles. J Med Chem 45:541–558

13. Olson GL, Bolin DR, Bonner MP, Bös M, Cook CM, Fry DC, Graves BJ, Hatada M, Hill DE, Kahn M, Madison VS, Rusiecki VK, Sarabu R, Sepinwall J, Vincent GP, Voss ME (1993) Concepts and progress in the development of peptide mimetics. J Med Chem 36:3039–3049
14. Gante J (1994) Peptidomimetics – tailored enzyme inhibitors. Angew Chem Int Ed 33:1699–1720
15. Ripka AS, Rich DH (1998) Peptidomimetic design. Curr Opin Chem Biol 2:441–452
16. Marshall GR (1993) A hierarchical approach to peptidomimetic design. Tetrahedron 49:3547–3558
17. Giannis A, Kolter T (1993) Peptidomimetics for receptor ligands – discovery, development, and medical perspectives. Angew Chem Int Ed 32:1244–1267
18. Hruby V (1982) Conformational restrictions of biologically active peptides via amino acid side chain groups. Life Sci 31:189–199
19. Toniolo C (1990) Conformationally restricted peptides through short-range cyclizations. Int J Pept Protein Res 35:287–300
20. Hruby VJ, Li G, Haskell-Luevano C, Shenderovich M (1997) Design of peptides, proteins and peptidomimetics in chi space. Biopolymers 43:219–266
21. Gibson (née Thomas) SE, Guillo N, Tozer MJ (1999) Towards control of χ-space: conformationally constrained analogues of Phe, Tyr, Trp and His. Tetrahedron 55:585–615
22. Choudhary A, Raines RT (2011) An evaluation of peptide-bond isosteres. ChemBioChem 12:1801–1807
23. Seebach D, Beck AK, Bierbaum DJ (2004) The world of β- and γ-peptides comprised of homologated proteinogenic amino acids and other components. Chem Biodiversity 1:1111–1239
24. Fowler SA, Blackwell HE (2009) Structure-function relationships in peptoids: recent advances toward deciphering the structural requirements for biological function. Org Biomol Chem 7:1508–1524
25. Chorev M, Goodman M (1993) A dozen years of retro-inverso peptidomimetics. Acc Chem Res 26:266–273
26. Hughes J (1975) Isolation of an endogenous compound from the brain with pharmacological properties similar to morphine. Brain Res 88:295–308
27. Hughes J, Smith T, Morgan B, Fothergill L (1975) Purification and properties of enkephalin – the possible endogenous ligand for the morphine receptor. Life Sci 16:1753–1758
28. Tipper DJ, Strominger JL (1965) Mechanism of action of penicillins: a proposal based on their structural similarity to acyl-D-alanyl-D-alanine. Proc Natl Acad Sci U S A 54:1133–1141
29. Yocum RR, Rasmussen JR, Strominger JL (1980) The mechanism of action of penicillins. J Biol Chem 255:3977–3986
30. Swindells DCN, White PS, Findlay JA (1978) The X-ray crystal structure of rapamycin, $C_{51}H_{79}NO_{13}$. Can J Chem 56:2491–2492
31. Choi J, Chen J, Schreiber SL, Clardy J (1996) Structure of the FKB12-rapamycin complex interacting with the binding domain of human FRAP. Science 273:239–242
32. Pictet A, Spengler T (1911) Über die bildung von Isochinolin-derivaten durch Einwirkung von Methylal auf Phenyl-äthylamin, Phenyl-alanin und Tyrosin. Chem Ber 44:2030–2036
33. Cox ED, Cook JM (1995) The Pictet-Spengler condensation: a new direction for an old reaction. Chem Rev 95:1797–1842
34. Tatsui G (1928) J Pharm Soc Jpn 48:453–459
35. Bailey PD, Hollinshead SP, McLay NR, Morgan K, Palmer SJ, Prince SN, Reynolds CD, Wood SD (1993) Diastereo- and enantio-selectivity in the Pictet-Spengler reaction. J Chem Soc Perkin Trans 1:431–439
36. Jacobs WA, Craig LC (1936) The ergot alkaloids* VIII. The synthesis of 4-carboline carbonic acids. J Biol Chem 113:759–765
37. Wadsworth A, Pangborn MC (1936) The reaction of formaldehyde with amino acids. J Biol Chem 116:423–436

38. Stöckigt J, Zenk MH (1977) Isovincoside (strictosidine), the key intermediate in the enzymatic formation of indole alkaloids. FEBS Lett 79:233–237
39. Hampp N, Zenk MH (1988) Homogeneous strictosidine synthase from cell suspension cultures of *Rauvolfia serpentina*. Phytochemistry 27:3811–3815
40. Stöckigt J, Zenk MH (1977) Strictosidine (isovincoside): the key intermediate in the biosynthesis of monoterpenoid indole alkaloids. J Chem Soc Chem Commun 646–648
41. Stöckigt J (1979) Enzymatic formation of intermediates in the biosynthesis of ajmalicine: strictosidine and cathenamine. Phytochemistry 18:965–971
42. O'Conner SE, Maresh JJ (2006) Chemistry and biology of monoterpene indole alkaloid biosynthesis. Nat Prod Rep 23:532–547
43. Ma X, Panjikar S, Koepke J, Loris E, Stöckigt J (2006) The structure of *Rauvolfia serpentina* strictosidine synthase is a novel six-bladed β-propeller fold in plant proteins. Plant Cell 18:907–920
44. McCoy E, Galan MC, O'Connor SE (2006) Substrate specificity of strictosidine synthase. Bioorg Med Chem Lett 16:2475–2478
45. Rueffer M, El-Shagi H, Nagakura N, Zenk MH (1981) (*S*)-Norlaudanosoline synthase: the first enzyme in the benzylisoquinoline biosynthetic pathway. FEBS Lett 129:5–9
46. Samanani N, Facchini PJ (2002) Purification and characterization of norcoclaurine synthase. J Biol Chem 277:33878–33883
47. Stadler R, Kutchan TM, Loeffler S, Nagakura N, Cassels B, Zenk MH (1987) Revision of the early steps of reticuline biosynthesis. Tetrahedron Lett 28:1251–1254
48. Stadler R, Zenk MH (1990) A revision of the generally accepted pathway for the biosynthesis of the benzyltetrahydroisoquinoline alkaloid reticuline. Liebigs Ann Chem 555–562
49. Rueffer M, Zenk MH (1987) Distant precursors of benzylisoquinoline alkaloids and their enzymatic formation. Z Naturforsch 42c:319–332
50. Facchini PJ, St-Pierre B (2005) Synthesis and trafficking of alkaloid biosynthetic enzymes. Curr Opin Plant Biol 8:657–666
51. Luk LYP, Bunn S, Liscombe DK, Facchini PJ, Tanner ME (2007) Mechanistic studies on norcoclaurine synthase of benzylisoquinoline alkaloid biosynthesis: an enzymatic Pictet-Spengler reaction. Biochemistry 46:10153–10161
52. Yan W, Ge HM, Wang G, Jiang N, Mei YN, Jiang R, Li SJ, Chen CJ, Jiao RH, Xu Q, Ng SW, Tan RX (2014) Pictet-Spengler reaction-based biosynthetic machinery in fungi. Proc Natl Acad Sci U S A 111:18138–18143
53. Stöckigt J, Antonchick AP, Wu F, Waldmann H (2011) The Pictet-Spengler reaction in nature and organic chemistry. Angew Chem Int Ed 50:8538–8564
54. Royer J, Bonin M, Micouin L (2004) Chiral heterocycles by iminium ion cyclization. Chem Rev 104:2311–2352
55. Taylor MS, Jacobsen EN (2004) Highly enantioselective catalytic acyl-Pictet-Spengler reactions. J Am Chem Soc 126:10558–10559
56. Mittal N, Sun DX, Seidel D (2014) Conjugate-base-stabilized Brønsted acids: catalytic enantioselective Pictet-Spengler reactions with unmodified tryptamine. Org Lett 16:1012–1015
57. Waldmann H, Schmidt G, Henke H, Burkard M (1995) Asymmetric Pictet-Spengler reactions employing N, N-phthaloyl amino acids as chiral auxiliary groups. Angew Chem Int Ed 34:2402–2403
58. Schmidt G, Waldmann H, Henke H, Burkard M (1996) Asymmetric control in the Pictet-Spengler reaction by means of *N*-protected amino acids as chiral auxiliary groups. Chem Eur J 2:1566–1571
59. Gremmen C, Wanner MJ, Koomen G-J (2001) Enantiopure tetrahydroisoquinolines via *N*-sulfinyl Pictet-Spengler reactions. Tetrahedron Lett 42:8885–8888
60. Gremmen C, Willemse B, Wanner MJ, Koomen G-J (2000) Enantiopure tetrahydro-*β*-carbolines via Pictet-Spengler reactions with *N*-sulfinyl tryptamines. Org Lett 2:1955–1958

61. Bailey PD, Beard M, Phillips TR (2009) Unexpected cis selectivity in the Pictet-Spengler reaction. Tetrahedron Lett 50:3645–3647
62. Ungemach F, DiPierro M, Weber R, Cook JM (1979) Stereospecific synthesis of *trans*-1,3-disubstituted-1,2,3,4-tetrahydro-β-carbolines. Tetrahedron Lett 35:3225–3228
63. Ungemach F, DiPierro M, Weber R, Cook JM (1981) Stereospecific synthesis of *trans*-1,3-disubstituted-1,2,3,4-tetrahydro-β-carbolines. J Org Chem 46:164–168
64. Julian PL, Karpel WJ, Magnani A, Meyer EW (1948) Studies on the indole series. X. Yohimbine (part 2). The synthesis of yobyrine, yobyrone and "tetrahydroyobyrine". J Am Chem Soc 70:180–183
65. Verschueren K, Toth G, Tourwé D, Lebl M, Van Binst G, Hruby V (1992) A facile synthesis of 1,2,3,4-tetrahydro-7-hydroxyisoquinoline-3-carboxylic acid, a conformationally constrained tyrosine analogue. Synthesis 458–460
66. Harvey DG, Miller EJ, Robson W (1941) The Adamkiewicz, Hopkins and Cole, and Rosenheim tests for tryptophan. An investigation of the configuration of the organic molecule responsible for the colour formation and its bearing on the constitution of yohimbine, with a note on the action of formaldehyde on tryptophan. J Chem Soc 153–159
67. Neuberger A (1944) The reaction between histidine and formaldehyde. Biochem J 38:309–314
68. Kazmierski W, Hruby VJ (1988) A new approach to receptor ligand design: synthesis and conformation of a new class of potent and highly selective μ opioid antagonists utilizing tetrahydroisoquinoline carboxylic acids. Tetrahedron 44:697–710
69. Kazmierski W, Wire WS, Lui GK, Knapp RJ, Shook JE, Burks TF, Yamamura HI, Hruby VJ (1988) Design and synthesis of somatostatin analogues with topographical properties that lead to highly potent and specific μ opioid receptor antagonists with greatly reduced binding at somatostatin receptors. J Med Chem 31:2170–2177
70. Schiller PW, Nguyen TM-D, Weltrowska G, Wilkes BC, Marsden BJ, Lemieux C, Chung NN (1992) Differential stereochemical requirements of μ vs. δ opioid receptors for ligand binding and signal transduction: development of a class of potent and highly δ-selective peptide antagonists. Proc Natl Acad Sci U S A 89:11871–11875
71. Lesma G, Salvadori S, Airaghi F, Murray TF, Recca T, Sacchetti A, Balboni G, Silvani A (2013) Structural and biological exploration of Phe^3-Phe^4-modified endomorphin-2 peptidomimetics. ACS Med Chem Lett 4:795–799
72. Wang H, Ganesan A (1999) The *N*-acyliminium Pictet-Spengler condensation as a multicomponent combinatorial reaction on solid-phase and its application to the synthesis of demethoxyfumitremorgin C analogues. Org Lett 1:1647–1649
73. van Loevezijn A, van Maarseveen JH, Stegman K, Visser GM, Koomen G-J (1998) Solid phase synthesis of fumitremorgin, verruculogen and tryprostatin analogs based on a cyclization/cleavage strategy. Tetrahedron Lett 39:4737–4740
74. van Loevezijn A, Allen JD, Schinkel AH, Koomen G-J (2001) Inhibition of BCRP-mediated drug efflux by fumitremorgin-type indolyl diketopiperazines. Bioorg Med Chem Lett 11:29–32
75. Lazarus LH, Bryant SD, Cooper PS, Guerrini R, Balboni G, Salvadori S (1998) Design of δ-opioid peptide antagonists for emerging drug applications. Drug Discov Today 3:284–294
76. Lesma G, Meschini E, Recca T, Sacchetti A, Silvani A (2007) Synthesis of tetrahydroisoquinoline-based pseudopeptides and their characterization as suitable reverse turn mimetics. Tetrahedron 63:5567–5578
77. Landoni N, Lesma G, Sacchetti A, Silvani A (2007) Pyrroloisoquinoline-based tetrapeptide analogues mimicking reverse-turn secondary structures. J Org Chem 72:9765–9768
78. Deaudelin P, Lubell WD (2008) Diastereoselective Pictet-Spengler approach for the synthesis of pyrrolo[3,2-e][1,4]diazepin-2-one peptide turn mimics. Org Lett 10:2841–2844
79. Boutard N, Dufour-Gallant J, Deaudelin P, Lubell WD (2011) Pyrrolo[3,2-e][1,4]diazepin-2-one synthesis: a head-to-head comparison of soluble versus insoluble supports. J Org Chem 76:4533–4545

80. Stazi F, Marcoux D, Poupon J-C, Latassa D, Charette AB (2007) Tetraarylphosphonium salts as soluble supports for the synthesis of small molecules. Angew Chem Int Ed 46:5011–5014
81. Dufour-Gallant J, Chatenet D, Lubell WD (2015) *De novo* conception of small molecule modulators based on endogenous peptide ligands: pyrrolodiazepin-2-one γ-turn mimics that differentially modulate urotensin II receptor-mediated vasoconstriction *ex vivo*. J Med Chem 58:4624–4637
82. Hanyu M, Takada Y, Hashimoto H, Kawamura K, Zhang M-R, Fukumura T (2013) Carbon-11 radiolabeling of an oligopeptide containing tryptophan hydrochloride via a Pictet-Spengler reaction using carbon-11 formaldehyde. J Pept Sci 19:663–668
83. Agarwal P, van der Weijden J, Sletten EM, Rabuka D, Bertozzi CR (2013) A Pictet-Spengler ligation for protein chemical modification. Proc Natl Acad Sci U S A 110:46–51
84. Agarwal P, Kudirka R, Albers AE, Barfield RM, de Hart GW, Drake PM, Jones LC, Rabuka D (2013) Hydrazino-Pictet-Spengler ligation as a biocompatible method for the generation of stable protein conjugates. Bioconjug Chem 24:846–851
85. Le Quement ST, Petersen R, Meldal M, Nielsen TE (2010) *N*-acyliminium intermediates in solid-phase synthesis. Biopolymers (Pept Sci) 94:242–256
86. Nielsen TE, Diness F, Meldal M (2003) The Pictet-Spengler reaction in solid-phase combinatorial chemistry. Curr Opin Drug Discov Devel 6:801–814
87. Pulka K, Feytens D, Misicka A, Tourwé D (2010) New tetracyclic tetrahydro-β-carbolines as tryptophan-derived peptidomimetics. Mol Divers 14:97–108
88. Pulka H, Kulis P, Tymecka D, Frankiewicz L, Wilczek M, Kozminski W, Misicka A (2008) Diastereoselective Pictet-Spengler condensation of tryptophan with α-amino aldehydes as chiral carbonyl components. Tetrahedron 64:1506–1514
89. Komnatnyy VV, Givskov M, Nielsen TE (2012) Solid-phase synthesis of structurally diverse heterocycles by an amide-ketone condensation/*N*-acyliminium Pictet-Spengler sequence. Chem Eur J 18:16793–16800
90. Dömling A, Ugi I (2000) Multicomponent reactions with isocyanides. Angew Chem Int Ed 39:3168–3210
91. El Kaim L, Gageat M, Gaultier L, Grimaud L (2007) New Ugi/Pictet-Spengler multicomponent formation of polycyclic diketopiperazines and α-keto acids. Synlett 3:500–502
92. Liu H, Dömling A (2009) Efficient and diverse synthesis of indole derivatives. J Org Chem 74:6895–6898
93. Wang W, Herdtweck E, Dömling A (2010) Polycyclic indole alkaloid-type compounds by MCR. Chem Commun 46:770–772
94. Lesma G, Cecchi R, Crippa S, Giovanelli P, Meneghetti F, Musolino M, Sachetti A, Silvani A (2012) Ugi 4-CR/Pictet-Spengler reaction as a short route to tryptophan-derived peptidomimetics. Org Biomol Chem 10:9004–9012
95. Sinha MK, Khoury K, Herdtweck E, Dömling A (2013) Tricycles by a new Ugi variation and Pictet-Spengler reaction in one pot. Chem Eur J 19:8048–8052
96. Cano-Herrera M-A, Miranda LD (2011) Expedient entry to the piperazinohydroisoquinoline ring system using a sequential Ugi/Pictet-Spengler/reductive methylation reaction protocol. Chem Commun 47:10770–10772
97. Airaghi F, Fiorati A, Lesma G, Musolino M, Sacchetti A, Silvani A (2013) The diketopiperazine-fused tetrahydro-β-carboline scaffold as a model peptidomimetic with an unusual α-turn secondary structure. Beilstein J Org Chem 9:147–154
98. Petersen R, Le Quement ST, Nielsen TE (2014) Synthesis of a natural product-like compound collection through oxidative cleavage and cyclization of linear peptides. Angew Chem Int Ed 53:11778–11782
99. Lesma G, Landoni N, Pilati T, Sacchetti A, Silvani A (2009) Tetrahydroisoquinoline-based spirocyclic lactam as a type II′ β-turn inducing peptide mimetic. J Org Chem 74:8098–8105
100. Lesma G, Cecchi R, Cagnotto A, Gobbi M, Meneghetti F, Musolino M, Sacchetti A, Silvani A (2013) Tetrahydro-β-carboline-based spirocyclic lactam as type II′ β-turn: application to

the synthesis and biological evaluation of somatostatine mimetics. J Org Chem 78:2600–2610
101. Sacchetti A, Silvani A, Lesma G, Pilati T (2011) Phe-Ala-based diazaspirocyclic lactam as nucleator of type II′ β-turn. J Org Chem 76:833–839
102. Wünsch B, Zott M (1992) Chirale 2-Benzopyran-3-carbonsäure-Derivate durch Oxa-Pictet-Spengler-Reaktion von (*S*)-3-Phenylmilchsäure-Derivaten. Liebigs Ann Chem 39–45
103. Schunk S, Linz K, Frormann S, Hinze C, Oberbörsch S, Sundermann B, Zemolka S, Englberger W, Germann T, Christoph T, Kögel B-Y, Schröder W, Harlfinger S, Saunders D, Kless A, Schick H, Sonnenschein H (2014) Discovery of spiro[cyclohexane-dihydropyrano[3,4-b]indole]-amines as potent NOP and opioid receptor agonists. ACS Med Chem Lett 5:851–856
104. Schunk S, Linz K, Hinze C, Frormann S, Oberbörsch S, Sundermann B, Zemolka S, Englberger W, Germann T, Christoph T, Kögel B-Y, Schröder W, Harlfinger S, Saunders D, Kless A, Schick H, Sonnenschein H (2014) Discovery of a potent analgesic NOP and opioid receptor agonist: cebranopadol. ACS Med Chem Lett 5:857–862
105. Gomez-Monterrey IM, Campiglia P, Bertamino A, Aquino C, Mazzoni O, Diurno MV, Iacovino R, Saviano M, Sala M, Novellino E, Grieco P (2008) Synthesis of novel indole-based ring systems by acid-catalysed condensation from α-amino aldehydes and L-Trp-OMe. Eur J Org Chem 1983–1992
106. Bai B, Li D-S, Huang S-Z, Ren J, Zhu H-J (2012) Chirality pairing recognition, a unique reaction forming spiral alkaloids from amino acids stereoselectively in one-pot. Nat Prod Bioprospect 2:53–58

Top Heterocycl Chem (2017) 49: 105–126
DOI: 10.1007/7081_2015_194

Published online: 14 December 2015

Peptidomimetics via Iminium Ion Chemistry on Solid Phase: Single, Fused, and Bridged Heterocycles

Agustina La-Venia, Pilar Ventosa-Andrés, and Viktor Krchňák

Abstract Iminium ion chemistry represents a versatile transformation capable of introducing structurally diverse constraints into peptide backbones. The compatibility of iminium ion chemistry with traditional solid-phase peptide synthesis methods enables the introduction of constraints without requiring solution-phase synthesis. This chapter describes the introduction of constrained molecular scaffolds composed of single, fused, and bridged heterocycles into peptide backbones.

Keywords Bridged heterocycles • Fused heterocycles • Iminium • Solid-phase synthesis

Contents

A. La-Venia and P. Ventosa-Andrés
Department of Organic Chemistry, Faculty of Science, Institute of Molecular and Translational Medicine, Palacky University, 771 46 Olomouc, Czech Republic

V. Krchňák (✉)
Department of Organic Chemistry, Faculty of Science, Institute of Molecular and Translational Medicine, Palacky University, 771 46 Olomouc, Czech Republic

Department of Chemistry and Biochemistry, University of Notre Dame, 251 Nieuwland Science Center, Notre Dame, IN 46556, USA
e-mail: vkrchnak@nd.edu

1 Introduction

1.1 General Strategy

The synthesis of peptidomimetics containing fused and bridged chiral heterocycles with a three-dimensional architecture requires robust and versatile synthetic methods. Among the plethora of chemical transformations used to achieve various peptide backbone constraints, the tandem *N*-acyliminium ion cyclization–nucleophilic addition reaction represents a particularly attractive option (Fig. 1). The chemistry of *N*-acyliminium ions has been applied in the synthesis of diverse heterocyclic compounds [1–5]. With respect to peptidomimetics, the most attractive features of the iminium-based synthetic strategy include (1) access to structurally diverse constraints, (2) the modular independent synthesis of individual ring precursors, and (3) compatibility with traditional Merrifield solid-phase peptide synthesis. In the general concept, an acyclic precursor is assembled and exposed to acid-mediated cyclic iminium ion formation and then a second ring closure by nucleophilic addition (Fig. 1). Acyclic precursors have been designed for the construction of two rings in scenarios yielding fused and bridged systems.

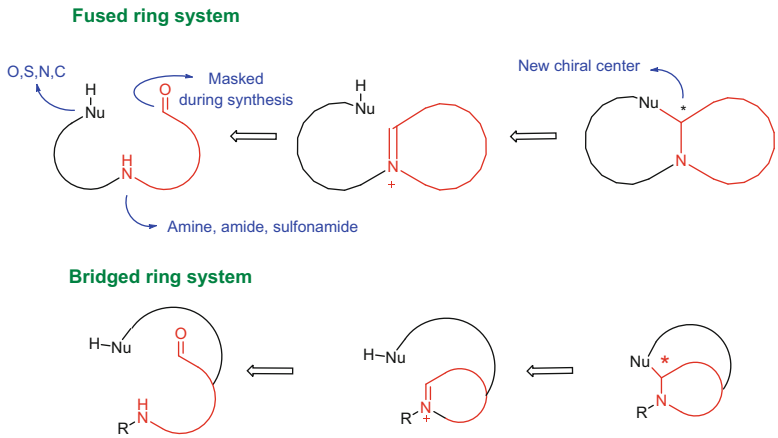

Fig. 1 General schemes of tandem *N*-acyliminium ion cyclization–nucleophilic addition reactions to fused and bridged ring systems

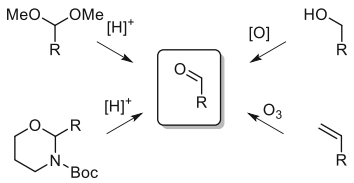

Fig. 2 Masked forms of aldehyde precursor for cyclic iminium ion formation

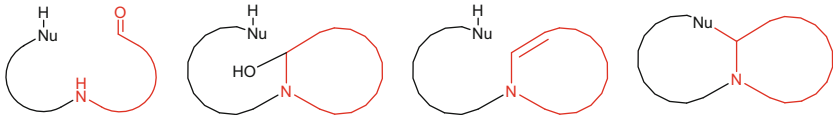

Fig. 3 Potential products from the exposure of acyclic intermediate to acid

Among the various methods for iminium ion synthesis, the condensation of secondary amides with aldehydes (and ketones) is regarded as one of the most versatile [3, 6–8]. This route has been particularly effective using peptide backbone amides for *N*-acyliminium ion formation. Typically, the acyclic precursor is prepared with "masked" aldehyde functionality (Fig. 2). Synthetic routes to the aldehyde precursor include acid-mediated acetal deprotection [9–11], alcohol oxidation, olefin oxidation by ozonolysis [12] and by OsO_4 catalysis [13], as well as acid-catalyzed 1,3-oxazinane cleavage [14, 15].

After assembly of the acyclic precursor is completed, acid (e.g., TFA and formic acid) is typically employed to form the cyclic iminium ion. Depending on the precursor structure, the conversion of the unprotected aldehyde to the iminium ion may proceed slowly providing mostly lineal aldehyde or stop at the cyclic geminal amino alcohol intermediate (Fig. 3). Similarly, attack of the internal nucleophile to the iminium ion may close the second ring forming the bicycle or may be impeded by steric and electronic factors, including formation of cyclic enamine instead. The spectrum of potential products depends largely on the structure of the intermediate and is discussed case by case because of the lack of general rules dictating cyclization.

1.2 Application to Peptides

As mentioned, compatibility with Merrifield solid-phase peptide synthesis is an attractive feature of the iminium ion strategy. The prerequisite aldehyde may be advantageously incorporated by attachment of a protected two-carbon unit to the peptide backbone amide nitrogen. The *N*-(2-oxo-ethyl)peptide derivative can in

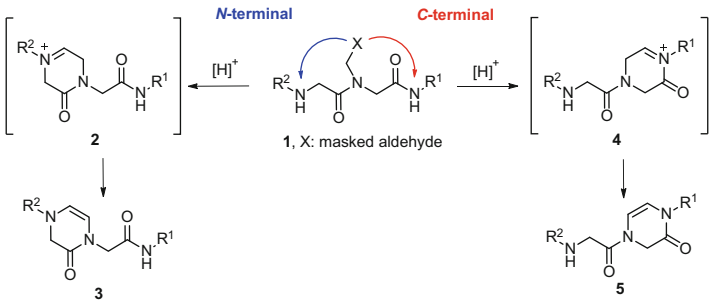

Scheme 1 Formation of cyclic *N*-acyliminium ions at the peptide *N*- and *C*-terminal

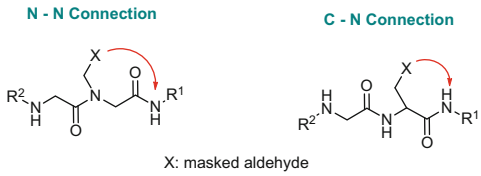

Fig. 4 Two scenarios (N–N and C–N) of peptide backbone bridging

principle form *N*-acyliminium species in two directions (Scheme 1) [16]. The cyclic *N*-acyliminium ion can, respectively, react in the direction of the peptide *N*- or *C*-terminal to give cyclic *N*-acyliminium ions **2** [9, 11, 17–19] and **4** [10]. Cyclization in either direction is viable, and both modes of *N*-acyliminium ion cyclization have been reported [9–11].

In the absence of nucleophile, intermediates **2** and **4** convert to 3,4-dihydropyrazin-2(1*H*)-ones **3** and **5**, respectively [20, 21]. Both scenarios have been documented for model compounds that provided selectively each of the two six-membered rings [22].

The masked aldehyde may also reside on the amino acid side chain, albeit this synthetic scenario has been documented in only a few examples [23]. In this case, the bridging element connects the C^{α} carbon and amide nitrogen (Fig. 4).

Cyclic *N*-acyliminium ions have been transformed into more complex structures by intramolecular nucleophilic addition to form fused bicyclic ring systems (e.g., **6**–**9**) [2–5, 24]. Peptide amide and amino acid side chains (O, S, N, C) have served as the nucleophile (Scheme 2).

2 Single Heterocycles

Although *N*-acyliminium ion chemistry is predisposed for a subsequent nucleophilic addition reaction, in the absence of a nucleophile, the cyclic iminium ion can undergo deprotonation in a neutral medium, forming dihydropirazinones which can

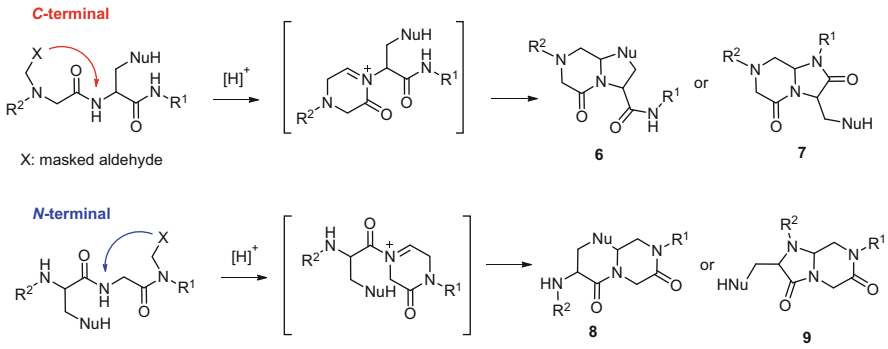

Scheme 2 Tandem fused ring formation in *C*- and *N*-terminal directions

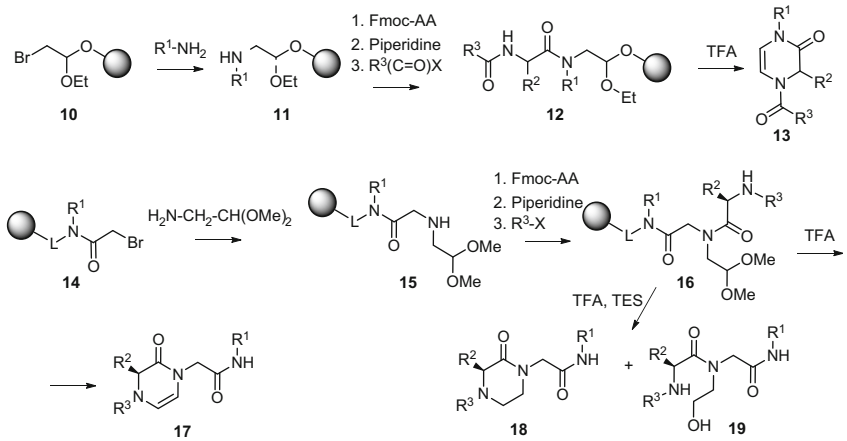

Scheme 3 Syntheses of piperazinones

be reduced to piperazinones. Piperazines and piperazinones are common pharmacophore components in numerous drugs and have thus been targeted by a variety of chemical routes (reviewed in [25]).

3,4-Dihydropyrazin-2(1*H*)-ones have been synthesized from linear 2-amino-*N*-(2,2-dimethoxyethyl)acetamide precursors by iminium ion cyclizations (Scheme 3) [20, 21]. For example, the bromide of bromoacetal resin **10** was displaced by various amines, and the resulting amino acetal **11** was acylated by different *N*-(Fmoc)amino acids [20]. After Fmoc group removal, amine acylation with various acids, acid chlorides, and isocyanates (**12**), followed by resin cleavage and cyclization, gave dihydropirazinones **13**. Alternatively, the protected aldehyde was introduced by bromoacetylation of the amine resin (**14**), followed by the nucleophilic displacement of bromine with the 2,2-dimethoxyethylamine providing **15** [21]. Piperazinones **18** have been prepared by reduction of the dihydropirazinones **17** by hydrogenation, typically using a palladium catalyst [26–28], and hydride

addition using triethylsilane (TES) [21, 29] and $NaCNBH_3$ [26]. Cleavage from the resin **16** carried out in the presence of TES provided direct access to piperazinones **18**, along with minor amount of alcohol **19** [21].

3 Fused Heterocycles

Bicyclic systems with different ring sizes have been assembled from acyclic substrates by intramolecular iminium ion formation and trapping with various internal nucleophiles. Key to these strategies has been the introduction of protected aldehydes into the peptide by different routes, featuring suitable polymeric supports and building blocks. Based on the ring size of the iminium ion intermediate, this section is divided into three parts: (1) five- and six-membered, (2) seven-membered, and (3) eight- and nine-membered iminium ion intermediates.

3.1 Fused Ring System Synthesis Using Five- and Six-Membered Iminium Ions

3.1.1 Synthetic Strategies to Access Acyclic Precursors

Acetal protection has been effectively used to introduce the aldehyde component for solid-phase iminium ion approaches to bi-, tri-, and tetracyclic heterocycles. For example, 5,6-fused 1-acyl-3-oxopiperazines **21** were synthesized using dipeptide amide **20** linked to the acetal attached to TentaGel OH resin. Treatment with TFA induced resin cleavage, iminium ion formation, and attack of the *N*-terminal carbamate to form conformationally rigid peptidomimetic bicycle **21** (Scheme 4a)

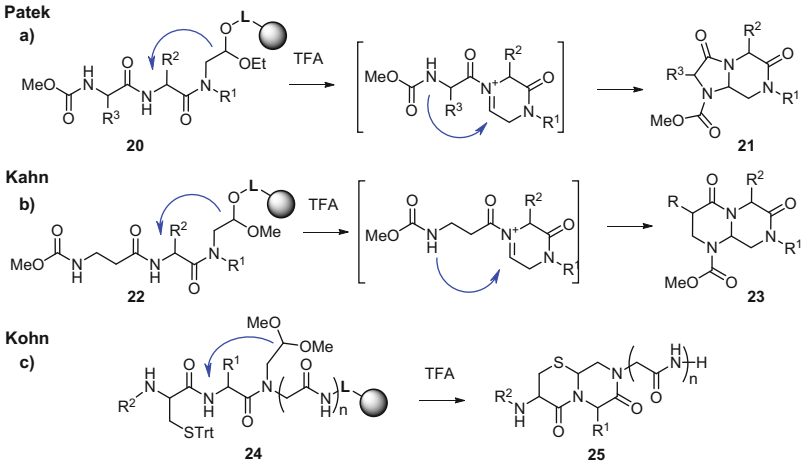

Scheme 4 Tandem iminium ion cyclizations on solid supports using acetal-protected aldehydes

[11]. 6,6-Fused bicycles **23** were prepared for use as β-turn mimics by employing β-amino acids at the *N*-terminal of dipeptide amide **22** in a similar strategy (Scheme 4b) [17–19]. Alternatively, by positioning of the acetal-protected aldehyde on a central amide of cysteine-containing polymer-supported peptides **24**, 6,6-fused bicycles **25** were prepared by trapping the iminium ion with the thiol side chain upon exposure of the acyclic precursor to TFA (Scheme 4c) [9].

N-Boc-1,3-Oxazinanes have served as masked aldehyde alternatives that are cleaved under milder conditions than acetals. For example, coupling of *N*-Boc-1,3-oxazinane-protected succinic semialdehyde to the amine of various phenylalanine derivatives gave linear precursors **26**, which on treatment with acid underwent intramolecular *N*-acyliminium ion Pictet–Spengler cyclizations to provide 1,5,6,10b-tetrahydro-2*H*-pyrrolo[2,1-a]isoquinoline-3-ones **27** (Scheme 5a) [14, 15, 30]. Employment of tryptophan analogs as well as β-(2-thienyl)-, β-(2-furyl)-, and 3-benzothienyl-alanines (**28**) in similar sequences provided a diverse series of tri- and tetracyclic ring systems **29** [14]. Olefins have also served as masked aldehydes that were revealed by oxidative cleavage using OsO_4/$NaIO_4$/DABCO in the presence of aromatic amino acid and *O*-trityl homoserine residues (**30**, **32**), prior to iminium ion cyclization and attack, respectively, from the aromatic ring and the alcohol to give multi-cyclic and tricyclic analogs **31** and **33** (Scheme 5b) [13]. Moreover, *tert*-butyldimethylsilyl ethers have been used as masked aldehydes in linear peptides possessing 3,4-dimethoxyphenylalanine and tryptophan residues **34** [13]. After alcohol liberation by silyl group cleavage with *tetra-n*-butylammonium fluoride, and oxidation with Dess–Martin periodinane, the aldehyde reacted in *N*-acyliminium ion Pictet–Spengler cyclizations to give, respectively, tri- and tetracyclic analogs **35** (Scheme 5c). Analogously, conformational constraints have been incorporated into peptides possessing 5-phenyldimethysilylproline residues, which undergo electrochemical anodic oxidation to provide *N*-acyliminium ions, followed by intramolecular nucleophilic addition to furnish bicyclic amino acid derivatives [31–33].

Among various masked aldehyde equivalents offering utility for the introduction of iminium ion precursors into linear peptides, acetals have often been used because of their versatility and simplicity. As mentioned, 2,2-dimethoxyethylamine has been used as a two-carbon building block that may be introduced into the peptide backbone by displacement of the bromide of a bromoacetamide residue (Scheme 3) [21]. In an alternative strategy, glycolaldehyde dimethyl acetal has been incorporated into supported *N*-sulfonyl amide peptides (**36**), providing *N*-alkyl-*N*-nitrobenzenesulfonyl (Nos) amides (**37**) under Mitsunobu reaction conditions. Removal of the Nos group enabled the extension of the peptidic chain (**38**) (Scheme 6) [24, 34].

3.1.2 Regioselectivity of the Iminium Ion Formation

Cyclizations have been performed in both directions with a preference for the *N*-terminal amide, albeit iminium ion formation on the *C*-terminal amide has been applied to make fused ring heterocycles usually in solution by reactions featuring

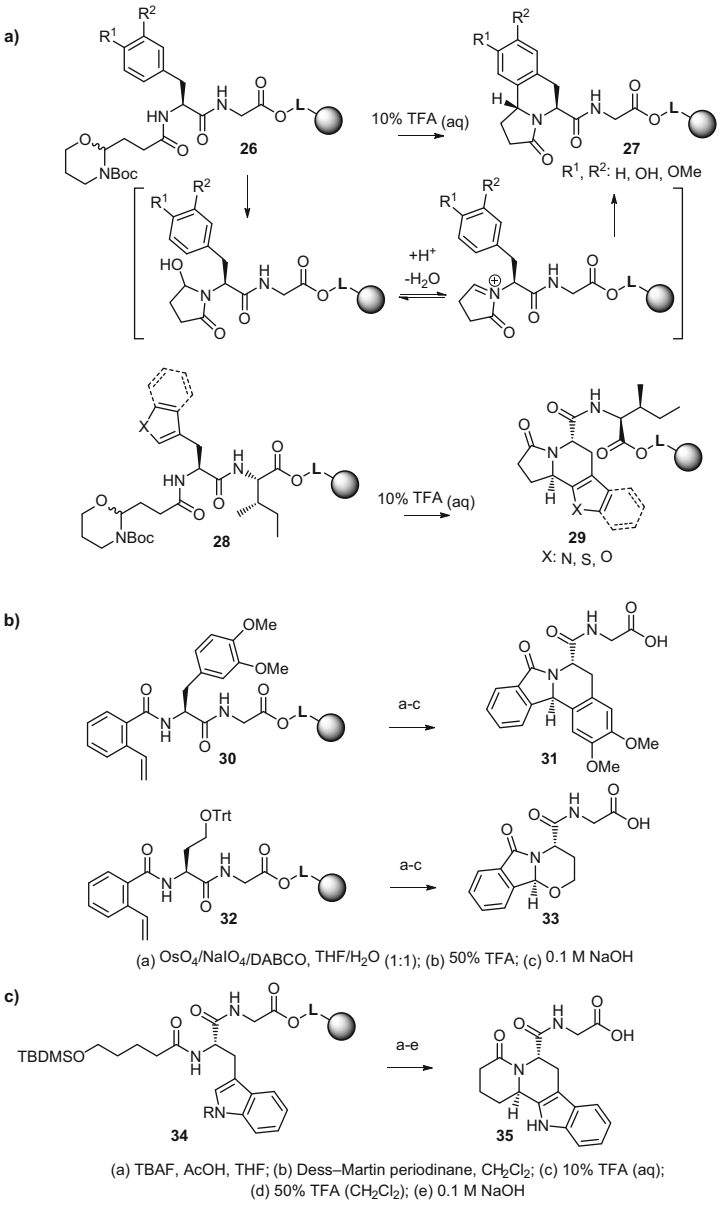

Scheme 5 Application of different masked aldehydes in tandem iminium ion cyclizations on solid support

amines, alcohols, thiols, and aromatic rings as internal nucleophiles [35–37]. The preferences for cyclic iminium ion formation using acetals that may react in both the *C*- and *N*-terminal directions have been studied using different internal

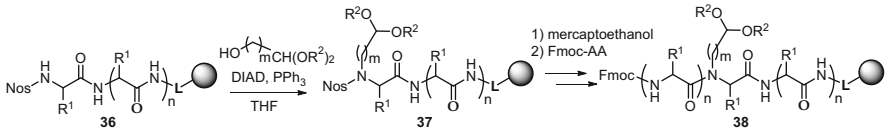

L = linker; R^1 = side chain of different amino acids; R^2 = methyl, ethyl; m = 1, 2

Scheme 6 Incorporation of an acetal-masked aldehyde by Mitsunobu alkylation of nitrosulfonamide

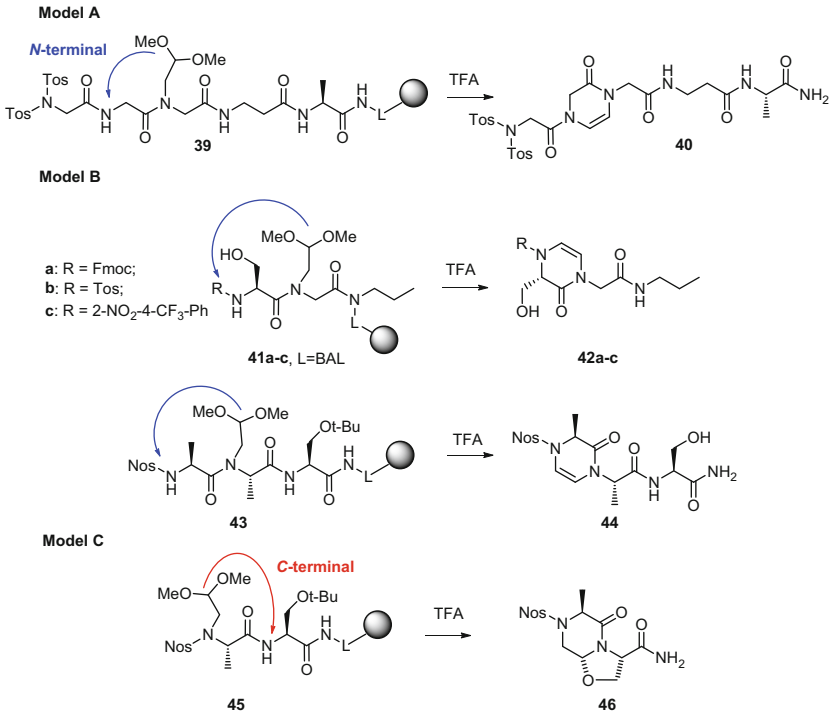

Scheme 7 Evaluation of the regioselectivity of cyclic iminium ion formation on a peptide backbone

nucleophiles: amides, sulfonamides, and anilines (Scheme 7) [38]. In all cases, the piperazine ring was exclusively formed on reaction at the peptide *N*-terminal. For example, treatment of solid-supported linear pentapeptide **39** with TFA gave only dihydropirazinone **40** (Model A, Scheme 7). Similarly, treatment of linear models **41a–c** and **43** led entirely to formation of heterocycles **42a–c** and **44** by reaction on the *N*-terminal amino group independent of the nucleophile, e.g., amide, urethane, sulfonamide, and aryl groups (Model B, Scheme 7). In the absence of the *N*-terminal amide (e.g., **45**), cyclization occurred at the *C*-terminal (e.g., **46**, Model C).

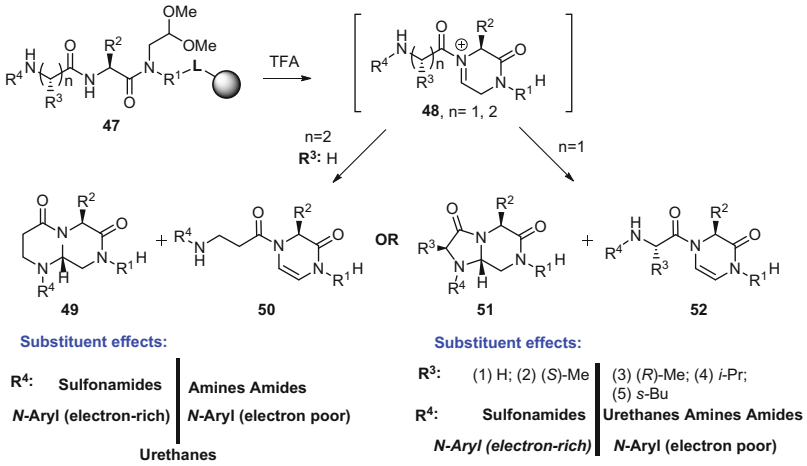

L: (1) BAL linker, (2) Rink linker; **R^1-H:** (1) -$CH_2CONHPr$, (2) -CH_2CONH_2; **R^2:** (1) H; (2) alkyl

Scheme 8 Substituent effects in the formation of 5,6- and 6,6-fused bicycles

3.1.3 Synthesis of 6,6- and 5,6-Fused Bicyclic Systems

Employing linear peptides **47** attached to the resin by acid-labile linkers, both 5,6- and 6,6-bicycles **49** and **51** were prepared, respectively, from their α- and β-amino acid counterparts using a set of internal nucleophiles (Scheme 8) [9, 38]. In the presence of 50% TFA in DCM, the resin-bounded linear precursors **47** were released from the polymer and converted to the cyclic iminium ion intermediate **48**. Formation of bicycles **49** and **51** by nucleophilic attack competed however with tautomerization of the iminium ion and proton loss to form the corresponding enamides (**50** and **52**). Considering the relative ratio of monocycle to bicycle product, the 6,6-fused ring systems were formed more efficiently than their 5,6-fused counterparts. In both cases, the nature of the R^4 group on the amine nucleophile was critical for bicycle formation. Sulfonamides gave bicycles **49** and **51** in 49–78% yields; however, amides and amines failed as nucleophiles in the annulation of the second heterocycle. For the *N*-alkyl precursors, amine protonation may inhibit cyclization. In the case of the *N*-acyl derivatives, switching from amide to carbamate gave partial cyclization to form 6,6-fused rings **49**. Furthermore, electron-rich aniline derivatives **47** formed bicycles **49** and **51**. Bulky R^3 side chains (e.g., *i*-Pr and *s*-Bu), as well as D-configuration at the amino acid (e.g., D-Ala, D-Val) bearing R^3, both hindered cyclization and afforded predominantly enamide (e.g., **52**) [38].

In the cyclization of **47** possessing *S*-configuration at the amino acid α-carbon bearing R^2, the iminium ion intermediate was attacked stereoselectively to provide

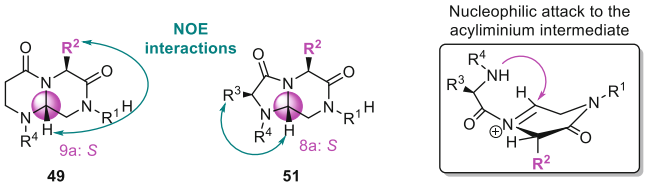

Fig. 5 Stereoselective attack of the cyclic iminium ion gives *S*,*S*-diastereomers

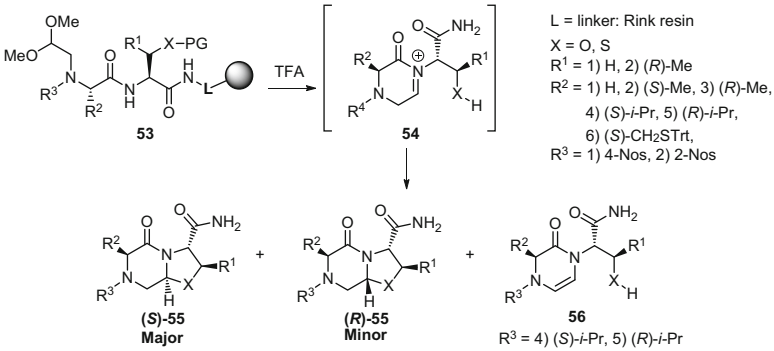

Scheme 9 Synthesis of 6,5-fused bicycles with alcohol and thiol internal nucleophiles

S,*S*-diastereomers **49** and **51** (Fig. 5). The *S*-configuration was assigned based on nuclear Overhauser effect (NOE) observed in ^{1}H NOESY and ROESY spectra. The NOE interactions between the protons at the ring fusion carbon (9a and 8a) and methyl substituent (R^2 and R^3) were, respectively, observed for bicycles **49** and **51** indicative of their proximity on the same face of the ring system. Nucleophilic attack occurs diastereoselectively at the least hindered face of the cyclic acyliminium ion intermediate opposite the R^2 substituent.

3.1.4 *C*-Terminal Cyclization with Amino Acid Side Chain Nucleophiles

6,5-Fused bicycles **55** have been synthesized by employing *N*-(dimethoxyethyl) peptides **53** possessing different *C*-terminal amino acids: L-Ser, L-Thr, and L-Cys (Scheme 9) [39]. Treatment of the polymer-supported dipeptides **53** with acid triggered resin release, removal of protecting groups from the aldehyde and internal nucleophile, endocyclic iminium ion formation (**54**) on the central *C*-terminal amide, and nucleophilic attack to provide bicycles **55**. Bicycles **55** were obtained in yields of up to 75% using alcohol and thiol nucleophiles; however, bulky *N*-terminal amino acids (e.g., L-Val, $R^2 = i$-Pr) hindered the second cyclization and provided product contaminated with enamide **56**.

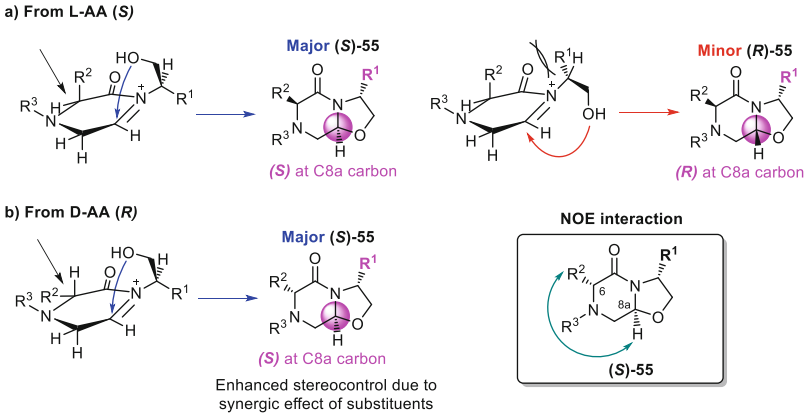

Fig. 6 Stereoselective nucleophilic attack of the six-membered iminium ion on route to 6,5-fused bicycles **55**

6,5-Fused bicycles **55** were obtained as diastereomeric mixtures contingent on the substitution pattern of dipeptide **53**. The configuration of the new ring fusion stereocenter was assigned using NOESY spectroscopy (Fig. 6). Specifically, the NOE interactions were observed between protons on the substituents at C6 and the ring fusion C8a carbon indicative of their location on the same face of the bicycle. Employing *N*-(4-Nos)dipeptides ($R^3 = 4$-Nos), the influence of the stereochemistry of the *C*-terminal residue (e.g., L-Ser, L-Thr, or L-Cys) dictated the preferential formation of the *S*-configuration at the newly formed ring fusion carbon. Although Gly and L-Ala at the *N*-terminal gave diastereomerically pure (*S*)-**55** (Fig. 6a), L-Val, an amino acid with bulkier side chain substituent ($R^2 = (S)$-*i*-Pr), decreased remarkably the stereoselectivity. With *N*-terminal amino acids possessing smaller side chains, attack of the appended nucleophile occurred preferentially on the same face as the R^2 group on the cyclic intermediate to avoid steric interactions between the amide carbonyl of the *N*-acyliminium ion and the *C*-terminal carboxamide (Fig. 6a). Bulkier R^2 groups may decrease selectivity by interfering with the incoming nucleophile. On the other hand, D-amino acids at the *N*-terminal enhanced stereoselectivity due to the synergic minimization of steric interactions between the R^1 and R^2 substituents on route to the ring fusion carbon with *S*-configuration (Fig. 6b).

3.1.5 Competition Between Nitrogen and Oxygen Nucleophiles

The introduction of serine as the *N*-terminal amino acid in supported dipeptides **57** was employed to study the competition between nitrogen and oxygen nucleophiles in the attack of iminium ion **58** to form, respectively, 5,6- and 6,6-fused bicycles **59**

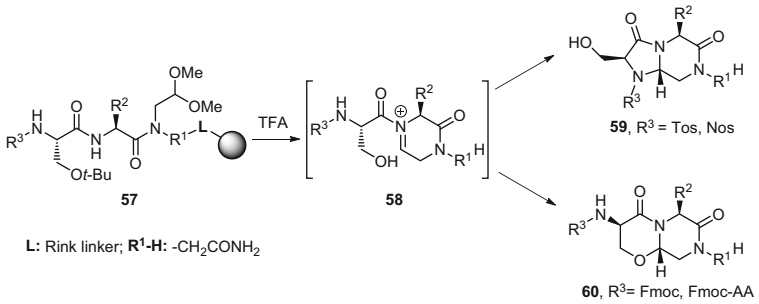

Scheme 10 Chemoselective control of attacking nucleophile in the tandem cyclization of serine derivatives **57**

and **60** (Scheme 10) [39]. In cases using *N*-Fmoc and *N*-(Fmoc)amino acyl serine residues, the alcohol was the favored nucleophile in the closure of the second heterocycle (e.g., **60**, 54–92% yields). On the other hand, *N*-(arylsulfonyl)serine residues (R^3 = Tos and Nos) reacted by the sulfonamide serving as nucleophile to give bicycles **59** (15–67% total yields). Selection of the R^3 substituent of linear dipeptide **57** provided thus chemoselective control over the attacking nucleophile in the tandem cyclization toward 5,6- and 6,6-fused bicycles **59** and **60**.

3.1.6 Benzoimidazopyrazinone Synthesis

Benzoimidazopyrazinones **62** and **64** have been synthesized by routes that employ 1-fluoro-2-nitrobenzene as a precursor to *o*-aminoanilines **61** and **63** by way of nucleophilic substitution of fluorine and nitro group reduction (Scheme 11). Treatment of *o*-aminoanilines **61** and **63** with TFA unmasked, respectively, the protected aldehydes, which condensed in a stepwise fashion onto aniline nitrogen to provide benzoimidazopyrazinones **62** and **64** [24, 40].

3.2 Fused Ring System Synthesis Using Seven-Membered Iminium Ions

Incorporation of a three-carbon protected aldehyde unit onto the peptide backbone has given access to bicycles bearing diazepanone ring systems (Scheme 12) [41]. The supported linear substrates were synthesized analogously as described in Scheme 6, employing alkylation of *N*-terminal 4-nitrobenzenesulfonamides (4-Nos) with 3,3-diethoxy-1-propanol under Mitsunobu reaction conditions to install the masked aldehyde [42]. In principle, this method may be used to convert linear peptides **65** and **68** into seven-membered iminium ion intermediates **66**, which on intramolecular reaction with various nucleophiles would furnish 7,5-

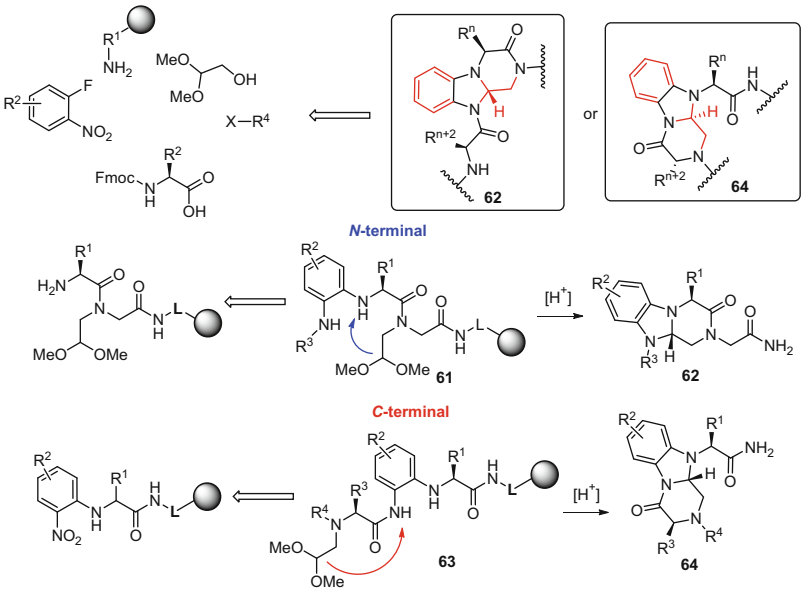

Scheme 11 Two synthetic routes to benzoimidazopyrazinones employing 1-fluoro-2-nitrobenzene

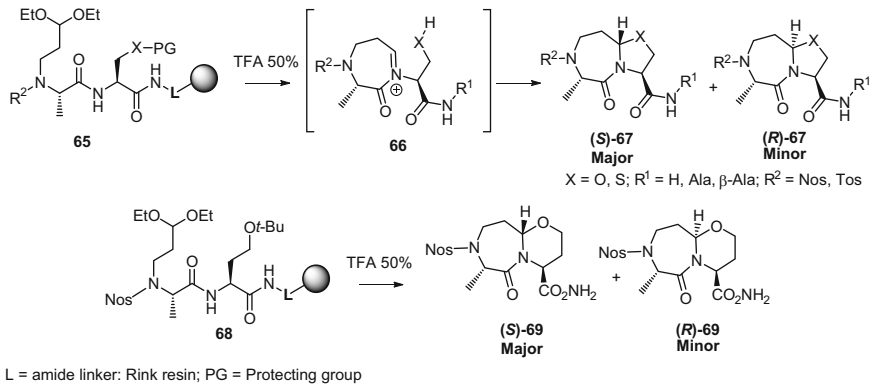

Scheme 12 Application of seven-membered iminium ions to prepare 7,5- and 7,6-fused ring systems

and 7,6-fused ring systems **67** and **69** (Scheme 12). For instance, the incorporation of Ser(O*t*-Bu) and Cys(OTrt) promoted the annulation of five-membered fused ring with good overall yields (23–58%), while Ser(O*t*-Bu) enabled the formation of 7,6-fused bicycles **69** with 20% total yield. L-Amino acids containing the internal nucleophile directed the new stereocenter preferentially toward the (*S*)-configuration (74–99 *d.e.*), while D-amino acids promoted the opposite (*R*)-configuration [41].

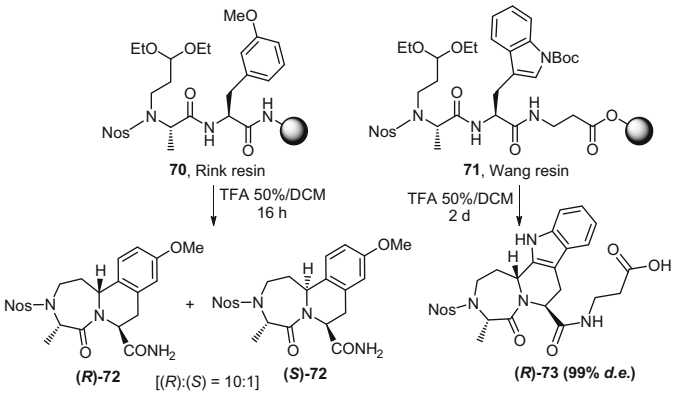

Scheme 13 Tri- and tetracycle synthesis by way of seven-membered iminium ion intermediates

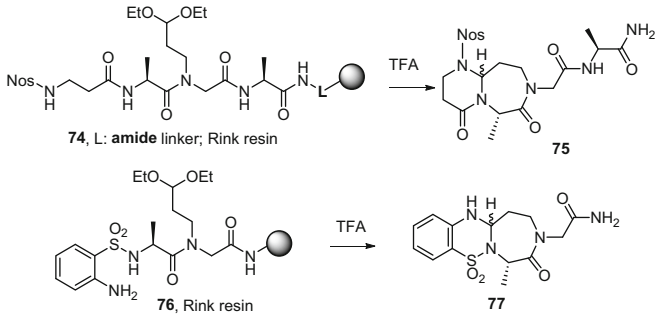

Scheme 14 Synthesis of 6,7-fused ring systems by way of seven-membered iminium ion intermediates

Employing *N*-acyliminium ion Pictet–Spengler reaction chemistry [43], linear peptides **70** and **71** possessing, respectively, *m*-methoxyphenylalanine and tryptophan residues were treated with TFA to provide, respectively, fused seven-membered tri- and tetracycles **72** and **73** in 25% and 15% yields with high regio- and stereoselectivity (Scheme 13) [41].

Rink resin support-bound linear peptides *N*-(Nos)-β-alaninyl-alaninyl-*N*-′-diethoxypropylamide **74** and *N*-(*o*-aminophenylsulfonyl)alaninyl-*N*-′-diethoxypropylamide **76** were, respectively, cleaved from resin with TFA to produce seven-membered iminium ions by condensation of masked aldehyde onto the *N*-terminal amide [44]. Subsequent attack of the sulfonamide and aniline nucleophiles provided, respectively, 6,7-fused heterocyclic ring systems **75** and **77** in up to 45% overall yields (Scheme 14).

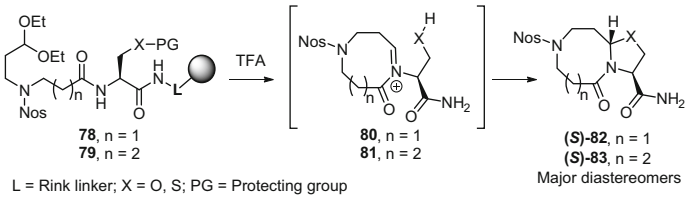

Scheme 15 Synthesis of 8,5- and 9,5-fused ring systems by way of eight- and nine-membered iminium ion intermediates [41]

3.3 Fused Ring System Synthesis Using Eight- and Nine-Membered Iminium Ions

The challenge of increasing the cyclic iminium ion ring size to make larger-ring heterocycles was addressed by combining the three-carbon masked aldehyde unit and longer-chain amino acids, such as β- and γ-amino acids (e.g., linear precursors **78** and **79**, respectively, Scheme 15) [41]. The incorporation of these extended amino acid units enabled the formation of eight- and nine-membered iminium ion intermediates (**80** and **81**), which led to 8,5- and 9,5-fused ring systems **82** and **83** with acceptable overall yields (26–41% and 4–18%, respectively, depending on the combination of building blocks). Moreover, the new stereocenter was generated with high selectivity.

4 Bridged Heterocycles

The iminium ion cyclization–nucleophilic addition strategy was also applied to the synthesis of bridged heterocycles on solid phase. The key difference in the synthesis of bridged instead of fused ring systems entails the connection of the nucleophile with respect to the iminium ion intermediate (Fig. 1). Bridged heterocycles may be considered constrained amino acids with potential to mimic peptide secondary structures, such as α-helices and β-turns.

This section is divided into two parts based on the ring size of the cyclic iminium ion: (1) six-membered and (2) seven-membered iminium ion intermediates. Both carbon–heteroatom and carbon–carbon bonds have been made using such iminium ions contingent on the nature of the nucleophile.

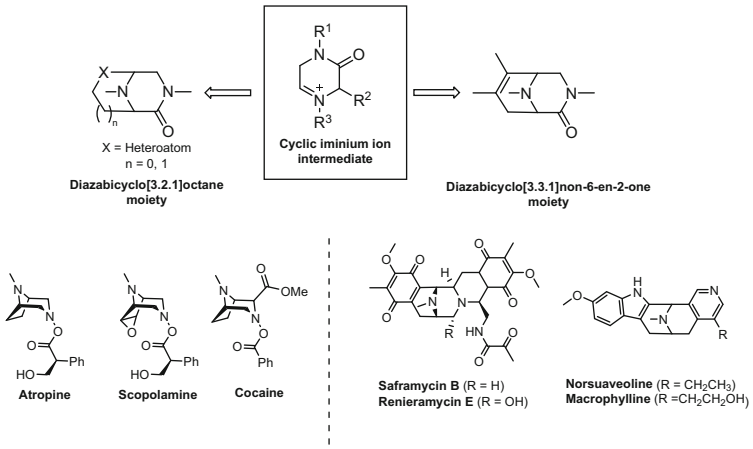

Fig. 7 Bridged frameworks present in bioactive natural products that may be synthesized from six-membered cyclic iminium ion intermediates

4.1 Bridged Ring System Synthesis Using Six-Membered Iminium Ion Intermediates

Natural products have inspired interest to develop synthetic methods aimed at making their complex frameworks. Synthetic analogs that mimic natural products have been used to develop biologically active compounds for applications such as medicine. Among natural products, those with bridged scaffolds, such as diazabicycle[3.2.1]octanes and diazabicycle[3.3.1]non-6-en-2-ones, have attracted interest, because of their interesting activity and challenging synthesis (Fig. 7). Application of such bridged scaffolds as peptidomimetics is intriguing because of their potential to orient side chains in ways that mimic natural peptide secondary structures.

Bridged diazabicyclo[3.2.1]octane frameworks are found in many natural products, such as the tropane alkaloids, atropine, cocaine, and scopolamine (Fig. 7) [45]. These bridged heterocycles exhibit intriguing pharmacological activities, in part due to their potential to mimic peptide structures as constrained isosteres.

Tandem iminium ion cyclization–nucleophilic addition chemistry has been developed using serine- and threonine-*N*′-dimethoxyethylamide moieties for the stereoselective polymer-supported synthesis of (1*S*,5*S*)-6-oxa-3,8-diazabicyclo[3.2.1]octanes (Scheme 16) [46]. A series of resin-bounded linear peptides **84** possessing three points of diversification (R^1, R^2, and R^3) were prepared on Wang and Rink resins. The Thr derivatives (R^2=CH_3) were acid stable, whereas the Ser derivatives (R^2=H) exhibited only partial acid stability. The nature of the R^3 substituent [sulfonamide versus amide] played an important role in the reactivity of iminium ion intermediate **85** and the acid stability of ring system **86**. The *N*-acyl derivatives **86** were more prone to convert to enamide under stronger acid

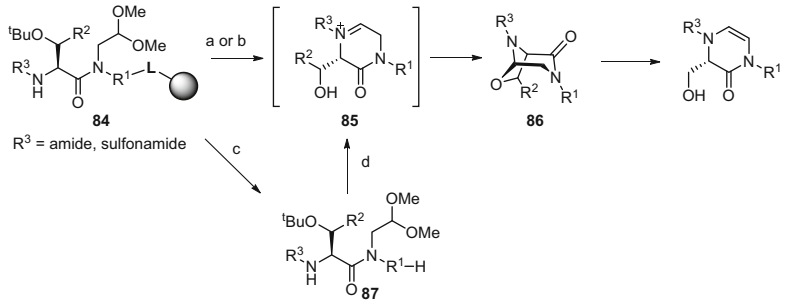

a) TFA in DCM, rt, 90 min; (b) TFA:H_2O (95:5), rt, 90 min; c) Only in Wang resin examples: 0.5 M NaOH in MeOH:THF (1:1), rt, 30 min; (d) neat formic acid, rt, 1 h.

Scheme 16 Synthesis of (1*S*,5*S*)-6-oxa-3,8-diazabicyclo[3.2.1]octanes **86**

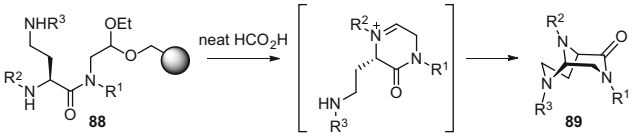

R^2 = Sulfonamide, amide, urea, carbamate

Scheme 17 Solid-phase synthesis of neurokinin antagonists and α-helix mimetics **89**

conditions (TFA) used for resin cleavage and better prepared by saponification of the Wang support with NaOH, followed by treatment with formic acid to induce cyclization of the linear peptide **87** in solution. Depending on the combination of building blocks, diazabicyclo[3.2.1]octanes **86** were prepared in >85% purity and 12–84% overall yields.

The syntheses of bridged heterocycles **89** from 2,3-diaminopropionic acid (Dap) peptides **88** anchored to Wang resin by way of an acetal linker were claimed in a patent (Scheme 17) [47]. The 2,7,9-triazabicyclo[3.3.1]nonan-6-one derivatives were claimed to mimic α-helix secondary structures and serve as neurokinin (tachykinin) antagonists.

Bridged 3,9-diazabicyclo[3.3.1]non-6-en-2-ones are present in saframycin, safracin, renieramycin, ecteinascidin, and related natural products, which exhibit properties such as antiproliferative and antitumoral activity (Scheme 18) [48]. Libraries of 3,9-diaza[3.3.1]non-6-en-2-ones **91** and **93** have been constructed from linear peptides **90** and **92** containing DOPA and Trp residues. Starting from a bromoacetal support that was prepared from Wang resin as noted above, the bridged heterocycle syntheses gave library members with average purity of 90% in 35–75% yield.

3,9-Diaza[3.3.1]non-6-en-2-one scaffold **95** was synthesized from *N*-(Boc)-5-hydroxytryptophan allyl ester [49], which was linked by way of a serine-based carbamate linker from the phenol to an aminomethylated SynPhase™ Lantern

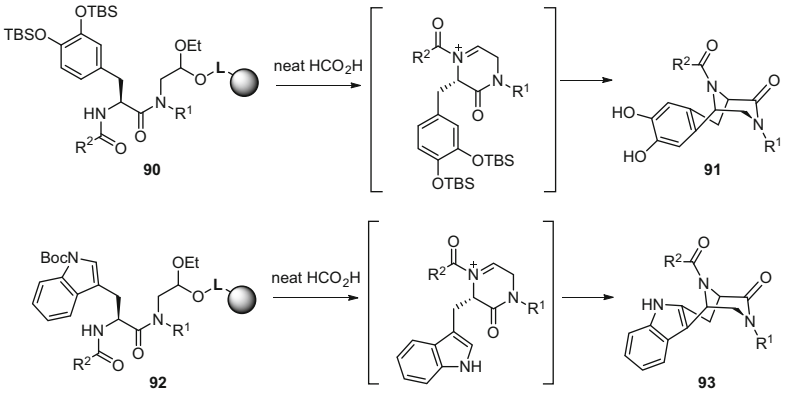

L: acetal linker, Wang resin

Scheme 18 Synthesis of diazabicyclo[3.3.1]non-6-en-2-one libraries **91** and **93**

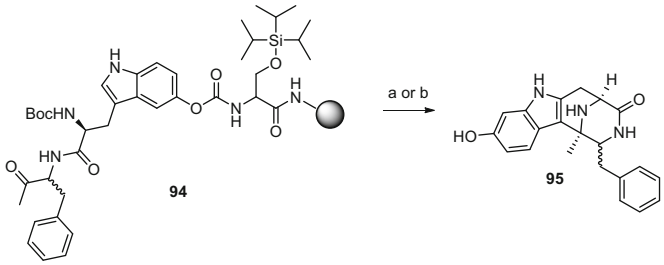

a) 20% TFA in DCM, 50ºC, 16 h; (b) 1 M TBAF in THF, rt, 2 h or 2 N NaOH (aq.):H_2O:THF (2:8:10)

Scheme 19 Solid-phase synthesis of 3,9-diaza[3.3.1]non-6-en-2-one **95** from ketone precursor **94**

(Scheme 19) [50]. The stability of the carbamate linker to TFA and organic bases was key in the synthesis, which featured coupling to phenylalanine and a Dakin–West reaction to convert the carboxylate to amino ketone **94**. The relatively less reactive ketone was converted to the bridged heterocycle using 20% TFA in DCM at 50 °C for 16 h, prior to resin cleavage using either TBAF in THF or NaOH. Scaffold **95** was obtained as a mixture of diastereomers in 85% purity and 35% overall yield and modified further by acylation and alkylation of the bridgehead nitrogen [49].

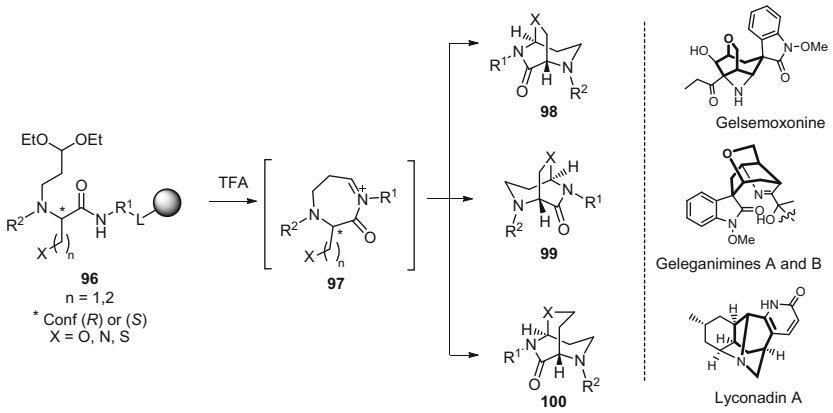

Scheme 20 Bicyclo[3.2.2] and [3.3.2]alkanes **98–100** and related natural products

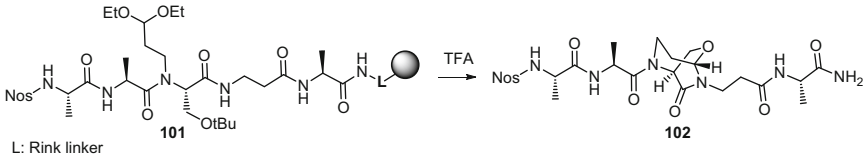

Scheme 21 Bridged heterocycle incorporation into a peptide backbone

4.2 Bridged Ring System Synthesis Using Seven-Membered Iminium Ions

Seven-membered *N*-acyliminium ions have served in the synthesis of bridged heterocycles (Scheme 20) [42]. Employing *N*-(Nos)-*N*-diethoxypropyl-Ser, Thr, homoserine, Cys, and Dap residues in linear peptide precursor **96**, various bicyclo [3.2.2] and [3.3.2]alkanes **98–100** were synthesized stereoselectively via seven-membered cyclic iminium ion intermediate **97**. Bridged heterocycles **98–100** may offer potential to mimic related alkaloid natural products in which similar ring systems are found.

In addition, Merrifield solid-phase peptide synthesis was used to introduce an *N*-(diethoxypropyl)serine residue into peptide **101**, which on treatment with 50% TFA in DCM provided stereoselectively in 24% overall yield bicyclo[3.2.2]alkane **102** to study the influence of the bridged amino acid constraint on peptide conformation (Scheme 21) [42].

5 Summary

In this chapter, we have described the solid-phase synthesis of peptidomimetics via iminium ion chemistry. This strategy has been applied for the synthesis of a broad variety of fused and bridged heterocycles from linear peptide precursors. The constrained systems offer potential to serve as peptidomimetics as well as natural product mimics. Incorporation of masked aldehydes into peptide frameworks has been key for the rapid construction of precursors that form iminium ion intermediates, which undergo intramolecular reactions with nucleophilic backbone and side chain groups to provide diverse molecular scaffolds. In particular, the acetal groups were employed in linkers, side chains, and backbone amide *N*-substituents in solid-phase approaches to prepare a wide range of resin-bounded acyclic precursors. Fused and bridged heterocycles were then assembled in one-pot processes featuring exposure of the precursors to acid conditions to cleave the polymer support, remove the acetal and side chain protecting groups, and induce formation and intramolecular nucleophilic attack of the cyclic iminium ion in tandem cyclizations. Different combinations of building blocks empowered formation of cyclic six-, seven-, eight-, and nine-membered iminium ions, which participated in a second annulation with various heteroatomic (e.g., alcohols, sulfonamides, thiols) and aromatic nucleophiles. Complex and diverse fused and bridged heterocycles were thus obtained effectively with notable regio-, chemo-, and stereocontrol. In light of the rapid construction of the linear precursors by solid-phase chemistry, the efficient tandem cyclization by way of iminium ion intermediates, and the power of the multiple ring products to mimic biologically active peptide conformations, this method may offer significant promise for the construction of peptidomimetics for applications in chemical biology and medicinal chemistry.

Acknowledgment This work was supported by the Department of Chemistry and Biochemistry, University of Notre Dame as well as the projects P207/12/0473 from Czech Science Foundation (GACR) and CZ.1.07/2.3.00/30.0060 and 1.07/2.3.00/30.0004 from the European Social Fund.

References

1. Daich A, Ghinet A, Rigo B (2014) Compr Org Synth II 2:682
2. Maryanoff BE, Zhang HC, Cohen JH, Turchi IJ, Maryanoff CA (2004) Chem Rev 104:1431
3. Royer J, Bonin M, Micouin L (2004) Chem Rev 104:2311
4. Yazici A, Pyne SG (2009) Synthesis 339
5. Yazici A, Pyne SG (2009) Synthesis 513
6. Overman LE (1992) Acc Chem Res 25:352
7. Remuson R, Gelas-Mialhe Y (2008) Mini Rev Med Chem 5:193
8. Speckamp WN, Moolenaar MJ (2000) Tetrahedron 56:3817
9. Kohn WD, Zhang L (2001) Tetrahedron Lett 42:4453
10. Min BJ, Gu X, Yamamoto T, Petrov RR, Qu H, Lee YS, Hruby VJ (2008) Tetrahedron Lett 49:2316

11. Vojkovsky T, Weichsel A, Patek M (1998) J Org Chem 63:3162
12. Paris M, Heitz A, Guerlavais V, Cristau M, Fehrentz JA, Martinez J (1998) Tetrahedron Lett 39:7287
13. Le Quement ST, Nielsen TE, Meldal M (2007) J Comb Chem 9:1060
14. Nielsen TE, Meldal M (2004) J Org Chem 69:3765
15. Nielsen TE, Le Quement S, Meldal M (2005) Org Lett 7:3601
16. Lewis JG, Bartlett PA (2003) J Comb Chem 5:278
17. Eguchi E, Kahn M (2002) Mini Rev Med Chem 2:447
18. Eguchi M, Lee MS, Nakanishi H, Stasiak M, Lovell S, Kahn M (1999) J Am Chem Soc 121:12204
19. Eguchi M, Lee MS, Stasiak M, Kahn M (2001) Tetrahedron Lett 42:1237
20. Lee SC, Park SB (2007) J Org Chem 9:828
21. Vankova B, Brulikova L, Wu B, Krchnak V (2012) Eur J Org Chem 2012:5075
22. Kim JH, Lee YS, Kim CS (1998) Heterocycles 48:2279
23. Cosford NDP, Vamos MD (2014) Patent WO2014085489A1
24. Cankarova N, Krchnak V (2012) J Org Chem 77:5687
25. Dinsmore CJ, Beshore DC (2002) Org Prep Proc Int 34:367
26. DiMaio J, Belleau B (1989) J Chem Soc Perkin Trans I:1687
27. Horwell DC, Lewthwaite RA, Pritchard MC, Ratcliffe GS, Rubin JR (1998) Tetrahedron 54:4591
28. Kitamura S, Fukushi H, Miyawaki T, Kawamura M, Konishi N, Terashita Z, Naka T (2001) J Med Chem 44:2438
29. Peng H, Carrico D, Thai V, Blaskovich M, Bucher C, Pusateri EE, Sebti SM, Hamilton AD (2006) Org Biomol Chem 4:1768
30. Nielsen TE, Meldal M (2005) J Comb Chem 7:599
31. Sun H, Martin C, Kesselring D, Keller R, Moeller KD (2006) J Am Chem Soc 128:13761
32. Sun H, Moeller KD (2002) Org Lett 4:1547
33. Sun H, Moeller KD (2003) Org Lett 5:3189
34. Fukuyama T, Jow C-K, Cheung M (1995) Tetrahedron Lett 36:6373
35. Airiau E, Spangenberg T, Girard N, Schoenfelder A, Salvadori J, Taddei M, Mann A (2008) Chem Eur J 14:10938
36. Ciofi L, Morvillo M, Sladojevich F, Guarna A, Trabocchi A (2010) Tetrahedron Lett 51:6282
37. Wirt U, Schepmann D, Wuensch B (2007) Eur J Org Chem 462
38. La-Venia A, Lemrova B, Krchnák V (2013) ACS Comb Sci 15:59
39. La-Venia A, Dolensky B, Krchnák V (2013) ACS Comb Sci 15:162
40. Ventosa Andrés P, Hradilova L, Krchnak V (2014) ACS Comb Sci 16:359
41. Ventosa Andrés P, La-Venia A, Ripoll CAB, Hradilova L, Krchnak V (2015) Chem Eur J 21:13112
42. La-Venia A, Ventosa-Andrés P, Hradilova L, Krchnák V (2014) J Org Chem 79:10378
43. Stockigt J, Antonchick AP, Wu F, Waldmann H (2011) Angew Chem Int Ed 50:8538
44. Ventosa Andrés P, La-Venia A, Ripoll CAB, Krchnak V (2015) Tetrahedron Lett 56:5424
45. Quirante J, Vila X, Bonjoch J, Kozikowski AP, Johnson KM (2004) Bioorg Med Chem 12:1383
46. Schütznerová E, Oliver AG, Zajícek J, Krchnák V (2013) Eur J Org Chem 2013:3158
47. Eguchi M, Huber V, Lee MS, Mathew J, Nakanishi H, Urban J (2003) Patent US20030236245 A1
48. Lee SC, Park SB (2005) J Comb Chem 8:50
49. Orain D, Canova R, Dattilo M, Kloppner E, Denay R, Koch G, Giger R (2002) Synlett 1443
50. Chou YL, Morrissey MM, Mohan R (1998) Tetrahedron Lett 39:757

Top Heterocycl Chem (2017) 49: 127–158
DOI: 10.1007/7081_2015_187

Published online: 20 November 2015

Synthesis of Peptidomimetics Through the Disrupted Ugi Reaction with Aziridine Aldehyde Dimers

Serge Zaretsky and Andrei K. Yudin

Abstract Aziridine aldehydes and isocyanides participate in a multicomponent reaction with amino acids or peptides. The reaction differs from a conventional Ugi reaction by virtue of the pendent aziridine nucleophile, which intercepts the mixed anhydride intermediate to deliver aziridine amide-containing piperazinones and peptide macrocycles for the respective reactions with amino acids and peptides. The diastereoselectivity of the process depends on the substitution of the amine component, and opposite diastereoselectivity was observed with primary versus secondary amino acids. The aziridine embedded within the piperazinone or cyclic peptides has been used for further transformation and diversification of products through nucleophilic ring opening with thiols, thioacids, and azides, as well as hydrogenolysis. The ring-opened products possess distinct structural organization elements, which have been used to develop rigid scaffolds with increased passive cellular permeability.

Keywords Aziridine · Cyclic peptide · Macrocycle · Multicomponent reaction · Peptidomimetic · Ugi reaction

Contents

S. Zaretsky and A.K. Yudin (✉)
Davenport Research Laboratories, Department of Chemistry, University of Toronto, 80 St. George Street, Toronto, ON, Canada M5S 3H6
e-mail: ayudin@chem.utoronto.ca

1 Multicomponent Reactions

In a multicomponent reaction (MCR) three or more starting materials are combined to form the final product in a single step. The major advantage of MCRs versus those of serial syntheses is the rapid increase in molecular complexity with each step (Fig. 1) [1]. This enabling feature has led to the application of MCRs in combinatorial [2, 3] and diversity-oriented syntheses [1].

Aldehydes and ketones form a crucial role in MCRs through condensation reactions with amines. The iminium ion intermediate that is formed upon condensation is a more reactive species which can participate in a subsequent reaction with an additional nucleophile [4], thereby completing the three-component reaction (Fig. 2). The Mannich reaction [5] and Strecker synthesis [6, 7] are two early examples of MCRs that take advantage of iminium ion chemistry.

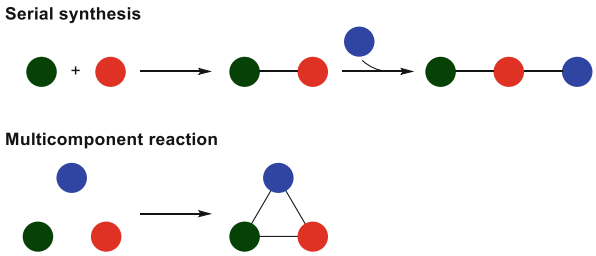

Fig. 1 Comparison of serial and MCRs

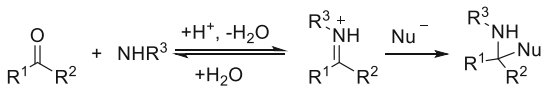

Fig. 2 General multicomponent reactivity through an iminium ion intermediate and a nucleophile

1.1 Amphoteric Molecules in MCRs

A common approach to make multiple bonds in an MCR involves the use of an amphoteric reagent. In chemistry, the term "amphoteric" is often ascribed to molecules that can act as both bases and acids, which is a thermodynamic property [8]. The simplest amphoteric molecule, water, conveniently illustrates this concept (Fig. 3a). α-Amino acids are another type of amphoteric molecule. Possessing both an amine and a carboxylic acid, they can either abstract or liberate protons from their zwitterionic forms (Fig. 3b).

Amphoterism, as a concept, can be extended beyond the Brønsted–Lowry constraints to include nucleophilic and electrophilic reactivity [8]. In this case, the molecules are considered kinetically amphoteric and are referred to by the relative positions of the nucleophilic and electrophilic moieties (Fig. 4) [9]. For example, an isocyanide would be a 1,1-amphoteric reagent.

Isocyanides form a privileged class of amphoteric molecules [10]. Historically, the terminal carbon of the isocyanide functionality has been drawn as a carbene to explain its electrophilic and nucleophilic nature (Fig. 5a). The zwitterionic depiction of the isocyanide functional group was later adopted to more closely match the physical properties of the functional group (Fig. 5b). More recent studies suggested that these representations form a false dichotomy and that a more valid representation would take into account both the carbene-like and zwitterion character. A computational study has provided a valence bond understanding of the isocyanide moiety [11], in which the carbenic resonance form was a major contributor and only partial triple bond character was present. A new depiction of an isocyanide was proposed with the nitrogen atom donating a lone pair of electrons to the carbon

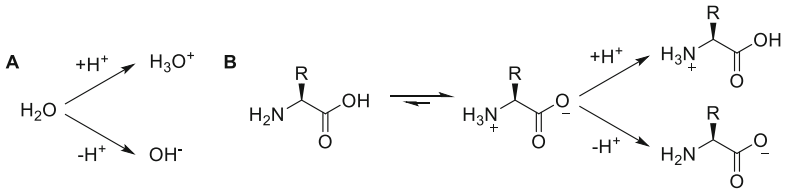

Fig. 3 (**a**) An amphoteric molecule of water acting as both base and acid; (**b**) α-amino acids behave as amphoteric molecules

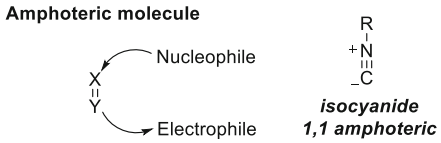

Fig. 4 Kinetically amphoteric molecules possess a combination of electrophilic and nucleophilic reactivity

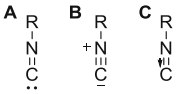

Fig. 5 Isocyanide representations as carbene form (**a**), zwitterion (**b**), and a hybrid-valence structure in which nitrogen lone pair donation stabilizes the carbene (**c**)

center, which takes into account the carbenic behavior and linear arrangement (Fig. 5c). Albeit more instructive, this depiction has not yet become standard [12].

1.2 Ugi and Passerini MCRs

Two of the most important MCRs with isocyanides are the closely related Passerini and Ugi reactions. In the Passerini reaction, three components are linked to produce α-acyloxycarboxamides (Fig. 6) [13, 14]. Activation of the carbonyl component by acid favors isocyanide attack, which, owing to its amphoteric nature, is in turn attacked by the carboxylate. This forms a mixed anhydride intermediate, which can undergo a 1,4-acyl shift to yield the final product. The mechanism of the Passerini reaction has not been fully established, and debate remains as to whether the addition of the isocyanide to the carbonyl component is a stepwise or concerted process [15].

The Ugi reaction expands the Passerini reaction into a four-component MCR through the addition of an amine to yield α-acylaminoamide products (Fig. 6) [10, 16, 17]. After imine/iminium ion formation, the reaction proceeds similarly to the Passerini reaction by way of a mixed anhydride intermediate. The Ugi reaction has been widely employed in the field of MCRs for target-driven synthesis [18–21], and diverse library synthesis [1, 22–26], with notable applications to prepare β-lactams, 2,5-diketopiperazines, and other peptidomimetics [23].

Interesting variations of the Ugi reaction entail the use of components that may intercept intermediates by intramolecular reactions leading to new scaffolds. For example, ester **1** was isolated following solvolysis of the mixed anhydride intermediate formed when proline was employed as both the source of the amine and carboxylic acid components (Fig. 7a) [27]. Lactone **2** resulted from application of L-homoserine as the amino acid component during an Ugi MCR, in which intramolecular attack of the hydroxyl side chain opened the mixed anhydride (Fig. 7b) [28]. The route to **2** suggests that other pendent nucleophiles may intercept the mixed anhydride intermediate to deliver novel, functionally rich scaffolds.

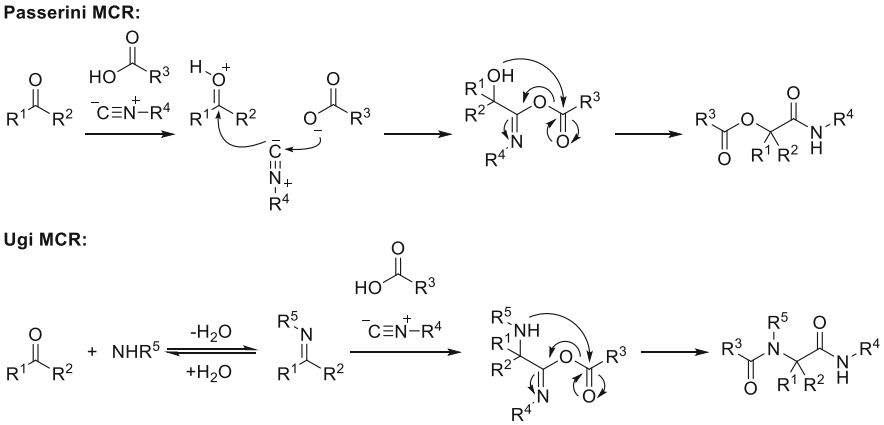

Fig. 6 The Passerini three-component and Ugi four-component MCRs

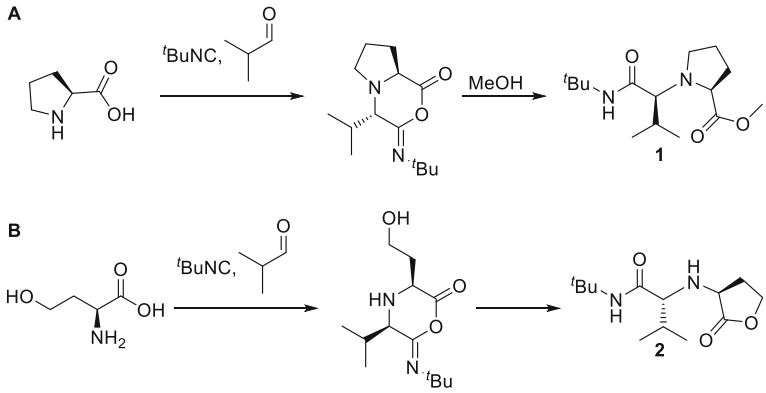

Fig. 7 (**a**) Ugi MCR with L-proline leads to methyl ester **1** after solvolysis of the mixed anhydride intermediate; (**b**) nucleophilic side-chain hydroxyl intercepts the mixed anhydride intermediate to form **2**

1.3 Aziridine Aldehydes

Unprotected amino aldehydes are desirable but seldom realized chemical entities, due to reactivity leading to imine and iminium ion formation [29]. Strategies for isolating unprotected amino aldehydes have centered on increasing chemical stability by employing strong acid conditions [30, 31] and steric encumbrance [32–37].

In 2006, the synthesis of bench-stable amphoteric aziridine aldehydes was reported [38]. Contrary to the expectation of having an amine and aldehyde in one molecule, these reagents did not self-condense with loss of water [8]. This behavior is both kinetically and thermodynamically controlled. The ring strain required to form an aziridine iminium disfavors condensation (Fig. 8); instead,

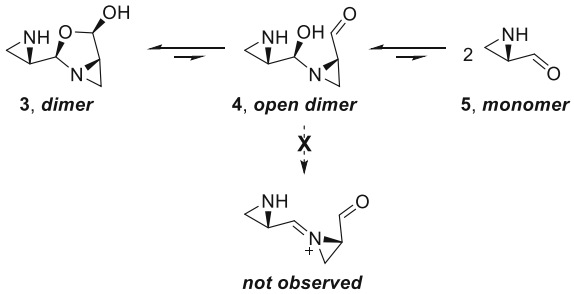

Fig. 8 Equilibrium of aziridine aldehydes in their dimer, open dimer, and monomeric forms

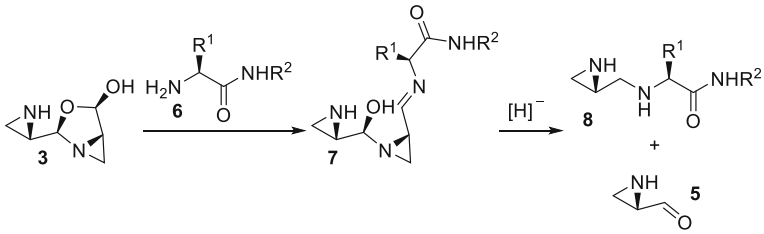

Scheme 1 Reductive amination with peptide **6** and aziridine aldehyde dimer **3**

the aziridine aldehyde reagent exists as acetal dimer **3**, which exhibits unfavorable dissociation to afford the open dimeric aldehyde **4** or monomer **5** [39].

In addition to applications in indium-promoted aldehyde allylation [40], rerouted aza-Michael reaction [41], intercepted Pictet–Spengler reaction [38], and others [8], we were interested in exploiting the rich functional density of the aziridine aldehyde in the synthesis of peptides and peptidomimetics. For example, in spite of the tendency for aziridine aldehydes to form dimer **3**, N-terminal aziridine 1,2-diamine products (e.g., **8**) containing only the monomeric skeleton were isolated from reductive aminations without epimerization at the α-carbon (Scheme 1) [38].

The presence of an electrophilic aziridine in **8** enabled further reactivity by aziridine ring opening [42]. For example, exposure of **8** to thioacids (e.g., **9**) caused regioselective ring opening to yield thioester **10**. Closely related to the intermediates of native chemical ligation [43], thioester **10** could be induced to undergo S → N-acyl transfer, through tetrahedral intermediate **11**, to produce reduced amide peptidomimetic **12** (Scheme 2). Desulfurization of sulfhydryl **12** would result in formal ligation of an alanine-reduced amide [44].

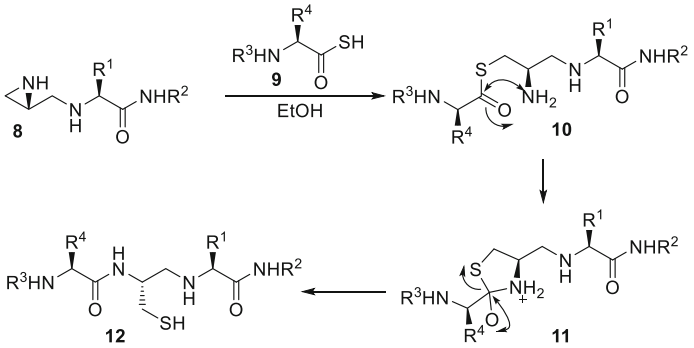

Scheme 2 Peptidomimetic ligation by aziridine ring opening with thioacids

2 Cyclic Peptide Synthesis

2.1 Conventional Cyclization

Peptides are valuable tools for evaluating biological pathways [45–49]. Their utility lies in their facile synthesis and ability to engage in native interaction with proteins. Peptides may, however, possess pharmacokinetic issues such as degradation by proteases and poor cellular permeability [50]. Cyclic peptides have offered a logical alternative to linear peptides [51], because they cannot effectively bind to endopeptidases that prefer extended conformations, nor do they possess amine and carboxylate ends for binding to exopeptidases [52]. Through modification by amide methylation and placement of hydrophobic groups, cyclic peptides have also been made cell permeable [53, 54]. Cyclic peptides occupy fertile chemical space for developing probes and therapeutics [55, 56].

Chemical synthesis remains a barrier to applying cyclic peptides in the study of biological pathways. Relative to the construction of linear peptides for which a wide variety of effective synthetic methods exist, successful approaches for stitching the two ends of a linear peptide to make its cyclic counterpart are typically sequence dependent [57]. Slow cyclization kinetics may necessitate the use of high dilution to avoid competitive oligomerization [55]. Moreover, carboxylic acid activation may disrupt the natural ion pair interaction between the termini of a linear peptide (Fig. 9) [58]. In the presence of an activating agent (HATU, PyBOP, etc.) under basic conditions, the equilibrium between unproductive conformers (e.g., **14**) and those well oriented for cyclization (e.g., **15**) becomes heavily dependent on sequence. Conformer **14** may ultimately react intermolecularly leading to reduced yield.

The sequence dependence for cyclization of a linear pentapeptide is instructively summarized in Fig. 10 [59]. Choice of linear substrate and amide bond-forming conditions on route to the cyclic peptide may dictate success or failure, lead to

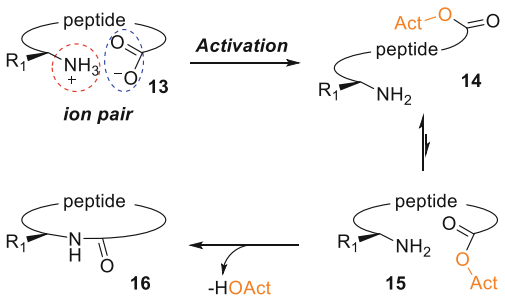

Fig. 9 Difficulty in attaining cyclization-conducive conformations after carboxylic acid activation

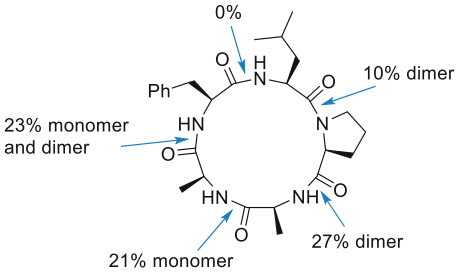

Fig. 10 Amide formation for cyclization can be dramatically affected by the choice of linear sequence

diastereomeric mixtures due to epimerization, as well as result in cyclic dimers and oligomers [57, 58].

2.2 Peptide Cyclization Through MCRs

Amide bond formation is a pivotal step in Ugi chemistry; however, few studies have employed such MCRs for the synthesis of macrocyclic lactams, such as cyclic peptides [10, 60, 61]. A notable use of the Ugi reaction for peptide cyclization of was reported by Götz and coworkers, albeit with low yield likely due to the choice of linear sequence [22, 62]. The Ugi reaction of the tripeptide $(glycine)_3$, isobutyraldehyde, and cyclohexyl isocyanide failed to give cyclic peptide **17**; instead, after multiple days of reaction, the product from integration of two equivalents of each reagent, cyclic dimer **18**, was isolated as a mixture of diastereomers in 12% yield (Scheme 3). Employing $(glycine)_6$ under similar Ugi conditions, the desired cyclic monomer **19** was isolated in 19% yield.

The Ugi reaction has been employed in the macrocyclization of poly-*N*-substituted glycines, so-called peptoids [63]. In contrast to peptides, peptoids may be substantially more flexible, due to *cis*-/*trans*-isomerization about their tertiary amide bonds [64, 65]. In the synthesis of depsipeptoid analogues of sansalvamide A (e.g., **20**) and a pentapeptoid analog of the RGD sequence [66], pseudo-high dilution was essential for ensuring selective formation of macrocyclic product, albeit in 33–49% yield in the case of the former (Fig. 11).

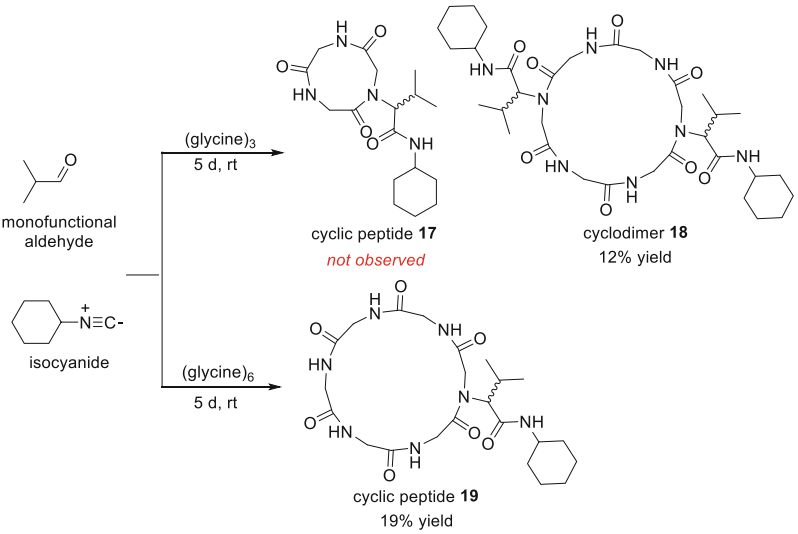

Scheme 3 The Ugi cyclization of glycine oligomers

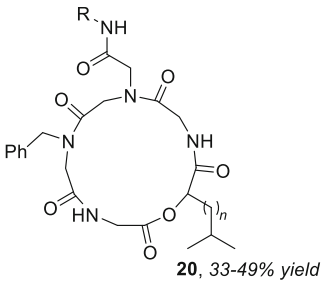

Fig. 11 Depsipeptoid analogues of sansalvamide A synthesized by Ugi macrocyclization (R = ^{i}Pr, ^{i}Bu, ^{t}Bu)

Ugi macrocyclization failed to provide ansacyclic cyclopeptide alkaloid **21**, due likely to the rigidity of isocyanide acid **21**; instead cyclodimer **23** was isolated (Scheme 4) [61].

Multiple Ugi reactions have been performed using diamine and diacid building blocks joined by rigid linkers [67], such as steroids [68], biarylethers [69–71], and other scaffolds [72–74], to form skeletally diverse macrocycles (Scheme 5) [61, 75].

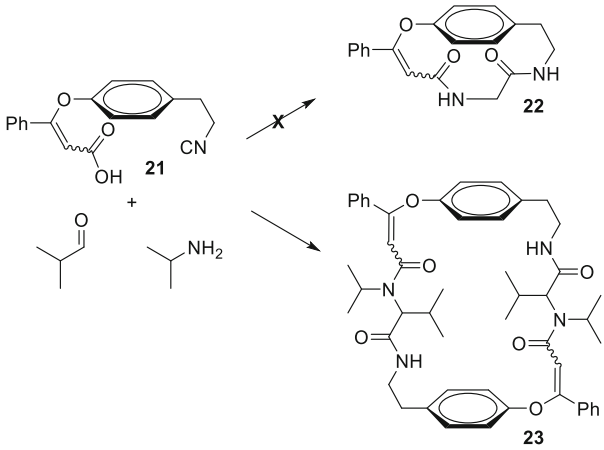

Scheme 4 Failed Ugi macrocyclization gives cyclic dimer

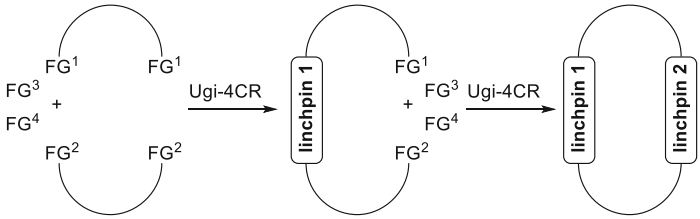

Scheme 5 Macrocyclization via multiple Ugi reactions

3 The Disrupted Ugi Reaction with Aziridine Aldehyde Dimers and Amino Acids

3.1 Four-Component Five-Center Ugi Reaction

Using aziridine aldehyde dimers as aldehydes in four-component Ugi reactions with secondary amines, carboxylic acids, and isocyanides gave novel aziridine amides (e.g., **25**) in 59–94% yields with up to 4:1 diastereoselectivity [76]. Aziridine amides **25** were rearranged to form lactones **26** during column chromatography on silica gel, or in the presence of *p*-toluenesulfonic acid, by a mechanism involving aziridine ring opening by intramolecular nucleophilic attack of the oxygen of the pendent amide (Scheme 6).

Replacement of secondary by primary amine components in the Ugi reaction with aziridine aldehyde **24** gave alternative products. For example, isopropylamine and benzylamine gave, respectively, a complex mixture and conventional Ugi product **29** (Scheme 7). Two possible pathways for the formation of **29** were hypothesized in which the benzylamine or aziridine nitrogen participated

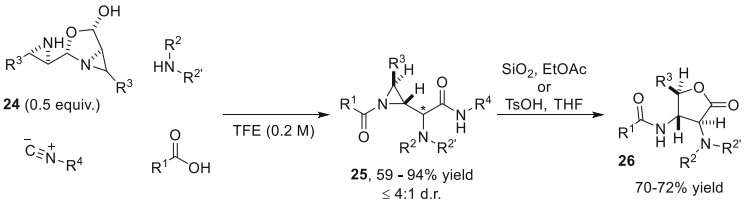

Scheme 6 Aziridine aldehyde dimers participate in Ugi four-component five-centered reactions to yield aziridine amides **25**, which undergo acid-catalyzed rearrangement to lactones **26**

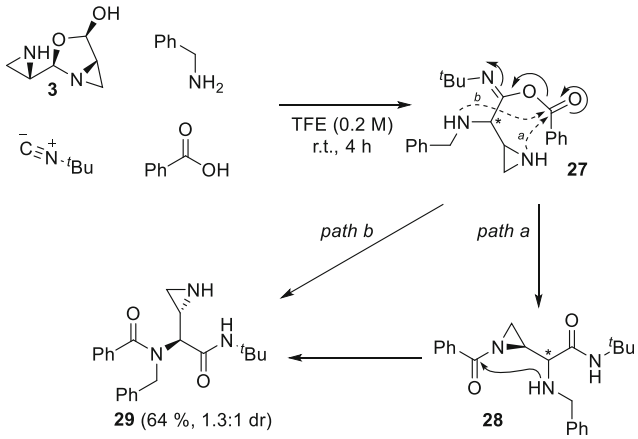

Scheme 7 Possible mechanistic pathways for Ugi reaction of aziridine aldehyde dimer and benzylamine

respectively in the *trans*-acylation reaction to render **29** directly or by way of **28**, which undergoes acyl migration from the aziridine to benzylamine nitrogen (Schemes 6 and 7).

3.2 Piperazinone Chemistry

The Ugi reaction of aziridine aldehyde dimer, isocyanide, and α-amino acid provided 6-membered piperazinone rings (e.g., **31**) possessing *trans*-relative stereochemistry (Scheme 8) [77]. In the proposed mechanism to **31**, the conventional Ugi-mixed anhydride intermediate **33** is intercepted by the pendent aziridine nucleophile to generate the lactam and liberate the side-chain carboxamide. This disrupted Ugi reaction afforded piperazinone rings **31** with stereocontrol from three readily available components in a single-step, thereby simplifying access and adding molecular complexity to these valuable heterocycles [78–81].

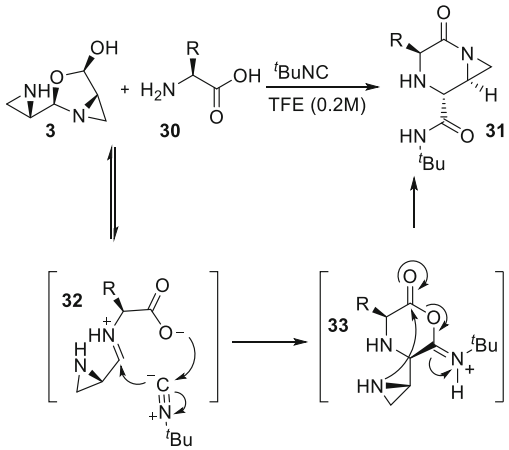

Scheme 8 Disrupted Ugi reaction with aziridine aldehyde, amino acid, and *tert*-butyl isocyanide

Table 1 Substrate scope of piperazinone formation by the disrupted Ugi reaction

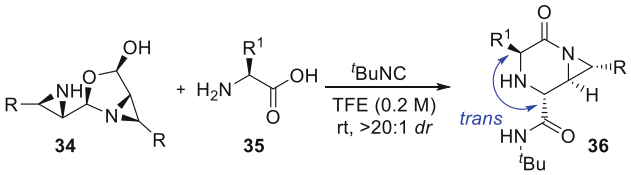

Entry	R	Amino acid	Yield (%)
1	$CH_2OTBDMS$	L-Phenylalanine	92
2	$CH_2OTBDMS$	D-Phenylalanine	90
3	$CH_2OTBDMS$	L-Alanine	82
4	$CH_2OTBDMS$	L-Proline	98
5	$CH_2{}^{i}Pr$	D-Arginine	83
6[a]	$CH_2{}^{i}Pr$	L-Lysine HCl[e]	76
7	$CH_2OTBDMS$	L-Glycine	80
8[b]	$CH_2{}^{i}Pr$	L-Aspartic acid	76
9[c]	$CH_2OTBDMS$	L-Cysteine	82
10[d]	$CH_2OTBDMS$	L-Histidine	88
11	$CH_2OTBDMS$	L-Serine	77

[a]HFIP/H_2O (20:1) was used as solvent
[b]Cyclization occurred at the α-carboxylate
[c]Degassed TFE was used
[d]HFIP was used as solvent
[e]ε-Amine protonated

A range of substrates was reported that encapsulated primary and secondary amino acids and two substituted aziridine aldehyde dimers (Table 1). The initial

trans-relative stereochemistry was assigned based on an X-ray analysis of piperazinone **36** (R = $CH_2OTBDMS$, R^1 = Bn) formed from L-phenylalanine. The favored reaction solvents were TFE and HFIP, both of which had been featured in prior work with aziridine aldehyde dimers [8].

On further investigation of the diastereoselectivity of the disrupted Ugi reaction, primary and secondary amino acids were found to give *trans*- and *cis*-relative stereochemistry, respectively (Scheme 9) [82]. For example, L-phenylalanine and L-leucine gave product with *trans*-selectivity (approx. 3:1 *trans*/*cis*). Conversely, L-proline reacted with excellent selectivity for the *cis*-isomer (>9:1 *cis*/*trans*). Diastereoselectivity with less bulky isocyanides (e.g., *n*-pentyl and benzyl isocyanides) was lower than with *tert*-butyl isocyanide.

The pairing of enantiomers with opposite configuration, such as (2*S*)-aziridine aldehyde from **41** with primary and secondary (2*R*)-amino acid substrates gave, respectively, products *trans*-**42** and *cis*-**43** with improved and diminished diastereoselectivity over similar reactions using substrates with similar configuration (Scheme 10).

Similar to the lactone formation that was detected in the Ugi four-component five-center reaction with aziridine aldehydes (Scheme 6), on stirring in TFE in the absence of external nucleophile, *cis*-piperazinone *cis*-**44** underwent aziridine ring opening from intramolecular attack of the neighboring amide oxygen to furnish bicyclic imidate **45** (Scheme 11). In contrast, the *trans*-diastereomer was unreactive under similar conditions.

The kinetics of the diastereoselective Ugi reaction to piperazinones **44** was further studied using HPLC/MS and ^{13}C NMR spectroscopy, which identified the

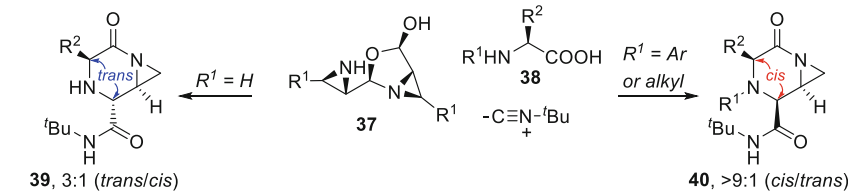

Scheme 9 Ugi reaction of aziridine aldehyde gives respectively *trans*- and *cis*-relative stereochemistry from primary and secondary amino acids

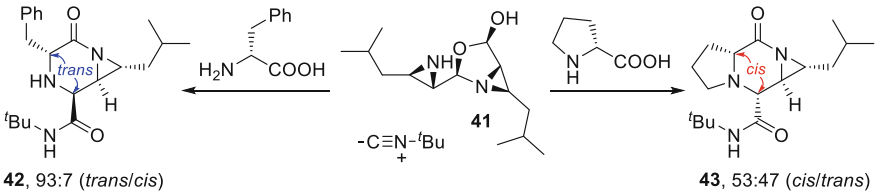

Scheme 10 Ugi reactions between primary and secondary (2*R*)-amino acids and (2*S*)-aziridine aldehyde dimer having unmatched configurations give respectively improved and lower diastereoselectivity

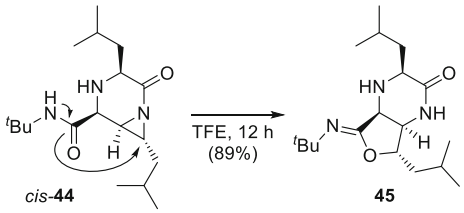

Scheme 11 Nucleophilic rearrangement of aziridine amide in piperazinone *cis*-**44** gave imidate **45**

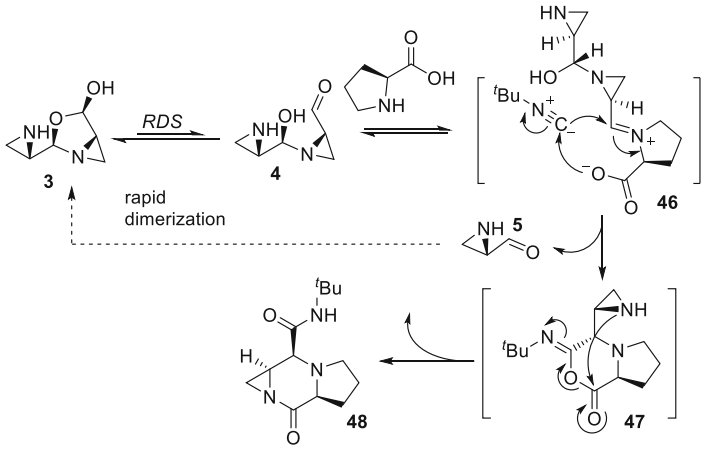

Scheme 12 Proposed mechanism for the disrupted Ugi reaction

rate-determining step of the reaction to be the formation of the open dimeric species of the aziridine aldehyde (Scheme 12). The mechanism from the open dimer to piperazinone was subsequently investigated by computational methods [83], using the MPWPW91/6-31G(d) [84, 85] level of theory. In the formation of proline adduct **48**, the attack of isocyanide onto the *re*- or *si*-face of the *trans*- or *cis*-iminium ion **46** proved pivotal. Among the four cases modeled, the addition to the *cis*-iminium ion leading to the *cis*-diastereomer was the most favorable, due to a major energetic contribution from the concomitant attacks of isocyanide onto the iminium ion and the carboxylate onto the isocyanide. In addition, the model suggesting this favorable concerted behavior predicted increased diastereoselectivity when substrates of opposite configuration were paired in the reaction with primary amines [82].

4 Peptide Macrocycles from Disrupted Ugi Reaction with Aziridine Aldehyde Dimers

4.1 Proposed Mechanism

Substitution of a linear peptide for the amino acid component in the disrupted Ugi reaction provided access to cyclic peptides (Scheme 13) [77]. A similar mechanism was proposed for this reaction, in which aziridine aldehyde dimer, isocyanide, and peptide bearing an N-terminal proline were combined. Condensation of the N-terminal proline and aziridine aldehyde generated an iminium ion intermediate that was attacked by the isocyanide with concomitant attack by the carboxylate to yield mixed anhydride **51**. Transacylation from the mixed anhydride onto the pendent aziridine nucleophile provided aziridine amide-bearing macrocycle **52**. This strategy provided access to a number of challenging cyclic peptides, as well as potential for downstream functionalization by aziridine-ring opening reactions. For example, aziridine opening with a thiocoumarin nucleophile provided a fluorescent probe [77, 86].

Ion pairing interactions have been implicated in the macrocyclization mechanism and supported by a computational study, which indicated a stable ion pair between the isonitrilium cation and carboxylate anion of intermediate **53** (Fig. 12) [87]. The application of ion pair interactions in macrocyclization chemistry has led to novel macrocyclization methodologies [88]. Subsequent studies on the

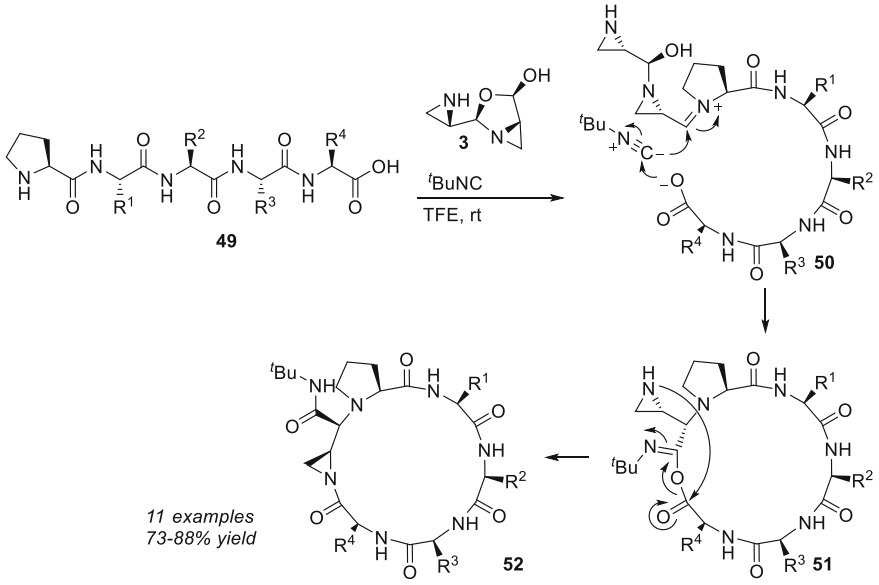

Scheme 13 Initially proposed mechanism for the formation of cyclic peptides from the disrupted Ugi reaction of aziridine aldehyde dimer and linear peptides

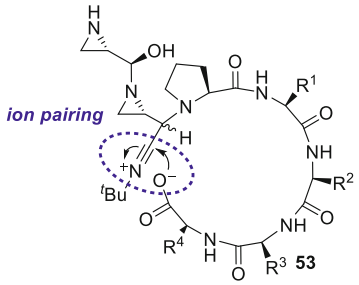

Fig. 12 Ion pair of carboxylate and nitrilium ions favors cyclization in the disrupted Ugi reaction

macrocyclization mechanism have uncovered the formation of amidine side products and the possible involvement of an imidoanhydride intermediate in the reaction pathway [89].

4.2 Increasing Molecular Complexity Using Functionalized Isocyanides

A uniquely enabling feature of macrocyclization through an MCR is the ability to add functionality during the stitching of the peptide ends. For example, cyclic peptides bearing fluorescent probes were prepared by employing disrupted Ugi reactions with aziridine aldehyde dimers and isocyanide **55**, which was synthesized by a route from anhydride **54** featuring formamide dehydration (Scheme 14).

Fluorescent piperazinones (67–93% yield) and cyclic peptides (e.g., **57**, 47–94% yield) were made by using isocyanide **55** in the aziridine aldehyde-mediated macrocyclization (Scheme 15) [90]. Macrocycles **57** of mitochondria-penetrating peptide sequences displayed higher mitochondrial fluorescence and cellular uptake than linear controls [90] and could be used for organelle-selective solvatochromic detection [91, 92].

A variety of thioester isocyanides **58** were made by amino acid *N*-formylation, coupling to ethanethiol, and dehydration with phosphoryl chloride [93]. Application of the thioester isocyanides in disrupted Ugi reactions provided cyclic peptides bearing handles for attachment onto N-terminal cysteine peptides (e.g., **62**, Scheme 16) using native chemical ligation [43, 44, 94].

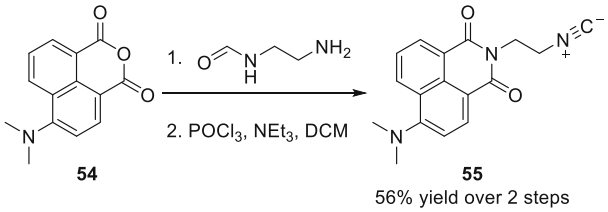

Scheme 14 Synthesis of solvatochromic isocyanide **1.50**

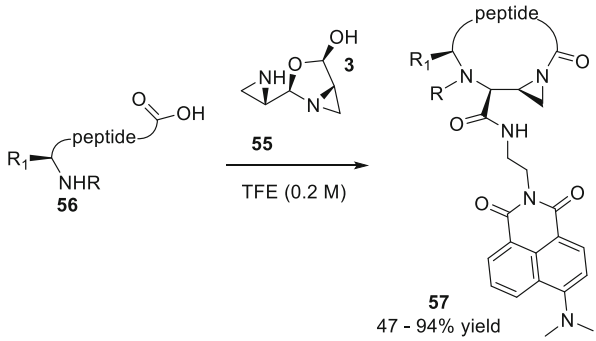

Scheme 15 Solvatochromic macrocyclic peptide probes derived from the disrupted Ugi reaction using fluorescent isocyanide **55**

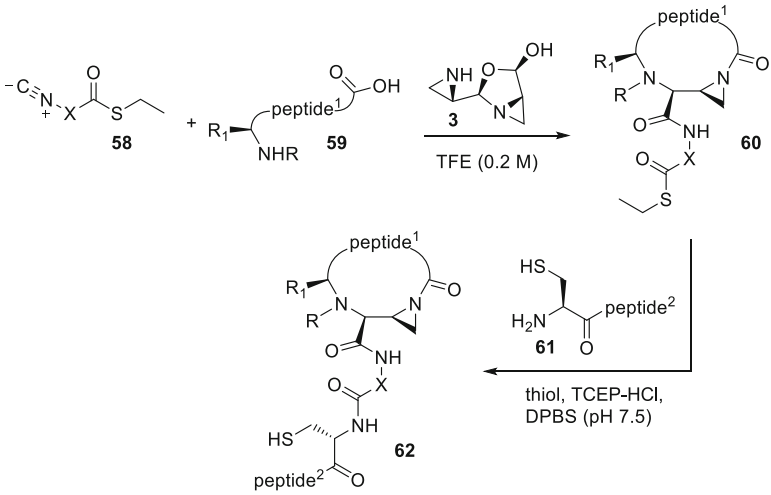

Scheme 16 Thioester isocyanides participate in the disrupted Ugi reaction to form macrocyclic substrates for native chemical ligation ($X = -CH_2CH_2^-$, $-C(CH_3)_2^-$)

4.3 Downstream Functionalization by Aziridine Ring Opening

Aziridines embedded within cyclic peptides enable late-stage modification by nucleophilic ring opening (Scheme 17), such that a parent precursor (**63**) may be diversified with different functionalities without affecting the remaining portion of the peptide [86, 95].

Aziridine **67** was ring opened effectively with excess sodium azide in anhydrous solvents (e.g., MeCN and DMF, Scheme 18) [96] to provide macrocycle **68**, which proved relatively more stable than the parent acyl aziridine during purification by reversed-phase chromatography, as well as when stirred in aqueous conditions at elevated temperatures. Aziridine ring opening proceeded typically in a regioselective manner at the methylene carbon.

The azide functionality served as an innocuous handle compatible with thiol functionalities during preparation of disulfide-bridged bicycle **70** from PCLFC (**69**, Scheme 19) [97].

In parallel to azide, thiols were studied as complementary nucleophiles with relatively soft nucleophilic character. Aliphatic and aromatic thiols participated in

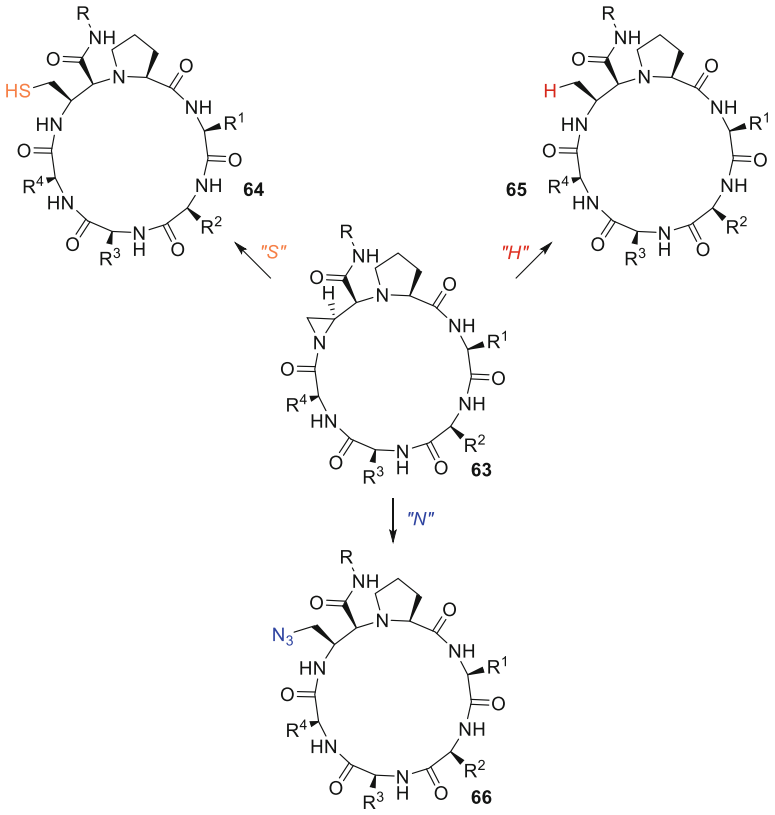

Scheme 17 Aziridine ring opening with a variety of nucleophiles

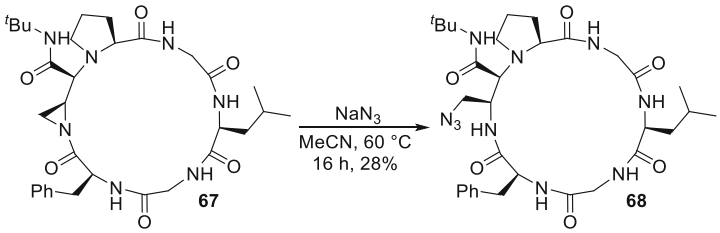

Scheme 18 Aziridine ring opening with sodium azide

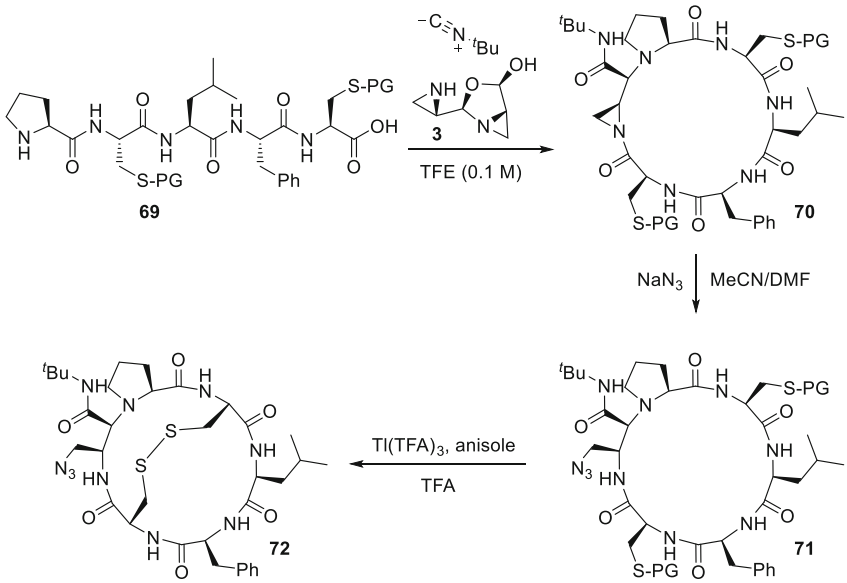

Scheme 19 Formation of bicycle derived from PCLFC by azide ring opening and disulfide formation

aziridine ring opening [86] and were used in a two-step protocol to append fluorescent functionalities to cyclic peptides (Scheme 20) [77, 95], such as isoform-specific integrin receptor ligands [95]. For example, aziridine **73** was ring opened with cysteamine to yield macrocycle **74** bearing an exocyclic amine that was subsequently coupled to a fluorescein *N*-hydroxysuccinimide ester to yield **76**. Ring size was found to be a dominant feature for ensuring a proper fit to the $\alpha_v\beta_3$ integrin receptor. The 18-membered ring cyclic peptide **76** that was derived from the protected linear precursor PRGDA exhibited μM affinity (IC_{50}) in a cell adhesion assay (Scheme 20).

Thioacids opened the aziridine ring regioselectivity at the methylene carbon and were used to prepare free thiols (e.g., **78**) by deacylation under basic conditions with K_2CO_3 in the presence of DTT (dithiothreitol) as reducing agent to prevent oxidation and disulfide bond formation (Scheme 21) [96]. Poorer conversions were

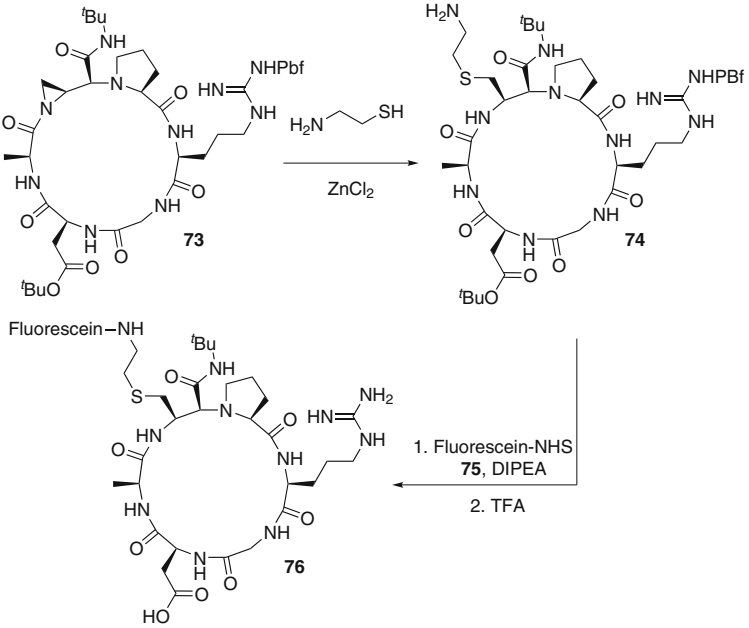

Scheme 20 Macrocycle functionalization via aziridine ring opening with cysteamine and conjugation to a fluorescein *N*-hydroxysuccinimide ester

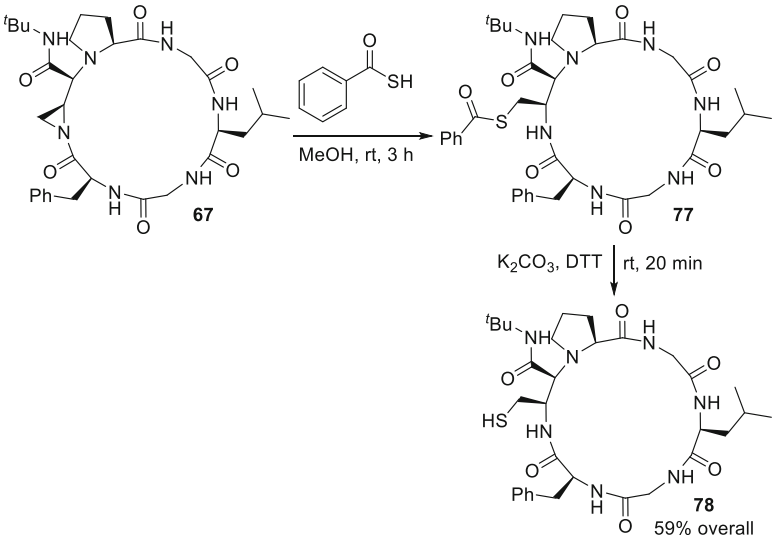

Scheme 21 Thiol synthesis by aziridine ring opening with thioacid followed by deacylation

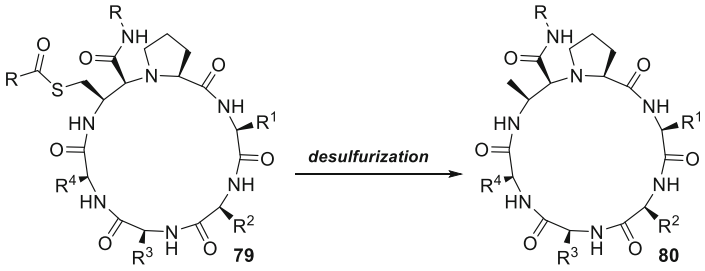

Scheme 22 Reductive hydrogenolysis replaces thioester with hydrogen

respectively obtained on employment of ethanolamine and TCEP (tris (2-carboxyethyl)phosphine) instead of K_2CO_3 and DTT, indicating that the latter may contribute to rate acceleration by *trans*-acylation to facilitate conversion.

Functionalization of cyclic peptides by ring opening of the aziridine with thiol and azide enabled further modifications respectively by conjugation and copper-catalyzed azide alkyne cyclization chemistry. Moreover desulfurization by reductive hydrogenolysis with Raney Ni was used to replace to the thioester (e.g., **79**) with hydrogen (Scheme 22) [98].

The reductive hydrogenolysis could be incorporated as the last step in a telescopic sequence of cyclization, opening of aziridine with thioacid, and desulfurization without solvent changes (Scheme 23). Employing this telescopic method, macrocycle **85** was obtained in 15% overall yield, after side-chain deprotection with a cocktail of TFA (trifluoroacetic acid), water (2.5% v/v), and TIPS (triisopropylsilane, 2.5% v/v), followed by HPLC purification [99]. Macrocycle **85** and another 18-membered ring analog were subsequently employed as the basis of a study of *ab initio* predictions of cyclic peptide NMR chemical shifts values [99].

Attempts to reduce directly the aziridine by hydrogenolysis were pursued using three different transition metal-catalyzed conditions, among which Raney Ni proved most effective as judged by the appearance of a "+2 amu" peak by LC/MS analysis (Scheme 24) [100–102].

In contrast to desulfurization (Scheme 23), Raney Ni-catalyzed reduction of the C–N bond of aziridine macrocycle **67** required positive hydrogen pressure throughout the reaction. After HPLC purification, macrocycle **87** was isolated in 14% yield. The regioselectivity of the hydrogenolysis reaction was analyzed by 2D NMR, which demonstrated the C_β–N bond of the aziridine was cleaved in identical fashion to the selectivity observed in ring opening with thioacid and azide [98].

An aziridine amide is more flexible than a simple secondary amide [103, 104]. Variable temperature NMR experiments of macrocycles containing aziridines lacked shielded amide NH signals. Moreover, cyclic peptides containing aziridines sometimes decomposed at elevated temperatures [98]. Conversely, after opening of the aziridine ring, the macrocycle derivatives were more rigid, thermally stable, and exhibited distinct amide NH signals, some of which were solvent shielded (Fig. 13).

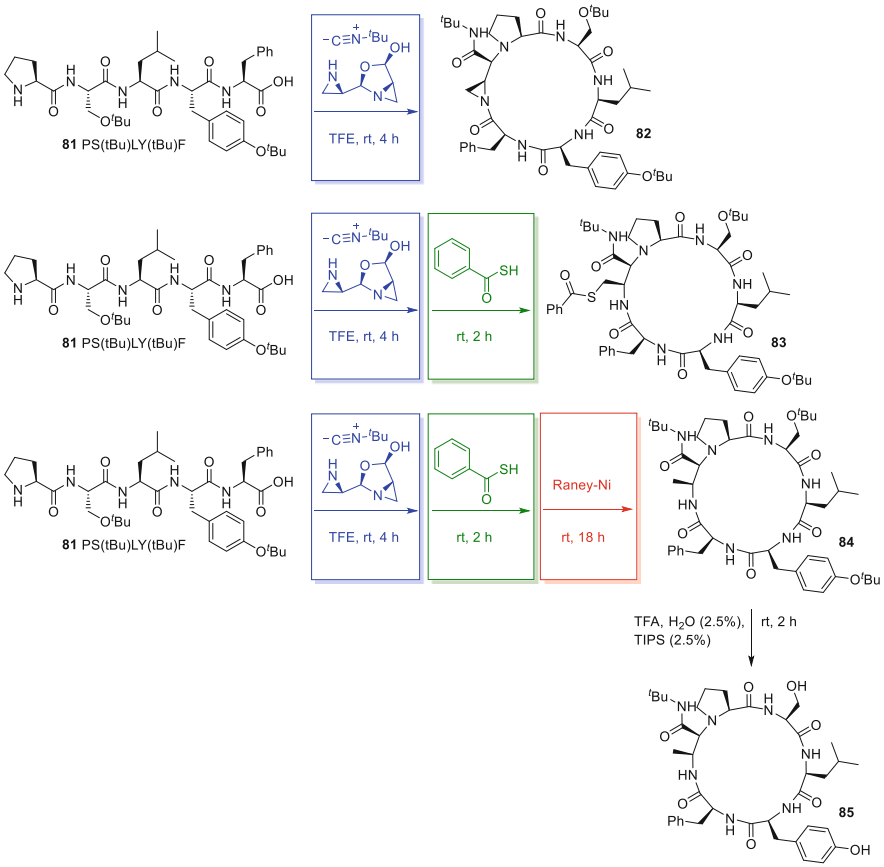

Scheme 23 Telescopic synthesis towards cyclic peptides

In the X-ray and NMR-derived structures of macrocycle **87**, the exocyclic amide was found to be a major contributor to the hydrogen bonding network [98]. The solid- and solution-phase structures of macrocycle **87** differed considerably however, and a different hydrogen bonding pattern was observed in the solution-phase structure. To increase rigidity, bicycle **89** was synthesized by a route featuring the use of *tert*-butyl isocyanoacetate in the Ugi cyclization to prepare macrocycle **88** possessing lysine amine and exocyclic glycine carboxylate for a second cyclization by conventional lactam formation (Scheme 25) [98]. The solution-phase structure of bicycle **89** was more similar to the solid- than the solution-phase structure of monocycle **87**. In spite of increased polarity, bicycle **89** exhibited greater permeability than monocycle **87** in a Caco-2 cell assay, suggesting that rigidity due to the hydrogen bonding of the exocyclic amide in the macrocycle may be important for this class of compounds to cross membrane environments.

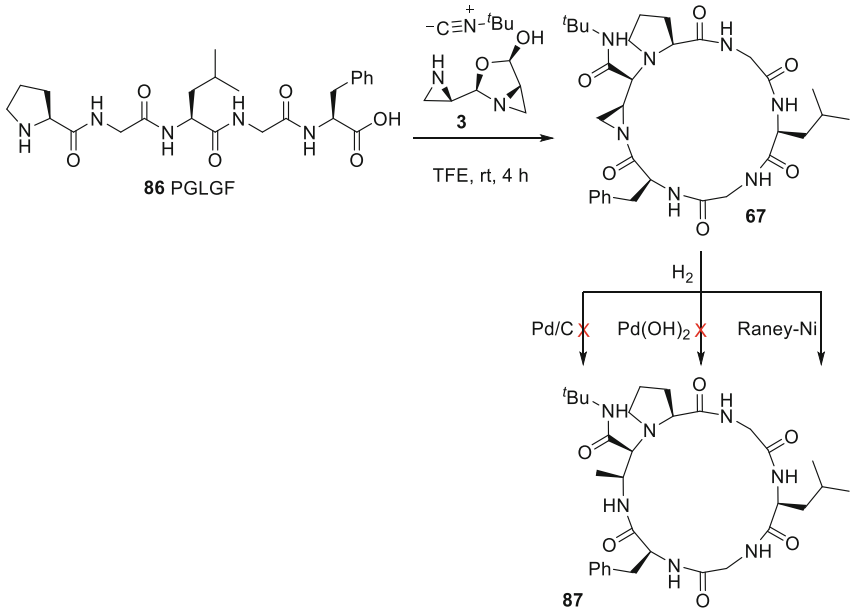

Scheme 24 Application of hydrogenation for opening the aziridine ring

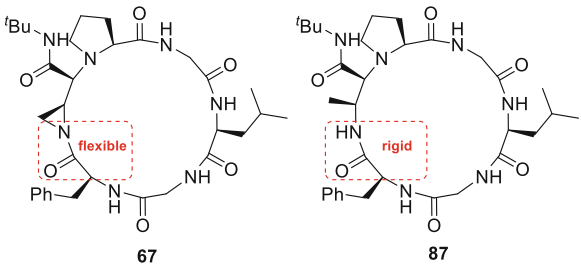

Fig. 13 Aziridine ring opening creates a more rigid, conventional amide

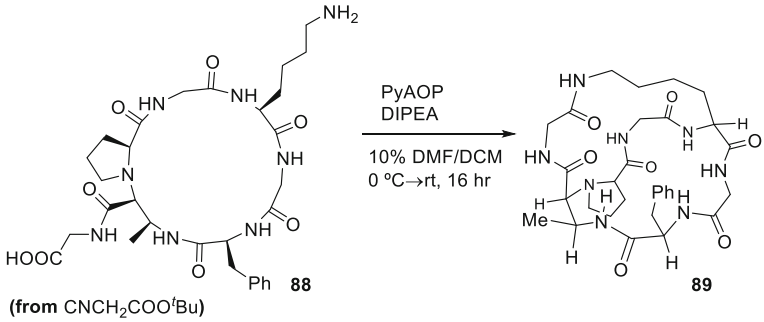

Scheme 25 Synthesis of bicycle **89**

5 Solid-Phase Synthesis Using the Disrupted Ugi Reaction

5.1 Piperazinone Synthesis

Solid-phase synthesis enables successive chemical reactions to be performed without product isolation [105], because reagents and solvents may be washed away by filtration. Reactions may also be pushed to completion by employing excess reagents [106]. Moreover, the solid support facilitates the creation of diverse libraries of molecules, such as natural products, by split and mix techniques [107, 108]. In addition, MCRs have been performed using components linked to the solid phase [109].

Aziridine aldehyde dimers have been used in the disrupted Ugi reaction on solid phase to synthesize piperazinones [110]. The amino acid component was initially linked onto FMP (4-(4-formyl-3-methoxyphenoxy)ethyl) resin through a reductive amination of the corresponding amino ester to provide resin **90**. After carboxylate deprotection, the disrupted Ugi reaction was performed on resin to furnish aziridine **91**, which was opened with a set of nucleophiles: thiols, thioacids, and azide. Cleavage of the resin with TFA gave piperazinones **92** in 9–38% overall yields (Scheme 26).

Consistent with the solution-phase reaction of secondary amino acids [82], *N*-linked amino acids gave piperazinones **91** with *cis*-selectivity (Scheme 27). This method served thus to produce the alternative diastereomer to that provided by the solution-phase *trans*-selective reaction.

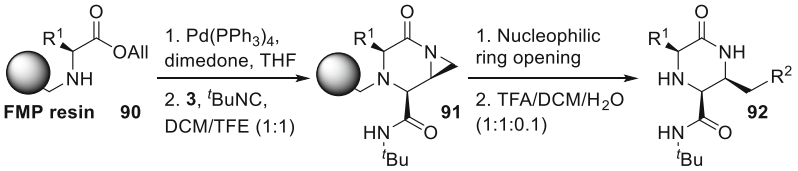

Scheme 26 Solid-phase synthesis of piperazinones by the disrupted Ugi reaction with aziridine aldehydes

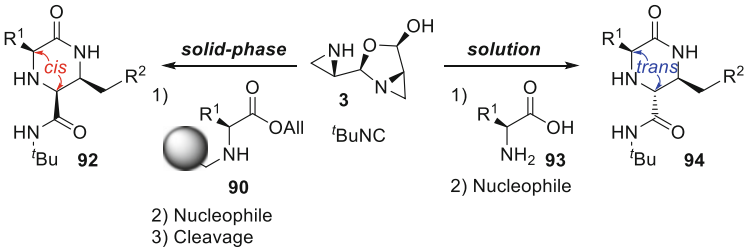

Scheme 27 Solution- and solid-phase syntheses produce, respectively, *trans*- and *cis*-piperazinone diastereomers

5.2 On-Resin Peptide Cyclization

Cyclic peptides have been synthesized on solid support by the disrupted Ugi reaction, employing a side-chain linking strategy [111]. Glutamine, glutamic acid, lysine, serine, and threonine were, respectively, anchored to the support by way of their side chains and employed as the C-terminal amino acid for peptide chain elongation. After attaching proline to the N-terminus [77], the C-terminal ester was removed, and the peptides were cyclized by the disrupted Ugi reaction with aziridine aldehydes (Scheme 28). Resin cleavage with concomitant protecting group removal provided cyclic peptides having 9- to 18-membered ring sizes that were isolated by HPLC purification in 7–32% overall yields. This solid-phase method has paved the way for parallel synthesis of topologically diverse cyclic peptides.

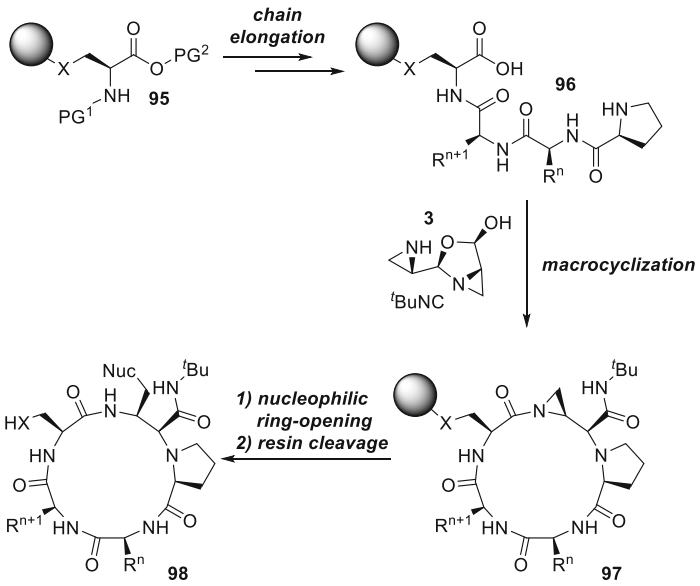

Scheme 28 Solid-phase cyclic peptide synthesis by disrupted Ugi cyclization with aziridine aldehyde dimers

6 Summary

The use of aziridine aldehydes in the Ugi reaction with amino acids and peptides has enabled the synthesis of functionally rich peptidomimetics. A variety of linear peptide, piperazinone, and macrocyclic peptide structures have been made by virtue of the interception of the pivotal Ugi-mixed anhydride intermediate through nucleophilic attack of the pendent aziridine group. Further modification by opening the resulting *N*-acyl aziridine with nitrogen and sulfur nucleophiles as well as hydrogenolysis has given access to diverse sets of novel piperazinones and cyclic peptide products. The potential for the cyclic peptides to exhibit specific hydrogen bonding patterns as well as to serve as fluorescent probes offers promise for the use of such scaffolds in future biological applications. Moreover, the disrupted Ugi reaction with aziridine aldehyde dimers has been effectively performed using resin-supported components, enabling solid-phase synthesis of diverse piperazinone and cyclic peptide libraries for biological screening. Remarkable precursors for the synthesis of heterocyclic peptidomimetics, aziridine aldehydes offer promise for the development of a range of tools for studying medicinal chemistry, peptide science, and chemical biology.

References

1. Ruijter E, Scheffelaar R, Orru RVA (2011) Multicomponent reaction design in the quest for molecular complexity and diversity. Angew Chem Int Ed 50:6234–6246. doi:10.1002/anie.201006515
2. Ganem B (2009) Strategies for innovation in multicomponent reaction design. Acc Chem Res 42:463–472. doi:10.1021/ar800214s
3. Hulme C, Gore V (2003) Multi-component reactions: emerging chemistry in drug discovery. From xylocain to crixivan. Curr Med Chem 10:51–80
4. Shiers JJ, Clarkson GJ, Shipman M, Hayes JF (2006) Rapid generation of molecular complexity using "hybrid" multi-component reactions (MCRs): application to the synthesis of alpha-amino nitriles and 1,2-diamines. Chem Commun 2:649–651. doi:10.1039/b516192d
5. Arend M, Westermann B, Risch N (1998) Modern variants of the Mannich reaction. Angew Chem Int Ed 37:1044–1070. doi:10.1002/(SICI)1521-3773(19980504)37:8<1044::AID-ANIE1044>3.0.CO;2-E
6. Wang J, Liu X, Feng X (2011) Asymmetric strecker reactions. Chem Rev 111:6947–6983. doi:10.1021/cr200057t
7. Strecker A (1850) Ueber die künstliche Bildung der Milchsäure und einen neuen, dem Glycocoll homologen Körper. Ann Chem Pharm 75:27–45. doi:10.1002/jlac.18500750103
8. He Z, Zajdlik A, Yudin AK (2014) Air- and moisture-stable amphoteric molecules: enabling reagents in synthesis. Acc Chem Res 47:1029–1040. doi:10.1021/ar400210c
9. Afagh NA, Yudin AK (2010) Chemoselectivity and the curious reactivity preferences of functional groups. Angew Chem Int Ed 49:262–310. doi:10.1002/anie.200901317
10. Dömling A, Ugi I (2000) Multicomponent reactions with isocyanides. Angew Chem Int Ed 39:3168–3210. doi:10.1002/1521-3773(20000915)39:18<3168::AID-ANIE3168>3.0.CO;2-U

11. Ramozzi R, Chéron N, Braïda B, Hiberty PC, Fleurat-Lessard P (2012) A valence bond view of isocyanides' electronic structure. New J Chem 36:1137–1140. doi:10.1039/c2nj40050b
12. Moss GP, Smith PAS, Tavernier D (1995) Glossary of class names of organic compounds and reactivity intermediates based on structure (IUPAC Recommendations 1995). Pure Appl Chem 67:1307–1375. doi:10.1351/pac199567081307
13. Passerini M, Simone L (1921) Gazz Chim Ital 51:181–189
14. Passerini M, Simone L (1921) Gazz Chim Ital 51:126–129
15. Maeda S, Komagawa S, Uchiyama M, Morokuma K (2011) Finding reaction pathways for multicomponent reactions: the Passerini reaction is a four-component reaction. Angew Chem Int Ed 50:644–649. doi:10.1002/anie.201005336
16. Ugi I (1962) The α-addition of immonium ions and anions to isonitriles accompanied by secondary reactions. Angew Chem Int Ed 1:8–21. doi:10.1002/anie.196200081
17. Ugi I, Meyr R, Fetzer U, Steinbrückner C (1959) Versuche mit isonitrilen. Angew Chem Int Ed 71:386
18. Endo A, Yanagisawa A, Abe M, Tohma S, Kan T, Fukuyama T (2002) Total synthesis of ecteinascidin 743. J Am Chem Soc 124:6552–6554. doi:10.1021/ja026216d
19. Tsukuda T, Suda A, Ohta A, Sudoh M, Shimma N (2001) Combinatorial synthesis of nikkomycin analogues on solid support. Heterocycles 55:1023. doi:10.3987/COM-01-9222
20. Bauer SM, Armstrong RW (1999) Total synthesis of motuporin (nodularin-V). J Am Chem Soc 121:6355–6366. doi:10.1021/ja9811243
21. Armstrong RW, Combs AP, Tempest PA, Brown SD, Keating TA (1996) Multiple-component condensation strategies for combinatorial library synthesis. Acc Chem Res 29: 123–131. doi:10.1021/ar9502083
22. Rotstein BH, Zaretsky S, Rai V, Yudin AK (2014) Small heterocycles in multicomponent reactions. Chem Rev 114:8323–8359. doi:10.1021/cr400615v
23. Koopmanschap G, Ruijter E, Orru RV (2014) Isocyanide-based multicomponent reactions towards cyclic constrained peptidomimetics. Beilstein J Org Chem 10:544–598. doi:10.3762/bjoc.10.50
24. Ayaz M, De Moliner F, Dietrich J, Hulme C (2012) Applications of isocyanides in IMCR s for the rapid generation of molecular diversity. In: Nenajdenko VG (ed) Isocyanide chemistry. Wiley-VCH, Weinheim, pp 335–384
25. Hulme C, Dietrich J (2009) Emerging molecular diversity from the intra-molecular Ugi reaction: iterative efficiency in medicinal chemistry. Mol Divers 13:195–207. doi:10.1007/s11030-009-9111-6
26. Hulme C, Gore V (2003) Multi-component reactions : emerging chemistry in drug discovery. From xylocain to crixivan. Curr Med Chem 10:51–80. doi:10.2174/0929867033368600
27. Demharter A, Hörl W, Herdtweck E, Ugi I (1996) Synthesis of chiral 1,1′-iminodicarboxylic acid derivatives from α-amino acids, aldehydes, isocyanides, and alcohols by the diastereoselective five-center–four-component reaction. Angew Chem Int Ed 35:173–175. doi:10.1002/anie.199601731
28. Park SJ, Keum G, Kang SB, Koh HY, Kim Y, Lee DH (1998) A facile synthesis of N-carbamoylmethyl- α -aminobutyrolactones by the Ugi multicomponent condensation reaction. Tetrahedron Lett 39:7109–7112. doi:10.1016/S0040-4039(98)01509-3
29. Layer RW (1963) The chemistry of imines. Chem Rev 63:489–510. doi:10.1021/cr60225a003
30. Myers AG, Kung DW, Zhong B (2000) Observations concerning the existence and reactivity of free α-amino aldehydes as chemical intermediates: evidence for epimerization-free adduct formation with various nucleophiles. J Am Chem Soc 122:3236–3237. doi:10.1021/ja000136x
31. Fischer E, Leuchs H (1903) Synthese desd-Glucosamins. Ber Dtsch Chem Ges 36:24–29. doi:10.1002/cber.19030360109

32. Donohoe TJ, Brian PM, Hargaden GC, O'Riordan TJC (2010) Synthesis of cylindricine C and a formal synthesis of cylindricine A. Tetrahedron 66:6411–6420. doi:10.1016/j.tet.2010.05.044
33. Fu P, Snapper ML, Hoveyda AH (2008) Catalytic asymmetric alkylations of ketoimines. Enantioselective synthesis of N-substituted quaternary carbon stereogenic centers by Zr-catalyzed additions of dialkylzinc reagents to aryl-, alkyl-, and trifluoroalkyl-substituted ketoimines. J Am Chem Soc 130:5530–5541. doi:10.1021/ja8001343
34. Ota H, Chyouma T, Iso S, Satoh T (2004) A novel synthesis of cyclic α-amino aldehydes, amino alcohols, and α-amino acid methyl esters from cyclic ketones through sulfinylaziridines. Tetrahedron Lett 45:3903–3907. doi:10.1016/j.tetlet.2004.03.124
35. Ooi T, Saito A, Maruoka K (2003) Asymmetric skeletal rearrangement of symmetrically alpha, alpha-disubstituted alpha-amino aldehydes: a new entry to optically active alpha-hydroxy ketones. J Am Chem Soc 125:3220–3221. doi:10.1021/ja0292851
36. De Kimpe N, Boeykens M, Boelens M, De Buck K, Cornelis J (1992) Synthesis of 2 (N-Alkylamino)Isobutyraldehydes. Org Prep Proced Int 24:679–681. doi:10.1080/00304949209356245
37. Satoh T, Oohara T, Ueda Y, Yamakawa K (1989) .alpha.,.beta.-Epoxy sulfoxides as useful intermediates in organic synthesis. 21. A novel approach to the asymmetric synthesis of epoxides, allylic alcohols, .alpha.-amino ketones, and .alpha.-amino aldehydes from carbonyl compounds through .alpha.,.beta. J Org Chem 54:3130–3136. doi:10.1021/jo00274a032
38. Hili R, Yudin AK (2006) Readily available unprotected amino aldehydes. J Am Chem Soc 128:14772–14773. doi:10.1021/ja065898s
39. Assem N, Hili R, He Z, Kasahara T, Inman BL, Decker S, Yudin AK (2012) Role of reversible dimerization in reactions of amphoteric aziridine aldehydes. J Org Chem 77:5613–5623. doi:10.1021/jo3007418
40. Hili R, Yudin AK (2008) Amphoteric amino aldehydes enable rapid assembly of unprotected amino alcohols. Angew Chem Int Ed 47:4188–4191. doi:10.1002/anie.200705776
41. Hili R, Yudin AK (2009) Amphoteric amino aldehydes reroute the aza-Michael reaction. J Am Chem Soc 131:16404–16406. doi:10.1021/ja9072194
42. Assem N, Natarajan A, Yudin AK (2010) Chemoselective peptidomimetic ligation using thioacid peptides and aziridine templates. J Am Chem Soc 132:10986–10987. doi:10.1021/ja104488d
43. Dawson P, Muir T, Clark-Lewis I, Kent S (1994) Synthesis of proteins by native chemical ligation. Science 266:776–779. doi:10.1126/science.7973629
44. Dawson PE (2011) Native chemical ligation combined with desulfurization and deselenization: a general strategy for chemical protein synthesis. Isr J Chem 51:862–867. doi:10.1002/ijch.201100128
45. Watkins HA, Au M, Hay DL (2012) The structure of secretin family GPCR peptide ligands: implications for receptor pharmacology and drug development. Drug Discov Today 17:1006–1014. doi:10.1016/j.drudis.2012.05.005
46. Schiller PW (2010) Bi- or multifunctional opioid peptide drugs. Life Sci 86:598–603. doi:10.1016/j.lfs.2009.02.025
47. Stein A, Aloy P (2008) Contextual specificity in peptide-mediated protein interactions. PLoS One 3:e2524. doi:10.1371/journal.pone.0002524
48. Wu C, Ma MH, Brown KR, Geisler M, Li L, Tzeng E, Jia CYH, Jurisica I, Li SS-C (2007) Systematic identification of SH3 domain-mediated human protein-protein interactions by peptide array target screening. Proteomics 7:1775–1785. doi:10.1002/pmic.200601006
49. Wavreille A, Garaud M, Zhang Y, Pei D (2007) Defining SH2 domain and PTP specificity by screening combinatorial peptide libraries. Methods 42:207–219. doi:10.1016/j.ymeth.2007.02.010
50. Craik DJ, Fairlie DP, Liras S, Price D (2013) The future of peptide-based drugs. Chem Biol Drug Des 81:136–147. doi:10.1111/cbdd.12055

51. Marsault E, Peterson ML (2011) Macrocycles are great cycles: applications, opportunities, and challenges of synthetic macrocycles in drug discovery. J Med Chem 54:1961–2004. doi:10.1021/jm1012374
52. Madala PK, Tyndall JDA, Nall T, Fairlie DP (2010) Update 1 of: proteases universally recognize beta strands in their active sites. Chem Rev 110:PR1–PR31. doi:10.1021/cr900368a
53. Hill TA, Lohman R, Hoang HN, Nielsen DS, Scully CCG, Kok WM, Liu L, Lucke AJ, Stoermer MJ, Schroeder CI, Chaousis S, Colless B, Bernhardt PV, Edmonds DJ, Griffith DA, Rotter CJ, Ruggeri RB, Price DA, Liras S, Craik DJ, Fairlie DP (2014) Cyclic penta- and hexaleucine peptides without N-methylation are orally absorbed. ACS Med Chem Lett 5: 1148–1151. doi:10.1021/ml5002823
54. Chatterjee J, Gilon C, Hoffman A, Kessler H (2008) N-methylation of peptides: a new perspective in medicinal chemistry. Acc Chem Res 41:1331–1342. doi:10.1021/ar8000603
55. Yudin AK (2015) Macrocycles: lessons from the distant past, recent developments, and future directions. Chem Sci 6:30–49. doi:10.1039/C4SC03089C
56. Terrett NK (2010) Methods for the synthesis of macrocycle libraries for drug discovery. Drug Discov Today Technol 7:e95–e146. doi:10.1016/j.ddtec.2010.06.002
57. White CJ, Yudin AK (2011) Contemporary strategies for peptide macrocyclization. Nat Chem 3:509–524. doi:10.1038/nchem.1062
58. Davies JS (2003) The cyclization of peptides and depsipeptides. J Pept Sci 9:471–501. doi:10.1002/psc.491
59. Schmidt U, Langner J (1997) Cyclotetrapeptides and cyclopentapeptides: occurrence and synthesis. J Pept Res 49:67–73. doi:10.1111/j.1399-3011.1997.tb01122.x
60. Wessjohann L, Rhoden C, Rivera D, Vercillo OE (2010) Cyclic peptidomimetics and pseudopeptides from multicomponent reactions. In: Orru RVA, Ruijter E (eds) Topics in heterocyclic chemistry. Springer, Berlin, pp 199–226
61. Wessjohann LA, Rivera DG, Vercillo OE (2009) Multiple multicomponent macrocyclizations (MiBs): a strategic development toward macrocycle diversity. Chem Rev 109: 796–814. doi:10.1021/cr8003407
62. Failli A, Immer H, Götz M (1979) The synthesis of cyclic peptides by the four component condensation (4 CC). Can J Chem 57:3257–3261. doi:10.1139/v79-533
63. Barreto A d FS, Vercillo OE, Wessjohann LA, Andrade CKZ (2014) Consecutive isocyanide-based multicomponent reactions: synthesis of cyclic pentadepsipeptoids. Beilstein J Org Chem 10:1017–1022. doi:10.3762/bjoc.10.101
64. Seo J, Lee B, Zuckermann R (2011) Peptoids – synthesis, characterization, and nanostructures. Compr Biomater 2:53–76
65. Yoo B, Shin SBY, Huang ML, Kirshenbaum K (2010) Peptoid macrocycles: making the rounds with peptidomimetic oligomers. Chem Eur J 16:5528–5537. doi:10.1002/chem.200903549
66. Vercillo OE, Andrade CKZ, Wessjohann LA (2008) Design and synthesis of cyclic RGD pentapeptoids by consecutive Ugi reactions. Org Lett 10:205–208. doi:10.1021/ol702521g
67. Wessjohann LA, Ruijter E (2005) Macrocycles rapidly produced by multiple multicomponent reactions including bifunctional building blocks (MiBs). Mol Divers 9: 159–169. doi:10.1007/s11030-005-1313-y
68. Wessjohann LA, Voigt B, Rivera DG (2005) Diversity oriented one-pot synthesis of complex macrocycles: very large steroid-peptoid hybrids from multiple multicomponent reactions including bifunctional building blocks. Angew Chem Int Ed 44:4785–4790. doi:10.1002/anie.200500019
69. Ricardo MG, Morales FE, Garay H, Reyes O, Vasilev D, Wessjohann LA, Rivera DG (2015) Bidirectional macrocyclization of peptides by double multicomponent reactions. Org Biomol Chem 13:438–446. doi:10.1039/c4ob01915f

70. Wessjohann LA, Westermann B, Michalik D, Schaks A, Kreye O, Wagner C, Merzweiler K (2007) Natural product inspired meta/para'-biaryl ether lactam macrocycles by double Ugi multicomponent reactions. Heterocycles 73:863. doi:10.3987/COM-07-S(U)21
71. Michalik D, Schaks A, Wessjohann LA (2007) One-step synthesis of natural product-inspired biaryl ether-cyclopeptoid macrocycles by double Ugi multiple-component reactions of bifunctional building blocks. Eur J Org Chem 2007:149–157. doi:10.1002/ejoc.200600354
72. Rivera DG, Wessjohann LA (2009) Architectural chemistry: synthesis of topologically diverse macromulticycles by sequential multiple multicomponent macrocyclizations. J Am Chem Soc 131:3721–3732. doi:10.1021/ja809005k
73. Rivera DG, Pando O, Bosch R, Wessjohann LA (2008) A biomimetic approach for polyfunctional secocholanes: tuning flexibility and functionality on peptidic and macrocyclic scaffolds derived from bile acids. J Org Chem 73:6229–6238. doi:10.1021/jo800708m
74. Rivera DG, Wessjohann LA (2006) Supramolecular compounds from multiple Ugi multicomponent macrocyclizations: peptoid-based cryptands, cages, and cryptophanes. J Am Chem Soc 128:7122–7123. doi:10.1021/ja060720r
75. Wessjohann LA, Filho RAWN, Rivera DG (2012) In: Nenajdenko VG (ed) Isocyanide chemistry. Wiley-VCH, Weinheim, pp 233–262
76. Rotstein BH, Yudin AK (2012) Aziridine-2-carboxaldehyde dimers undergo homo-Ugi 4-component-5-center reactions. Synthesis 44:2851–2858. doi:10.1055/s-0030-1260261
77. Hili R, Rai V, Yudin AK (2010) Macrocyclization of linear peptides enabled by amphoteric molecules. J Am Chem Soc 132:2889–2891. doi:10.1021/ja910544p
78. Mata L, Avenoza A, Busto JH, Peregrina JM (2013) Chemoselectivity control in the reactions of 1,2-cyclic sulfamidates with amines. Chem Eur J 19:6831–6839. doi:10.1002/chem.201204392
79. Jang JI, Kang SY, Kang KH, Park YS (2011) Dynamic resolution of α-halo chiral esters for the synthesis of 3-substituted piperazin-2-ones. Tetrahedron 67:6221–6226. doi:10.1016/j.tet.2011.06.055
80. Pollini GP, Baricordi N, Benetti S, De Risi C, Zanirato V (2005) A simple entry to chiral non-racemic 2-piperazinone derivatives. Tetrahedron Lett 46:3699–3701. doi:10.1016/j.tetlet.2005.03.163
81. Dinsmore CJ, Beshore DC (2009) Synthesis and transformations of piperazinone rings. A review. Org Prep Proced Int 34:367–404. doi:10.1080/00304940209458075
82. Zaretsky S, Adachi S, Rotstein BH, Hickey JL, Scully CCG, St. Denis JD, Courtemanche R, Yu JCY, Chung BKW, Yudin AK (2014) Stereocontrolled disruption of the Ugi reaction toward the production of chiral piperazinones: substrate scope and process development. J Org Chem 79:9948–9957. doi:10.1021/jo5018316
83. Belding L, Zaretsky S, Rotstein BH, Yudin AK, Dudding T (2014) Shifting the energy landscape of multicomponent reactions using aziridine aldehyde dimers: a mechanistic study. J Org Chem 79:9465–9471. doi:10.1021/jo501242r
84. Adamo C, Barone V (1998) Exchange functionals with improved long-range behavior and adiabatic connection methods without adjustable parameters: the mPW and mPW1PW models. J Chem Phys 108:664–675
85. Perdew JP, Jackson KA, Pederson MR, Singh DJ, Fiolhais C (1992) Atoms, molecules, solids, and surfaces: applications of the generalized gradient approximation for exchange and correlation. Phys Rev B 46:6671–6687. doi:10.1103/PhysRevB.46.6671
86. Rotstein BH, Rai V, Hili R, Yudin AK (2010) Synthesis of peptide macrocycles using unprotected amino aldehydes. Nat Protoc 5:1813–1822. doi:10.1038/nprot.2010.127
87. Scully CCG, Rai V, Poda G, Zaretsky S, Burns DC, Houliston RS, Lou T, Yudin AK (2012) Bending rigid molecular rods: formation of oligoproline macrocycles. Chem Eur J 18:15612–15617. doi:10.1002/chem.201203266
88. Londregan AT, Farley KA, Limberakis C, Mullins PB, Piotrowski DW (2012) A new and useful method for the macrocyclization of linear peptides. Org Lett 14:2890–2893. doi:10.1021/ol301173m

89. Zaretsky S, Hickey JL, Tan J, Pichugin D, St. Denis MA, Ler S, Chung BKW, Scully CCG, Yudin AK (2015) Mechanistic investigation of aziridine aldehyde-driven peptide macrocyclization: the imidoanhydride pathway. Chem Sci 6:5446–5455. doi:10.1039/C5SC01958C
90. Rotstein BH, Mourtada R, Kelley SO, Yudin AK (2011) Solvatochromic reagents for multicomponent reactions and their utility in the development of cell-permeable macrocyclic peptide vectors. Chem Eur J 17:12257–12261. doi:10.1002/chem.201102096
91. Yousif LF, Stewart KM, Horton KL, Kelley SO (2009) Mitochondria-penetrating peptides: sequence effects and model cargo transport. Chembiochem 10:2081–2088. doi:10.1002/cbic.200900017
92. Horton KL, Stewart KM, Fonseca SB, Guo Q, Kelley SO (2008) Mitochondria-penetrating peptides. Chem Biol 15:375–382. doi:10.1016/j.chembiol.2008.03.015
93. Rotstein BH, Winternheimer DJ, Yin LM, Deber CM, Yudin AK (2012) Thioester-isocyanides: versatile reagents for the synthesis of cycle-tail peptides. Chem Commun 48:3775–3777. doi:10.1039/c2cc16027g
94. Dawson PE, Kent SB (2000) Synthesis of native proteins by chemical ligation. Annu Rev Biochem 69:923–960. doi:10.1146/annurev.biochem.69.1.923
95. Roxin A, Chen J, Scully CCG, Rotstein BH, Yudin AK, Zheng G (2012) Conformational modulation of in vitro activity of cyclic RGD peptides via aziridine aldehyde-driven macrocyclization chemistry. Bioconjug Chem 23:1387–1395. doi:10.1021/bc300239a
96. Zaretsky S, Tan J, Hickey JL, Yudin AK (2015) Macrocyclic templates for library synthesis of peptido-conjugates. In: Derda R (ed) Methods in molecular biology: peptide libraries. Springer, New York, pp 67–68
97. Chung BKW, Hickey JL, Scully CCG, Zaretsky S, Yudin AK (2013) Bicycle synthesis through peptide macrocyclization using aziridine aldehydes followed by late stage disulfide bond installation. Medchemcomm 4:1124. doi:10.1039/c3md00054k
98. Zaretsky S, Scully CCG, Lough AJ, Yudin AK (2013) Exocyclic control of turn induction in macrocyclic peptide scaffolds. Chem Eur J 19:17668–17672. doi:10.1002/chem.201303453
99. Zaretsky S, Hickey JL, St. Denis MA, Scully CCG, Roughton AL, Tantillo DJ, Lodewyk MW, Yudin AK (2014) Predicting cyclic peptide chemical shifts using quantum mechanical calculations. Tetrahedron 70:7655–7663. doi:10.1016/j.tet.2014.07.070
100. Zhou P, Chen B, Davis F (2006) Asymmetric syntheses with aziridinecarboxylate and aziridinephosphonate building blocks. In: Yudin AK (ed) Aziridines and epoxides in organic synthesis. Wiley-VCH, Weinheim, pp 73–115
101. Xiong C, Wang W, Cai C, Hruby VJ (2002) Regioselective and stereoselective nucleophilic ring opening reactions of a phenyl-substituted aziridine: enantioselective synthesis of β-substituted tryptophan, cysteine, and serine derivatives. J Org Chem 67:1399–1402. doi:10.1021/jo010860d
102. Davis FA, Deng J, Zhang Y, Haltiwanger RC (2002) Aziridine-mediated asymmetric synthesis of quaternary β-amino acids using 2H-azirine 2-carboxylate esters. Tetrahedron 58:7135–7143. doi:10.1016/S0040-4020(02)00727-5
103. Glover SA, Rosser AA (2012) Reliable determination of amidicity in acyclic amides and lactams. J Org Chem 77:5492–5502. doi:10.1021/jo300347k
104. Shao H, Jiang X, Gantzel P, Goodman M (1994) Tilted amides in amino acid and peptide derivatives. Chem Biol 1:231–234. doi:10.1016/1074-5521(94)90015-9
105. Hermkens PHH, Ottenheijm HCJ, Rees D (1996) Solid-phase organic reactions: a review of the recent literature. Tetrahedron 52:4527–4554. doi:10.1016/0040-4020(96)00216-5
106. Drewry D, Coe D, Poon S (1999) Solid-supported reagents in organic synthesis. Med Res Rev 19:97–148. doi:10.1002/(SICI)1098-1128(199903)19:2<97::AID-MED2>3.0.CO;2-Y
107. Nandy JP, Prakesch M, Khadem S, Reddy PT, Sharma U, Arya P (2009) Advances in solution- and solid-phase synthesis toward the generation of natural product-like libraries. Chem Rev 109:1999–2060. doi:10.1021/cr800188v

108. Hall DG, Manku S, Wang F (2001) Solution- and solid-phase strategies for the design, synthesis, and screening of libraries based on natural product templates: a comprehensive survey. J Comb Chem 3:125–150. doi:10.1021/cc0001001
109. Dax SL, McNally JJ, Youngman MA (1999) Multi-component methodologies in solid-phase organic synthesis. Curr Med Chem 6:255–270
110. Treder AP, Tremblay M, Yudin AK, Marsault E (2014) Solid-phase synthesis of piperazinones via disrupted Ugi condensation. Org Lett 16:4674–4677. doi:10.1021/ol5023118
111. Treder AP, Hickey JL, Tremblay M-CJ, Zaretsky S, Scully CCG, Mancuso J, Doucet A, Yudin AK, Marsault E (2015) Solid-phase parallel synthesis of functionalised medium-to-large cyclic peptidomimetics through three-component coupling driven by aziridine aldehyde dimers. Chem Eur J 21:9249–9255. doi:10.1002/chem.201500068

Top Heterocycl Chem (2017) 49: 159–202
DOI: 10.1007/7081_2015_188

Published online: 21 November 2015

Recent Studies on Gramicidin S Analog Structure and Antimicrobial Activity

Sudip Pal, Uttam Ghosh, Ravi Sankar Ampapathi, and Tushar Kanti Chakraborty

Dedicated to Prof. S. Chandrasekaran on the occasion of his 70th birthday.

Abstract Gramicidin S, the most notable example of cationic antimicrobial peptides (CAPs), has remained in the forefront of worldwide research for development of new antibiotics for over seven decades now. Hundreds of papers have been published over the years on this molecule and its numerous analogs, delineating their structures and biological activities with an aim to achieve selective antimicrobial activities with reduced cytotoxicity for potential therapeutic applications. The present review attempts to capture the essence of some of the recent studies with the aims to chronicle the journey traversed by this fascinating molecule so far and to decipher what is needed for future success.

Keywords Antibiotics • Antimicrobial activities • Cationic antimicrobial peptides • Gramicidin S

Contents

S. Pal and R.S. Ampapathi
CSIR-Central Drug Research Institute, Lucknow 226031, India

U. Ghosh and T.K. Chakraborty (✉)
Department of Organic Chemistry, Indian Institute of Science, Bangalore 560012, India
e-mail: tushar@orgchem.iisc.ernet.in

1 Introduction

1.1 General

The increasing emergence of resistant strains of many pathogenic bacteria warrants serious attention toward the development of new therapeutic agents with novel mechanisms of action targeting receptors different from those of the conventional drugs [1, 2]. Cationic antimicrobial peptides (CAPs), known as part of the biological defense system of wide-ranging microorganisms, have been pursued for sometime as potential sources of new antibiotics, in part because resistance against antimicrobial peptides by pathogens has been found to be rare to date [3–5]. In general, bacteria develop resistance by genetic alteration to render inactive those antibiotics, which interact with specific enzymes, receptors, and metabolic processes. Typically, the genetically altered target no longer recognizes the antibiotic. By targeting the cellular lipid bilayer, instead of a particular component, certain CAPs offer potential to combat microbes without incurring resistance, because modification of the cellular envelope may be fatally detrimental to microbial fitness [6, 7].

In spite of their potential as antimicrobial agents with novel mechanism of actions, very few CAPs have been approved for clinical use. Notably, polymyxin E, which is obtained from gram-positive bacterium *Bacillus polymyxa*, is currently used as a drug of last resort to treat multidrug-resistant *Pseudomonas aeruginosa* infections [8, 9]. Many CAPs have failed at different stages of clinical trials, due to their inability to demonstrate increased efficacy over existing treatments. Moreover, many natural antibiotics possess hemolytic activity and kill human blood cells, which restrict their usage as therapeutic agent [10].

Gramicidin S (GS, **1**) is one of the most studied membrane-disrupting CAPs [11]. Produced non-ribosomally by *Bacillus brevis*, GS is active against both gram-positive and gram-negative bacteria, as well as fungi. GS perturbs lipid packing, induces pore formation, and causes extrusion of intracellular content by localizing in the glycerol backbone region of the lipid bilayer below the polar head groups and above the hydrocarbon chains [12–14]. GS interacts, however, with both mammalian and microbial cell membranes causing changes and destruction of membrane integrity, leading to cell lysis and death [15, 16]. For over 70 years, efforts have

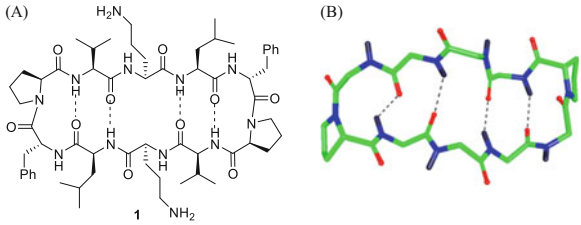

Fig. 1 Gramicidin S chemical structure (**A**) and the solution structure (**B**)

been made to develop modified versions of GS with enhanced potency, decreased mammalian cytotoxicity, and improved therapeutic index. Some of the recent research mainly published since 2000 are discussed here to understand the structure-activity relationships toward the ultimate aim to develop GS-based antimicrobial therapies.

1.2 Structure and Conformation

The structure and conformation of GS have been studied in detail by many researchers worldwide [17]. The C_2 symmetric structure of this cyclic decapeptide, *cyclo*-(D-Phe-Pro-Val-Orn-Leu)$_2$, adopts a β-pleated sheet structure in which the Val, Orn, and Leu residues are positioned along the two antiparallel β-strands. In the gas phase, sodiated and protonated GS adopt, respectively, β-sheet (β-hairpin) and collapsed random coil type conformations [18] (Fig. 1).

The D-Phe-Pro sequences adopt type II′ β-turns, which position the two β-strands in antiparallel orientation in GS. In the cold gas-phase electronic spectra of doubly protonated GS, the aromatic Phe chromophores were weakly coupled to one another but interacted strongly with the charged Orn side chains [19]. Conformer-specific highly resolved IR spectra of the amide I and II regions supported the symmetrical structure, because the CO double-bond stretches were observed as unresolved doublets [19]. Recently, low-temperature IR spectra of doubly protonated GS with computational study and density functional calculations (DFT) have yielded three lower energy conformations in the gas phase in which the lowest one had C_2 symmetry [20].

1.3 Mechanism of Action

The amphiphilic nature of GS is important for activity and results from the opposite orientations of the hydrophobic (Val and Leu) and hydrophilic (ornithine) residues. Although the mechanism of GS action is not completely understood, the destruction of bacterial cells arises likely through destabilization of the cellular membrane by displacement of lipid molecules in a way that creates an outflow of intracellular

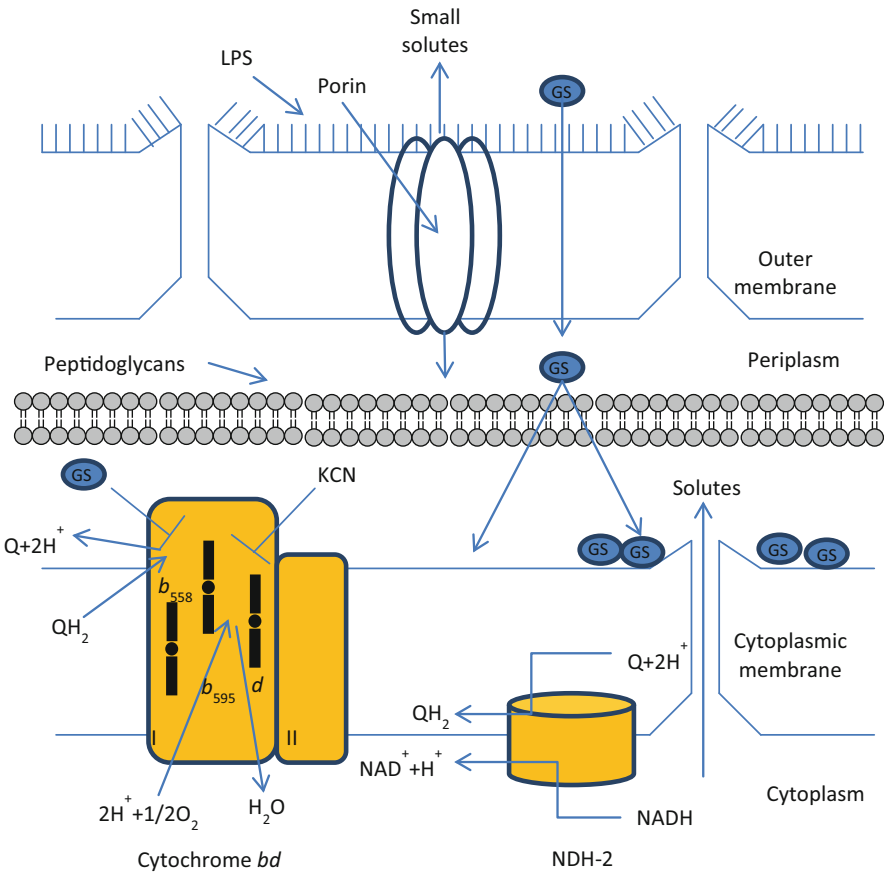

Fig. 2 Interaction of GS in the cell surface of the gram-negative bacteria [8]

components [15] (Fig. 2). Molecular dynamics simulations of the hydrated dimyristoylphosphatidylcholine (DMPC) bilayer have shown that GS exhibited minor influences on membrane dipole potential and water permeability. Indirect and direct interaction of GS with lipids promoted, respectively, ordered and disordered states, the latter being more fluid [21].

Densitometry and sound velocimetry studies on large multi- and unilamellar vesicles composed of DMPC have also suggested that GS disordered the lipid bilayer both in liquid crystal and gel states [12]. According to Krivanek et al. [12], GS decreases progressively phase transition temperature and co-operativity of the main phase transition at relatively higher concentrations creating a strong disordering of the membrane at the phase transition region. Through X-ray studies of GS interacting with lipid bilayers of *Acholeplasma laidlawii* B (*A. laidlawii* B) and *Escherichia coli* (*E. coli*), Lohner et al. found that GS promoted the formation of bicontinuous inverted cubic phases in these two

model lipid membranes [22]. Through scanning electron microscopy (SEM) and transmission electron microscopy (TEM), GS was shown to disrupt and penetrate into the outer membrane of the lipid bilayer by replacing bivalent cations, through a probable mechanism of action featuring insertion inside the inner membrane to cause lateral expansion and folding of the membrane near the polar part of the cell [15]. In the presence of GS, the cell membrane becomes leaky and loses regulatory control over turgor pressure.

1.4 Effect of Cholesterol

Cholesterol has been observed by spectroscopic studies to diminish the interaction of GS with phosphatidylcholine and phosphatidylethanolamine model membrane systems. Although introduction of cholesterol did not change the basic conformation of GS, the ability of the peptide to induce lipid bilayer membrane permeabilization was reduced according to calcein leakage experiments [23]. Calorimetric [24] and FTIR spectroscopic [25] studies have indicated that the strength of GS interactions with various phospholipid bilayers increased with their degree of negative charge and fluidity in model membranes. Moreover, studies using ^{31}P-NMR spectroscopy [26], X-ray diffraction, and differential scanning calorimetry (DSC) have suggested that GS destabilized lipid bilayers by increasing their negative (monolayer) curvature stress through interaction with inverted non-lamellar phase-forming phospholipids and glycolipids [22]. The exact mechanism by which cholesterol influences GS activity remains unknown.

1.5 Activity

GS is active against both gram-positive and gram-negative bacteria with a minimum inhibitory concentration (MIC) value of 3–11 μM; however, the hemolytic activity of GS has restricted its application as medicine to topical use only [27, 28]. A detailed study was made by Overhand et al. to find the morphological changes of RBCs caused by GS using giant unilamellar vesicles as models [29] and concluded that the increase in the surface tension caused probably the rupture of the membrane. The task to prepare GS analogs that retain antimicrobial power without hemolytic activity is particularly challenging due to similarities between bacteria and mammalian cell membranes as well as insufficient knowledge of the mechanisms of GS action. In a recent study [30], GS was found to be active also against platelets causing shape changes, swelling, and disaggregation of aggregates. Generally, GS did not destroy platelets depending on concentration; however, disaggregation of platelet aggregates might cause excessive bleeding. To respectively induce hemolysis and disaggregation of platelet aggregates, the binding of 35×10^9 GS molecules per red blood cell and 22×10^7 GS molecules per platelet cell were

required. The relatively larger surface area and increased cholesterol level in the lipid bilayer of red blood cells versus platelets may account for the greater number of GS molecules needed for hemolysis. Such issues must be addressed to develop safe antimicrobial drugs based on the structure of GS.

In addition to stopping bacterial infection by altering membrane permeability, GS inhibits the cytochrome *bd*-type quinol oxidase of *E. coli* [31], NADH oxidation, quinone reduction, and the type II NADH-quinone oxidoreductases (NDH-2) of *Mycobacterium Tuberculosis* (*M. Tuberculosis*) [$IC_{50} = 2$ μM, better than trifluoroperazine ($IC_{50} = 12$ μM)] and of *Mycobacterium smegmatis* (*M. smegmatis*) [32], as well as P-type ATPases, such as the plasma membrane Mg^{2+}/K^{+}-ATPase from tobacco leaves ($IC_{50} = 24$ μM) [33], rat heart plasma membrane Ca^{2+}-ATPase ($IC_{50} = 3$ μM), sarcoplasmic reticulum Ca^{2+}-ATPase ($IC_{50} = 6$ μM) [34], and human red blood cell membrane Ca^{2+}-ATPase [35]. In addition, GS inhibits in vitro amyloid β-peptide aggregation, which is a characteristic of Alzheimer's disease [36]. These examples demonstrate that GS targets more than the cellular membrane and binds to peripheral and intrinsic membrane proteins after absorption into the membrane [8].

Instead of targeting genetic material, such as DNA and RNA, or any particular protein within the bacterial cell, GS interacts primarily with the bacterial cell membrane, and hence bacteria have difficulties to develop resistance to GS [37]. Proof that GS interacts specifically with the bacterial cell membrane instead of intracellular components comes from experimentation with the retro-enantiomer of GS, which exhibited activity on par with its natural counterpart [38]. Resistance against membrane-disrupting antibiotics would likely necessitate a mechanism by which the antibiotic is destroyed or specifically blocked from accumulating in the lipid bilayer. Considering that such a path to resistance may be difficult to develop through genetic modification, GS continues to attract attention from researchers around the globe.

2 Modifications and Consequences

Efforts to modify the strand and turn regions of GS have been pursued to increase its therapeutic index by maintaining antimicrobial activity while decreasing cytotoxicity. Structure-activity relationships identified from these studies have furnished understanding of characteristics of GS which are necessary for activity, e.g., hydrophobicity, amphiphilicity, ring size, β-sheet structure, and β-turn geometry. In addition to modifying the turn and strand regions, the size of the cycle has been expanded by adding additional amino acid residues to the sequence. Although some analogs have exhibited a better therapeutic index, none has demonstrated sufficient improvement for use beyond topical applications.

The search for new active non-cytotoxic GS analogs has generally employed the following methods: (a) design and synthesis of novel GS analogs, (b) the secondary structure analysis of these compounds in aqueous solution, and (c) the activity study

on both bacterial strains and erythrocytes. In the current review, we have discussed some of the recent examples of GS modifications reported by different groups during the last decade.

2.1 Ring Size

The ring size of GS has been expanded to 14 amino acids in so-called GS14 analogs **2a** possessing variations at the stereocenters of the lysine residues (Fig. 3)

Fig. 3 Structures of **2a–c**

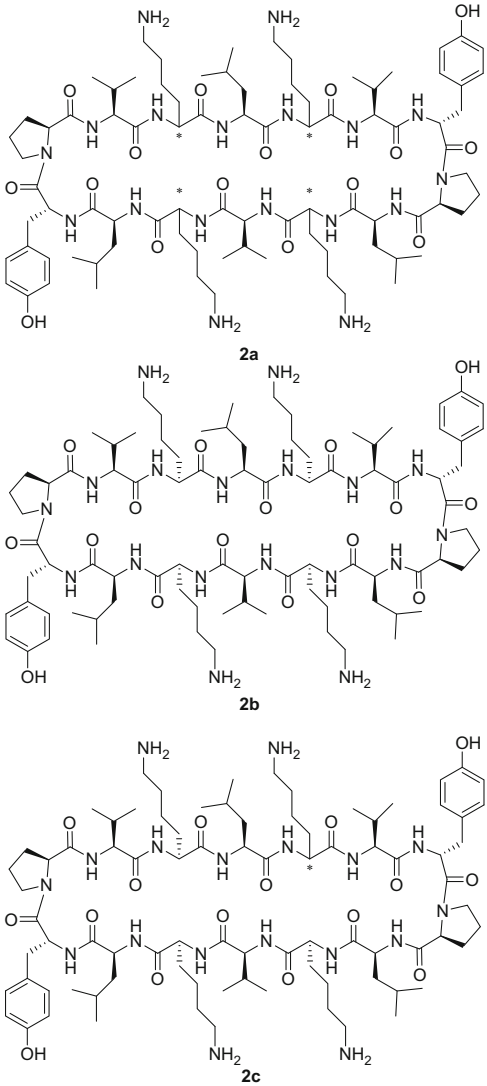

[39]. Circular dichroism (CD) spectroscopy was used to analyze the analogs and revealed that the GS14 analog **2b** having the sequence *cyclo*-(Val-Lys-Leu-Lys-Val-D-Tyr-Pro-Leu-Lys-Val-Lys-Leu-D-Tyr-Pro) exhibited molar ellipticity that was considerably greater than that of the other derivatives and a curve shape indicative of a predominant antiparallel β-sheet orientation with type II′ β-turn structures. In addition, GS14 analog **2b** showed the maximum permeabilization of phospholipid vesicles composed of 1-palmitoyl-2-oleoyl-*sn*-glycero-3-phosphocholine (POPC). All the other analogs showed lower activity, which diminished with the number and position of the enantiomeric inversions. Against fungal growth and *A. laidlawii* B, GS14 **2b** exhibited the best activity followed by analogs possessing single and multiple enantiomeric inversions; however, the therapeutic indices decreased in the order single stereocenter inversion of Lys analogs > multiple inversion analogs > GS14 **2b**.

To study the effect of cholesterol on membrane binding, isothermal titration calorimetry (ITC) studies were performed with GS and [D-Lys^4]-GS14 (**2c**) using large unilamellar vesicles composed of various zwitterionic (POPC) and anionic phospholipids {1-palmitoyl-2-oleoyl-*sn*-glycero-3-[phospho-*rac*-(glycerol)] [POPG] and 1-palmitoyl-2-oleoyl-*sn*-glycero-3-[phosphoserine] [POPS]} in the presence and absence of cholesterol [40, 41]. The interactions of [D-Lys^4]-GS14 (**2c**) with lipid micelles and bilayer membranes was also studied using FTIR spectroscopy [42]. Relative to that of GS, [D-Lys^4]-GS14 (**2c**) exhibited a slightly distorted β-sheet conformation, almost identical antimicrobial potency, but was 15–20-fold less hemolytic. The orientation of the D-Lys^4 side chain toward the hydrophobic part of [D-Lys^4]-GS14 (**2c**) was suggested to increase its hydrophilic and decrease its amphiphilic properties diminishing the tendency to aggregate in hydrophilic environments and augmenting interactions with hydrophobic moieties relative to GS14 (**2b**) [43].

The capability of [D-Lys^4]-GS14 (**2c**) to bind, disrupt phospholipid model membranes, and permeabilize large unilamellar vesicles was also studied using a fluorescent dye leakage assay [44]. Binding affinity varied distinctively with the charge and to some extent with the polar head-group structure of the phospholipid, as well as with the cholesterol content of the model membrane. Peptide **2c** bound much more tightly to anionic than to zwitterionic phospholipids and much less tightly to cholesterol-containing than to cholesterol-free model membranes. The binding affinity of peptide **2c** correlated more strongly with its antimicrobial and hemolytic activities than its influence on the rate and extent of dye leakage in model membrane systems.

In permeabilization studies of lipid bilayers composed of mixtures of zwitterionic diphytanoylphosphatidylcholine and anionic diphytanoylphosphatidylglycerol, as well as single zwitterionic unsaturated phosphatidylcholines of various hydrocarbon chain lengths, in the presence and absence of cholesterol, GS did not form discrete, well-defined, channel-like structures in the phospholipid bilayers but instead brought about a wide variety of transient, differently sized defects which served to compromise the bilayer barrier properties toward small electrolytes [45].

The preparation and CD analysis of a GS analog (GS10, **3a**) in which the Orn and D-Phe residues were, respectively, replaced by Lys and D-Tyr demonstrated that the β-sheet conformation was retained but was less structured compared to GS in aqueous and membrane mimetic solvent [46]. Less associative in water than GS, GS10 was more polar and exhibited weaker antibacterial activity against *A. laidlawii* B. Fourteen diastereomers of GS14 were also synthesized; each contained a different single enantiomeric substitution within the framework of GS14. The β-sheet structure of all GS14 diastereomers was disrupted as determined by CD and NMR spectroscopy under aqueous conditions. It was observed that compounds with high amphipathicity resulted in high hemolytic activity and low antimicrobial activity. The best diastereomer exhibited 130-fold less hemolytic activity compared with GS14 with increased antimicrobial activities for a number of microorganisms. The therapeutic indices of this peptide were significantly higher than GS with greater specificity for gram-negative microorganisms [47, 48].

Ten- to sixteen-meric analogs of GS were prepared by, respectively, substituting the Orn and Phe residues with Lys and Tyr: *cyclo*-(VKL*d*YP^{5}VKL*d*YP^{10}) (GS10, **3a**), *cyclo*-(VKLK*d*YP^{6}KVKL*d*YP^{12}) (GS12, **3b**), *cyclo*-(VKLK*d*YP^{6}*VKL*d*YP^{11}) (GS12-K7, **3c**), *cyclo*-(VKL**d*YP^{5}KVKL*d*YP^{11}) (GS12-K4, **3d**), *cyclo*-(VK*K*d*YP^{5}KVKL*d*YP^{11}) (GS12-L3, **3e**), *cyclo*-(VKLKV*d*YP^{7}LKVKL*d*YP^{14}) (GS14, **3f**), *cyclo*-(VKLK**d*YP^{6}LKVKL*d*YP^{13}) (GS14-V5, **3g**), *cyclo*-(VKL*V*d*YP^{6}LKVKL*d*YP^{13}) (GS14-K4, **3h**), *cyclo*-(VK*KV*d*YP^{6}LKVKL*d*YP^{14}) (GS14-L3, **3i**), *cyclo*-(VKL KVK*d*YP^{8}KLKVKL*d*YP^{16}) (GS16, **3j**), *cyclo*-(VKLKV**d*YP^{7}KLKVKL*d*YP^{15}) (GS16-K6, **3k**), *cyclo*-(VKLK*K*d*YP^{7}KLKVKL*d*YP^{15}) (GS16-V5, **3l**), and *cyclo*-(VKL*VK*d*YP^{7}KLKVKL*d*YP^{15}) (GS16-K4, **3m**) (Fig. 4, note, * indicates a deleted amino acid compared to the parent peptide) [49]. Among the CD spectra of **3a–m**, that of GS10 (**3a**) exhibited two negative maxima at 205 and 222 nm characteristic of a β-sheet – β-turn structure. In contrast, the higher homologues were found to have CD spectra indicative of disrupted β-sheet structure. Although almost all of the expanded GS analogs were potent against gram-positive bacteria, they possessed hemolytic activity. Relative to GS, GS14-L3 (**3i**) and GS16 (**3j**) exhibited better (up to sixfold) therapeutic indices with **3i** exhibiting the best efficacy against *Streptococcus aureus* (*S. aureus*), *Streptococcus mitis* (*S. mitis*), and *Streptococcus pneumoniae* (*S. pneumoniae*) and **3j** combating best *Staphylococcus epidermis* (*S. epidermis*). In a similar way, GS16-K4 (**3m**) exhibited high therapeutic indices for *Enterococcus faecalis* (*E. faecalis*), *Streptococcus pyogenes* (*S. pyogenes*), and *Corynebacterium jeikeium* (*C. jeikeium*). Lower MIC values were obtained for gram-negative compared to gram-positive bacteria with GS16 (**3j**) exhibiting the best therapeutic index values against *Enterobacter cloacae* (*E. cloacae*), *E. coli*, *Klebsiella pneumoniae* (*K. pneumoniae*), and *Pseudomonas aeruginosa* (*P. aeruginosa*). Similarly, against *Acinetobacter calcoaceticus* (*A. calcoaceticus*) and *Stenotrophomonas maltophilia* (*S. maltophilia*), GS16-V5 (**3l**) and GS16-K4 (**3m**) exhibited, respectively, the highest therapeutic index values. Against fungi such as *Candida albicans* (*C. albicans*) and *Cryptococcus neoformans* (*C. neoformans*), GS14-L3 (**3i**) had the highest therapeutic index. The expanded

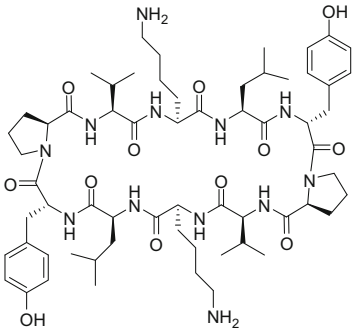

3a cyclo-(VKL*d*YP^{5}VKL*d*YP^{10}) GS10

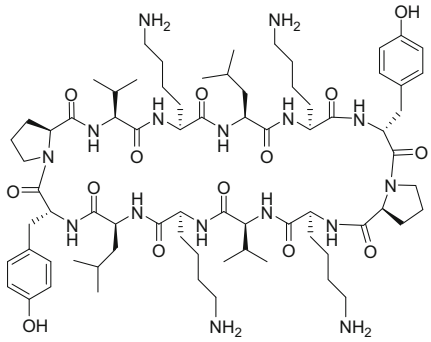

3b cyclo-(VKLK*d*YP^{6}KVKL*d*YP^{12}) GS12

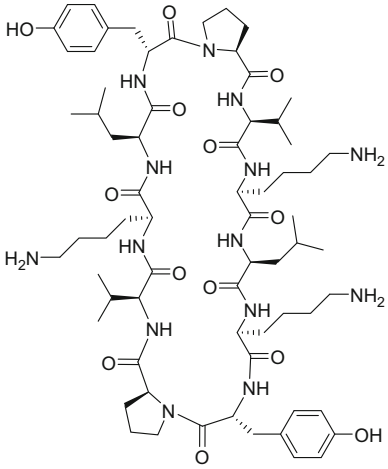

3c cyclo-(VKLK*d*YP^{6}*VKL*d*YP$_{11}$) GS12-K7

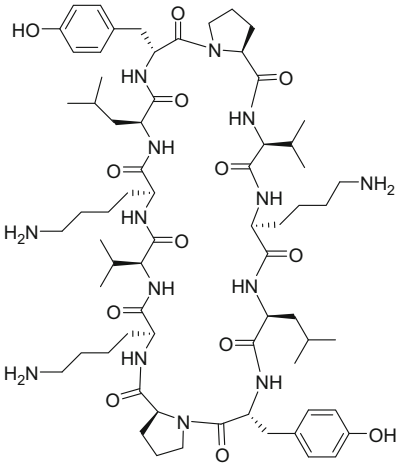

3d cyclo-(VKL**d*YP^{5}KVKL*d*YP^{11}) GS12-K4

Fig. 4 (continued)

GS analogs with CD spectra indicating a disrupted β-sheet conformation tended to exhibit lower hemolytic activity.

Extended reverse GS derivatives **4a–j** were synthesized and studied by NMR spectroscopy [50]. The proline residue chemical shift perturbation values ($\Delta\delta = 0.8$–0.9 ppm) were indicative of its presence in a β-hairpin with similar amount of β-sheet content among analogs **4a–j** (Fig. 5). The presence of the β-sheet – β-hairpin conformation for **4a–j** – was supported by their CD spectra which displayed characteristic negative maximum at 210 and 220 nm. Extended reverse GS derivatives **4a** and **4j** showed the lowest antibacterial activity, and **4c**, **4e**, and **4g** were more potent than GS (**1**). Analog **4a** was the least hemolytic in the series, and **4b** and **4c** were comparatively less hemolytic than GS (**1**). Other analogs were more hemolytic than GS. Comparison of hemolytic activity with HPLC

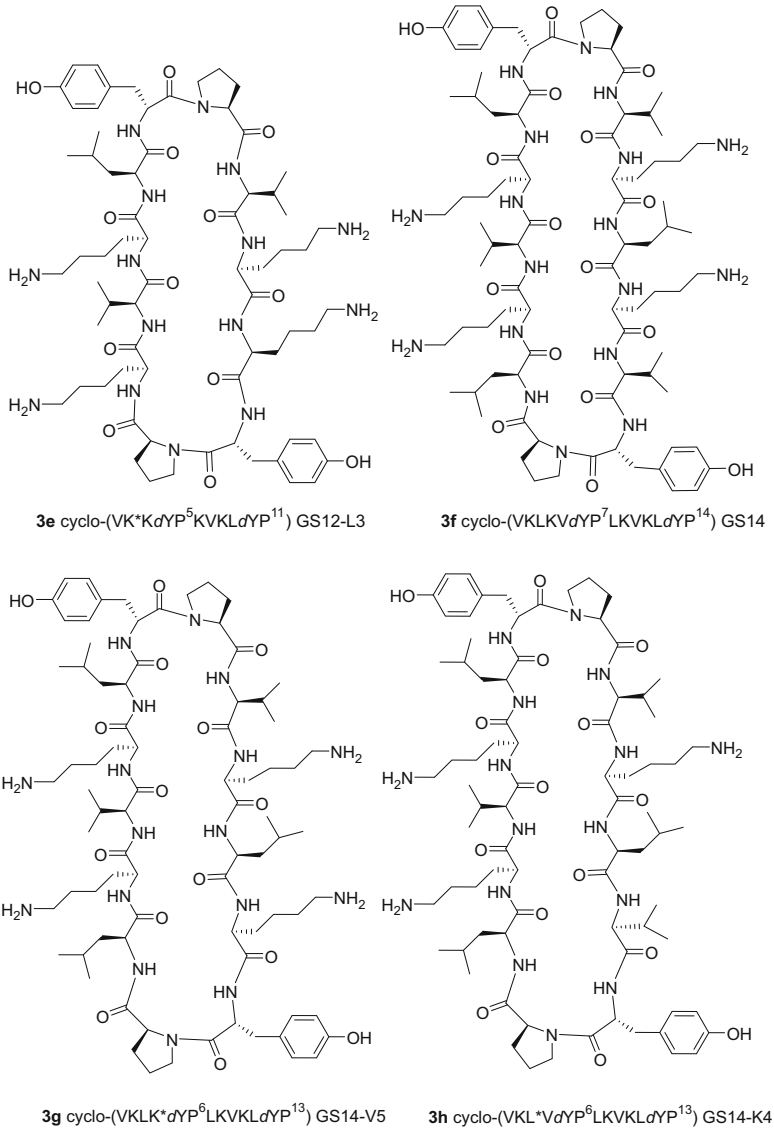

Fig. 4 (continued)

retention time revealed that the most and least hydrophobic analogs **4j** and **4a** exhibited, respectively, the highest and lowest hemolytic activity in the series.

Ring-extended GS analogs **5** with four basic amino acid residues, as well as sugar amino acids (SAA) serving as dipeptide surrogates, were synthesized and studied by NMR spectroscopy (Fig. 6) [51]. The 7–9 Hz $^3J_{\text{NH-C}\alpha\text{H}}$ coupling constants and chemical shift perturbation values ($\Delta\delta$ $C_\alpha H > 0.1$) for the Val, Leu, and

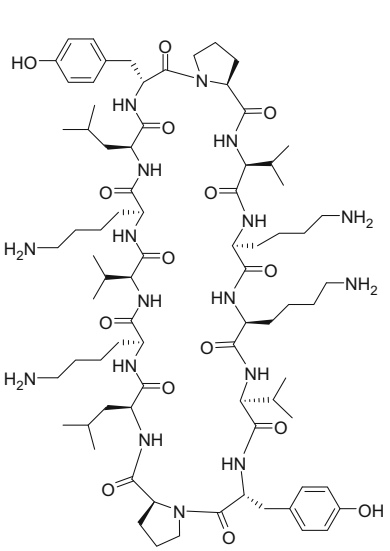

3i cyclo-(VK*KV*d*YP^{6}LKVKL*d*YP^{14}) GS14-L3

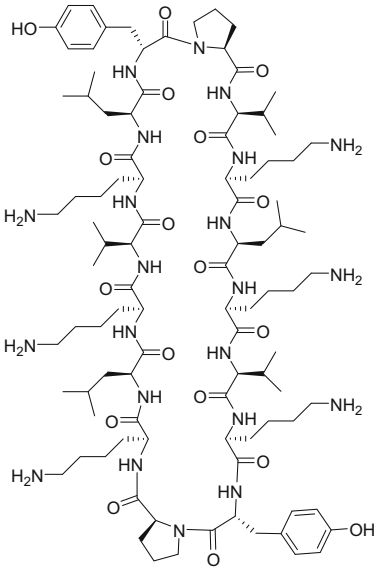

3j cyclo-(VKLKVK*d*YP^{8}KLKVKL*d*YP^{16}) GS16

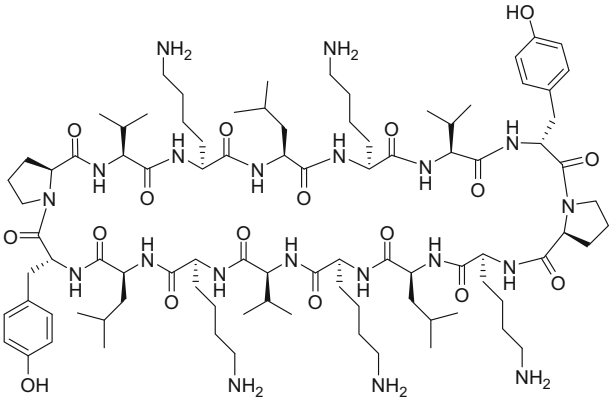

3k cyclo-(VKLKV**d*YP^{7}KLKVKL*d*YP^{15}) GS16-K6

Fig. 4 (continued)

Orn residues of **5c** suggested their presence in an extended β-strand conformation. The 2–4 Hz coupling constants for the D-Phe residues and $\Delta\delta$ of $C_{\alpha}H < 0$ for the Pro and D-Phe residues implied their presence in a turn motif. Incorporation of a SAA residue for one of the D-Phe-Pro dipeptides was inferred to disrupt the β-hairpin structure, because **5e–g** exhibited, respectively, lower coupling constants and smaller chemical shift perturbations than **5c**.

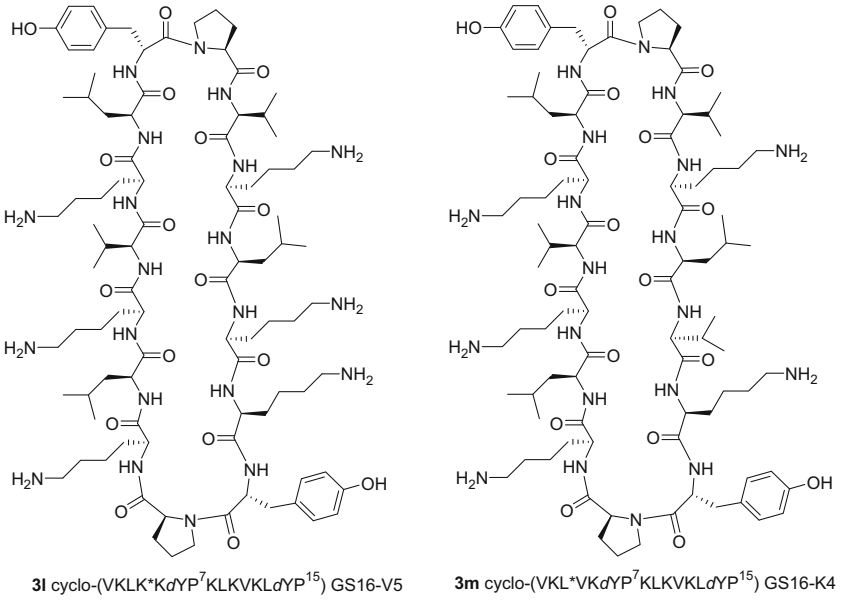

Fig. 4 Structures of **3a–m**

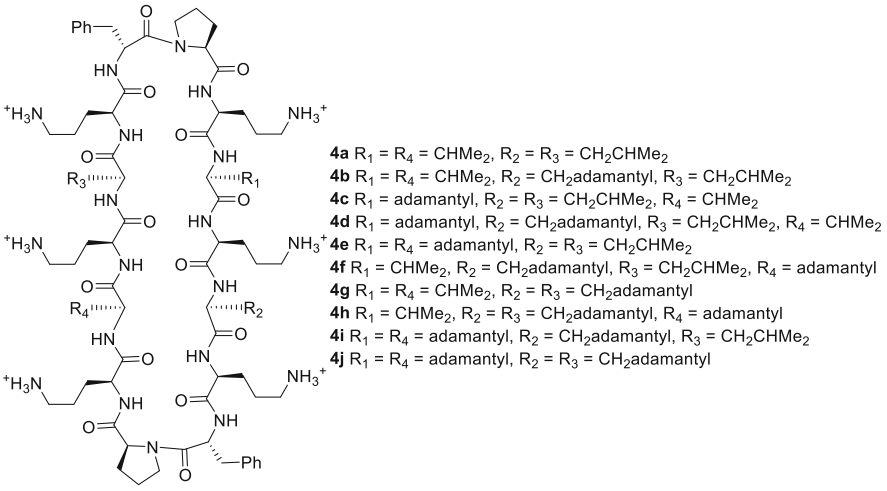

Fig. 5 Structures of **4a–j**

The CD spectrum of **5c** had two negative maximum around 205 and 222 nm; however, the spectra of **5e–g** had a weaker negative maximum around 220 nm. Relative to **5a**, **5c** had better antibacterial activity against both gram-positive and gram-negative bacteria, as well as lower hemolytic activity. The SAA-GS analogs

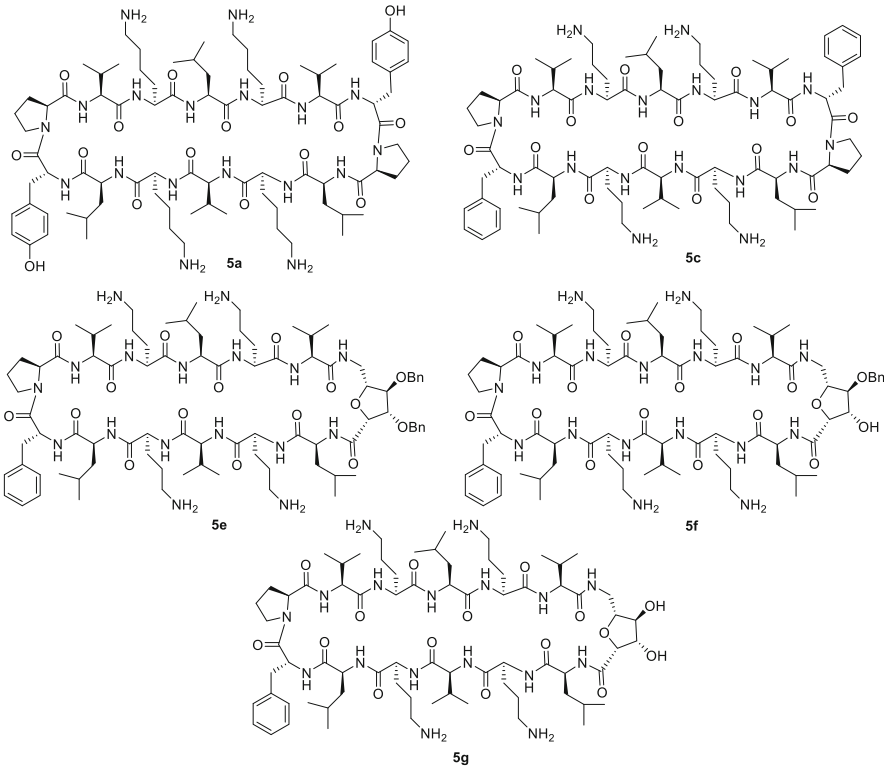

Fig. 6 Structures of **5a**, **5c**, **5e–g**

5e–g possessed similar bactericidal activity as **5c** with lower hemolytic activity. The improved therapeutic profiles for **5e–g** may be due to distortion of the β-hairpin structure and reduced hydrophobicity at the SAA turn.

Diastereomeric analogs **5d** and **5h–j**, in which the configuration of one of the Orn residues was inverted (Fig. 7), showed well-resolved NMR spectra indicating the presence of a single stable β-hairpin–β-sheet secondary structure in solution: $^3J_{\text{NH-C}\alpha\text{H}}$ coupling constants of 7–9 Hz for the Val, Leu, and Orn residues and of 4 Hz for the D-Phe residues; $C_\alpha H$ chemical shift perturbation values of $\Delta\delta > 0.1$ for the Val, Leu, Orn residues; and $\Delta\delta < 0$ for D-Phe and Pro residues.

Relatively lower values for the amide coupling constants and chemical shift perturbations of the Val, Leu, Orn residues of **5e–g** and **5h–j** compared to those of their parent counterparts **5c** and **5d** indicated that introduction of SAA moiety disrupted the hairpin secondary structure. Inversion of the stereochemistry of one Orn residue did not apparently alter the peptide secondary structure in CD_3OH, albeit CD spectra in TFE/H_2O indicated that **5e–g** adopted a more ordered secondary structure compared to diastereomers **5h–j**. Like GS, analogs **5c** and **5d** exhibited negative ellipticity at 220 and 205 nm. Analogs **5e–g** had spectra most indicative of the stable β-hairpin–β-sheet secondary structure and proved the most

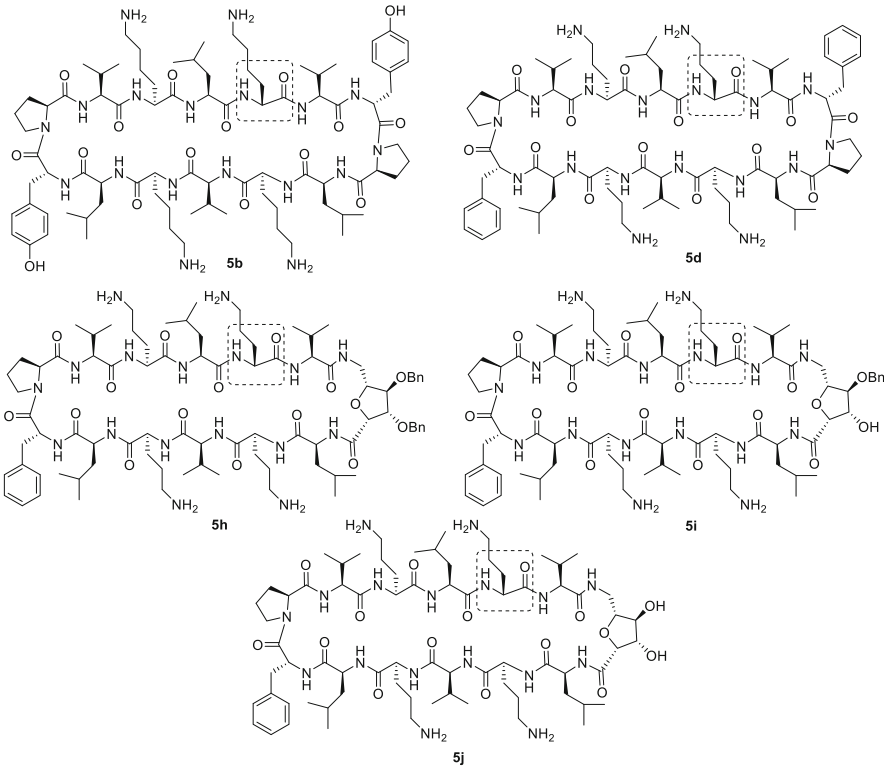

Fig. 7 Structures of **5b**, **5d**, **5h–j**

potent against both gram-positive and gram-negative bacteria but maintained significant hemolytic activity. In terms of therapeutic index, analog **5h** gave the best results because of its relatively high antibacterial potency and significantly reduced hemolytic activity. Based on HPLC retention times, D-Orn analogs **5b**, **5d**, and **5h–j** were, respectively, less hydrophobic than their L-Orn diastereomers **5a**, **5c**, and **5e–g**, with the promising D-Orn analog **5h** in the middle of the hydrophobic range of the series [52].

Undecapeptide GS analogs of the structure *cyclo*-(Val^1-Orn^2-Leu^3-Xaa^4-D-Phe^5-Pro^6-Val^7-Orn^8-Leu^9-D-Phe^{10}-Pro^{11}) (**6a–e**, Fig. 8) were synthesized and studied by NMR spectroscopy [53]: Xaa was Leu, Ala, Orn, Lys, and Arg. Analogs **6** were monomeric over a wide concentration range. The absolute values of the temperature coefficients ($\Delta\delta/\Delta T$) of the amide NHs for the Val^{1,7} and Leu^{3,9} residues were relatively low, and those for the Orn^{2,8}, Leu^4, and D-Phe^{5,10}, residues were high indicative of solvent shielded and exposed protons; the former involved in intramolecular hydrogen bonds. The relatively larger $^3J_{\text{NH-C}\alpha\text{H}}$ coupling constant values for the Val^1, Orn^2, Leu^3, Val^7, Orn^8, and Leu^9 residues were consistent with their ϕ dihedral values around $-120°$, as found in a β-sheet conformation. The ROE cross peaks observed between D-Phe^{5}CαH and Pro^{6}CαH, as well as the D-Phe^{10}CαH and

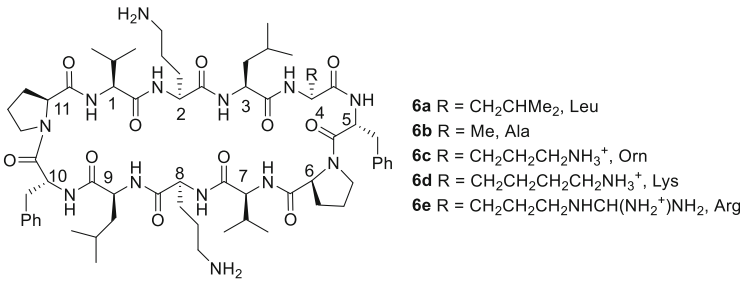

Fig. 8 Structures of **6a–e**

Pro[11]δCH_2 protons, indicated, respectively, prolyl amide *cis*- and *trans*-conformations, the latter in a type II′ β-turn. All analogs **6** showed similar conformations, which was supported by similar CD spectra. Relative to GS, analogs **6** had comparable activity against gram-positive but weaker effects on gram-negative bacteria. Leucine and alanine analogs **6a** and **6b** exhibited, respectively, similar and lower toxicity against sheep red blood cells as GS. Analogs **6c–e** with cationic residues showed much lower toxicity indicating selectivity for bacteria versus mammalian membranes.

β-Amino acid containing analogs of GS [*cyclo*-$(\alpha\beta^3\alpha\beta^2\alpha)_2$ **7a–b**, *cyclo*-$(\alpha\beta^2\alpha\beta^3\alpha)_2$ **7c–e**, in addition to GS diastereomer **7f** (Fig. 9)] was synthesized and studied by NMR spectroscopy. Although analog **7c** containing two (*S*)-β^2-homovaline and two (*R*)-β^3-homoleucine was modestly active, analogs containing two (*R*)-β^3-homovaline and two (*R*)-β^2-homoleucine residues were largely inactive [54].

Inactive analogs **7a** and **7b**, as well as the analog **7c** with the best antibacterial activity, all were found to adopt β-hairpin structures using a combination of NMR spectroscopy and X-ray analysis. Placing the hydrophobic side chains of the β-homoLeu and β-homoVal residues closer to the Orn residue might have influenced the charge density in **7c** to favor an improved activity. The authors speculated that inclusion of proper *anti*-$\beta^{2,3}$-amino acids [55] would lead to the rigid conformations effective in terms of activity.

2.2 *Effect of* N-*Methylation*

Intramolecular hydrogen bonds between Val and Leu residues play an important role in maintaining the antiparallel β-sheet arrangement of GS. The roles of other nitrogen protons, including those of the free amine of the Orn residues in the antiparallel sheet structure, were evaluated by X-ray crystallographic analysis of bis-Boc-tetra-*N*-methyl-GS (**8**, Fig. 10) [56].

Although the expected arrangement of hydrogen bonds was observed for methylated GS analog **8**, the antiparallel β-sheet exhibited a slight twist, and an extra

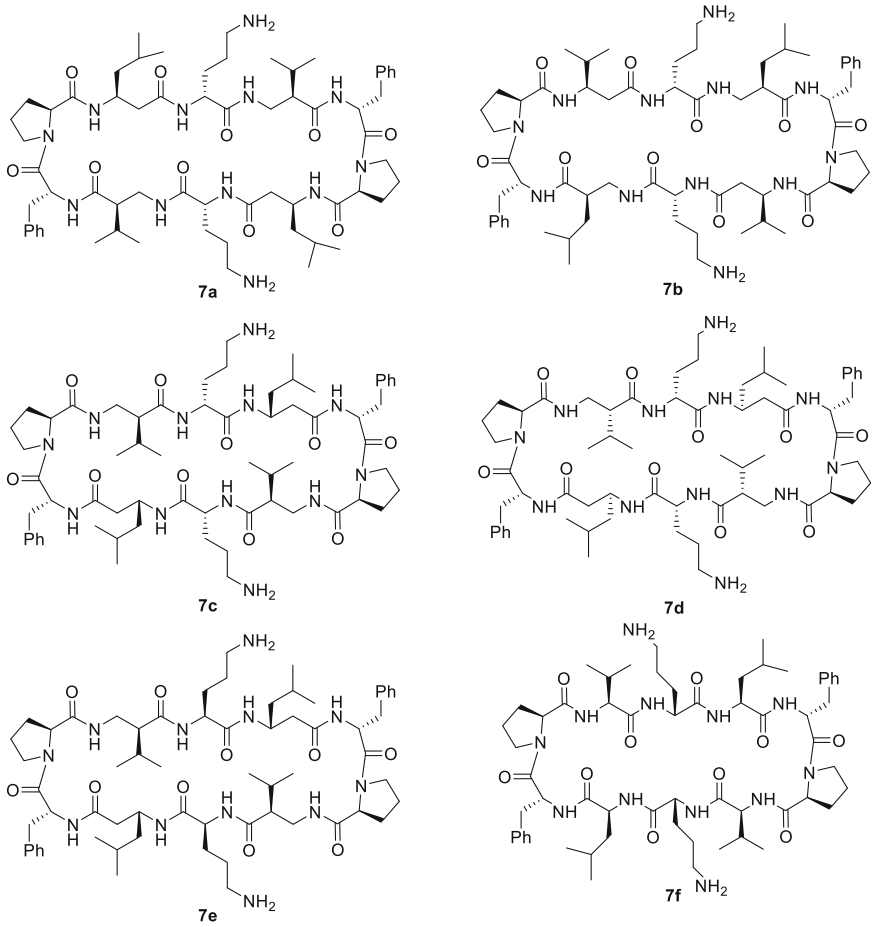

Fig. 9 Structures of **7a–f**

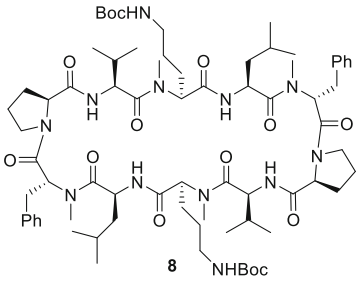

Fig. 10 Structure of **8**

hydrogen bond was observed between the carbonyl groups of the D-Phe residues and the urethane NHs of the protected ornithine side chains. The sense of the twist was opposite to that reported for bis-N^{δ}-(trichloroacetyl) and bis-N^{δ}-(*m*-

bromobenzoyl) derivatives of GS. The importance of amide protons in GS was further investigated by the synthesis and analysis in which one, two or three residues were, respectively, replaced with *N*-methylamino acid residues (*N*-Me-Ala, *N*-Me-Phe, and *N*-Me-Leu, **9a–l**, Fig. 11) [57].

Four analogs were studied by NMR spectroscopy in DMSO-d_6: [Me-Leu^5]-GS (**9e**), [Me-Leu^5, Me-Ala^7]-GS (**9h**), [Me-Ala^2, Me-Ala^7]-GS (**9j**), and [Me-Ala^2, Me-Leu^5, Me-Ala^7]-GS (**9k**). The larger $^3J_{\text{NH-C}\alpha\text{H}}$ coupling constants and lower temperature coefficients ($\Delta\delta/\Delta T$) for the Val, Orn, and Leu amide NHs in the proton NMR spectra of **9j** compared to GS suggest a distortion from the β-sheet–β-turn structure indicating that replacement of the proline residues by *N*-(methyl)alanine decreased structural rigidity. The structures of **9e** and **9k** both possess a *N*-(methyl)leucine residue at the 5-position and exhibited coupling constant values indicating their similar backbone conformations. Relative to their respective parent counterpart GS, **9j**, **9e**, and **9k** exhibited similar $^3J_{\text{NH-C}\alpha\text{H}}$ coupling constants except for the D-Phe residue which was significantly higher indicating a conformational change about the β-turn region. In an observation of a significant increase in the $\Delta\delta/\Delta T$ temperature coefficient for the amide NH of the Val^8 residue of **9k** compared to that in GS, **9e** and **9j** indicated strengthening of the intramolecular bond with the carbonyl of the *N*-(methyl)leucine^5 residue. As in the case of **9e** and **9k**, [Me-Leu^5, Me-Ala^7]-GS (**9h**) exhibited a change in the coupling constant for the D-Phe^1 residue indicating perturbation of the turn region. In addition, the temperature coefficient of the amide NH of Val^3 of **9h** increased significantly indicating involvement in an internal hydrogen bond. The CD spectra of [Me-Ala^2]-GS (**9d**) and [Me-Ala^2, Me-Ala^7]-GS (**9j**) were measured in water, and their curve shapes were found to be similar to that of GS with a negative maximum at 207 nm and a shoulder at 217 nm indicating that replacement of Pro with Me-Ala had limited effect on the overall type II′ β-sheet–β-turn conformation. On the other hand, all of the other methylated GS analogs showed curve shapes indicative of major deviation from GS conformation: e.g., [Me-Ala^4]-GS (**9b**) showed broad negative maximum at 207–213 nm, and [Me-Ala^3]-GS (**9c**) exhibited a shifted negative maximum at 202 nm. Relative to GS, the IC_{90} values increased 15–20-fold for analogs **9a** and **9c** against gram-positive bacteria. Moreover, analogs **9d** and **9j** were similarly as active as GS against gram-positive bacteria indicating that replacement of Pro with *N*-Me-Ala did not affect the activity. Retained antibacterial activity for [Me-Ala^4]-GS (**9b**) and [Me-D-Phe^6]-GS (**9f**) suggested that methylation of the externally exposed amides did not affect the activity and that only one positively charged Orn residue was sufficient for retained activity. Up to a fivefold decrease in hemolytic activity relative to GS was observed on *N*-methylation of the internal amide hydrogen bonding NH of the Leu^5 residue (e.g., **9a**, **9e**, **9g**, **9h**, and **9k**). *N*-Methylation of the amide NH of specific β-turn and β-strand residues was thus shown useful for dissociating antimicrobial and hemolytic activity.

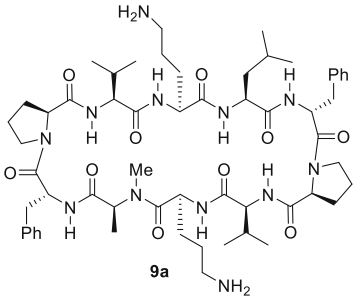

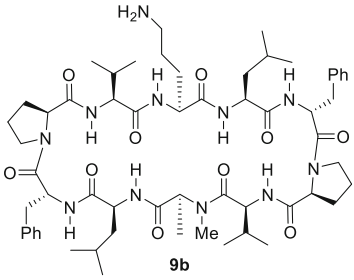

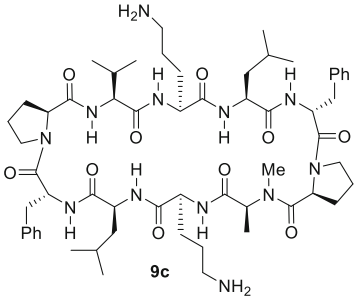

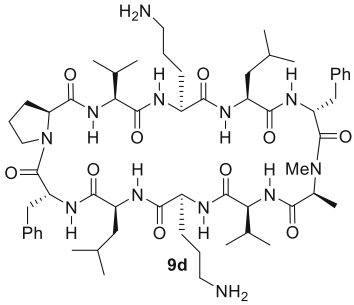

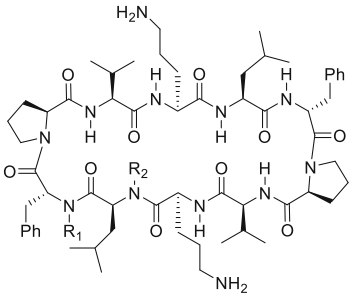

9e R_1 = H, R_2 = Me; **9f** R_1 = Me, R_2 = H

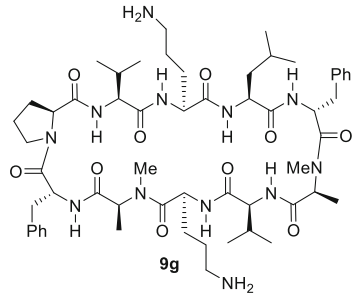

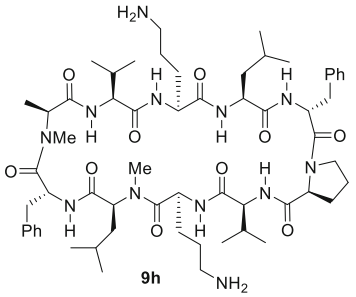

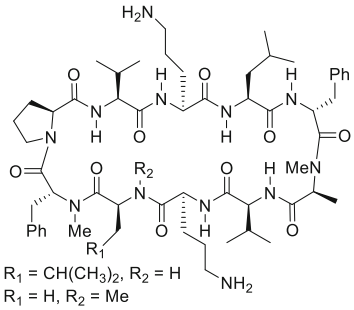

9i R_1 = $CH(CH_3)_2$, R_2 = H
9l R_1 = H, R_2 = Me

Fig. 11 (continued)

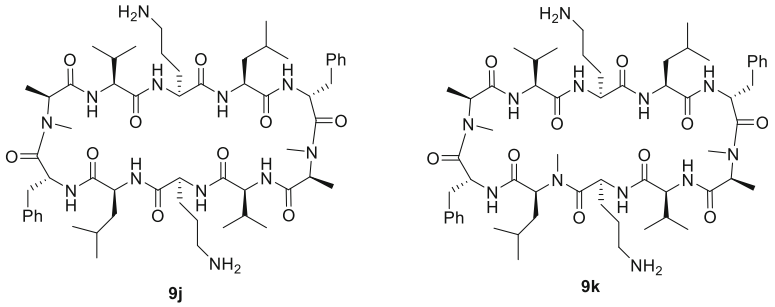

Fig. 11 Structures of **9a–l**

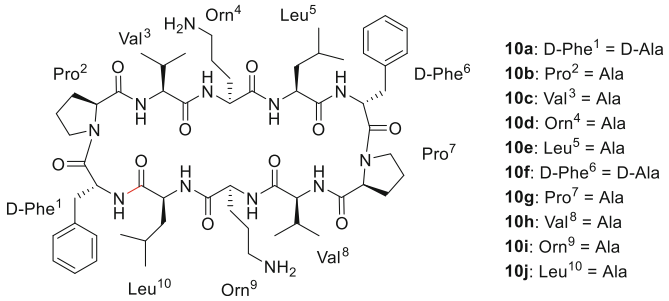

Fig. 12 Structures of **10a–j**

2.3 Exchange of Amino Acid

Solid-phase peptide synthesis using Fmoc protocol and on-resin macrolactamization without side-chain protection afforded cyclic GS analogs **10** in high yield and high purity. The pre-organized conformation of the linear precursors was cited for the high specificity of the cyclization reactions. Head-to-tail cyclization of a linear thioester precursor was used to close the ring at D-Phe^1-Leu^{10} amide bond (shown in red, Fig. 12). To demonstrate the general applicability of the method, an alanine-scan series of GS analogs **10a–j** was synthesized in which each residue was systematically replaced by alanine (Fig. 12) [58]. The biological activities of the analogs were not reported. This method was compared with an earlier reported chemoenzymatic approach in which the isolated thioesterase domain of gramicidin synthase was used for enzymatic cyclization of GS precursors containing up to three consecutive modifications of the amino acid residues in the sequence without significant affect on the cyclization rate [59].

The size and orientation of the D-Phe residues have been studied by the synthesis and analysis of GS analogs possessing aromatic amino acids **11a–f** N-terminal to the prolyl residues (Fig. 13) [60]. In all cases, the major isomer observed by NMR

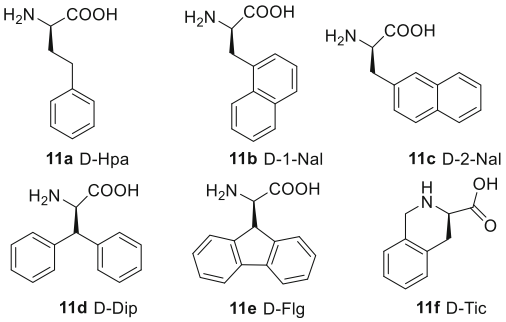

Fig. 13 Structures of the residues used to replace D-Phe in GS analogs **11a–f**

spectroscopy possessed amide *trans*-isomers N-terminal to the two Pro residues and an overall conformation that was similar to GS as indicated by similar ^{1}H, ^{13}C, and ^{15}N chemical shifts. In certain cases (e.g., **11e** and **11f**), the chemical displacements of some protons were shifted due to ring current effects from the aromatic residues. In addition, Nuclear Overhauser Effects (NOE) from the transfer of magnetization between the Orn-CαH and the Val and the Leu amide NHs supported the presence of the sheet structure for **11a–c**.

For GS and analogs **11** (except **11b**, which had low solubility), NOEs were observed between the side-chain protons of the Val and Leu residues suggesting a β-sheet structure. Relative to the temperature coefficients of GS, the $\Delta\delta/\Delta T$ values were similar for the solvent-exposed Orn and D-Phe amide NH protons, except for **11e**, and for the solvent-shielded NH of the Leu residues. The temperature coefficients for the Val residue NHs were higher in **11** than in GS indicating a relatively weaker participation in an intramolecular hydrogen bond, except for **11f** in which the $\Delta\delta/\Delta T$ value was low. Except for the D-Tic analog **11f**, all of the aromatic amino acid analogs **11a–e** were potent against bacterial strains; however, they exhibited hemolytic activity equal to or greater than GS.

Another series of GS analogs modified at the turn region were prepared by replacing the D-Phe-Pro sequence with D-Pro-Phe and employing a series of constrained amino acids **12a–l** to replace the phenylalanine moiety (Fig. 14) [61]. In all cases, the Leu-D-Pro amide bond was observed to be in a *trans*-arrangement in the major conformer, which existed in some cases in equilibrium with amide *cis*-isomer as well as conformers not related to prolyl amide *cis–trans*-isomerism. In contrast to GS and analogs **11**, the Val residues in **12** exhibited coupling constants and temperature coefficients indicative of a stronger intramolecular hydrogen bond. With the exception of **12a**, which possessed a $^{3}J_{\text{NH-C}\alpha\text{H}}$ value of 5.7 Hz for the Orn residue, analogs **12** exhibited large (8.0–9.8 Hz) $^{3}J_{\text{NH-C}\alpha\text{H}}$ coupling constants for the Val, Orn, and Leu residues indicative of a β-strand conformation. With the exception of **12k**, analogs **12** exhibited solvent-shielded temperature coefficients ($\Delta\delta/\Delta T > -5.1$ pbb/K) for the Val and Leu residue amide NH protons, as well as solvent-exposed values ($\Delta\delta/\Delta T < -7.0$ pbb/K) for the Orn and D-Phe residue amide NH protons, a pattern indicating a β-sheet–β-turn

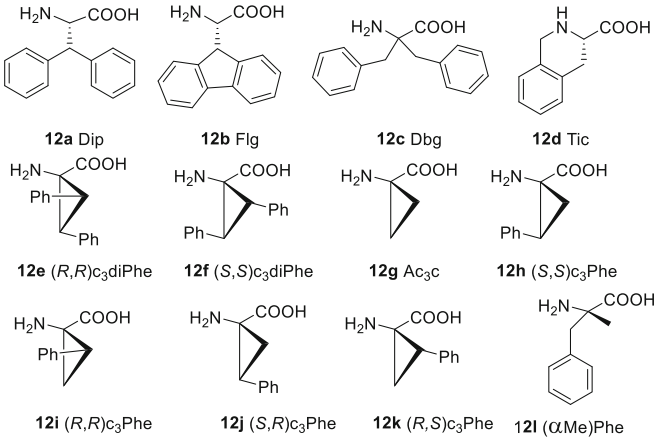

Fig. 14 Structures of amino acids used to replace Phe in [D-Pro[1,6]-Phe[2,7]]GS analogs **12a–l**

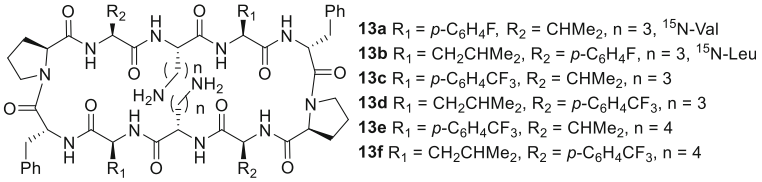

Fig. 15 Structures of **13a–f**

conformation. Similarly, with the exceptions of **12a** and **12k**, analogs **12** exhibited three cross-strand NOEs characteristic of a symmetrical GS structure, between (i) the CαH protons of the Orn residues, (ii) the CαH proton of the Orn residues, and the amide NH of the Leu residues, as well as (iii) the amide NH protons of the Val and Leu residues. In the case of **12a** and **12k**, NOE between the Val and Leu side chains suggested their proximity on an amphiphilic structure that differed from the canonical β-sheet structure of GS. The parent reversed analog exhibited lower antibacterial and hemolytic activity compared to GS; however, certain analogs (e.g., **12a**, **12b** and **12d**) had comparable or better activity than GS but retained hemolytic activity like GS.

The starting amino acid proved critical for good overall yield in the synthesis of GS and analogs **13** bearing ^{19}F-labeled *p*-fluoro- and *p*-trifluoromethylphenylglycine as well as ^{15}N-labeled Leu and Val residues (Fig. 15) [62]. The latter analogs were synthesized for use in solid-state NMR structure analysis of GS in biologically relevant membranes [63, 64].

Replacement of one of the D-Phe residues with *N*-substituted and unsubstituted D-triazolyl alanines, as well as D-histidine, gave analogs **14** (Fig. 16) [65], which maintained characteristics of the parent type II′ β-sheet–β-turn structure: i.e., the

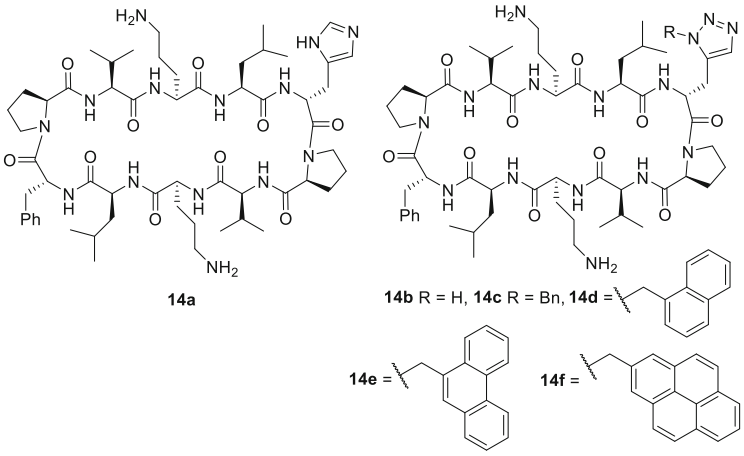

Fig. 16 Structures of **14a–f**

$^3J_{NH\text{-}C\alpha H}$ values were relatively small (2.5–3.5 Hz) for the D-His, D-triazolyl alanine, and D-Phe residues and high (>8 Hz) for the strand residues. X-ray structures of histidine and *N*-benzyl triazolyl alanine analogs **14a** and **14c** were also in accordance with the NMR data and confirmed the predicted secondary structure. Relative to the parent triazolyl alanine analog **14b**, **14c–e** showed higher antimicrobial activity indicating the importance of the aromatic substituent. Bulky pyrene analog **14f** was, however, less potent compared to **14c–e** indicating the limits of aromatic ring size for activity. Analogs **14d–f** exhibited higher hemolytic activity than GS. Although analogs **14b** and **14c** were less hemolytic than GS, histidine analog **14a** was the most promising lead, having the best antibacterial activity with least cytotoxicity, likely due to the relatively higher basicity of the imidazole moiety.

The importance of the basic ornithine residues was demonstrated by replacement with glutamine in a series of analogs **15** bearing different D-Phe, Val, and Leu residue surrogates (Fig. 17) [66].

Although antibacterial activity was abolished against a panel of organisms [e.g., *Streptococcus agalactiae* (*S. agalactiae*) methicillin-resistant *S. aureus* (MRSA), *E. coli*, and *P. aeruginosa*], except *S. pyogenes*, against which a few analogs exhibited marginal activity, analogs **15** retained significant hemolytic activity.

Exploring the affinity that GS shows toward carbohydrates, a series of analogs **16** was prepared in which the hydrophobic Val residue of GS was replaced by Asn, Asp, and Gln, and the Leu residue was substituted with Trp (Fig. 18). Analogs **16** demonstrated selective affinity for neutral carbohydrates, such as glucose, lactulose, galactose, and fructose [67].

Removal of the D-Phe-Pro sequence to produce smaller ring size GS analogs, *cyclo*-[δ-Orn(-Val-Pro-D-Phe-H)-Leu]$_2$ **17a** and *cyclo*-(δ-Orn-Leu)$_2$ **17b**, abolished activity against both gram-positive and gram-negative bacteria in the case of the

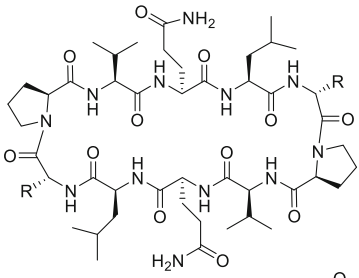

15a R = D-Tyrosine, **15b** R = D-Phenylamine
15c R = D-Naphthylalanine, **15d** R = D-Tryptophan
15e R = D-Phenylglycine, **15f** R = D-Thienylalanine
15g R = D-4-Flurophenylalanine
15h R = D-4-Iodophenylalanine

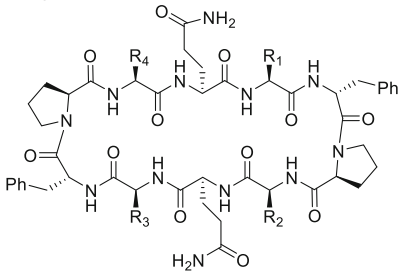

15i R_1 = $CHMe_2$, R_2 = $CHMe_2$, R_3 = $CHMe_2$, R_4 = $CHMe_2$
15j R_1 = $CHMe_2$, R_2 = $CHMe_2$, R_3 = $CHMe_2$, R_4 = CH_2CHMe_2
15k R_1 = $CHMe_2$, R_2 = $CHMe_2$, R_3 = CH_2CHMe_2, R_4 = $CHMe_2$
15l R_1 = $CHMe_2$, R_2 = CH_2CHMe_2, R_3 = $CHMe_2$, R_4 = $CHMe_2$
15m R_1 = $CHMe_2$, R_2 = $CHMe_2$, R_3 = CH_2CHMe_2, R_4 = CH_2CHMe_2
15n R_1 = $CHMe_2$, R_2 = CH_2CHMe_2, R_3 = CH_2CHMe_2, R_4 = $CHMe_2$
15o R_1 = CH_2CHMe_2, R_2 = $CHMe_2$, R_3 = CH_2CHMe_2, R_4 = $CHMe_2$
15p R_1 = $CHMe_2$, R_2 = CH_2CHMe_2, R_3 = CH_2CHMe_2, R_4 = CH_2CHMe_2
15q R_1 = CH_2CHMe_2, R_2 = CH_2CHMe_2, R_3 = CH_2CHMe_2, R_4 = CH_2CHMe_2

Fig. 17 Structures of **15a–q**

latter, and the former retained 1/2 to 1/8 the activity of GS against gram-positive bacteria [68].

Modification of the D-Phe-Pro turn was examined by the synthesis of GS analogs **18** [69], in which the D-Phe residues were substituted by D-Tyr and *O*-benzyl D-Tyr, and the Pro residues were replaced with (2*S*,4*R*)- and (2*S*,4*S*)-azidoproline (*R*- and *S*-Azp, **18c** and **18d**), (2*S*,4*R*)- and (2*S*,4*S*)-aminoproline (**18e** and **18f**), as well as their carbamate (**18g** and **18h**) and succinamide (**18i** and **18j**) counterparts (Fig. 19). Similar to GS, analogs **18**, all showed the respective large and small vicinal spin–spin $^3J_{NH\text{-}C\alpha H}$ coupling constants for the extended β-strand and turn conformations. Relative to GS, only the hydrophobic *O*-benzyl-D-Tyr and Azp peptides (**18b**, **18c** and **18d**) possessed comparable antibacterial activity.

On the other hand, single replacement of D-Phe with *p*-*N*-benzylamino and *p*-*N*, *N*-dibenzylamino-D-Phe gave analogs **19k** and **19l**, which failed to show antibacterial potency, further illustrating that introduction of a relatively basic amine into the turn region was detrimental to activity (Fig. 20) [70].

Extensive NMR studies in solution and X-ray analysis established that analogs **19** maintained the cyclic β-hairpin secondary structure of GS. Analogs **19** illustrated general trends in which potent antimicrobial analogs exhibited high hemolytic activity, and optimal size and hydrophobicity was important for potency.

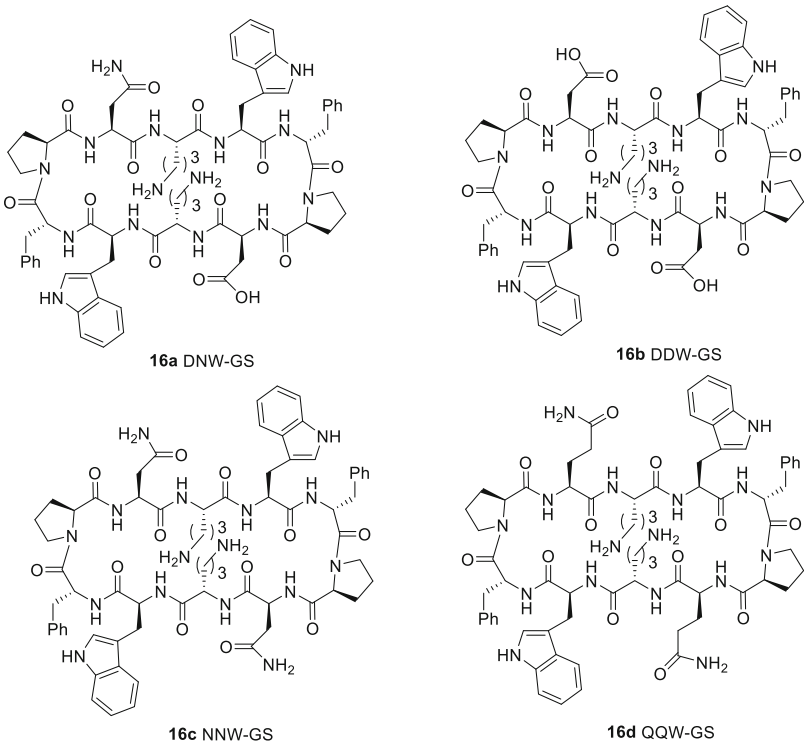

Fig. 18 Structures of **16a–d**

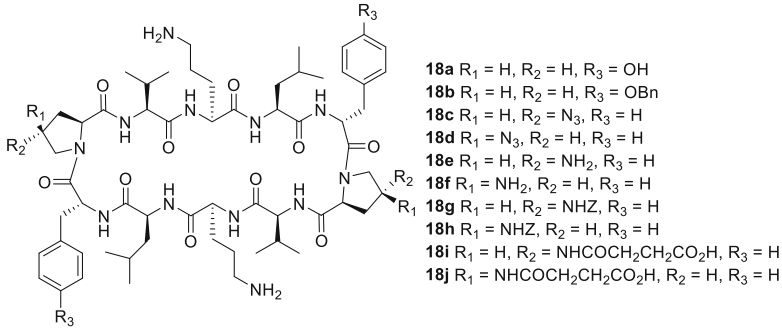

Fig. 19 Structures of **18a–j**

The importance of the amphiphilic sequence was demonstrated by replacement of the hydrophobic Val and Leu residues with hydrophilic amino acids (e.g., His, Lys, Orn, Dab, and Dap) and the hydrophilic Orn residues with Leu as a hydrophobic amino acid (Fig. 21), which produced the series of analogs **20** that had lower antibacterial and hemolytic activity than GS [71]. Replacement of one proline

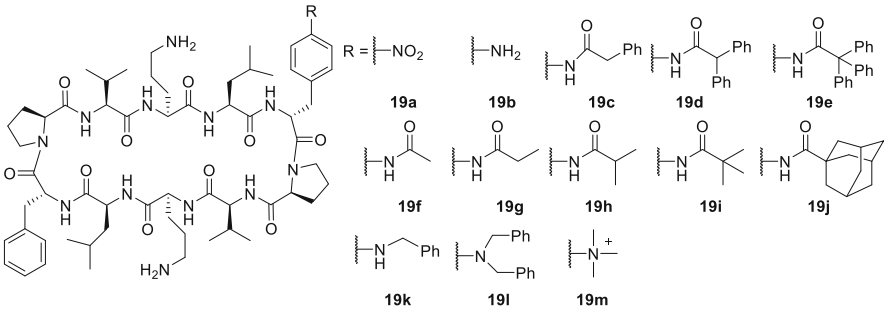

Fig. 20 Structures of **19a–m**

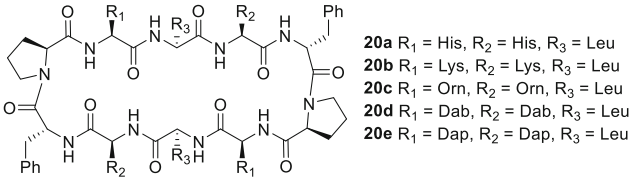

Fig. 21 Structures of **20a–e**

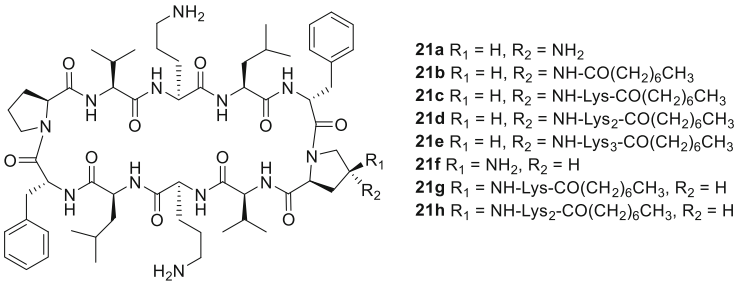

Fig. 22 Structures of **21a–h**

residue with (2*S*,4*S*)-aminoproline, as well as its *N*-octanoyl and octanoyl-(lysyl)$_n$ counterparts ($n = 1$–3), gave analogs **21**, which maintained CD spectra characteristic of the β-sheet structure of GS with a negative maximum at ~207 nm and small negative band at ~220 nm (Fig. 22) [72]. Analogs **21** exhibited antibacterial activities similar to GS, with hemolytic activity comparable (**21b**, **21c**, and **21g**) and lower (**21a**, **21d–f**, and **21h**) than that of GS.

A major conformer similar to GS and a few minor conformations were exhibited by *cyclo*-(L-Leu-L-Lys-L-Leu-D-Leu-L-Leu)$_2$ (**22**), in which Leu replaced the Val, D-Phe, and Pro residues, and Lys was substituted for the Orn residue (Fig. 23) [73], albeit **22** had 1/8 to 1/4 antimicrobial activity of GS.

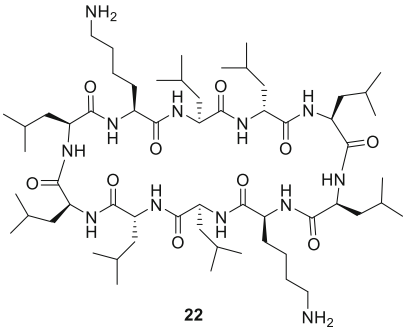

Fig. 23 Structure of **22**

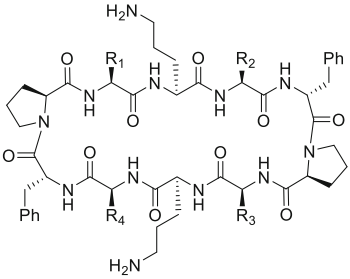

23a R_1 = adamantyl, R_2 = CH_2CHMe_2, R_3 = $CHMe_2$, R_4 = CH_2CHMe_2
23b R_1 = adamantyl, R_2 = CH_2CHMe_2, R_3 = adamantyl, R_4 = CH_2CHMe_2
23c R_1 = $CHMe_2$, R_2 = CH_2adamantyl, R_3 = $CHMe_2$, R_4 = CH_2CHMe_2
23d R_1 = $CHMe_2$, R_2 = CH_2adamantyl, R_3 = $CHMe_2$, R_4 = CH_2adamantyl
23e R_1 = adamantyl, R_2 = CH_2adamantyl, R_3 = adamantyl, R_4 = CH_2adamantyl
23f R_1 = CMe_3, R_2 = CH_2CMe_3, R_3 = CMe_3, R_4 = CH_2CMe_3
23g R_1 = C_6H_{11}, R_2 = $CH_2C_6H_{11}$, R_3 = C_6H_{11}, R_4 = $CH_2C_6H_{11}$

Fig. 24 Structures of **23a–g**

To examine the importance of the hydrophobic residues, GS analogs **23** were synthesized possessing (*S*)-*tert*-butylglycine, (*S*)-cyclohexylglycine, and (*S*)-adamantylglycine as hydrophobic valine replacements and (*S*)-*tert*-butylalanine, (*S*)-cyclohexylalanine, and (*S*)-adamantylalanine as the corresponding leucine replacements (Fig. 24) [74].

In agreement with the GS spectrum, the $^3J_{NH\text{-}C\alpha H}$ values of the adamantylglycyl, adamantylalanyl, Orn, Val, and Leu residues, all were between 8 and 12 Hz and those for the D-Phe residue were between 2 and 4 Hz indicating their respective presence in the strand and turn portions of the β-hairpin structure for analogs **23a–e**. Moreover, the NOEs, as well as the X-ray structures of **23b** and **23f** confirmed the presence of the β-hairpin secondary structure. Except analogs **23d** and **23e**, all the hydrophobic GS analogs were potent against various gram-positive, gram-negative strains (with **23f** against MRSA strains also); however, all were found to be significantly hemolytic.

Similarly, peptides **24** composed of four Orn residues sandwiching central hydrophobic amino acids, with unaltered turn regions, exhibited potent activity

against gram-negative and gram-positive bacteria, as well as human erythrocytes (Fig. 25) [75].

To study the inhibition of aggregation of amyloid Aβ(1–40) peptides, GS analogs **25** were synthesized and examined using thioflavine T fluorescence assays and scanning probe microscopy (Fig. 26) [36]. Analogs **25** and GS with hydrophobicity on the β-strand, as well as suitable aromatic components at the D-Phe

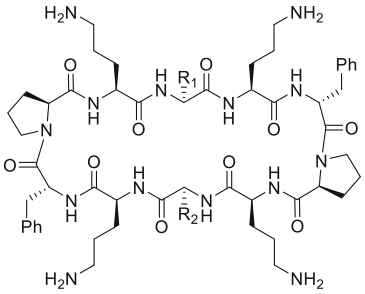

24a $R_1 = R_2 = CHMe_2$
24b $R_1 = R_2 =$ adamantyl
24c $R_1 = CHMe_2$, $R_2 = CMe_3$
24d $R_1 = R_2 = CH_2CHMe_2$
24e $R_1 = CH_2CHMe_2$, $R_2 = CH_2CMe_3$
24f $R_1 = R_2 = CMe_3$
24g $R_1 = R_2 = CH_2CMe_3$
24h $R_1 =$ adamantyl, $R_2 = CHMe_2$
24i $R_1 = CH_2$adamantyl, $R_2 = CH_2CHMe_2$
24j $R_1 =$ adamantyl, $R_2 = CMe_3$
24k $R_1 = CH_2$adamantyl, $R_2 = CH_2CMe_3$
24l $R_1 = C_{10}H_{21}$, $R_2 = CHMe_2$
24m $R_1 = R_2 = CH_2$adamantyl
24n $R_1 = R_2 = C_{10}H_{21}$

Fig. 25 Structures of **24a–n**

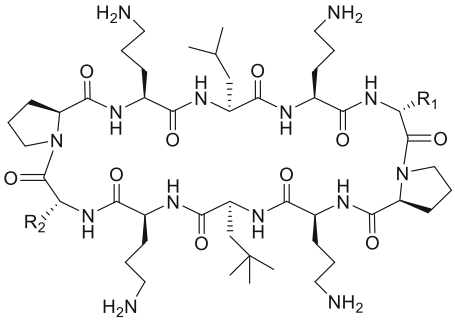

25a $R_1 =$ Bn, $R_2 = C_8H_{17}$
25b $R_1 = R_2 = C_8H_{17}$

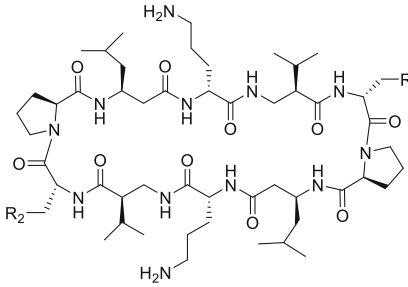

25c $R_1 = R_2 =$ Ph **25d** $R_1 = R_2 =$ 
25e $R_1 = R_2 =$ 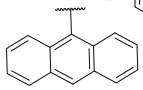
25f $R_1 =$ 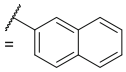 $R_2 =$ 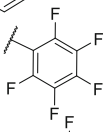
25g $R_1 =$ 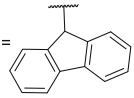 $R_2 =$ 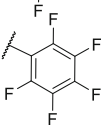

Fig. 26 Structures of **25a–g**

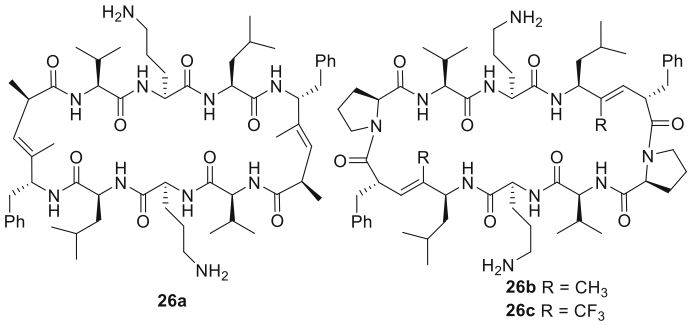

Fig. 27 Structures of **26a–c**

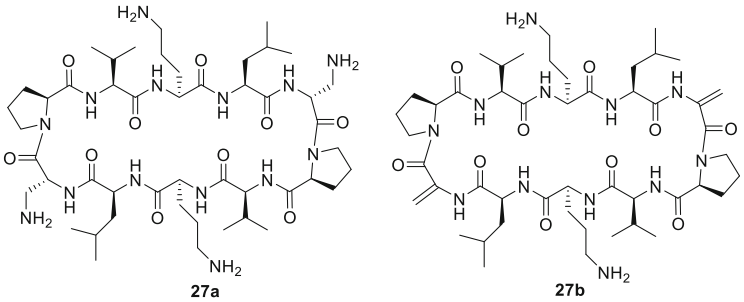

Fig. 28 Structures of **27a** and **27b**

position, were shown to inhibit fibrillization and to dissolve preformed amyloid fibrils by a mechanism that was ascertained through in silico docking to involve interaction at a channel of the Aβ fibril composed of hydrophobic and hydrophilic residues [36].

The D-Phe-Pro region of GS has been replaced with different turn surrogates. For example, replacement of D-Phe-Pro with a trisubstituted *E*-alkene dipeptide isostere (TEADI) gave analog **26a** (Fig. 27), which exhibited the characteristic antiparallel β-sheet structure and a MIC value of 20 μg/mL against *Bacillus subtilis* (15 μg/mL for GS) [76]. Replacement of the Leu-D-Phe residue with TEADI analogs with methyl and trifluoromethyl substituents gave **26b** and **26c** with MIC activities of 5–15 μg/mL against *Bacillus subtilis*, the latter showing better β-pleated sheet structure [77].

The replacement of the D-Phe residues with D-2,3-diaminopropionic acid added two additional cationic residues in **27a** which retained activity against gram-negative bacteria but was less effective against gram-positive bacteria than GS. On the other hand, replacement of the D-Phe residues with α,β-dehydroalanine gave analog **27b** which showed antibacterial activity comparable to GS (Fig. 28) [78].

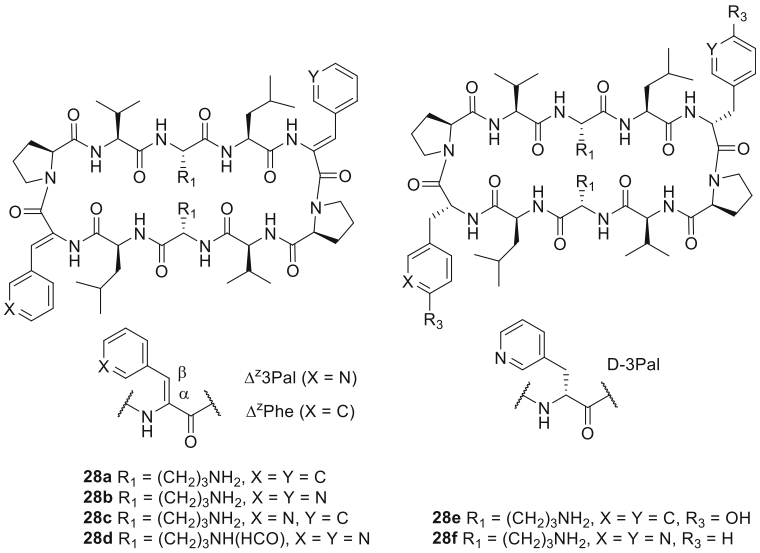

Fig. 29 Structures of **28a–f**

A related series of GS analogs **28** was synthesized in which the D-Phe residue was, respectively, substituted by (*Z*)-(β-3-pyridyl)-α,β-dehydroalanine (Δ^{Z}3Pal), (β-3-pyridyl)-D-alanine (D-3Pal), and (*Z*)-α,β-dehydrophenylalanine (Δ^{Z}Phe) (Fig. 29). In the spectra of the Δ^{Z}3Pal-containing analogs, variable-temperature experiments indicated intramolecular hydrogen bonds between the Val and Leu residues and $^{3}J_{\text{NH-C}\alpha\text{H}}$ values (8.6–9.5 Hz) for the Val, Orn, and Leu residues indicative of a β-sheet conformation. In contrast, the temperature coefficient ($\Delta\delta/\Delta T$) and the $^{3}J_{\text{NH-C}\alpha\text{H}}$ value of the D-3Pal containing analogs differed slightly from those of GS suggesting a slight distortion from the β-sheet conformer [79].

The CD spectra indicated similarly antiparallel β-sheet conformations for analogs **28**, except D-3Pal analog **28f**, which exhibited a negative maximum of much weaker intensity. The Δ^{Z}3Pal and Δ^{Z}Phe analogs **28a–c** and D-Tyr analog **28e** all had antibacterial activity comparable to GS against gram-positive *S. aureus*. Higher hemolytic activity than GS was exhibited by Δ^{Z}Phe analog **28a** relative to GS, but the other analogs showed reduced toxicity to red blood cells. The D-3Pal analog **28f** lost both antimicrobial and hemolytic activity, perhaps due to a loss of hydrophobic to hydrophilic residue balance as suggested by HPLC on which it was more polar than the other analogs. Replacement of one and both Orn residues by Ala gave Δ^{Z}3Pal analogs **28g** and **28h**, which exhibited reduced and no antibacterial activity, albeit they were much less hemolytic than GS and **28e** (Fig. 30) [80].

Net positive charge and amphiphilicity were suggested to control membrane selectivity for analogs **28**, with the hydrophilic pyridyl group in the β-turn region reducing interactions with red blood cells. The mechanism of antibacterial action was suggested to implicate membrane disruption with K^{+} ion efflux [81, 82].

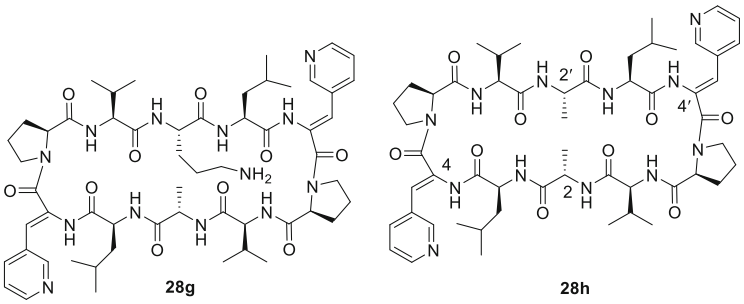

Fig. 30 Structures of **28g** and **28h**

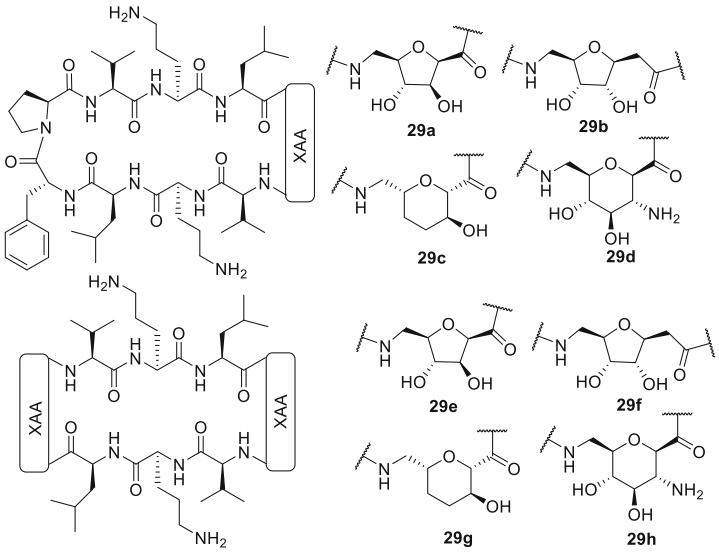

Fig. 31 Structures of **29a–h**

2.4 SAA-Based Analogs

The D-Phe-Pro sequence has also been replaced with sugar amino acids (SAAs) in GS analogs **29**, which were observed by NMR spectroscopy to maintain antiparallel β-sheet structure (Fig. 31) [83]. Lower antibacterial activity compared to GS was exhibited by SAA analogs **29**, with **29c** exhibiting the highest relative activity in the series, and disubstituted SAA analogs completely losing activity. Singly substituted SAA-GS analogs **29** exhibited hemolytic activity at around 500 μM, and disubstituted SAA analogs **29** were without toxicity against human red blood cells.

Fig. 32 Structure of **30**

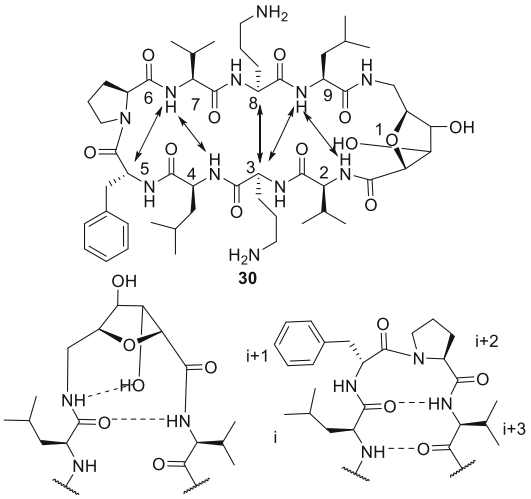

Furanoid SAA analog **30** was reported to adopt an unusual reverse turn structure with three hydrogen bonds between opposing Leu and Val residues (Fig. 32) [84]. Several short-range NOEs were observed between strands of **30**: between the amide NHs of Val^2 and Leu^9 and between Val^7 and Leu^4; amide NH and α-protons between Val^7 and D-Phe and between Leu^9 and Orn^3; and α-proton–α-proton NOEs between the Orn^3 and Orn^8 residues. Moreover, a strong NOE that was observed between the amide NHs of the SAA and Val^2 residues indicated a distortion from normal turn conformation. Crystallographic analysis of **30** indicated a β-pleated sheet structure with two hydrogen bonds shared between the Leu^4 and Val^7 residues and one between the amide NH of Leu^9 and carbonyl oxygen of Val^2 similar to those inside GS, but with a larger right-handed twist [85]. An unusual reverse turn structure positioned the SAA amide NH in close proximity to its C3 hydroxyl group. Chakraborty et al. had previously observed similar hydrogen bonds between amide NH and hydroxyl groups in furanoid SAA peptides in solution [86, 87]. The furanoid C_3-*endo* conformation was accounted for the close proximity of the hydroxyl function in the turn region [88]. In the crystal structure, molecular packing of six crystallographically equivalent molecules of **30** were observed with the hydrophilic Orn side-chain residues projected into the core and the hydrophobic Val, Leu, and D-Phe residues at periphery attributing to supramolecular amphiphilic character. The resulting hexameric β-barrel complex was stabilized by intermolecular hydrogen bonds between the SAA carbonyl and Orn^3 amide NH, as well as the Pro carbonyl and Orn^8 amide NH, respectively, corresponded to a twelve-stranded β-barrel of approximately 13 Å in length. Many pore-forming proteins, including cytolytic bacterial toxins such as perfringolysin O and α-hemolysin, adopt β-barrels to achieve their mode of action [89].

The D-Phe-Pro sequence of GS has also been replaced by furanoid SAAs having *O*-arylmethyl C_4-OH substituents in analogs **31** (Fig. 33) [90]. Consistent with the β-sheet structure exhibited by **30**, similar vicinal coupling constant ($^3J_{NH\text{-}C\alpha H}$) and

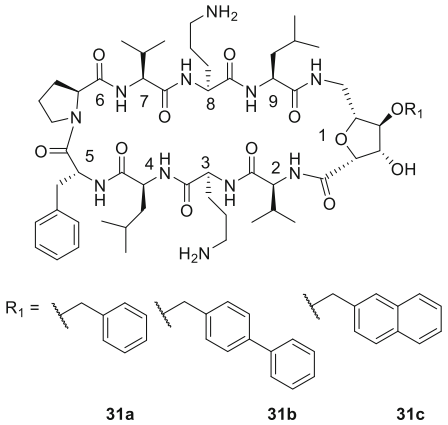

Fig. 33 Structures of **31a–c**

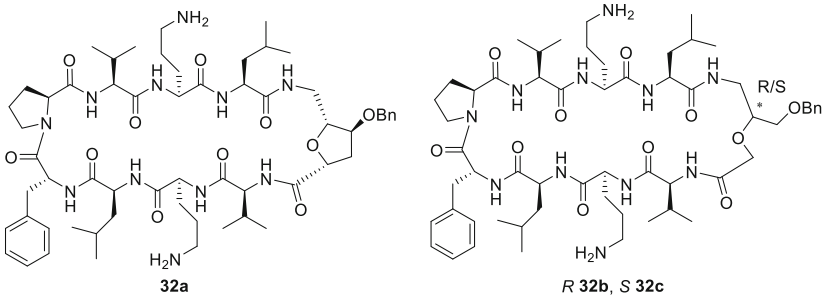

Fig. 34 Structures of **32a–c**

CαH chemical shift perturbations were observed for the corresponding arylmethyl ethers **31** [91]. In the case of benzyl ether **31a**, the preservation of NOEs between the amide NH protons of Val^7 and Leu^4, Val^2 and Leu^9, as well as SAA^1 and Leu^9 supported the β-sheet structure. Moreover, a characteristic NOE between the amide NH of the SAA^1 and Val^2 residues was discerned in support of a similar structure as **30**. Similar spectroscopic data was observed for the biphenylmethyl and naphthylmethyl analogs. X-ray analysis of naphthylmethyl ether **31c** confirmed β-sheet structure and found a pore-like assembly of 12 individual cyclic peptides in the molecular packing of the unit cell. Both the antibacterial and hemolytic activity of analogs **31** were comparable to GS.

Employing an alternative furanoid SAA and linear aminoethoxy acetic acid as dipeptide isosteres, GS analogs **32** were synthesized to explore further the relationship between the carbohydrate moiety and activity (Fig. 34) [92].

Both hydroxyl groups were deemed less important for conformational constraint of 3,4-dihydroxy SAA peptide **30**, because the NMR spectra of counterpart **32a** exhibited similar features including a low ($^3J_{\text{NH-C}\alpha\text{H}}$ <4 Hz) coupling constant for the D-Phe residue, negative chemical shift perturbations of the D-Phe and Pro

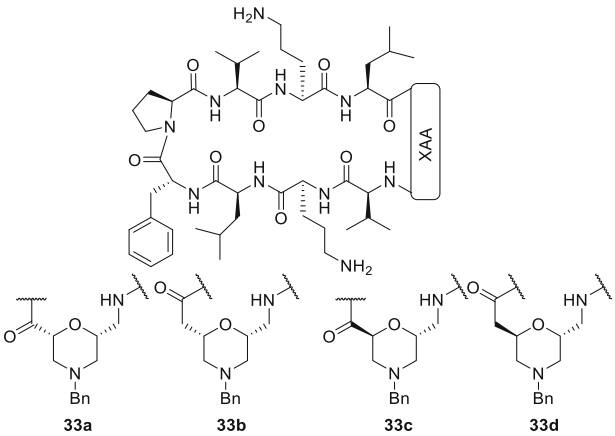

Fig. 35 Structures of **33a–d**

residues, as well as characteristic NOEs between amide NH protons of neighboring SAA, Val, and Leu residues indicative of an unusual reverse turn structure. On the other hand, conformational restriction by the SAA residue was deemed important, because more flexible analogs **32b** and **32c** lacked characteristic NOEs. Analogs **32** were generally inactive against gram-negative bacteria, such as *E. coli* and *P. aeruginosa*, but retained potency against gram-positive bacteria relative to GS. Analogs **32a** and **32b** had significant hemolytic activity, but *S*-aminoethoxy acetic acid analog **32c** exhibited 90% hemolysis at 500 μM concentration.

Morpholine amino acids (MAA) have also been substituted for the D-Phe-Pro sequence in analogs **33** (Fig. 35). Except for analog **33d** which appeared to exist in equilibrium between multiple conformations, the relatively large coupling constant $^3J_{\text{NH-C}\alpha\text{H}}$ values (8–12 Hz) for the Orn, Val, and Leu residues and small values (2–4 Hz) for the D-Phe residue indicated the β-hairpin structure. Relative to GS, analogs **33** had comparable activity against both gram-positive and gram-negative bacteria and weaker hemolytic activity [93].

Variations in ring size were examined in four-, five-, and six-membered SAA homologues **34** (Fig. 36), which all displayed β-hairpin structure with a similar pattern of high (7–9 Hz) and low (4 Hz) $^3J_{\text{NH-C}\alpha\text{H}}$ values and chemical shift perturbations as GS. Relative to GS, pyranoid **34c** showed comparable antibacterial activity that was better than the other analogs, and all had moderate hemolytic activity [94].

Chakraborty et al. had previously reported SAA-based C_2 symmetric 24-membered cyclic CAPs that were found to match the dumbbell shaped of the loloatin cyclopeptides better than the typical β-sheet structures of GS and tachyplesins [95]. Their promising biological activities inspired design and synthesis of new SAA peptides **35** (Fig. 37) in search of CAP-based drugs.

The order of antibacterial activity (lethal concentration against gram-positive and gram-negative bacteria) and corresponding hemolytic activity of analogs **35b** > **35c** > **35f** > **35e** >> **35a** > **35d** indicated that distance between the

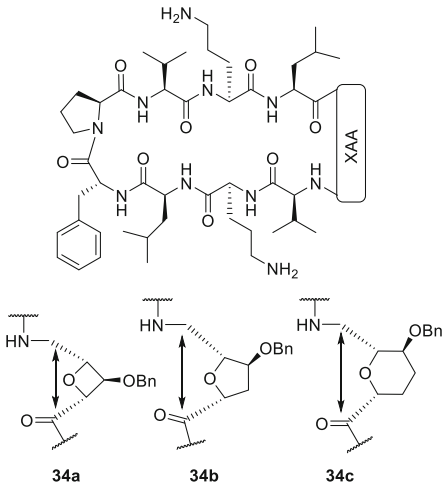

Fig. 36 Structures of **34a–c**

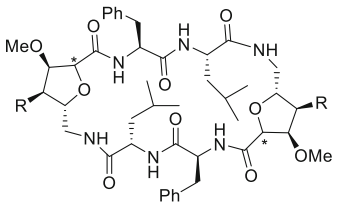

35a R = NH_3^+, * = *S*, **35d** R = NH_3^+, * = *R*
35b R = $NHCOCH_2CH_2NH_3^+$, * = *S*, **35e** R = $NHCOCH_2CH_2NH_3^+$, * = *R*
35c R = $NHCOCH(NH_3^+)(CH_2)_4NH_3^+$, * = *S*, **35f** R = $NHCOCH(NH_3^+)(CH_2)_4NH_3^+$, * = *R*

Fig. 37 Structures of **35a–f**

backbone and amine and a *trans*-relative stereochemistry for the furanoid rings enhanced activity.

Replacement of the D-Phe-Pro sequence with 4-amino(methyl)-1,3-thiazole-5-carboxylic acids as reverse turn mimics gave analog **36**, which had slightly lower antibacterial activity compared to GS, but sixfold decreased hemolytic activity (Fig. 38) [96].

Conformational analysis of **36** indicated the Val, Orn, and Leu residues aligned in a β-strand with relatively high $^3J_{NH\text{-}C\alpha H}$ coupling constants, and temperature coefficients for the amide protons of the Orn and γ-amino acid residues are comparatively higher than those of the Val and Leu residues, indicating their solvent-exposed and solvent-shielded natures. Furthermore, NOE between the Val and Leu residues and the CγH of the γ-amino acid and Val amide proton supported a distorted antiparallel β-sheet structure with the γ-amino acid acting as a reverse turn mimic.

Employing analogs of spirocyclic glucose-proline hybrids Glc3′(*S*)-5′(*R*)(CH_2OH)HypH and Glc3′(*S*)-5′(*S*)(CH_2OH)HypH inside tetrapeptide models **37**

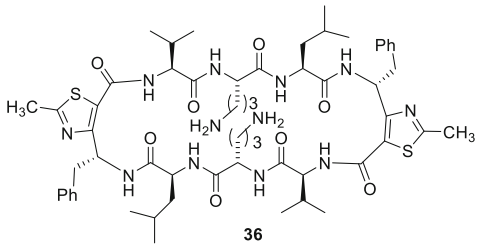

Fig. 38 Structure of **36**

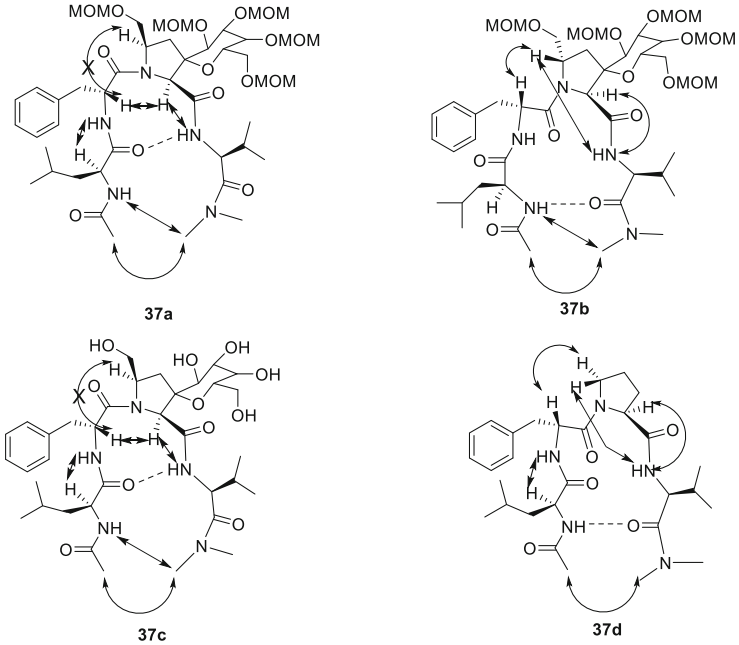

Fig. 39 Structures of **37a–d**

(Ac-Leu-D-Phe-Pro-Val-NMe_2) derived from GS, the 5*S* and 5*R* stereochemistries were shown to dictate turn conformation, which adopted, respectively, type II′ and type VI β-turn geometry (Fig. 39) [97].

Employing tetrahydrofuran amino acids (TAA) as surrogates of the D-Phe-Pro unit in GS analogs **38**, the Chakraborty laboratory explored their potential to differentiate antibacterial and hemolytic activity (Fig. 40) [98].

Examination of their ^{1}H NMR spectra in $CDCl_3$ (**38a–d**) and in DMSO-d_6 (**38e–h**) indicated preferred conformations similar to that of GS with NOEs between the Val amide NH and TAA C^5H and between the TAA C^6H and Leu amide NH. Amide proton temperature coefficients for the Val and Leu residues were lower than the Orn and TAA residues suggesting the former participated in the hydrogen bonds. Structural variation was observed at the turn region. Analogs **38e–**

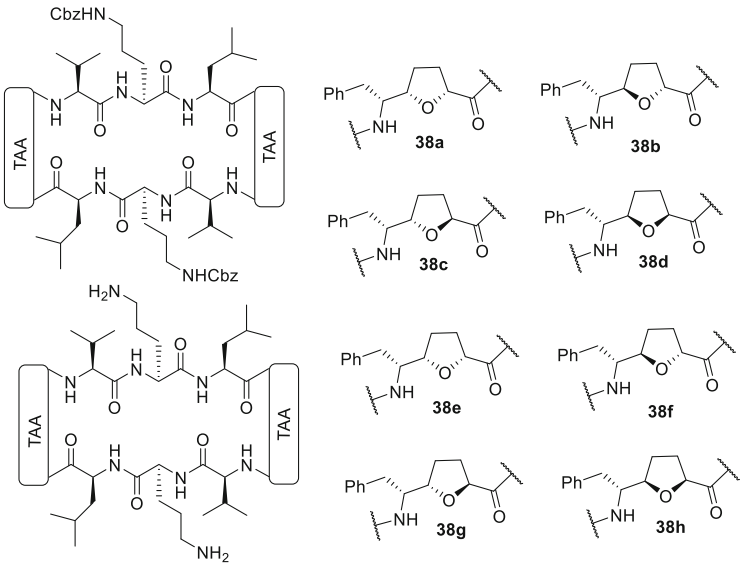

Fig. 40 Structures of **38a–h**

g were tested against two gram-positive (*S. aureus* and *B. subtilis*) and two gram-negative (*E. coli* and *P. aeruginosa*) bacteria. The most active analog **38e** exhibited comparable activity to GS but nearly fivefold lower hemolytic activity. The other analogs were less active but nontoxic. Analogs **38g** and **38h** were active against *M. tuberculosis* (MICs = 6.25 μM) with lower hemolytic activity than GS. Their potency against *M. tuberculosis*, without hemolytic activity and toxicity against Vero cells, make analogs **38g** and **38h** promising candidates for future study.

3 GS Dimers and Polymers

A series of GS-dimers **39** were synthesized by, respectively, substituting the D-Phe and Pro residues with D-Glu and 4-aminoproline and linking the two macrocycle peptides by a succinamide cross-link and by side chain to side-chain amide bonds to join the inserted residues (Fig. 41).

GS-dimers were generally without antibacterial activity, except dimer **39e**, which had limited activity against gram-positive bacteria, such as *S. epidermidis*. The dimers displayed, however, significant increase in hemolytic activity relative to GS. In conductance-increasing studies, succinyl-tethered **39a** and amide **39f** exhibited membrane-disruptive properties but were not observed to form discrete channels [99].

Polymerization of methacrylate GS **40** occurred in a controlled manner without loss of β-sheet character (Fig. 42) [100]. The biological activity of this polymeric substrate was not reported.

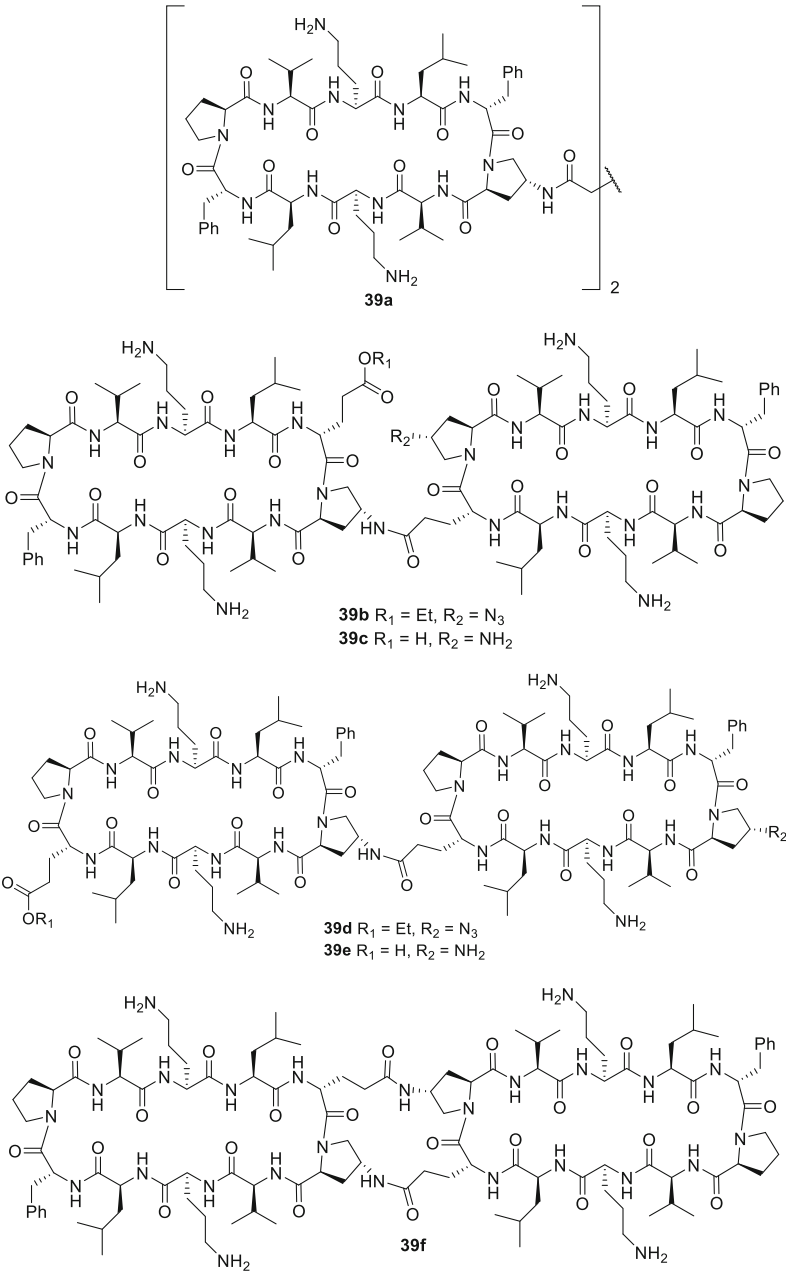

Fig. 41 Structures of **39a–f**

Fig. 42 Structure of **40**

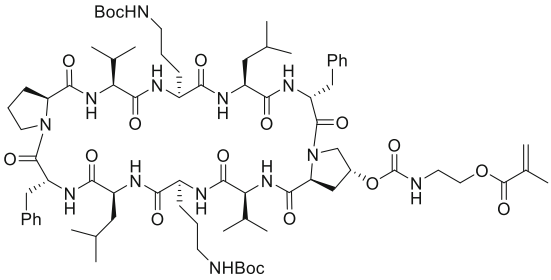

Fig. 43 Structures of **41a–c**

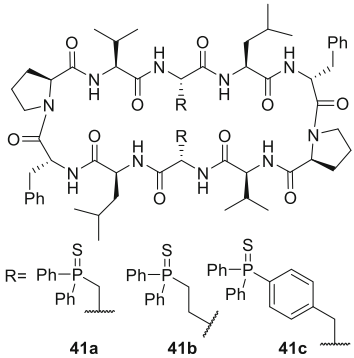

4 GS as Catalyst

Bisphosphine-functionalized GS analogs **41** and **42** were designed and used to coordinate transition metals (Figs. 43 and 44) [101].

Poor solubility of **41a** necessitated elevated temperatures to obtain the NMR spectra, which indicated a close arrangement of the $CH_2P(S)Ph_2$ groups in a characteristic β-hairpin structures. X-ray crystallographic analyses found, respectively, less and more twisted conformation for **41b** and **41c** than GS.

Phosphine GS analogs **42** (Fig. 44) were employed as ligands in Rh-catalyzed asymmetric hydrogenation and Pd-catalyzed allylic substitution giving, respectively, products with up to 52 % and 15 % enantiomeric excess (ee) [102]. Metal coordination was confirmed by ^{31}P NMR spectroscopy and MALDI-TOF mass spectrometry. Structure-activity relationships of various GS analogs [103] suggested that the amphiphilic β-sheet and β-turn structure was required for catalytic activity of GS analogs.

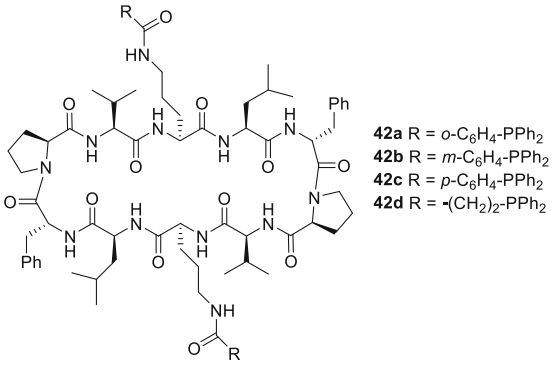

Fig. 44 Structures of **42a–d**

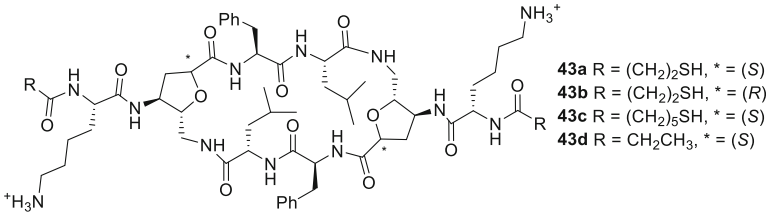

Fig. 45 Structures of **43a–d**

5 Synergistic Effect

Employment of GS with $AgNO_3$ as well as silver nanoparticles identified synergistic effects against bacteria with reduced hemolytic activity [104]. Cyclic cationic SAA peptides **43** (Fig. 45) and their gold nanoparticle complexes exhibited similar antimicrobial activities with lower hemolytic activity for the latter [105].

The *cis*-SAA analog **43b** was more effective than the *trans*-counterparts. The thiol was necessary for coordination to gold (**43d** did not attach to gold), gave broader spectrum antimicrobial activity, and reduced hemolytic activity, which was in some cases abolished at the observed MICs. Initial studies of the mechanism of action of **43** with transmission electron microscopy suggested that bacterial death may be due to cell membrane perforation.

6 Conclusions

Owing to its wide-ranging activities against both gram-positive and gram-negative bacteria, gramicidin S has been an attractive lead compound for antibiotic development for several decades. In spite of potent bactericidal properties, a similar

molecular mode of action against erythrocytes has limited application of GS. Efforts to understand the mechanism by which GS disrupts the integrity of cell membrane lipid bilayers to cause cell lysis have been pursued using various analytical techniques as well as the synthesis and structure-activity analysis of a wide spectrum of analogs with the ultimate goal of developing GS antibiotics that selectively target bacteria. With greater understanding of the interactions of these molecules, light is beginning to be shed on how to differentiate activity against bacterial and human cell membranes. Further study is, however, still needed to rationally design selective molecules that would kill only bacteria without hemolytic activity.

References

1. Lewis K (2013) Nat Rev Drug Discov 12:371
2. Walsh CT, Wencewicz TA (2014) J Antibiot 67:7
3. Fox JL (2013) Nat Biotechnol 31:379
4. Fjell CD, Hiss JA, Hancock REW, Schneider G (2012) Nat Rev Drug Discov 11:37
5. Karstad R, Isaksen G, Brandsdal B-O, Svendsen JS, Svenson J (2010) J Med Chem 53:5558
6. O'Connell KMG, Hodgkinson JT, Sore HF, Welch M, Salmond GPC, Spring DR (2013) Angew Chem Int Ed 52:10706
7. Herzog IM, Green KD, Berkov-Zrihen Y, Feldman M, Vidavski RR, Eldar-Boock A, Satchi-Fainaro R, Eldar A, Garneau-Tsodikova S, Fridman M (2012) Angew Chem Int Ed 51:5652
8. Mogi T, Kita K (2009) Cell Mol Life Sci 66:3821
9. Falagas ME, Kasiakou SK (2005) Clin Infect Dis 40:1333
10. Moual HL, Thomassin J-L, Brannon JR (2013) J Clin Cell Immunol S13:4
11. Gause GF, Brazhnikova MG (1944) Nature 154:703
12. Krivanek R, Rybar P, Prenner EJ, McElhaney RN, Hianik T (2001) Biochim Biophys Acta Biomembranes 1510:452
13. Dergunov AD, Kaprel'yants AS, Ostrovskii DN (1981) Biokhim 46:1499
14. Prenner EJ, Lewis RNAH, McElhaney RN (1999) Biochim Biophys Acta Biomembranes 1462:201
15. Hartmann M, Berditsch M, Hawecker J, Ardakani MF, Gerthsen D, Ulrich AS (2010) Antimicrob Agents Chemother 54:3132
16. Kondejewski LH, Farmer SW, Wishart DS, Hancock RE, Hodges RS (1996) Int J Pept Protein Res 47:460
17. Schmidt GMJ, Hodgkin DC, Oughton BM (1957) Biochem J 65:744
18. Routolo BT, Tate CC, Russell DH (2004) J Am Soc Mass Spectrom 15:870
19. Nagornova NS, Rizzo TR, Boyarkin OV (2010) J Am Chem Soc 132:4040
20. Joshi K, Semrouni D, Ohanessian G, Clavaguéra C (2012) J Phys Chem B 116:483
21. Mihailescu D, Smith JC (2000) Biophys J 79:1718
22. Staudegger E, Prenner EJ, Kriechbaum M, Degovics G, Lewis RNAH, McElhaney RN, Lohner K (2000) Biochim Biophys Acta Biomembranes 1468:213
23. Prenner EJ, Lewis RNAH, Jelokhani-Niaraki M, Hodges RS, McElhaney RN (2001) Biochim Biophys Acta Biomembranes 1510:83
24. Prenner EJ, Lewis RNAH, Kondejewski LH, Hodges RS, McElhaney RN (1999) Biochim Biophys Acta Biomembranes 1417:211
25. Lewis RNAH, Prenner EJ, Kondejewski LH, Flach CR, Mendelsohn R, Hodges RS, McElhaney RN (1999) Biochemistry 38:15193

26. Prenner EJ, Lewis RNAH, Neuman KC, Gruner SM, Kondejewski LH, Hodges RS, McElhaney RN (1997) Biochemistry 36:7906
27. Ando S, Nishikawa H, Takiguchi H, Lee S, Sugihara G (1993) Biochim Biophys Acta Biomembranes 1147:42
28. Kondejewski LH, Farmer SW, Wishart DS, Kay CM, Hancock REW, Hodges RS (1996) J Biol Chem 271:25261
29. Semrau S, Monster MWL, van der Knaap M, Florea BI, Schmidt T, Overhand M (2010) Biochim Biophys Acta Biomembranes 1798:2033
30. Hackl EV, Berest VP, Gatash SV (2012) J Pept Sci 18:748
31. Mogi T, Ui H, Shiomi K, Ōmura S, Kita K (2008) FEBS Lett 582:2299
32. Yano T, Li L-S, Weinstein E, Teh J-S, Rubin H (2006) J Biol Chem 281:11456
33. Kasamo K (1982) Plant Cell Physiol 23:195
34. Zhao D, Dhalla NS (1989) Can J Physiol Pharmacol 67:546
35. Iglesias RO, Rega AF (1987) Biochim Biophys Acta Biomembranes 905:383
36. Luo J, Otero JM, Yu C-H, Wärmländer SKTS, Gräslund A, Overhand M, Abrahams JP (2013) Chem Eur J 19:17338
37. Zhang L, Parente J, Harris SM, Woods DE, Hancock REW, Falla TJ (2005) Antimicrob Agents Chemother 49:2921
38. Shemyakin MM, Ovchinnikov YA, Ivanov VT, Ryabova ID (1967) Experientia 23:326
39. Prenner EJ, Kiricsi M, Jelokhani-Niaraki M, Lewis RNAH, Hodges RS, McElhaney RN (2005) J Biol Chem 280:2002
40. Abraham T, Lewis RNAH, Hodges RS, McElhaney RN (2005) Biochemistry 44:11279
41. Abraham T, Lewis RNAH, Hodges RS, McElhaney RN (2005) Biochemistry 44:2103
42. Lewis RNAH, Kiricsi M, Prenner EJ, Hodges RS, McElhaney RN (2003) Biochemistry 42:440
43. Jelokhani-Niaraki M, Prenner EJ, Kondejewski LH, Kay CM, McElhaney RN, Hodges RS (2001) J Pept Res 58:293
44. Abraham T, Marwaha S, Kobewka DM, Lewis RNAH, Prenner EJ, Hodges RS, McElhaney RN (2007) Biochim Biophys Acta Biomembranes 1768:2089
45. Ashrafuzzaman M, Andersen OS, McElhaney RN (2008) Biochim Biophys Acta Biomembranes 1778:2814
46. Abraham T, Prenner EJ, Lewis RNAH, Mant CT, Keller S, Hodges RS, McElhaney RN (2014) Biochim Biophys Acta Biomembranes 1838:1420
47. Kondejewski LH, Jelokhani-Niaraki M, Farmer SW, Lix B, Kay CM, Sykes BD, Hancock REW, Hodges RS (1999) Biochem J 274:13181
48. Kiricsi M, Prenner EJ, Jelokhani-Niaraki M, Lewis RNAH, Hodges RS, McElhaney RN (2002) Eur J Biochem 269:5911
49. Jelokhani-Niaraki M, Kondejewski LH, Wheaton LC, Hodges RS (2009) J Med Chem 52:2090
50. Knijnenburg AD, Kapoerchan VV, Spalburg E, de Neeling AJ, Mars-Groenendijk RH, Noort D, van der Marel GA, Overkleeft HS, Overhand M (2010) Bioorg Med Chem 18:8403
51. Knijnenburg AD, Spalburg E, de Neeling AJ, Mars-Groenendijk RH, Noort D, Grotenbreg GM, van der Marel GA, Overkleeft HS, Overhand M (2009) ChemMedChem 4:1976
52. Knijnenburg AD, Kapoerchan VV, Grotenbreg GM, Spalburg E, de Neeling AJ, Mars-Groenendijk RH, Noort D, Otero JM, Llamas-Saiz AL, van Raaij MJ, Ravensbergen B, Nibbering PH, van der Marel GA, Overkleeft HS, Overhand M (2011) Bioorg Med Chem 19:3402
53. Tamaki M, Sasaki I, Kokuno M, Shindo M, Kimura M, Uchida Y (2010) Org Biomol Chem 8:1791
54. van der Knaap M, Basalan F, van de Mei HC, Busscher HJ, van der Marel GA, Overkleeft HS, Overhand M (2012) Chem Biodivers 9:2494
55. Seebach D, Beck AK, Bierbaum DJ (2004) Chem Biodivers 1:1111

56. Yamada K, Unno M, Kobayashi K, Oku H, Yamamura H, Araki S, Matsumoto H, Katakai R, Kawai M (2002) J Am Chem Soc 124:12684
57. Li Y, Bionda N, Yongye A, Geer P, Stawikowski M, Cudic P, Martinez K, Houghten RA (2013) ChemMedChem 8:1865
58. Bu X, Wu X, Ng NLJ, Mak CK, Qin C, Guo Z (2004) J Org Chem 69:2681
59. Wu X, Bu X, Wong KM, Yan W, Guo Z (2003) Org Lett 5:1749
60. Solanas C, de la Torre BG, Fernández-Reyes M, Santiveri CM, Jiménez MÁ, Rivas L, Jiménez AI, Andreu D, Cativiela C (2009) J Med Chem 52:664
61. Solanas C, dela Torre BG, Fernández-Reyes M, Santiveri CM, Jiménez MÁ, Rivas L, Jiménez AI, Andreu D, Cativiela C (2010) J Med Chem 53:4119
62. Wadhwani P, Afonin S, Ieronimo M, Buerck J, Ulrich AS (2006) J Org Chem 71:55
63. Ulrich AS, Wadhwani P, Dürr UHN, Afonin S, Glaser RW, Strandberg E, Sachse C, Tremouilhac P, Berditchevskaia M, Grage SL (2006) In: Ramamoorthy A (ed) NMR spectroscopy of biological solids. CRC, Boca Raton, pp 215–236
64. Salgado J, Grage SL, Kondejewski LH, Hodges RS, McElhaney RN, Ulrich AS (2001) J Biomol NMR 21:191
65. van der Knaap M, Lageveen LT, Busscher HJ, Mars-Groenendijk R, Noort D, Otero JM, Llamas-Saiz AL, van Raaij MJ, van der Marel GA, Overkleeft HS, Overhand M (2011) ChemMedChem 6:840
66. Derbal S, Hensler M, Fang W, Nizet V, Ghedira K, Nefzi A (2010) Bioorg Med Chem Lett 20:5701
67. Niidome T, Murakami H, Kawazoe M, Hatakeyama T, Kobashigawa Y, Matsushita M, Kumaki Y, Demura M, Nitta K, Aoyagi H (2001) Bioorg Med Chem Lett 11:1893
68. Tamaki M, Ishii R, Kikuchi S, Watanabe E (2005) J Antibiot 58:293
69. Grotenbreg GM, Spalburg E, de Neeling AJ, van der Marel GA, Overkleeft HS, van Boom JH, Overhand M (2003) Bioorg Med Chem 11:2835
70. van der Knaap M, Engels E, Busscher HJ, Otero JM, Llamas-Saiz AL, van Raaij MJ, Mars-Groenendijk RH, Noort D, van der Marel GA, Overkleeft HS, Overhand M (2009) Bioorg Med Chem 17:6318
71. Tamaki M, Fujinuma K, Harada T, Takanashi K, Shindo M, Kimura M, Uchida Y (2011) J Antibiot 64:583
72. Tamaki M, Fujinuma K, Harada T, Takanashi K, Shindo M, Kimura M, Uchida Y (2012) Bioorg Med Chem Lett 22:106
73. Ono S, Lee S, Kodera Y, Aoyagi H, Waki M, Kato T, Izumiya N (1987) FEBS Lett 220:332
74. Kapoerchan VV, Knijnenburg AD, Niamat M, Spalburg E, de Neeling AJ, Nibbering PH, Mars-Groenendijk RH, Noort D, Otero JM, Llamas-Saiz AL, van Raaij MJ, van der Marel GA, Overkleeft HS, Overhand M (2010) Chem Eur J 16:12174
75. Kapoerchan VV, Knijnenburg AD, Keizer P, Spalburg E, de Neeling AJ, Mars-Groenendijk RH, Noort D, Otero JM, Llamas-Saiz AL, van Raaij MJ, van der Marel GA, Overkleeft HS, Overhand M (2012) Bioorg Med Chem 20:6059
76. Xiao J, Weisblum B, Wipf P (2006) Org Lett 8:4731
77. Xiao J, Weisblum B, Wipf P (2005) J Am Chem Soc 127:5742
78. Ando S, Aoyagi H, Shinagawa S, Nishino N, Waki M, Kato T, Izumiya N (1983) FEBS Lett 161:89
79. Yamada K, Shinoda S-S, Oku H, Komagoe K, Katsu T, Katakai R (2006) J Med Chem 49:7592
80. Yamada K, Kodaira M, Shinoda S-S, Komagoe K, Oku H, Katakai R, Katsu T, Matsuo I (2011) MedChemComm 2:644
81. Katsu T, Kobayashi H, Fujita Y (1986) Biochim Biophys Acta Biomembranes 860:608
82. Katsu T, Kuroko M, Morikawa T, Sanchika K, Fujita Y, Yamamura H, Uda M (1989) Biochim Biophys Acta Biomembranes 983:135

83. Grotenbreg GM, Kronemeijer M, Timmer MSM, Oualid FE, van Well RM, Verdoes M, Spalburg E, van Hooft PAV, de Neeling AJ, Noort D, van Boom JH, van der Marel GA, Overkleeft HS, Overhand M (2004) J Org Chem 69:7851
84. Grotenbreg GM, Timmer MSM, Llamas-Saiz AL, Verdoes M, van der Marel GA, van Raaij MJ, Overkleeft HS, Overhand M (2004) J Am Chem Soc 126:3444
85. Wang L, O'Connell T, Tropsha A, Hermans J (1996) J Mol Biol 262:283
86. Chakraborty TK, Jayaprakash S, Diwan PV, Nagaraj R, Jampani SRB, Kunwar AC (1998) J Am Chem Soc 120:12962
87. Chakraborty TK, Ghosh S, Jayaprakash S, Sharma JARP, Ravikanth V, Diwan PV, Nagaraj R, Kunwar AC (2000) J Org Chem 65:6441
88. Altona C, Sundaralingam M (1972) J Am Chem Soc 94:8205
89. Montoya M, Gouaux E (2003) Biochim Biophys Acta Biomembranes 1609:19
90. Grotenbreg GM, Buizert AEM, Llamas-Saiz AL, Spalburg E, van Hooft PAV, de Neeling AJ, Noort D, van Raaij MJ, van der Marel GA, Overkleeft HS, Overhand M (2006) J Am Chem Soc 128:7559
91. Wüthrich K (1986) NMR of proteins and nucleic acids. Wiley, New York
92. Tuin AW, Palachanis DK, Buizert A, Grotenbreg GM, Spalburg E, de Neeling AJ, Mars-Groenendijk RH, Noort D, van der Marel GA, Overkleeft HS, Overhand M (2009) Eur J Org Chem 4231
93. Kapoerchan VV, Spalburg E, de Neeling AJ, Mars-Groenendijk RH, Noort D, Otero JM, Ferraces-Casais P, Llamas-Saiz AL, van Raaij MJ, van Doorn J, van der Marel GA, Overkleeft HS, Overhand M (2010) Chem Eur J 16:4259
94. Knijnenburg AD, Tuin AW, Spalburg E, de Neeling AJ, Mars-Groenendijk RH, Noort D, Otero JM, Llamas-Saiz AL, van Raaij MJ, van der Marel GA, Overkleeft HS, Overhand M (2011) Chem Eur J 17:3995
95. Chakraborty TK, Koley D, Ravi R, Krishnakumari V, Nagaraj R, Kunwar AC (2008) J Org Chem 73:8731
96. Legrand B, Mathieu L, Lebrun A, Andriamanarivo S, Lisowski V, Masurier N, Zirah S, Kang YK, Martinez J, Maillard LT (2014) Chem Eur J 20:6713
97. Zhang K, Schweizer F (2010) Carbohydr Res 345:1114
98. Pal S, Singh G, Singh S, Tripathi JK, Ghosh JK, Sinha S, Ampapathi RS, Chakraborty TK (2015) Org Biomol Chem 13:6789
99. Grotenbreg GM, Witte MD, van Hooft PAV, Spalburg E, Reiß P, Noort D, de Neeling AJ, Koert U, van der Marel GA, Overkleeft HS, Overhand M (2005) Org Biomol Chem 3:233
100. Ayres L, Grotenbreg GM, van der Marel GA, Overkleeft HS, Overhand M, van Hest JCM (2005) Macromol Rapid Commun 26:1336
101. Burck S, van Assema SGA, Lastdrager B, Slootweg JC, Ehlers AW, Otero JM, Dacunha-Marinho B, Llamas-Saiz AL, Overhand M, van Raaij MJ, Lammertsma K (2009) Chem Eur J 15:8134
102. Guisado-Barrios G, Muñoz BK, Kamer PCJ, Lastdrager B, van der Marel G, Overhand M, Vega-Vázquez M, Martin-Pastor M (2013) Dalton Trans 42:1973
103. Izumiya N, Kato T, Aoyagi H, Waki M, Kondo M. Synthetic aspects of biologically active cyclic peptides – gramicidin S, tyrocidines. Kodansha/Wiley, Tokyo/New York
104. Ruden S, Hilpert K, Berditsch M, Wadhwani P, Ulrich AS (2009) Antimicrob Agents Chemother 53:3538
105. Pal S, Mitra K, Azmi S, Ghosh JK, Chakraborty TK (2011) Org Biomol Chem 9:4806

Top Heterocycl Chem (2017) 49: 203–234
DOI: 10.1007/7081_2016_202

Published online: 29 March 2016

Anti-amyloidogenic Heterocyclic Peptides

Marina Chemerovski-Glikman, Michal Richman, and Shai Rahimipour

Abstract The amyloid fibril is a highly ordered proteinous aggregate, originally discovered in the context of the self-assembly of soluble proteins into insoluble extracellular plaques. The molecular structure of amyloidosis, an energetically stable conformation with a thermodynamic local minimum, is of particular interest because of its possible pathogenicity. Amyloidogenic diseases (amyloidoses) are often fatal, widely heterogenic, and caused by sporadic, genetic, or infectious pathogens. Consequently, major effort has been directed in the past few decades to identify and develop agents that decrease the concentration of the pathogenic aggregates either by interfering with the self-assembly of the proteins or by modulating their physiological concentration. Heterocyclic peptides of natural and synthetic origin have gained special attention because of their demonstrated ability to interact with various amyloids. In addition to interfering with the amyloid aggregation process, many of the discovered peptides also inhibit the formation of fibrils, disassemble preformed fibrils, and prevent the pathogenic seeding effect. Others are instrumental candidates for passive vaccination against amyloid deposits. The promising preliminary results described here, together with the broad chemical diversity of heterocyclic peptides and their amenability to large-scale production, make these compounds promising for anti-amyloidogenic research and for pharmacological therapy of amyloidoses.

Keywords Alzheimer's disease • Amyloidosis • Cyclic D,L-α-peptides • Heterocyclic peptides

M. Chemerovski-Glikman, M. Richman, and S. Rahimipour (✉)
Department of Chemistry, Bar-Ilan University, Ramat-Gan 5290002, Israel
e-mail: rahimis@biu.ac.il

Contents

1 Introduction

The term "amyloid" was first used in 1854 by the German physician Rudolph Virchow, who considered initially the amyloidogenic material to be starch ("amylum," in Latin), based on crude iodine-staining techniques. Later, the presence of protein and the absence of carbohydrate in the aggregates shifted the scientific view toward considering amyloids to be a class of protein (reviewed in [1, 2]).

Amyloids were traditionally defined as formerly soluble proteins that had accumulated in the extracellular space of various tissues as insoluble deposits comprised of 10 nm-wide fibrils that were rich in β-sheet structures and that possessed characteristic dye-binding properties [3]. However, the modern biophysical definition is broader and includes any polypeptide that self-assembles to form a cross-β X-ray fiber diffraction pattern, in vivo or in vitro, in which the β-strands are spaced 4.8 Å apart and run parallel to the ~10 Å-thick fibril axis (reviewed in [4]).

This definition is supported by the observation that even "ordinary" globular proteins, such as muscle myoglobin [5] and others [6], are capable of forming amyloidogenic deposits under native conditions (reviewed in [7]) and that protein accumulation can also occur intracellularly, as happens in Parkinson's disease (PD).

Eisenberg et al. were the first to reveal the atomic structure of the molecular organization of the cross-β spine shared by all amyloids [8]. They selected the prion-like infective yeast protein Sup35 and isolated its seven-residue fragment, GNNQQNY, which displays all the common characteristics of amyloid fibrils. Using X-ray micro-crystallography, the researchers confirmed the cross-β spine characteristics established by other methods. Importantly, they coined the term "steric zipper" to describe the result of the hydrogen bonding that occurs between the self-complementing side chains protruding from each of the paired β sheets (Fig. 1). This steric zipper, together with backbone–backbone hydrogen-bonding interactions, binds every segment within each β sheet to its two neighboring segments and thereby holds the sheets together. In contrast to the dry internal interface of the steric zipper, the external interface of the paired sheets was found

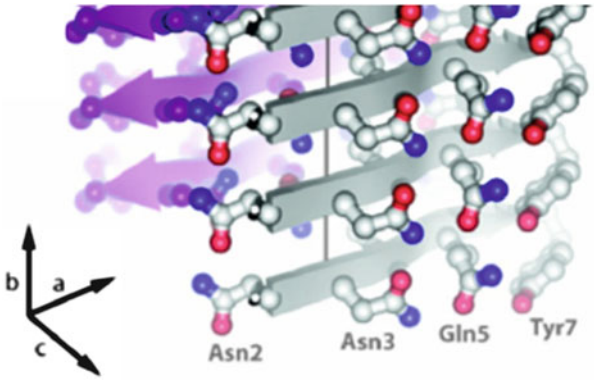

Fig. 1 The "steric zipper." The cross-β spine structure of the fibril-forming peptide GNNQQNY, showing the backbone of each β-strand as an *arrow*, with ball and stick side chains protruding. The interfaces between sheets are dry, whereas the external interfaces are hydrated. Carbon atoms are colored in *purple* or *gray*. The hydrogen bonds lie parallel to amyloid fibril axis b. Adapted from [8]

to be highly hydrated [8]. This and other studies presented the amyloidogenic fibril as a generic structure that is determined by nonspecific hydrogen, hydrophobic, and aromatic bonds, rather than by specific interactions between residue constituents [9, 10].

Although the ability to form amyloid fibrils seems to be a generic feature of polypeptide chains regardless of their sequence, and not necessarily associated with any disease, amyloids are still best known for their biochemical and biophysical correlations with a large number of heterogeneous disorders [11, 12], collectively called "protein deposition diseases." Only correctly folded proteins are able to maintain stability in the crowded cellular environment and to selectively interact with their natural ligands. Not surprising, failure to fold correctly can lead to complex pathological outcomes.

More than 40 different human pathologies involve the accumulation of a specific peptide or protein as a misfolded, thermodynamically highly stable fibrillar plaque. Among the different molecular pathways that may lead to this final outcome are various aging processes, high protein concentration in serum or tissue, mutations in the original protein sequence, and faulty remodeling of precursor proteins [13]. Despite their wide range of epidemiology and clinical symptoms, the amyloidosis can be divided among three types, based on their organ distribution (reviewed in [13] and [14]):

- *Non-neuropathic systemic amyloidosis* is generally characterized by large amounts of amyloid deposits in the extracellular spaces of multiple organs, including the spleen, kidneys, and liver. The systemic amyloidosis usually breaks out upon the worsening of other pathological conditions that elevate the concentration of an aggregation-prone protein, as happens for serum amyloid A (SAA) protein that accumulates as an amyloid during the acute-phase response

to inflammatory disorders, such as rheumatoid arthritis. Another reason for some systemic amyloidosis is the failure to clear an amyloid-prone protein (such as β_2-microglobulin in hemodialysis-related amyloidosis), which increases its concentration.

- *Organ-limited localized amyloidosis* is characterized by a fibrillogenic accumulation of a protein adjacent to its site of cellular production, mostly in the extracellular space in one organ. In type II diabetes mellitus, for example, amylin hormone deposits are formed in the spleen, while cataract-induced vision loss is derived from a pathological process of protein aggregation and formation of amyloid assemblies on the lens [15].
- *Neurodegenerative disorders* are usually classified separately, because the aggregates are formed in small quantities in the central nervous systems in most of these conditions. These disorders include Alzheimer's, Parkinson's, and prion diseases that are associated with the deposition of tau and amyloid beta (Aβ), alpha-synuclein (α-syn), and the prion protein (PrP), respectively.

The combined process of protein self-assembly and amyloid formation exhibits a typical nucleation-elongation profile (Fig. 2A). Nucleation occurs during a lag phase via the initial assembly of monomers into soluble oligomers and their subsequent growth into high molecular weight prefibrillar aggregates (Fig. 2B). When a critical nucleus is formed, the oligomers further elongate into fibrils at an exponential rate through monomer addition. Upon reaching an equilibrium that is dramatically shifted toward fibril formation, the process slows down and reaches a plateau [19] (Fig. 2). Although all the initial interactions occurring during amyloid self-assembly are non-covalent and hence reversible, the process is strongly shifted toward the thermodynamically most favored and stable fibril structure [13].

The *amyloid cascade hypothesis*, proposed in 1991 by John Hardy and David Allsop, suggests that the mature fibrillar deposits produced during the final stage of Aβ oligomerization underlie the pathologies of Alzheimer's disease (AD) [20, 21]. Nevertheless, increasing evidence has led to a new consensus that the toxic species are the early oligomeric assemblies formed during the lag or fast logarithmic polymerization phases, which precede considerably the formation of the mature fibril state [13, 22–25]. Despite the yet unknown structure of these soluble oligomers, their toxicity is believed to arise from their interaction with lipids and cellular membrane receptors and the consequent disruption of cell homeostasis [13, 26, 27]. Lately, a causative connection was established between the structure of the oligomers of an amyloid model protein, namely, the *N*-terminal domain of the prokaryotic hydrogenase maturation factor (HypF-N), and its toxicity [28]. In this study, the authors suggested that the primary determinants of the ability of oligomeric species to cause cell toxicity were their structural flexibility and relatively few hydrophobic inter-protein interactions, the latter of which correlated with an improved ability of the oligomeric assemblies to penetrate the cell membrane [28]. This finding supports the proposition that hydrophobic misfolded proteins induce the most significant membrane damage by forming ion channels (reviewed in [29]). Other factors promoting toxicity and tissue damage include

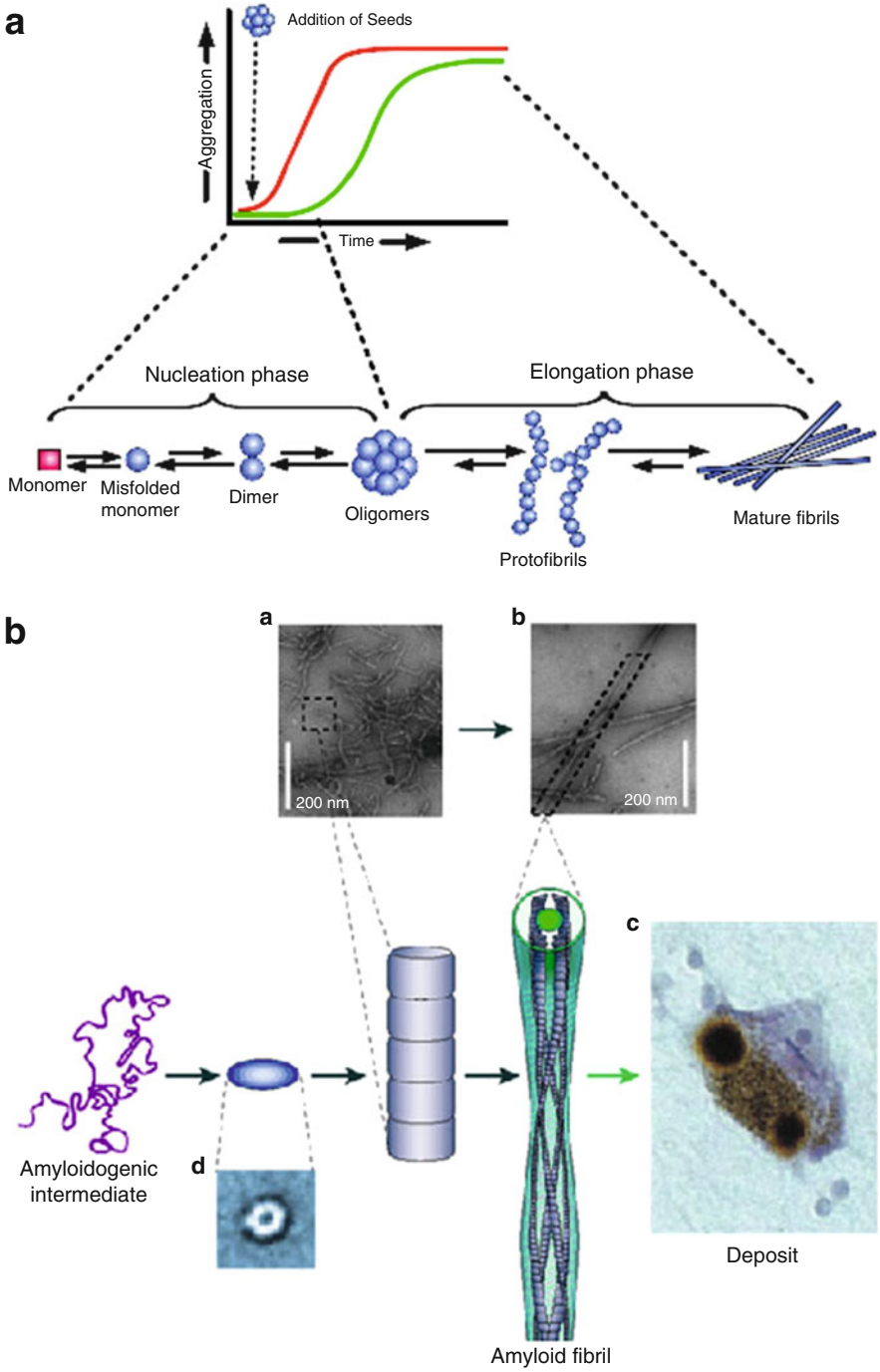

Fig. 2 The mechanism of amyloid aggregation. (**A**) A schematic representation of amyloid aggregation kinetics (Adapted from [16]). (**B**) The general mechanism of aggregation of amyloidogenic proteins to form amyloid fibrils. TEM images of (*a*) amyloid protofibrils and (*b*)

physical damage to tissue architecture due to large quantities of amyloid deposits, the inflammatory response promoted by the soluble toxic aggregates, oxidative stress, and activation of apoptotic pathways [13].

Despite the consensus that deposited amyloidogenic fibrils are nontoxic by themselves, a new approach focuses on their contribution to the pool of toxic oligomers. In their study, Cohen et al. [30] suggested that deposited fibrils of Aβ42 may promote the nucleation of toxic protofibrils from their monomers [30]. Dissociation of the deposited fibrils into fragments may also promote a local increase in the concentration of toxic intermediates which alter neuronal metabolism [31].

In light of the observed similarities between different amyloidogenic pathologies, the associated conditions have been considered as conformational diseases, raising the possibility that they might even be transmissible in the same manner as prion disease [32–36]. Unfortunately, due to the complexity of these disorders and the lack of robust available biomarkers, the diagnosis of different amyloidogenic diseases relies on clinical symptoms, which are believed to appear long after the initial molecular events. All of these factors, together with a lack of efficient therapies, make amyloidosis a major cause of morbidity and mortality.

Contemporary therapy addresses only the symptoms of amyloidogenic diseases. Intensive research is however focused on developing new diagnostic and pharmacologic interventions. Promising strategies for the therapy of amyloidogenic diseases include promoting amyloid resorption or otherwise reducing the concentration of the precursor proteins to reduce the amyloidogenic protein level below a critical threshold concentration, reducing the expression of the corresponding genes, and stabilizing the native protein structure with specific structure-based ligands. Other encouraging approaches include inhibiting the formation and remodeling nuclei and seeds into incompetent structures, removing metal ions that are vital for amyloid formation using chelating agents, antioxidative and free radical suppressive approaches, and immunization against amyloidogenic proteins [13, 37].

This chapter focuses mainly on heterocyclic peptides as potential anti-amyloidogenic agents. These compounds represent the most promising leads in each of the general anti-amyloidogenic approaches listed above.

Fig. 2 (continued) mature fibrils (Images are from [17]). (*c*) Optical microscopy of Lewy body plaques. (*d*) EM of early aggregates (Image is from [18])

2 Anti-amyloidogenic Heterocyclic Peptides

The search for amyloid inhibitors originally began from organic compounds, such as cinnamon, curcumin, porphyrins, and polyphenols, which were demonstrated to possess a degree of activity against different amyloidogenic peptides and proteins in vitro and in vivo [38–45]. Research expanded to the development of peptide inhibitors, which are now of considerable interest because of their low toxicity and the relative ease with which they can be designed, synthesized, and screened through the use of combinatorial library technology. Despite these benefits, peptides are generally susceptible to fast proteolysis and have usually short half-lives and low bioavailability. However, advances in the field of modern peptide chemistry enable chemical modifications to the backbone and side chains of the peptides, in order to stabilize strategically against enzymatic degradation and to enhance potency.

Cyclization is a widely used chemical approach to increase peptide potency and stability [46]. The constrained structure created by cyclization has been demonstrated to enhance the binding affinity of cyclic peptides [47], to increase intestinal permeability, and to improve resistance to cellular proteases and bioavailability. Cyclization reduces the conformational flexibility of natural and synthetic peptides by inducing a structural constraint, which often makes cyclic peptides and their different chemical derivatives potent bioactive compounds. Moreover, their intrinsic characteristics and ability to bind to large surfaces enable various cyclic and bicyclic peptides to be utilized to modulate protein–protein interactions (reviewed in [48]).

Currently, there are more than 68 approved macrocyclic drugs (predominantly of natural origin and ranging in size from 12 atoms up to 30 amino acids) on the market, and at least 35 more are in various phases of clinical development [49]. Most of these drugs are approved to treat infections and various types of cancers. From a chemical viewpoint, they are equally distributed between heterocyclic peptides and macrolides. With one exception, all of the heterocyclic peptides that are in clinical use are administered by parenteral dosage because of insufficient oral bioavailability; however, certain candidates under investigation in ongoing clinical trials exhibit increased drug-like membrane permeability and are being considered for oral administration (reviewed in [49]).

There are many methods to create libraries of cyclic peptides (reviewed in [50]), some of which have been implemented in the search for anti-amyloidogenic agents. As mentioned before, heterocyclic peptides have been studied in many anti-amyloidogenic therapeutic approaches. This chapter will concentrate on the latest developments concerning heterocyclic peptide agents as direct inhibitors of various amyloidogenic proteins.

2.1 Conformational Mimics

Peptide supramolecular assemblies are complex structures formed by a "bottom-up" process from small and simple building blocks [51]. This description characterizes the building up process of both amyloid fibrils and other self-assembled systems, such as cyclic D,L-α-peptide nanotubes. In these supramolecular structures, the monomeric building blocks associate through specific non-covalent interactions to form well-ordered three-dimensional nanostructures. As implied by the name of this category, the cyclic peptide inhibitors gain their mechanism of action from their structural and biochemical similarities to amyloid fibrils.

2.1.1 Cyclic D,L-α-Peptides

Cyclic D,L-α-peptides are composed of an even number of alternating D- and L-α-amino acids, which force the cyclic peptide ring to adopt a low-energy flat conformation. In such a conformation, all backbone amide functionalities lie perpendicular to the plane of the peptide ring (Fig. 3) [2, 52]. Under conditions that favor hydrogen-bond formation, the cyclic peptide subunits stack on top of each other through backbone–backbone intermolecular hydrogen bonds to produce a contiguous β-sheet nanotube structure.

The first suggestion that cyclic peptides can self-assemble was made in 1974 based on theoretical studies [53]. In 1993, Ghadiri et al. were the first to report on the design, synthesis, and characterization of the *cyclo*[-(D-Ala-Glu-D-Ala-Gln)$_2$-] nanostructure [52]. Electron microscopy (EM) and X-ray diffraction studies revealed that, upon protonation, the peptide self-assembles into highly ordered tubular structures of length 10–30 μm and width 100–500 nm. The nanotube has an internal diameter of 7–8 Å and an axial spacing of 4.73 Å (Fig. 3) [52].

The cyclic D,L-α-peptide self-assembly process results in a predictable structural dynamic network. Unlike proteins in which the sequence of the polypeptide chain

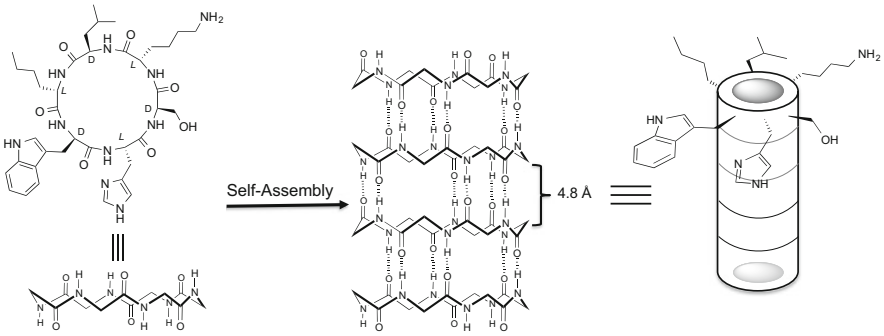

Fig. 3 Schematic diagram of nanotube assembly from cyclic D,L-α-peptide *CP-2*. For clarity, most of the peptide side chains have been omitted

encodes their structure and function, in cyclic D,L-α-peptide nanotubes, the alternating D- and L-α-amino acid configuration is the primary determinant of self-assembly and function, whereas the peptide's primary structure dictates only the conditions under which self-assembly occurs. Thus, the most important factors that need to be considered in the design of cyclic D,L-α-peptide nanotubes are those that directly affect the self-assembly process, rather than the individual characteristics of the residues. Factors that directly affect self-assembly include the ring size, backbone–backbone hydrogen-bond interactions (which dictate the ring stacking arrangements), and the relative sheet register and sequence selection in terms of the influence of the side chains on the three-dimensional nanotube structure [54]. Consequently, the external dimensions and surface of cyclic D,L-α-peptide nanotubes are relatively easy to control through a rational choice of amino acid side chains and size prior to the synthesis of the cyclic peptide ring. An approach based on chemical synthesis opens the door for the design of a wide range of cyclic D,L-α-peptides to produce tubular structures with specific characteristics and various possible applications [2, 55–60].

Recently, theoretical studies using molecular dynamics and umbrella sampling have suggested that the polarity of the solvent plays an important role in the dissociation mechanism of the cyclic D,L-α-peptide nanotubes. Cylindrical structures were less dynamic and therefore more stable in nonpolar rather than polar solvent [61]. More efficient hydrogen bond-induced self-assembly is thus favored in a nonpolar milieu, such as that provided by cellular membranes and by the hydrophobic core of the amyloids.

Based on the rationale that cyclic D,L-α-peptides with appropriate hydrophobic side chains may partition into lipid bilayers and increase membrane permeability upon their self-assembly, the first cyclic peptide-based transmembrane ion channel was reported [55]. Channel-mediated membrane modulation was subsequently applied to designing cyclic D,L-α-peptides with potent antimicrobial [56, 62] and antiviral [57, 63] activity.

Cyclic D,L-α-peptides with various modifications were also studied for other applications, such as biosensors and photo-responsive materials [64, 65]. Lately, we have shown that His-rich self-assembled cyclic D,L-α-peptides stimulate non-insulin-dependent glucose uptake in skeletal muscle cells by increasing the translocation of GLUT1 and GLUT4 receptors. The cell-permeable His-rich cyclic peptides catalytically decompose large amounts of H_2O_2 in vitro and so protect muscle cells against oxidative stress damage induced under hyperglycemic conditions. These His-rich cyclic peptides are candidates for the treatment of diabetes mellitus [59].

Moreover, we have recently demonstrated that self-assembled cyclic D,L-α-peptides and amyloids exhibit several common structural and functional characteristics (Fig. 4). (a) The intermolecular cross-β-sheet structure of both amyloids and cyclic D,L-α-peptides is generated by hydrogen bonds that run parallel to the fibril axis and perpendicular to the plane of the peptide chains. (b) Similar to the 3D structure of amyloids, the structure of self-assembled cyclic D,L-α-peptides is dictated mainly by backbone hydrogen bonding and not by the amino acid

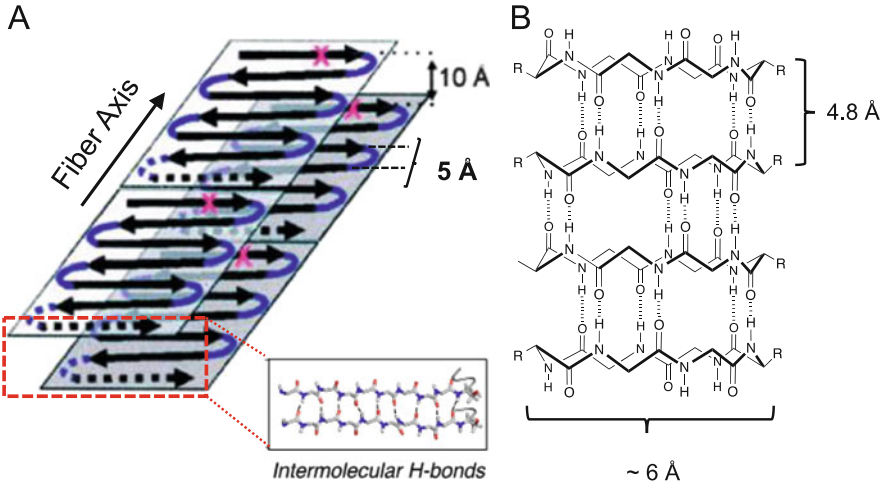

Fig. 4 Self-assembled cyclic D,L-α-peptides and amyloids exhibit common structural characteristics. Structural similarities between the self-assembly process of (**a**) α-syn protein and (**b**) cyclic D,L-α-hexapeptides. For clarity, all the side chains have been omitted. The amyloid structure is adapted from [66], while the structure of the cyclic hexapeptide is based on the known core structure of cyclic D,L-α-peptide octamer [52]

sequence. (c) Each cyclic peptide in the nanotube assembly is separated from its neighbors by ~4.8 Å, which resembles closely the distance between β-strands in the amyloids. (d) The mechanisms of action of bioactive cyclic D,L-α-peptides and amyloids both involve membrane interactions and perturbation through the formation of nonspecific ion channels or pores that disrupt integrity resulting in cytotoxicity [2, 26, 27, 56, 67].

The similarities between self-assembled cyclic D,L-α-peptides and amyloids manifest in their similar interactions with polyclonal antibodies (A11) raised against prefibrillar assemblies of Aβ peptide [25] and are responsible for amyloid cross-interactions. For example, Aβ interacts specifically and modulates the aggregation of various amyloidogenic proteins, including tau [68], α-synuclein (α-syn) [69], transthyretin [70], and IAPP [71].

Based on the close structural and functional similarities between amyloids and cyclic D,L-α-peptides, we designed and synthesized a library of cyclic peptide hexamers and screened it for peptides that interact with Aβ and its aggregates [58]. The "one-bead-one-compound" combinatorial approach was employed to identify analogs exhibiting anti-amyloidogenic activity and probe their topological requirements in general. Thus, representative amino acids with different functional side chains, such as Lys, Glu, Ser, Leu, Trp, and His, were introduced at five positions on cyclic D,L-α-peptide hexamers, in which position one was fixed with Lys that was linked to the support by way of the side-chain amine to allow "on-resin" cyclization.

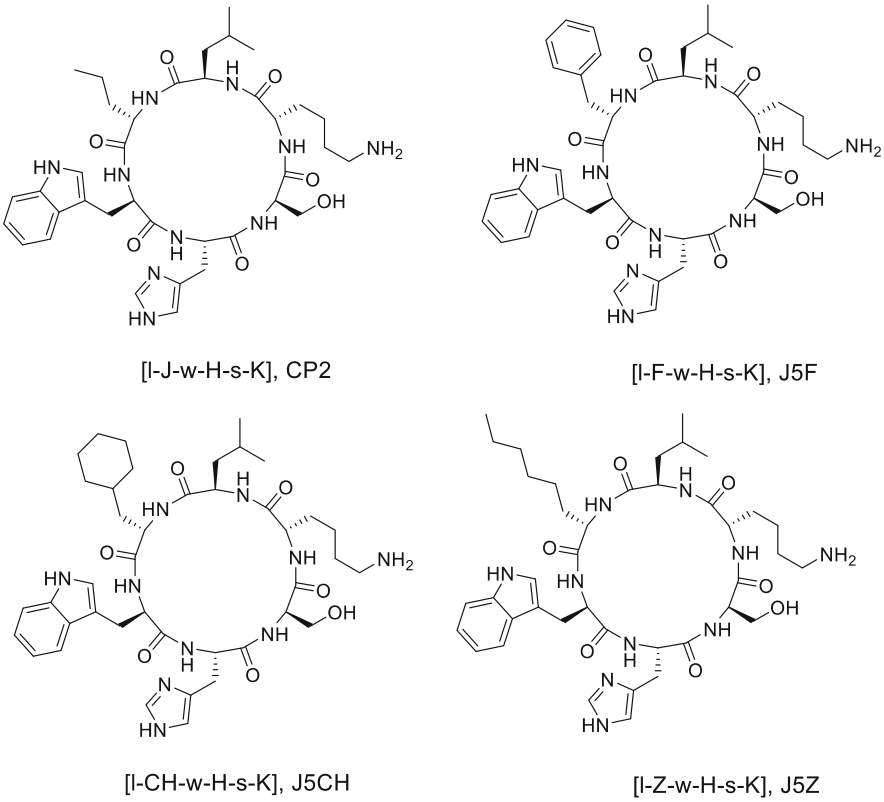

Fig. 5 Chemical structures of four cyclic D,L-α-peptides discovered in our studies. *Upper and lower case letters* represent L- and D-α-amino acids, respectively. *Square brackets* indicate a cyclic structure. J, CH, and Z denote norleucine, cyclohexylalanine, and 2-aminooctanoic acid, respectively [58, 72]

Five hundred members of the library were screened for anti-amyloidogenic activity against Aβ40 as a model amyloidogenic protein. Figure 5 illustrates some of the structures of the identified amyloid-binding cyclic D,L-α-peptides. Thioflavin T (ThT), which produces a strong fluorescent signal on binding to amyloid fibrils, was used as indicator of the aggregation process. Through this approach, two potent cyclic peptides were discovered and their sequences were optimized to yield the cyclic D,L-α-peptide [lJwHsK] (*CP-2*; upper and lower case letters represent L- and D-α-amino acids, respectively; square brackets indicate a cyclic structure; J denotes norleucine).

We found that *CP-2* caused a dose-dependent reduction in Aβ aggregation with superior activity to that of the anti-amyloidogenic Ac-KLVFF-NH_2 peptide [73] that was used as a positive control. Transmission electron microscopy (TEM) analysis suggested that co-incubation of *CP-2* with soluble Aβ drastically reduced fibril formation. Moreover, we showed that *CP-2* decreased dose-dependently the

aggregation kinetics of Aβ40 and arrested completely the aggregation of Aβ42 at as high as a 1:1 Aβ:*CP-2* concentration ratio, suggesting that *CP-2* has a somewhat stronger inhibitory effect on the more neurotoxic Aβ42 peptide [58]. Most importantly, we demonstrated that *CP-2* was recognized by the A11 conformational antibody, suggesting that it could be used as a structural mimic to cross-interact and interfere with the aggregation and toxicity of different amyloids [58, 72, 74].

The importance of π–π stacking interactions in the molecular recognition and self-assembly process of amyloid formation is well documented [75–78]. By conducting an Ala scan study and using the ThT assay to determine the contribution of each amino acid of the lead cyclic peptide, we showed that substitution of the aromatic D-Trp with D-Ala completely abolished anti-amyloidogenic activity. On the other hand, replacement of Nle (J) in position 5 with the aromatic residue Phe (to generate *J5F* [lFwHsK], Fig. 5) increased significantly this activity and confirmed the importance of aromatic interactions for anti-amyloidogenic activity [72].

The cyclic nature of *CP-2* and the intermolecular hydrogen bonds formed during its self-assembly were deemed vital for activity. Reports have previously emphasized the importance of intermolecular hydrogen bonds and the cyclic nature of the macrocyclic subunit for self-assembly as well as antiviral and antibacterial activity of cyclic peptides [56, 63]. The combined results of ThT, critical micelle concentration, and NMR analyses of *CP-2* confirmed that self-assembly was essential for anti-amyloidogenic activity and that the bioactive form of *CP-2* was probably self-assembled [58].

To investigate the mechanism of action of *CP-2*, we tested its effect on the kinetics of amyloid aggregation under seeding conditions. Amyloid fibrils are seeding-competent structures that can efficiently convert soluble and monomeric proteins to their aggregated state [79]. We found that co-incubation of *CP-2* with monomeric Aβ40 in the presence of 5% Aβ40 seeds inhibited completely formation of Aβ amyloids, suggesting that *CP-2* interacted with the monomers of Aβ, or bound and remodeled the seeds to incompetent structures. Using dot blotting and ELISA assays and employing the amyloid oligomer-specific polyclonal antibody A11 and the Aβ oligomer-specific monoclonal antibody (OMAB), we showed that *CP-2* reduced dramatically the amount of Aβ toxic soluble oligomers. In addition, the dot-blot immunoassay confirmed that the inhibitory effect of *CP-2* was stronger toward the more toxic Aβ42. These findings collectively suggested that *CP-2* interacted and altered the aggregation of Aβ to an "off-pathway" mechanism [38, 58].

Our ThT, TEM, and immunochemical analyses indicated that at a near-stoichiometric ratio, *CP-2* disassembled effectively preformed fibrils without generating a new pool of toxic oligomers. Moreover, the results of photo-induced cross-linking of unmodified proteins (PICUP) suggested that *CP-2* generated relatively stable co-aggregates with monomeric or small 1–3-mers of Aβ and shifted the aggregation equilibrium toward these early-assembled species [58].

From the clinical perspective, the aggregation of Aβ has been associated with AD [21]. Hence, we probed whether *CP-2* could reduce Aβ-induced toxicity in a neuronal-like model of rat pheochromocytoma PC12 cells. These viability assays

showed that *CP-2* significantly decreased Aβ-induced toxicity, with the maximal increase in cell viability occurring when Aβ was incubated with a five- to tenfold excess of the cyclic peptide [58].

As mentioned in the introduction, the strong structural and functional similarities between the different deposited amyloidogenic proteins may be related to their cross-reactivity. The generic nature of amyloid aggregates has also been strongly supported by the finding that antibodies can cross-interact with early aggregates of different proteins and inhibit their toxicity [25]. This phenomenon was further supported by the finding that fibrillar aggregated species of globular proteins possessed cell toxicity, implying a common mechanism for different amyloidoses [5, 6].

In order to show that the anti-amyloidogenic activity of *CP-2* stems from its structural and functional similarities to pathogenic amyloids, we tested its effect on the aggregation and toxicity of PD-associated α-syn. Using kinetic ThT assays, TEM, dot-blot immunoassays, and circular dichroism (CD) spectroscopy, we demonstrated that *CP-2* inhibited effectively the aggregation of α-syn and disassembled preformed fibrils, again by an "off-pathway" mechanism. Moreover, *CP-2* reduced significantly the toxicity of α-syn to PC12 and neuronal cells [74].

Overall, we have shown that a simple self-assembled system of cyclic D, L-α-peptides may be used to modulate the aggregation and toxicity of pathogenic amyloids because of their close structural and functional similarities. Our results support previous studies that proposed that amyloids may have common structural and functional properties [25], by which they may cross-react and modulate each other's aggregation and toxicity. Our cyclic D,L-α-peptide system represents a new methodological platform for designing amyloidogenic and neurodegenerative inhibitors.

2.2 Sequence Mimics

Most of the cyclic peptides described as sequence mimics were generated by rational design. These include cyclic peptides, possessing sequences homologous to those of the central amyloidogenic sequence of different amyloid proteins and peptides. The rationale of this approach is based on employing the sequence homology between such synthetic cyclic peptides and the amyloids to favor specific binding that interferes with aggregation of the amyloid parent protein. This strategy is usually accompanied by insertion of a β-breaking residue or motif into the synthetic inhibitor. The β-breaker property introduces a folding constraint or a steric hindrance into a cross-β-sheet structure, which may arrest the growth of the fibril.

2.2.1 Cyclic Modular β-Sheets

The supramolecular interactions of β-sheets play an important role in their ability to bind to other β-sheet-containing proteins by complementary hydrogen-bonding interactions. In an elegant series of publications, Nowick's group introduced a model of a macrocyclic protein β-sheet [80] and demonstrated its use to study and inhibit the aggregation of several amyloidogenic proteins [81–83]. These cyclic modular β-sheets were initially developed as water-soluble templates for β-strand mimics [80]. The macrocyclic rings [84] (Fig. 6a) contain a pentapeptide in the "upper" strand, two natural α-amino acids in the "lower" strand, two δ-linked ornithine amino acids as β-hairpin turn mimics, and the synthetic tripeptide Hao [85], which is a rigid β-sheet mimic that serves as a template for the folding of the upper strand and blocks the self-aggregation of the lower strand [86].

Structural studies using NMR spectroscopy demonstrated that well-folded β-sheet conformations with cross-strand aromatic–aromatic interactions were adopted by certain 42-membered macrocycles, which contained the hydrophobic sequences KLVFF and LVFFA that were derived from $A\beta_{16–20}$ and $A\beta_{17–21}$, respectively [80]. This approach was also used to study the antiparallel-layered parallel β-sheets formed by amyloids. In particular, a short peptide, Ac-VQIVYK-NH_2 (Ac-PHF6), derived from AD-associated tau protein, was chosen as a model for amyloid aggregation. A macrocyclic peptide that delayed the onset of Ac-PHF6 aggregation in a thioflavin S (ThS) assay was prepared by incorporating, respectively, the Ac-PHF6-derived VQIVY sequence and the Hao motif into the upper and lower strands of the macrocycle (Fig. 6b) [81]. A related macrocycle containing the more hydrophilic sequence, Ac-PHF6-derived QIVYK, showed no significant

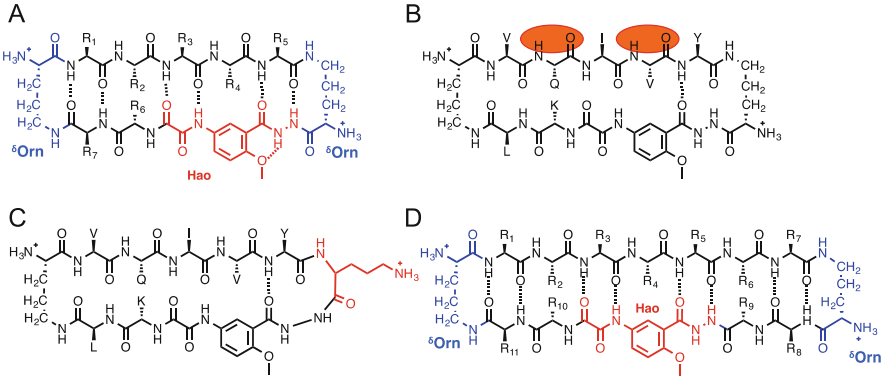

Fig. 6 Cyclic modular β sheets. (**a**) General template for the cyclic modular β sheets [80]. (**b**) Cyclic modular β sheets containing a tau-derived sequence (PHF6, VQIVY pentapeptide) incorporated in its upper strand. (**c**) α-Linked ornithine macrocycle, a mutant of cyclic modular β sheet (**b**) [81]. (**d**) Aβ-sheet mimic (ABSM), a 54-membered ring, comprising a heptapeptideβ-strand (*black, the upper strand*), one Hao unit (*red*) flanked by two dipeptides (*black, the lower strand*) and two δ-linked ornithine (*blue*, *$^{\delta}$Orn*) turns [83]. In (**b**) and (**c**), amino acid side chains are signified by the respective one letter code of the amino acid

effect on Ac-PHF6 aggregation. The β-sheets were suggested to grow mainly in one favorable direction, because only one of the two macrocycles, which were targeted to bind different hydrogen-bonding surfaces of Ac-PHF6, exhibited an inhibitory effect on aggregation [81]; a similar selectivity was demonstrated in the case of Aβ [87]. By preparing linear and α-linked ornithine mutants of the original cyclic modular β sheet (Fig. 6c), the lower strand of the macrocycle was demonstrated to be active in blocking β-sheet interactions, and preorganization of the macrocycle β-sheet structure was shown to be crucial for activity [81]. Systematic studies of different analogs revealed that anti-amyloidogenic macrocycles interacted with the antiparallel-layered amyloid parallel β-sheet and bound the edges of the β-sheet layers to inhibit their growth [81]. Facial hydrophobicity was shown to play an important role in the recognition of the layered parallel β-sheets of amyloids by the anti-amyloidogenic macrocycles [81].

In a separate work, a detailed SAR study sought to characterize the effect exerted by each component of the macrocyclic β-sheet peptide (peptide **1**) on its inhibitory activity against the tau protein-derived peptide Ac-VQIVYK-NH_2 (Ac-PHF6). The study supported the important role of the hydrophobic surface displayed by the macrocycle for interaction with the β-sheet layers of the amyloid and inhibition of aggregation [82]. Moreover, the nonlinear effect of macrocycle concentration on the lag time of Ac-PHF6 aggregation indicated that inhibition was a cooperative process in which at least two macrocycles were bound to the growing fibril [81]. Based on X-ray crystallographic and solution state NMR spectroscopic studies of the lead macrocycles, as well as the crystal structure of the more hydrophilic QIVYK peptide, models for Ac-PHF6 amyloidogenic growth and inhibition were proposed. Growth of the amyloid of Ac-PHF6 was hypothesized to involve addition of peptide strands alternately to each layer of the layered β-sheets, and inhibition of β-sheet growth entailed cooperative binding of the macrocycles to two layers [81].

To further study the inhibitory effect of macrocycles on amyloid aggregation, a new family of 54-membered macrocycles was designed and named amyloid–βsheet mimics (ABSMs, Fig. 6d) [83]. Different heptapeptide sequences of several amyloids were incorporated into the upper strand of the ABSMs. In the lower β-strand, two additional amino acid residues were added to the *N*-terminal of the Hao mimic unit, and the δ-ornithine turn motifs were kept constant. The ABSMs were incubated with their parent amyloid proteins and tested for anti-amyloidogenic activity using ThT, EM, and cell viability assays. The different ABSMs inhibited the aggregation of their parent amyloidogenic proteins [e.g., Aβ40, Aβ42, human β2-microglobulin ($h\beta_2M$), and truncated human α-syn1-100] and rescued cells from parent amyloid-induced toxicity, probably through β-sheet interactions. Moreover, structurally homologous ABSMs cross-interacted with different amyloids and inhibited their toxicity [83].

To exploit the possibility that linking two macrocyclic β-sheet structures [80] may produce a multivalency effect [88], several divalent macrocyclic β-sheets were designed and tested for anti-amyloidogenic activity. ThT fluorescent assay results suggested that these inhibitors exhibited enhanced activity against Aβ aggregation compared with their monovalent components [89]. Based on these results showing

improved anti-Aβ aggregation activity for the divalent relative to the monovalent ABSMs [83], and in light of the hypothesis that amyloid deposition is a nucleation-dependent polymerization process, the authors presented a model for the inhibition of Aβ aggregation in which the macrocycles bind early β-structured oligomers to create new aggregation pathways that blocked the Aβ oligomer-to-nucleus transition [83]. Further investigation of this model enabled characterization of the structure of the oligomers formed by the Aβ peptide using X-ray crystallography of a macrocycle that incorporated Aβ residues 15–23 [90].

It is evident from these studies that cyclic modular β-sheets represent an instrumental tool for amyloid research. In light of Cheng's proposed model for amyloidogenic aggregation [91],the inhibitory effects of the cyclic modular β-sheets offer deeper insights into the supramolecular chemistry of β-sheets that may enable the design of therapeutic agents to treat amyloid-related pathologies [92, 93]. Although these macromolecules may have limited oral bioavailability, they may be administered by parenteral dosage.

2.2.2 Cyclic KLVFF Derivatives

The linear peptide fragment KLVFF from $A\beta_{16–20}$ binds to the full-length peptide at a self-recognition region and inhibits aggregation [73]. Moreover, a related 5-residue linear synthetic peptide *iAβ5* (LPFFD), derived from the KLVFF sequence, but containing Pro as a β-sheet breaker inhibited the formation of amyloids and disassembled amyloid fibrils in vitro and in vivo [94]. Modifications to *iAβ5*, through cyclization via a disulfide bond between two Cys residues sandwiching the LPFFD sequence was pursued to enhance resistance to proteolysis [95]; however, the resulting cyclic peptide analog was devoid of anti-amyloidogenic activity in the ThT assay [95]. Alternatively, head-to-tail cyclization of the KLVFF sequence gave *cyclo-[KLVFF]* (Fig. 7a), which along with its D-amino acid enantiomer, at a threefold excess, inhibited the aggregation of full-length Aβ, as demonstrated in the ThT assay [99]. Structure–activity relationship (SAR) studies demonstrated that the side chains of LVFF rather than the backbone amide moieties were responsible for the inhibitory activity of *cyclo-[KLVFF]* and guided the synthesis of non-peptidic Aβ aggregation inhibitors [99]. Extensive SAR studies on *cyclo-D-[KLVFF]* led to incorporation of an additional phenyl group at the β-position of the Phe^4 residue to afford *cyclo-D-[KLVF(β-Ph)F]*, which demonstrated superior anti-Aβ activity compared to the parent peptide [100]. Various biochemical and biophysical analyses suggested that the inhibitory mechanism of *cyclo-D-[KLVF(β-Ph)F]* involved interaction with Aβ to produce off-pathway Aβ oligomers, which possessed lower β-sheet content, lower seeding ability, and lower toxicity than oligomers derived from full-length Aβ42. A chemical modification of *cyclo-KLVF(β-Ph)F* with a diazirine moiety altered strongly the extent of the cross-β-sheet structure, as well as the characteristics of amyloid aggregation and the toxicity of Aβ42 [100]. Different cyclic derivatives of the potent aggregation inhibitor KLVFF, derived from the Aβ sequence, were demonstrated to exhibit

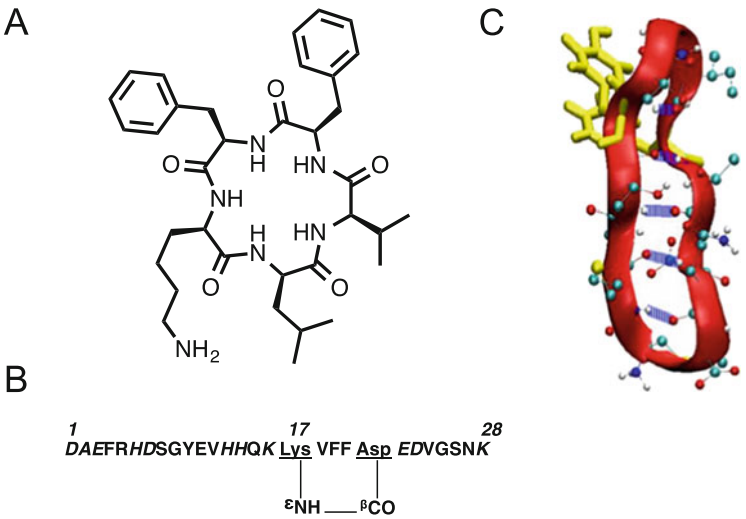

Fig. 7 Structures of several sequence mimics. (**a**) Chemical structure of cyclic KLVFF derived from Aβ16-20 (*cyclo-[KLVFF]*) [96]. (**b**) Schematic presentation of cyclo^{17,21}-[Lys^{17}, Asp^{21}]Aβ (1-28), a cyclic derivative of a full-length Aβ [97]. (**c**) Ribbon and CPK representation of the Janus cyclic peptide *cyc[60–70]* showing the persistent intramolecular backbone hydrogen bonds in *blue* [98]

enhanced potency relative to linear analogs; however, a threefold excess of inhibitor was typically necessary to obtain significant inhibition.

2.2.3 Conformational Restrictors

Inspired by the β-sheet-breaking strategy [94], the amyloidogenic sequence of Aβ28 was transformed into a non-amyloidogenic peptide by restraining its conformation through cyclization by an intramolecular lactam bridge [97]. Applying an *i* to *i*+4 side-chain to side-chain cyclization approach, a Lys^{i} and Asp^{i+4} pair was installed within the Aβ sequence to create the lactam *cyclo^{17,21}-[Lys^{17},Asp^{21}]Aβ(1–28)* (Fig. 7b). Based on the hypothesis that the region of residues 13–20 adopts a helical conformation that unfolds during the aggregation process in which the hydrophobic Val^{18} and Phe^{19,20} residues directly contribute to self-recognition and aggregation of Aβ, the lactam was placed within this portion of the sequence to inhibit unfolding [101]. Atomic force microscopy (AFM), CD spectroscopy, and EM showed that no amyloid fibrils were formed upon aging of *cyclo^{17,21}-[Lys^{17},Asp^{21}]Aβ(1–28)*. In addition, aged *cyclo^{17,21}-[Lys^{17},Asp^{21}]Aβ(1–28)* did not bind Congo red (a typical amyloid stain), in contrast to aged Aβ28 and linear [Lys^{17},Asp^{21}]Aβ(1–28) controls. The CD curve shape, a pull-down assay in combination with NuPAGE gel electrophoresis, and Western blotting studies all suggested that *cyclo^{17,21}-[Lys^{17},Asp^{21}]Aβ (1–28)* contained higher amounts of α-helical structures than Aβ28 and that the two

peptides interacted to prevent the generation of Aβ amyloid. Moreover, a 3-(4,5-dimethylthiazol-2-yl)-2,5-diphenyltetrazolium bromide (MTT) reduction assay suggested that *cyclo*^{17,21}*-[Lys*^{17}*,Asp*^{21}*]Aβ(1–28)* protected human glioblastoma/astrocytoma cells from Aβ28-induced toxicity. Exclusion chromatography results further suggested that the interaction between the two peptides created aggregation-resistant heterodimers of Aβ28 and the cyclic analog disassembled dimeric and multimeric Aβ28 assemblies back to monomers [97].

Collectively, these results demonstrated that conformational restriction of an amyloid core, by means of intramolecular cyclization, inhibited amyloidogenic potential and reduced cytotoxicity of the native sequence [97]. This approach may be further implemented to develop therapeutic and diagnostic candidates for use in studies of amyloid aggregation, because the cyclic constraint does not affect amyloidogenic recognition and interactions.

2.2.4 Janus Cyclic Peptide

As implied by its name, the fibril formation inhibitor cyclic peptide, *cyc[60–70]* (Fig. 7c), has two contrasting faces, one hydrophobic and the other hydrophilic [98, 102]. *Cyc[60–70]* was derived from the amyloidogenic sequence of human apolipoprotein C-II (apoC-II), which self-assembles readily into fibrils upon removal of the lipid component. ApoC-II has been identified in amyloid plaques [103] and, together with Aβ40, was demonstrated to induce macrophage inflammatory response and initiate early events in heart disease [104]. In a preliminary study conducted using molecular dynamics simulations, apoC-II[60–70] and apoC-II[56–76], peptides derived from the core of apoC-II amyloid, were shown to preferentially form β-hairpin-like structure in solution [105]. *Cyc[60–70]* possesses a disulfide cross-link formed between cysteine residues linked to both ends of the apoC-II[60–70] peptide and was designed to investigate the potential of the constrained hairpin-like structure to disrupt the fibrillogenesis of apoC-II[60–70] and apoC-II[56–76] [102].

Using ThT fluorescence and EM, sub-stoichiometric concentrations of *cyc[60–70]* were demonstrated to completely inhibit apoC-II[60–70] and apoC-II[56–76] fibril formation, in contrast to reduced and scrambled *cyc[60–70]* derivatives which exhibited decreased inhibitory activity[102]. *Cyc[60–70]* possessed anti-amyloidogenic activity against full-length apoC-II, albeit at much higher molar ratios, but exhibited no effect on Aβ40 aggregation. Moreover, ThT assay results showed that *cyc[60–70]* did not disassemble preformed apoC-II[60–70] and apoC-II[56–76] fibrils, and sedimentation equilibrium analytical centrifugation experiments suggested that *cyc[60–70]* did not bind strongly to either peptide.

The molecular mechanism utilized by *cyc[60–70]* was examined by NMR spectroscopy which revealed an elongated conformation with hairpin-like turns and the Janus characteristics of distinct hydrophobic and hydrophilic faces [102]. Molecular dynamics simulations and quantum calculations were used to determine the structures formed and the dynamics of the interactions between

apoC-II(60–70) and *cyc[60–70]*. The results suggested a mechanism in which *cyc [60–70]* induces increased flexibility in apoC-II(60–70) and prevents its β-hairpin-like fibril-favoring conformation from being adopted [98]. Hydrophobic interactions between the two molecules were suggested to inhibit formation of fibrils by altering the dynamic equilibrium [102]. The hydrophobic surface of the Janus cyclic peptide may protect the fibril-forming face of the amyloidogenic protein while the exposed hydrophilic surface inhibits fibril growth [98, 102]. In agreement with other studies [81, 106], targeting of hydrophobic interactions was shown to be an important aim for anti-amyloidogenic research.

2.3 Cyclic Peptide Inhibitors that Interfere with Amyloidogenic Signal Transduction

Synthetic heterocyclic peptides that were reported to exhibit anti-amyloidogenic activity without interacting directly with amyloids include several cyclic peptide inhibitors that interfere with amyloidogenic pathways with partially understood mechanisms. For example, some of the heterocyclic peptides were designed to target protease enzymes. Others act on various receptors and cellular pathways that have yet to be associated directly with amyloid pathology.

2.3.1 Cyclic Peptides Selected by In Vivo Screening

Although the mechanism of action of these cyclic peptides is not yet understood, the method for their selection has important value in anti-amyloidogenic research. Libraries of head-to-tail cyclic peptides were generated in vivo to enable chemical genetic selection [107]. Using an in vivo yeast model for Parkinson's disease (PD) and other synucleinopathies, rapid phenotypic selection identified peptides that reduced specifically α-syn toxicity [108]. From an original pool of 5 million cyclic octapeptides, two cyclic peptides (CPWCSTRV and CALCDPWW, Fig. 8a, b) were isolated and their activity was validated in additional filtering assays. Studies of SAR by point mutagenesis revealed that the biological activity of both cyclic peptides requires the presence of Cys in the first position of a common CXΦX motif, in which X is any residue and Φ is a hydrophobic amino acid. The two selected cyclic peptides reduced significantly dopaminergic neuron loss in a nematode synucleinopathy PD model. Immuno-electron and EM results demonstrated that both cyclic peptides permitted the growth and division of the dopaminergic neurons despite the presence of hindered pools of α-syn vesicles that killed control cells. The cyclic peptides were hypothesized to target cell pathways downstream of α-syn-mediated vesicle trafficking defects and to alter likely cellular functions distinct from those linked to α-syn toxicity [108]. In addition to discovering new lead compounds, this study accomplished development of a novel

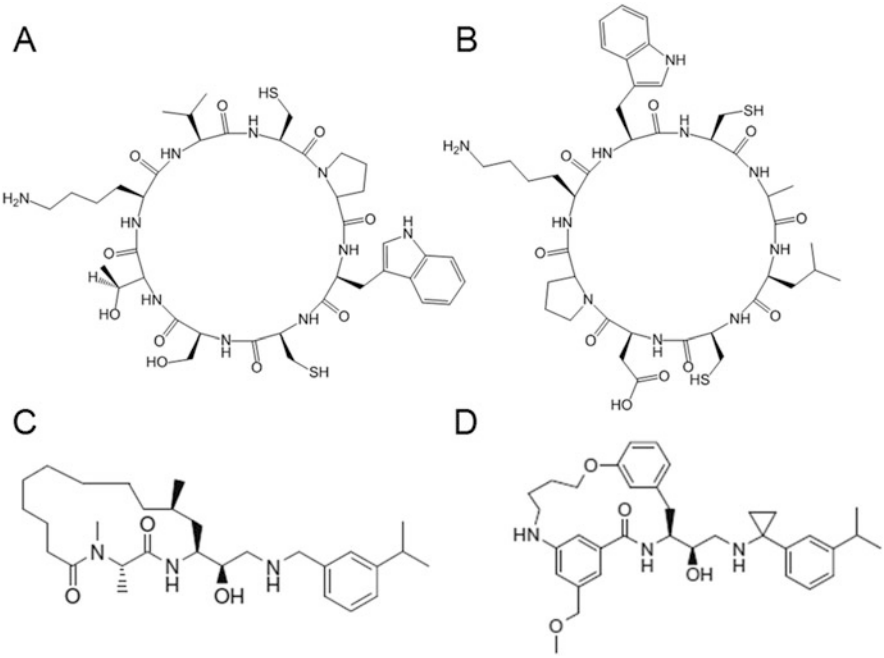

Fig. 8 Structures of some cyclic peptides that interfere with amyloidogenic signal transduction: (**a**) CP1R7K, (**b**) CP2W7K cyclic peptides discovered by screening chemical genetic drug candidates in vivo [108], (**c**) β-secretase inhibitor NB-544, and (**d**) macrocycleNB-216 [109, 110]

technology for screening chemical genetic drug candidates in vivo. The method has been utilized in various disease models, including those difficult to address in vitro, and may prove a lower-cost, higher throughput alternative to traditional small molecule screening.

2.3.2 Transmembrane Neurotrophin p75 Receptor ($p75^{NTR}$) Antagonist

The neurotoxicity of extracellular Aβ oligomers may be mediated by signaling through various receptors. For example, Aβ oligomers may induce nerve growth factor (NGF) receptor-mediated neuronal death by binding to the transmembrane neurotrophin p75 receptor ($p75^{NTR}$) [111] and activation of apoptotic signaling [112, 113].

A cyclic peptide antagonist was designed based on the structure of the mutated NGF and Aβ ligands of the $p75^{NTR}$ receptor. The sequence CATDIKGAEC is homologous to the β-hairpin loop of mutated NGF(28–36) and contains the KGA tripeptide fragment shared with Aβ(28–30). A cyclic peptide was prepared by attachment of two cysteines to the termini of the linear sequence followed by

disulfide bond formation [114]. Using immunoprecipitation, Northern blotting, and cell viability assays, the cyclic peptide was shown to displace Aβ40 from the p75 ^{NTR} receptor, to inhibit the Aβ40-mediated signaling process, and to prevent Aβ40-mediated neuronal death in vitro [114]. Moreover, administration of the cyclic peptide antagonist in vivo reduced Aβ42-induced inflammation in mice [115]. Together, these results indicate that blockage of the binding of Aβ to the p75 ^{NTR} receptor may reduce AD-associated neuroinflammation and neuronal loss. Caution must however be used in the generation of disulfide bonds for the synthesis of cyclic anti-amyloidogenic agents [114],because the amyloidogenic properties of natural peptides, such as 4 kDa *ABri* peptide, which comprises the amyloid of rare familial British dementia, have been shown to be contingent on disulfide bond formation [116, 117].

2.3.3 Protease Inhibitors

A general anti-amyloidogenic approach involves inhibition of the proteases responsible for the generation of amyloidogenic fragments. Especially relevant to AD research, inhibitors of β- and γ-secretases have been developed to prevent cleavage of amyloid precursor protein (APP) to generate Aβ pathogenic peptide [118, 119].

Peptide isosteres have proven useful for probing the active site of γ-secretase and characterizing the catalytic subunit, albeit without inhibiting activity (reviewed in [120]). Several studies have reported macroheterocyclic peptidomimetic inhibitors of β-secretases (Fig. 8c, d) that fit into the relatively large-size active site of the aspartic peptidase [109, 121–124]. Macrocyclic ethers and lactones have been used to pre-organize and stabilize bioactive conformations with improved activity and physicochemical properties relative to the linear counterparts (reviewed in [125]). For example, macrocyclic β-secretase inhibitors (Fig. 8d) have reduced Aβ40 levels in mice brains after oral administration [110]. Although small molecule secretase inhibitors have been more commonly pursued toward clinical trials because of improved bioavailability (reviewed in [125]), issues concerning their selectivity and toxicity remain unresolved [13, 126, 127].

2.4 Natural Inhibitors

Naturally occurring linear and heterocyclic amyloid-binding peptides have been isolated and shown to modulate amyloid formation. For example, gramicidin S has exhibited potent anti-amyloidogenic activity [106].

2.4.1 Gramicidin S and Derivatives

Gramicidin S (GS, Fig. 9a) is a natural cyclic decapeptide antibiotic (*cyclo*-(Val-Orn-Leu-D-Phe-Pro)$_2$) effective against both Gram-positive and Gram-negative bacteria as well as some fungi. Produced by the Gram-positive bacterium *Bacillus brevis* [128], GS possesses a secondary structure comprised of an extended β-sheet conformation created by two antiparallel β-strands (Val-Orn-Leu) connected by two β-turns (D-Phe-Pro). The structure of GS is amphiphilic with hydrophobic and polar side chains facing opposite sides of the β-sheet. The relatively stable cyclic β-hairpin conformation of GS has been studied using ^{1}H and ^{13}C NMR spectroscopy [129].

Based on previous studies of modular β-sheets and conformational synthetic β-sheet mimics [58, 72, 81–83, 89], and using the ThT fluorescence assay and AFM, natural GS and analogs were shown to inhibit fibril formation by Aβ40 and Aβ42 [106]; however, GS was suggested not to interact with monomeric Aβ based on NMR spectroscopy. Instead, molecular docking methods using the Aβ(18–42) hairpin-stacked structure as amyloid model identified a possible site in which GS binds the Aβ fibril [130]. The structure of GS identified by crystallography [129] was shown to dock into the β-hairpin-like structure of Aβ(18–42) with its hydrophobic and hydrophilic residues interacting, respectively, with the apolar hydrophobic and polar hydrophilic interfaces within the amyloidogenic fibrillar tubes [106]. A family of mixed $(\alpha\beta\alpha\beta\alpha)_2$ cyclopeptides was designed based on GS and shown to form β-hairpin-like structures [131] that fit the channel interface of Aβ better than GS, probably because of the increased flexibility [106]. Further ThT assays and docking simulations performed on the GS derivatives illustrated the importance of hydrophilic and aromatic residues for interactions with the fibrils. In particular, the amyloidogenic residues clustered about Phe19 and Phe20 of Aβ were

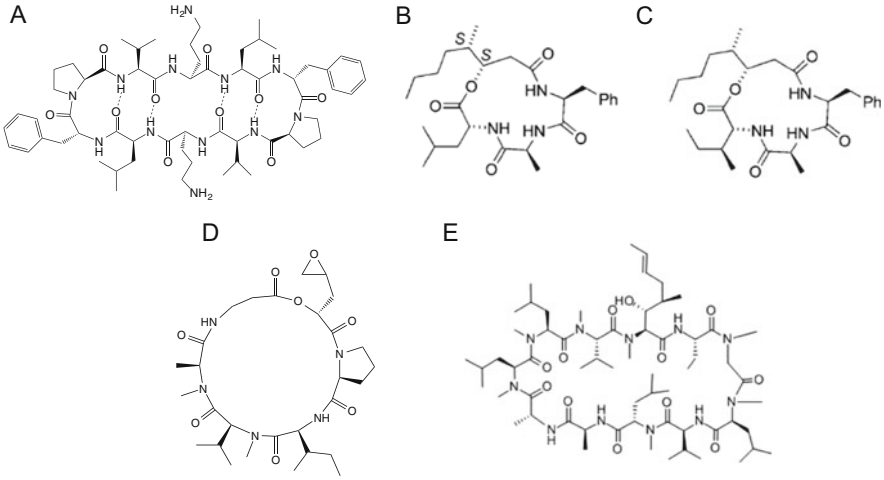

Fig. 9 Natural amyloid inhibitors:(**a**) gramicidin S, (**b**) beauveriolide I, (**c**) beauveriolide III a fungal metabolite, (**d**) destruxin E, and (**e**) cyclosporin A

suggested to recognize and bind to the aromatic side chains in the β-turns of the GS-derived cyclopeptides by π-stacking interactions [58, 72, 75, 106]. Although GS and analogs dissolved preformed amyloid fibrils [106], their ability to reduce amyloid-induced cell toxicity awaits to be studied.

2.4.2 Cyclodepsipeptides

Cyclodepsipeptides are a wide variety of structurally diverse class of cyclic peptides of natural origin that possess at least one ester linkage and a wide range of biological activities and molecular architectures [132]. The biological effects of cyclodepsipeptides include immunosuppressant, antibiotic, antifungal, anti-inflammatory, and antitumor activities (reviewed in [132]). Certain cyclodepsipeptides are being evaluated in clinical trials (reviewed in [133]); others are useful tools in research of biological processes involved in cellular regulation.

A few cyclodepsipeptides have been reported to exhibit anti-amyloidogenic activity without clear mechanisms of action. Some may interfere with cell signaling [134, 135], and others may exhibit β-sheet-breaking anti-amyloidogenic activity [136].

Beauveriolides I and III (Fig. 9b, c) are fungal metabolites that were originally isolated during screening for anti-atherosclerotic agents [137] and demonstrated to reduce atherogenic lesions in mouse models by inhibiting acyl-CoA cholesterol acyltransferase (ACAT) [138, 139], an enzyme which catalyzes the production of cholesteryl esters (CEs). Cellular levels of CEs correlate with Aβ secretion and ACAT may play a regulatory role in Aβ processing [140]. By inhibiting ACAT, Beauveriolides I and III may alter Aβ metabolism [134]. The depsipeptides were shown to dose-dependently decrease cholesterol esterification in cells expressing amyloid precursor protein [141]. Furthermore, in a quantitative ELISA assay, they decreased the secretion levels of Aβ40 and Aβ42, with beauveriolide III exhibiting greater potency. Immunolabeling and microscopy studies revealed that beauveriolide III did not alter the known endosomal localization of Aβ [141] but may decrease the biogenesis of Aβ from amyloid precursor protein by modifying cellular CE levels [134].

Destruxin E (Fig. 9d) is a cyclic hexadepsipeptide that inhibited Aβ generation in cell culture [135]. Secreted by entomopathogenic fungi [142], destruxin E contains one α-hydroxy acid and was shown using biochemical, immunohistochemical, and cellular assays to inhibit cleavage of amyloid precursor protein to generate Aβ without affecting β- and γ-secretases [135]. The mechanism of Aβ regulation by destruxin E remains to be elucidated.

Aplidine is a member of the proline-rich didemnin cyclodepsipeptide family isolated from marine invertebrates [143]. Under evaluation in clinical trials for anticancer activity [144], aplidine was observed by EM to inhibit aggregation of peptide from the prion amyloidogenic region $PrP_{106–141}$ in vitro at equimolecular concentrations [136]. The inhibitory effect of aplidine was suggested to not be due to a nonspecific binding, because aggregation of $PrP_{106–141}$ was not affected at high

concentrations using Pro-rich peptide controls. Aplidine dissolved preformed $PrP_{106–141}$ fibrils. At a fourfold mass excess, examination of a shift in the amide II region of the FTIR spectrum indicated that aplidine caused a drastic change of the $PrP_{106–141}$ β-sheet structure to a set of unstructured conformers; however, no inhibitory effect of aplidine was observed on the $A\beta_{25–35}$ fragment [136].

The collective anti-amyloidogenic activities of the beauveriolides I and III and destruxin E warrant further in vivo testing, especially in light of the oral bioavailability of beauveriolide III [138]. The specificity of aplidine should be further examined, because of its potential as anti-prion therapy. In general, cyclodepsipeptides merit further examination for potential to regulate signaling and regulatory mechanisms of Aβ and other amyloids.

2.4.3 Cyclosporin

Cyclosporin (Fig. 9e) is a cyclic nonribosomal peptide of 11 amino acids that contains a single D-amino acid [145]. Originally isolated from the fungus *Tolypocladium inflatum ganus* found in a soil sample, cyclosporin is a potent orally bioavailable immunomodulator that affects immune function by multiple pathways which are not fully understood. Although its usage may be accompanied by side effects, cyclosporin was approved by the FDA for the prevention and treatment of graft-versus-host diseases following various transplantations, rheumatoid arthritis, and psoriasis. In addition to these indications, cyclosporin was used to treat severe atopic dermatitis accompanied by Lichen amyloidosis. This chronic skin disorder features formation of degenerated keratin amyloid depositions across large areas of the skin [146]. Two case studies reported that oral treatment with cyclosporin completely flattened disease-associated papules and kept patients asymptomatic [147, 148]. Although the mechanism of action of cyclosporin in this disorder was not studied, the authors suggested modulation of various inflammatory cellular proteins [148]. In a mouse model of systemic amyloidosis, therapeutic doses of cyclosporin reduced substantially the rate of disease progression, probably by intervening in immune mechanisms [149]. One of the effects of cyclosporin in cells is inhibition of the mitochondrial permeability transition pore, which results in inhibition of cytochrome c release and apoptosis [150]. In this context, cyclosporine was reported to protect primary cholinergic neurons against Aβ42-induced cytotoxicity [151]. Determination of cell morphology and cell viability together with expression levels of anti-apoptotic proteins revealed that cyclosporin exerts significant protective effects on the viability of cultured rat primary basal forebrain cholinergic neurons by ameliorating the decrease in Bcl-2 anti-apoptotic protein and the increase in apoptotic cytochrome c and caspase-3 activity induced by Aβ42 [151].

Additionally, cyclosporin was proposed to possess neuroprotective activity following traumatic brain injury, probably through downregulation of APP expression, which is elevated after this event. Using reverse-transcription polymerase chain reaction and immunocytochemistry, cyclosporin was demonstrated to reduce

the mRNA expression of APP following traumatic brain injury [152]. Although the exact mechanism associated with neuroprotection by cyclosporin is unknown, Aβ causes toxic mitochondrial permeability transition pore opening. The neuroprotective action of cyclosporin may thus arise from the inhibition of APP expression, promoting mitochondrial protection and mitochondrial permeability transition pore inhibition [152].

Together, these results suggest that the inhibition of mitochondrial pathways may play a role in Aβ-induced cytotoxicity and neuronal damage. The established oral bioavailability of cyclosporin and its approved usage in humans make it a preferred candidate for anti-amyloidogenic treatment.

2.5 Cyclic Peptides as Anti-amyloidogenic Pharmacological Tools

In some cases, heterocyclic peptides do not associate with the amyloid themselves but act as scaffolds that induce or enhance an anti-amyloidogenic response.

2.5.1 Multivalent Scaffolds

Cyclic peptide scaffolds have been utilized to enhance the multivalency of anti-amyloidogenic chemical agents, such as quinacrine. For example, multimeric conjugation of quinacrine to a cyclic decapeptide scaffold resulted in more efficient anti-amyloidogenic activity than that which was demonstrated by a quinacrine monomer [153]. A peptide scaffold has served as an advantageous biodegradable and nontoxic transport system for improving quinacrine active [153].

2.5.2 Antibody-Derived Vaccination/Passive Immunotherapy

Anti-Aβ antibodies were previously demonstrated to dissolve Aβ fibrils and plaques and to prevent neurotoxic effects [154, 155]. An initial clinical trial of anti-amyloid vaccination was however halted when active immunization of fibrillar Aβ42 caused severe brain inflammation [156]. Research in vivo has also reported side effects associated with passive immunization [157]. Recently, the first successful attempt in this field was published [158, 159], opening the door for other methods.

In the search for safer anti-Aβ immunization methods, the cyclic peptide *C44* exhibited neuroprotective effects against Aβ42 in neurons [158, 160]. The 15-amino-acid sequence of *C44* (CASVRGWYVRSVFDPAC) was based on the complementarity-determining region of the variable heavy (V_H) domain of a potent recombinant Ig antibody fragment, as displayed on a phage clone. Additional cysteine residues were added to the sequence to form the disulfide loop mimic,

which exhibited binding to Aβ in an ELISA assay, and neuroprotective effects against Aβ-mediated toxicity in vitro [160].

Molecular mechanics and dynamics simulations were used to model the interaction between *C44* and Aβ42 [161] and found the hydrophobic face of the macrocycle was recognized by two regions of Aβ42, including the amyloidogenic-prone central V^{18} and F^{19} residues. Considering the *C44* sequence was derived from a recombinant anti-Aβ antibody fragment (V_H), the potency of the latter was suggested to be also due to binding to the central region of Aβ42 [160, 161]. In the study of anti-amyloid immunization, synthetic cyclic peptides based on lead antibody complementarity-determining regions offer potential for passive immunization against Aβ and other amyloids.

3 Summary

Amyloid fibrils are products of complex self-assembly reactions, mediated by thermodynamic forces that drive multiple intermediate states to proteinous deposits associated with aging and disease. Although mature fibrils have been extensively studied, the structures of the toxic soluble aggregates are just starting to be elucidated.

Treatments for different amyloidoses are major unmet medical needs. In particular, effective disease-halting therapy is urgently required to combat the pandemic of neurodegenerative brain diseases, including AD and PD. In the search for amyloid inhibitors, the oligomeric states that are responsible for toxicity have become important pharmacological targets. Fueled by a growing body of structural information on amyloids, including their toxic oligomers, as well as evidence that the formation of amyloids entails equilibrium processes, the last few decades have seen major efforts directed toward designing and developing inhibitors that target such equilibria. Heterocyclic peptides are attractive for this purpose, because they can be effectively synthesized and diversified by chemical methods (reviewed in [162]).

The abilities of cyclic and heterocyclic peptides to mimic the strands and turns of natural proteins and to engage in protein–protein interactions (reviewed in [163]) have made them important tools in basic research on fibril assembly. For example, cyclic D,L-α-peptides hold great potential as anti-amyloidogenic agents and tools for studying structural similarities between different amyloids that lead to their cross-interactions. Nanotubes derived from D,L-α-peptides are particularly relevant conformational mimics for studying the properties of toxic amyloids to inhibit specific pathogenic structures. Macrocyclic β-sheets have been valuable tools for elucidating the toxic structures of Aβ oligomers. Balancing amyloid-sequence homology with potential to break and inhibit the folding of β-sheets, sequence-derived cyclic peptides have served to study the physical and chemical forces driving amyloid formation. Natural heterocyclic peptides have inhibited fibril formation with increased binding specificity to specific amyloids, as well as severed to identify

new pathways for therapeutic intervention by attacking amyloid-associated signal transduction and metabolism in native and pathogenic cellular environment. Finally, heterocyclic peptides offer use as pharmacological tools for multivalent drug transport and anti-amyloidogenic immunization.

A critical requirement for targeting neurodegenerative diseases using anti-amyloidogenic agents is penetration of the blood–brain barrier. In this light, anti-amyloidogenic macrocycles may be more attractive for treating systemic or organ-limited amyloidosis. Potential to develop peptide macrocycle analogs that penetrate the blood–brain barrier, enter cell membranes, and exhibit enhanced bioavailability all may arrive from synthetic modifications such as *N*-methylation of amide groups on the peptide backbone, which has increased oral bioavailability in the case of cyclosporin.

Another possible application of anti-amyloidogenic heterocyclic peptides could be related to the detection of amyloid deposits in vitro and in histological segments. The low-molecular mass and ability for conformational mimicry of heterocyclic peptides may enhance their consideration for the detection and imaging of toxic oligomers in vivo, because they are expected to bind early oligomers.

Macrocycles, such as cyclic peptides, have already proven valuable as pharmaceutical agents [49]. Ongoing development of cyclic heteropeptide drugs for oncology and infectious disease may open the door further for their application as diagnostics and therapeutic agents in amyloidogenic diseases. Considering their potential for high affinity, specificity, and metabolic stability, as well as their effective preparation by chemical and biotechnological synthetic methods, heterocyclic peptides offer significant potential for the development of anti-amyloidogenic therapies.

References

1. Sipe JD, Cohen AS (2000) J Struct Biol 130:88
2. Bong DT, Clark TD, Granja JR, Ghadiri MR (2001) Angew Chem Int Ed Engl 40:988
3. Glenner GG (1980) N Engl J Med 302:1283
4. Fandrich M (2007) Cell Mol Life Sci 64:2066
5. Fandrich M, Fletcher MA, Dobson CM (2001) Nature 410:165
6. Bucciantini M, Giannoni E, Chiti F, Baroni F, Formigli L, Zurdo J, Taddei N, Ramponi G, Dobson CM, Stefani M (2002) Nature 416:507
7. Chiti F, Dobson CM (2009) Nat Chem Biol 5:15
8. Nelson R, Sawaya MR, Balbirnie M, Madsen AO, Riekel C, Grothe R, Eisenberg D (2005) Nature 435:773
9. Chiti F, Dobson CM (2006) Annu Rev Biochem 75:333
10. Dobson CM (2003) Nature 426:884
11. Dobson CM (2001) Philos Trans R Soc Lond B Biol Sci 356:133
12. Dobson CM (1999) Trends Biochem Sci 24:329
13. Merlini G, Bellotti V (2003) N Engl J Med 349:583
14. Selkoe DJ (2003) Nature 426:900
15. Meehan S, Berry Y, Luisi B, Dobson CM, Carver JA, MacPhee CE (2004) J Biol Chem 279:3413

16. Kumar S, Walter J (2011) Aging 3:803
17. Fandrich M, Dobson CM (2002) EMBO J 21:5682
18. Lashuel HA, Hartley D, Petre BM, Walz T, Lansbury PT Jr (2002) Nature 418:291
19. Xue WF, Homans SW, Radford SE (2008) Proc Natl Acad Sci U S A 105:8926
20. Hardy J, Allsop D (1991) Trends Pharmacol Sci 12:383
21. Hardy J, Selkoe DJ (2002) Science 297:353
22. Silveira JR, Raymond GJ, Hughson AG, Race RE, Sim VL, Hayes SF, Caughey B (2005) Nature 437:257
23. Haass C, Selkoe DJ (2007) Nat Rev Mol Cell Biol 8:101
24. Kirkitadze MD, Condron MM, Teplow DB (2001) J Mol Biol 312:1103
25. Kayed R, Head E, Thompson JL, McIntire TM, Milton SC, Cotman CW, Glabe CG (2003) Science 300:486
26. Yip CM, McLaurin J (2001) Biophys J 80:1359
27. Kelly BL, Ferreira A (2006) J Biol Chem 281:28079
28. Campioni S, Mannini B, Zampagni M, Pensalfini A, Parrini C, Evangelisti E, Relini A, Stefani M, Dobson CM, Cecchi C, Chiti F (2010) Nat Chem Biol 6:140
29. Kourie JI, Henry CL (2002) Clin Exp Pharmacol Physiol 29:741
30. Cohen SI, Linse S, Luheshi LM, Hellstrand E, White DA, Rajah L, Otzen DE, Vendruscolo M, Dobson CM, Knowles TP (2013) Proc Natl Acad Sci U S A 110:9758
31. Spires-Jones TL, Hyman BT (2014) Neuron 82:756
32. Yagi H, Kusaka E, Hongo K, Mizobata T, Kawata Y (2005) J Biol Chem 280:38609
33. Westermark GT, Westermark P (2009) FEBS Lett 583:2685
34. Desplats P, Lee H-J, Bae E-J, Patrick C, Rockenstein E, Crews L, Spencer B, Masliah E, Lee S-J (2009) Proc Natl Acad Sci 106:13010
35. Guo JL, Lee VM (2014) Nat Med 20:130
36. Nath S, Agholme L, Kurudenkandy FR, Granseth B, Marcusson J, Hallbeck M (2012) J Neurosci 32:8767
37. Cheng B, Gong H, Xiao H, Petersen RB, Zheng L, Huang K (2013) Biochim Biophys Acta Gen Subj 1830:4860
38. Ehrnhoefer DE, Bieschke J, Boeddrich A, Herbst M, Masino L, Lurz R, Engemann S, Pastore A, Wanker EE (2008) Nat Struct Mol Biol 15:558
39. Grelle G, Otto A, Lorenz M, Frank RF, Wanker EE, Bieschke J (2011) Biochemistry 50:10624
40. Masuda M, Suzuki N, Taniguchi S, Oikawa T, Nonaka T, Iwatsubo T, Hisanaga S, Goedert M, Hasegawa M (2006) Biochemistry 45:6085
41. Wang MS, Boddapati S, Emadi S, Sierks MR (2010) BMC Neurosci 11:57
42. Bieschke J, Russ J, Friedrich RP, Ehrnhoefer DE, Wobst H, Neugebauer K, Wanker EE (2010) Proc Natl Acad Sci U S A 107:7710
43. Ahmad B, Lapidus LJ (2012) J Biol Chem 287:9193
44. Howlett D, Cutler P, Heales S, Camilleri P (1997) FEBS Lett 417:249
45. Taniguchi S, Suzuki N, Masuda M, Hisanaga S, Iwatsubo T, Goedert M, Hasegawa M (2005) J Biol Chem 280:7614
46. Wen JJ, Spatola AF (1997) J Pept Res 49:3
47. Horton DA, Bourne GT, Smythe ML (2002) J Comput Aided Mol Des 16:415
48. Nevola L, Giralt E (2015) Chem Commun (Camb) 51:3302
49. Giordanetto F, Kihlberg J (2014) J Med Chem 57:278
50. Foster AD, Ingram JD, Leitch EK, Lennard KR, Osher EL, Tavassoli A (2015) J Biomol Screen 20:563
51. Gazit E (2007) Chem Soc Rev 36:1263
52. Ghadiri MR, Granja JR, Milligan RA, McRee DE, Khazanovich N (1993) Nature 366:324
53. De Santis P, Morosetti S, Rizzo R (1974) Macromolecules 7:52
54. Hartgerink JD, Granja JR, Milligan RA, Ghadiri MR (1996) J Am Chem Soc 118:43
55. Ghadiri MR, Granja JR, Buehler LK (1994) Nature 369:301

56. Fernandez-Lopez S, Kim HS, Choi EC, Delgado M, Granja JR, Khasanov A, Kraehenbuehl K, Long G, Weinberger DA, Wilcoxen KM, Ghadiri MR (2001) Nature 412:452
57. Horne WS, Wiethoff CM, Cui C, Wilcoxen KM, Amorin M, Ghadiri MR, Nemerow GR (2005) Bioorg Med Chem 13:5145
58. Richman M, Wilk S, Chemerovski M, Warmlander SK, Wahlstrom A, Graslund A, Rahimipour S (2013) J Am Chem Soc 135:3474
59. Shapira R, Rudnick S, Daniel B, Viskind O, Aisha V, Richman M, Ayasolla KR, Perelman A, Chill JH, Gruzman A, Rahimipour S (2013) J Med Chem 56:6709
60. Mizrahi M, Zakrassov A, Lerner-Yardeni J, Ashkenasy N (2012) Nanoscale 4:518
61. Vijayaraj R, Van Damme S, Bultinck P, Subramanian V (2012) J Phys Chem B 116:9922
62. Motiei L, Rahimipour S, Thayer DA, Wong CH, Ghadiri MR (2009) Chem Commun (Camb):3693
63. Montero A, Gastaminza P, Law M, Cheng G, Chisari FV, Ghadiri MR (2011) Chem Biol 18:1453
64. Horne WS, Ashkenasy N, Ghadiri MR (2005) Chemistry 11:1137
65. Ashkenasy N, Horne WS, Ghadiri MR (2006) Small 2:99
66. Der-Sarkissian A, Jao CC, Chen J, Langen R (2003) J Biol Chem 278:37530
67. Quist A, Doudevski I, Lin H, Azimova R, Ng D, Frangione B, Kagan B, Ghiso J, Lal R (2005) Proc Natl Acad Sci U S A 102:10427
68. Manczak M, Reddy PH (2013) J Alzheimers Dis 36:285
69. Mandal PK, Pettegrew JW, Masliah E, Hamilton RL, Mandal R (2006) Neurochem Res 31:1153
70. Schwarzman AL, Goldgaber D (1996) Ciba Found Symp 199:146
71. Yan LM, Velkova A, Tatarek-Nossol M, Andreetto E, Kapurniotu A (2007) Angew Chem Int Ed Engl 46:1246
72. Chemerovski-Glikman M, Richman M, Rahimipour S (2014) Tetrahedron 70:7639
73. Tjernberg LO, Naslund J, Lindqvist F, Johansson J, Karlstrom AR, Thyberg J, Terenius L, Nordstedt C (1996) J Biol Chem 271:8545
74. Chemerovski-Glikman M, Rozentur-Shkop E, Grupi A, Richman M, Getler A, Cohen HY, Wallin C, Wärmländer KTS, Haas E, Gräslund A, Chill J, Rahimipour S (Unpublished)
75. Gazit E (2002) FASEB J 16:77
76. Hochdorffer K, Marz-Berberich J, Nagel-Steger L, Epple M, Meyer-Zaika W, Horn AH, Sticht H, Sinha S, Bitan G, Schrader T (2011) J Am Chem Soc 133:4348
77. Waters ML (2002) Curr Opin Chem Biol 6:736
78. Philp D, Stoddart JF (1996) Angew Chem Int Ed Engl 35:1154
79. Harper JD, Lansbury PT Jr (1997) Annu Rev Biochem 66:385
80. Woods RJ, Brower JO, Castellanos E, Hashemzadeh M, Khakshoor O, Russu WA, Nowick JS (2007) J Am Chem Soc 129:2548
81. Zheng J, Liu C, Sawaya MR, Vadla B, Khan S, Woods RJ, Eisenberg D, Goux WJ, Nowick JS (2011) J Am Chem Soc 133:3144
82. Zheng J, Baghkhanian AM, Nowick JS (2013) J Am Chem Soc 135:6846
83. Cheng PN, Liu C, Zhao M, Eisenberg D, Nowick JS (2012) Nat Chem 4:927
84. Nowick JS, Brower JO (2003) J Am Chem Soc 125:876
85. Nowick JS, Chung DM, Maitra K, Maitra S, Stigers KD, Sun Y (2000) J Am Chem Soc 122:7654
86. Nowick JS, Lam KS, Khasanova TV, Kemnitzer WE, Maitra S, Mee HT, Liu R (2002) J Am Chem Soc 124:4972
87. Ban T, Hoshino M, Takahashi S, Hamada D, Hasegawa K, Naiki H, Goto Y (2004) J Mol Biol 344:757
88. Mammen M, Choi S-K, Whitesides GM (1998) Angew Chem Int Ed 37:2754
89. Cheng PN, Spencer R, Woods RJ, Glabe CG, Nowick JS (2012) J Am Chem Soc 134:14179
90. Pham JD, Chim N, Goulding CW, Nowick JS (2013) J Am Chem Soc 135:12460

91. Cheng PN, Pham JD, Nowick JS (2013) J Am Chem Soc 135:5477
92. Pham JD, Demeler B, Nowick JS (2014) J Am Chem Soc 136:5432
93. Pham JD, Spencer RK, Chen KH, Nowick JS (2014) J Am Chem Soc 136:12682
94. Soto C, Sigurdsson EM, Morelli L, Kumar RA, Castano EM, Frangione B (1998) Nat Med 4:822
95. Adessi C, Frossard MJ, Boissard C, Fraga S, Bieler S, Ruckle T, Vilbois F, Robinson SM, Mutter M, Banks WA, Soto C (2003) J Biol Chem 278:13905
96. Arai T, Sasaki D, Araya T, Sato T, Sohma Y, Kanai M (2014) Chembiochem 15:2577
97. Kapurniotu A, Buck A, Weber M, Schmauder A, Hirsch T, Bernhagen J, Tatarek-Nossol M (2003) Chem Biol 10:149
98. Todorova N, Yeung L, Hung A, Yarovsky I (2013) PloS One 8
99. Arai T, Araya T, Sasaki D, Taniguchi A, Sato T, Sohma Y, Kanai M (2014) Angew Chem Int Ed Engl 53:8236
100. Kino R, Araya T, Arai T, Sohma Y, Kanai M (2015) Bioorg Med Chem Lett 25:2972
101. Barrow CJ, Yasuda A, Kenny P, Zagorski MG (1992) J Mol Biol 225:1075
102. Griffin MD, Yeung L, Hung A, Todorova N, Mok Y-F, Karas JA, Gooley PR, Yarovsky I, Howlett GJ (2012) J Mol Biol 416:642
103. Stewart CR, Haw A, Lopez R, McDonald TO, Callaghan JM, McConville MJ, Moore KJ, Howlett GJ, O'Brien KD (2007) J Lipid Res 48:2162
104. Medeiros LA, Khan T, El Khoury JB, Pham CL, Hatters DM, Howlett GJ, Lopez R, O'Brien KD, Moore KJ (2004) J Biol Chem 279:10643
105. Legge FS, Treutlein H, Howlett GJ, Yarovsky I (2007) Biophys Chem 130:102
106. Luo J, Otero JM, Yu CH, Wärmländer SK, Gräslund A, Overhand M, Abrahams JP (2013) Chem Eur J 19:17338
107. Horswill AR, Benkovic SJ (2005) Cell Cycle 4:552
108. Kritzer JA, Hamamichi S, McCaffery JM, Santagata S, Naumann TA, Caldwell KA, Caldwell GA, Lindquist S (2009) Nat Chem Biol 5:655
109. Machauer R, Laumen K, Veenstra S, Rondeau JM, Tintelnot-Blomley M, Betschart C, Jaton AL, Desrayaud S, Staufenbiel M, Rabe S, Paganetti P, Neumann U (2009) Bioorg Med Chem Lett 19:1366
110. Lerchner A, Machauer R, Betschart C, Veenstra S, Rueeger H, McCarthy C, Tintelnot-Blomley M, Jaton AL, Rabe S, Desrayaud S, Enz A, Staufenbiel M, Paganetti P, Rondeau JM, Neumann U (2010) Bioorg Med Chem Lett 20:603
111. Yamamoto N, Matsubara E, Maeda S, Minagawa H, Takashima A, Maruyama W, Michikawa M, Yanagisawa K (2007) J Biol Chem 282:2646
112. Perini G, Della-Bianca V, Politi V, Della Valle G, Dal-Pra I, Rossi F, Armato U (2002) J Exp Med 195:907
113. Kuner P, Schubenel R, Hertel C (1998) J Neurosci Res 54:798
114. Yaar M, Zhai S, Panova I, Fine RE, Eisenhauer PB, Blusztajn JK, Lopez-Coviella I, Gilchrest BA (2007) Neuropathol Appl Neurobiol 33:533
115. Yaar M, Arble BL, Stewart KB, Qureshi NH, Kowall NW, Gilchrest BA (2008) Cell Mol Neurobiol 28:1027
116. El-Agnaf OM, Sheridan JM, Sidera C, Siligardi G, Hussain R, Haris PI, Austen BM (2001) Biochemistry 40:3449
117. El-Agnaf OM, Nagala S, Patel BP, Austen BM (2001) J Mol Biol 310:157
118. Blennow K, de Leon MJ, Zetterberg H (2006) Lancet 368:387
119. Mattson MP (2004) Nature 430:631
120. Olson RE, Albright CF (2008) Curr Top Med Chem 8:17
121. Hanessian S, Yang G, Rondeau J-M, Neumann U, Betschart C, Tintelnot-Blomley M (2006) J Med Chem 49:4544
122. Barazza A, Gotz M, Cadamuro SA, Goettig P, Willem M, Steuber H, Kohler T, Jestel A, Reinemer P, Renner C, Bode W, Moroder L (2007) Chembiochem 8:2078

123. Rojo I, Martin JA, Broughton H, Timm D, Erickson J, Yang HC, McCarthy JR (2006) Bioorg Med Chem Lett 16:191
124. Machauer R, Veenstra S, Rondeau JM, Tintelnot-Blomley M, Betschart C, Neumann U, Paganetti P (2009) Bioorg Med Chem Lett 19:1361
125. Ghosh AK, Brindisi M, Tang J (2012) J Neurochem 120(Suppl 1):71
126. De Strooper B, Vassar R, Golde T (2010) Nat Rev Neurol 6:99
127. Ghosh AK, Tang J (2015) ChemMedChem 10:1463
128. Gause G, Brazhnikova M (1944) Nature 154:703
129. Llamas-Saiz AL, Grotenbreg GM, Overhand M, van Raaij MJ (2007) Acta Crystallogr D Biol Crystallogr 63:401
130. Luhrs T, Ritter C, Adrian M, Riek-Loher D, Bohrmann B, Dobeli H, Schubert D, Riek R (2005) Proc Natl Acad Sci U S A 102:17342
131. Otero JM, van der Knaap M, Llamas-Saiz AL, van Raaij MJ, Amorín M, Granja JR, Filippov DV, van der Marel GA, Overkleeft HS, Overhand M (2013) Cryst Growth Des 13:4355
132. Sarabia F, Chammaa S, Ruiz AS, Ortiz LM, Herrera FL (2004) Curr Med Chem 11:1309
133. Pelay-Gimeno M, Tulla-Puche J, Albericio F (2013) Mar Drugs 11:1693
134. Witter DP, Chen Y, Rogel JK, Boldt GE, Wentworth P Jr (2009) Chembiochem 10:1344
135. Itoh N, Okochi M, Tagami S, Nishitomi K, Nakayama T, Yanagida K, Fukumori A, Jiang J, Mori K, Hosono M, Kikuchi J, Nakano Y, Takinami Y, Dohi K, Nishigaki A, Takemoto H, Minagawa K, Katoh T, Willem M, Haass C, Morihara T, Tanaka T, Kudo T, Hasegawa H, Nishimura M, Sakaguchi G, Kato A, Takeda M (2009) Neurodegener Dis 6:230
136. Perez M, Sadqi M, Munoz V, Avila J (2003) Biochim Biophys Acta 1639:133
137. Namatame I, Tomoda H, Si S, Yamaguchi Y, Masuma R, Omura S (1999) J Antibiot 52:1
138. Namatame I, Tomoda H, Ishibashi S, Omura S (2004) Proc Natl Acad Sci U S A 101:737
139. Puglielli L, Konopka G, Pack-Chung E, Ingano LAM, Berezovska O, Hyman BT, Chang TY, Tanzi RE, Kovacs DM (2001) Nat Cell Biol 3:905
140. Huttunen HJ, Greco C, Kovacs DM (2007) FEBS Lett 581:1688
141. Huttunen HJ, Puglielli L, Ellis BC, MacKenzie Ingano LA, Kovacs DM (2009) J Mol Neurosci 37:6
142. Pedras MS, Irina Zaharia L, Ward DE (2002) Phytochemistry 59:579
143. Geldof AA, Mastbergen SC, Henrar RE, Faircloth GT (1999) Cancer Chemother Pharmacol 44:312
144. Broggini M, Marchini SV, Galliera E, Borsotti P, Taraboletti G, Erba E, Sironi M, Jimeno J, Faircloth GT, Giavazzi R, D'Incalci M (2003) Leukemia 17:52
145. Borel JF (2002) Wien Klin Wochenschr 114:433
146. Kumakiri M, Hashimoto K (1979) J Invest Dermatol 73:150
147. Behr FD, Levine N, Bangert J (2001) Arch Dermatol 137:553
148. Kang MJ, Kim HS, Kim HO, Park YM (2009) J Dermatolog Treat 20:368
149. Scheinberg MA, Bakkenist VA, Benson MD (1991) Cyclosporin reduces the incidence of amyloid disease in casein treated mice. In: Natvig JB et al (eds) Amyloid and amyloidosis 1990. Springer, Dordrecht, p 874
150. Zoratti M, Szabo I (1995) Biochim Biophys Acta 1241:139
151. Zeng X, Wang T, Jiang L, Ma G, Tan S, Li J, Gao J, Liu K, Zhang Y (2013) Neurol Res 35:529
152. Van Den Heuvel C, Donkin JJ, Finnie JW, Blumbergs PC, Kuchel T, Koszyca B, Manavis J, Jones NR, Reilly PL, Vink R (2004) J Neurotrauma 21:1562
153. Dolphin GT, Chierici S, Ouberai M, Dumy P, Garcia J (2008) Chembiochem 9:952
154. Solomon B, Koppel R, Frankel D, Hanan-Aharon E (1997) Proc Natl Acad Sci U S A 94:4109
155. Schenk D, Barbour R, Dunn W, Gordon G, Grajeda H, Guido T, Hu K, Huang J, Johnson-Wood K, Khan K, Kholodenko D, Lee M, Liao Z, Lieberburg I, Motter R, Mutter L, Soriano F, Shopp G, Vasquez N, Vandevert C, Walker S, Wogulis M, Yednock T, Games D, Seubert P (1999) Nature 400:173

156. Orgogozo JM, Gilman S, Dartigues JF, Laurent B, Puel M, Kirby LC, Jouanny P, Dubois B, Eisner L, Flitman S, Michel BF, Boada M, Frank A, Hock C (2003) Neurology 61:46
157. Pfeifer M, Boncristiano S, Bondolfi L, Stalder A, Deller T, Staufenbiel M, Mathews PM, Jucker M (2002) Science 298:1379
158. Liu P, Reed MN, Kotilinek LA, Grant MK, Forster CL, Qiang W, Shapiro SL, Reichl JH, Chiang AC, Jankowsky JL, Wilmot CM, Cleary JP, Zahs KR, Ashe KH (2015) Cell Rep 11:1760–1771
159. Underwood E (2015) Science 349:464
160. Manoutcharian K, Acero G, Munguia ME, Becerril B, Massieu L, Govezensky T, Ortiz E, Marks JD, Cao C, Ugen K, Gevorkian G (2004) Neurobiol Dis 17:114
161. Solorzano-Vargas RS, Vasilevko V, Acero G, Ugen KE, Martinez R, Govezensky T, Vazquez-Ramirez R, Kubli-Garfias C, Cribbs DH, Manoutcharian K, Gevorkian G (2008) Mol Immunol 45:881
162. Luo J, Abrahams JP (2014) Chemistry 20:2410
163. Hill TA, Shepherd NE, Diness F, Fairlie DP (2014) Angew Chem Int Ed Engl 53:13020

Top Heterocycl Chem (2017) 49: 235–252
DOI: 10.1007/7081_2015_186

Published online: 30 October 2015

Lipoylated Peptides and Proteins

Cédric Rentier, Giulia Pacini, Francesca Nuti, Paolo Rovero, and Anna-Maria Papini

Abstract Lipoic acid is a heterocyclic sulfur-containing derivative of octanoic acid that is characterized by a 1,2-dithiolane ring. Found in nature as an essential protein cofactor, lipoic acid is implicated in cellular metabolic reactions. In particular, lipoylation is an essential posttranslational modification involved in cellular energetic metabolism performed by mitochondria. In this chapter, we highlight the different pathways to obtain lipoylated peptides and proteins and the antioxidant properties of lipoic acid analogs, including their therapeutic potential in fields such as autoimmunity.

C. Rentier and A.-M. Papini (✉)
French-Italian Interdepartmental Laboratory of Peptide and Protein Chemistry and Biology, PeptLab, Sesto Fiorentino, Italy

PeptLab@UCP Platform and Laboratory of Chemical Biology EA4505, University of Cergy-Pontoise, 5 mail Gay-Lussac, 95031 Cergy-Pontoise, France

Department of Chemistry "Ugo Schiff", Via della Lastruccia 13, University of Florence, 50019 Sesto Fiorentino, Italy
e-mail: annamaria.papini@unifi.it

G. Pacini and P. Rovero
French-Italian Interdepartmental Laboratory of Peptide and Protein Chemistry and Biology, PeptLab, Sesto Fiorentino, Italy

Department of Neurosciences, Psychology, Drug Research and Child Health, Section of Pharmaceutical Sciences and Nutraceutics, Via Ugo Schiff 6, University of Florence, 50019 Sesto Fiorentino, Italy

F. Nuti
French-Italian Interdepartmental Laboratory of Peptide and Protein Chemistry and Biology, PeptLab, Sesto Fiorentino, Italy

Department of Chemistry "Ugo Schiff", Via della Lastruccia 13, University of Florence, 50019 Sesto Fiorentino, Italy

Keywords Lipoic acid · Lipoylated lysine · Lipoylated Self Assembled Monolayers · In vivo lipoylation · Lipoic acid supplements · Reactive Oxygen Species · Antioxidant properties

Contents

1 Lipoic Acid

Lipoic acid was described in the literature as thioctic acid, 6,8-thioctic acid, 6,8-dithioctane acid, 1,2-dithiol-3-valeric acid, lipoate acid, and α-lipoic acid. A sulfur-containing heterocycle derived from octanoic acid, lipoic acid possesses a terminal carboxylic acid and a chiral 1,2-dithiolane ring (Fig. 1). The C-6 carbon of lipoic acid can exist in both (*R*)-(+)- and (*S*)-(-)-enantiomers, as well as a racemic mixture. The 1,2-dithiolane sulfur atoms at C-6 and C-8 exist in vivo in the oxidized disulfide bond, which may be reduced to form the respective dithiol, dihydrolipoic acid (DHLA, Fig. 2).

Lipoic acid was first isolated and characterized by Reed et al. in 1951 [1]. After a 300,000-fold purification, approximately 10 tons of insoluble "liver residue" yielded about 30 mg of the pure lipoic acid [2]. The correct structure of 6,8-dithiooctanoic acid was assigned through chemical synthesis as a by-product from the synthesis of its 5,8-dithiooctanoic acid regioisomer by Bullock et al. in 1953 [3]. An optimized synthesis of lipoic acid was later conceived and is represented in Scheme 1. The synthetic process starts with acylation of ethylene with ethyl adipoyl chloride in the presence of aluminum chloride to yield the α,β-unsaturated ketone **1**. Conjugate addition of thioacetic acid, followed by sodium borohydride reduction and saponification, gave racemic 8-thiol-6-hydroxyoctanoic acid (**2**). 6,8-Dithioloctanoic acid (**3**) was assembled from alcohol **2** by treatment with thiourea and hydriodic acid followed by hydrolysis of the intermediate thiouronium salt. Finally, oxidation of dithiol acid **3** to the disulfide was achieved using gaseous oxygen and catalytic ferric iron to give racemic lipoic acid (**4**).

Enantiomerically pure lipoic acid was subsequently prepared by resolution of the racemate by formation of diastereomeric salts using respectively (*R*)- and (*S*)-α-methylbenzylamine [4].

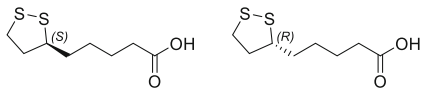

Fig. 1 (*S*)- and (*R*)-lipoic acid

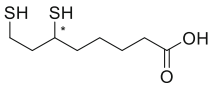

Fig. 2 Dihydrolipoic acid (DHLA)

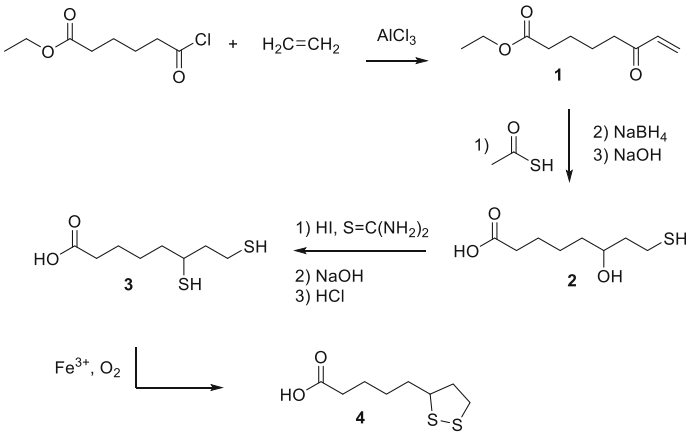

Scheme 1 Synthesis of racemic lipoic acid by Bullock et al.

2 Lipoylation: In Vivo Pathways and Naturally Occurring Lipoylated Proteins

Attachment of lipoic acid to a molecule is called lipoylation. In vivo, lipoylation occurs on the side chain of a lysine residue in the form of the amino acid itself to give so-called lipoyl-Lys or in a protein to provide the "lipoylated protein" (Fig. 3). Lipoylation is a posttranslational modification with a strong structural requirement for lysine [5]; however, various amino acids are tolerated at the neighboring residues [6], in contrast to *N*-glycosylation, which requires typically a clear consensus sequence [7].

Although lipoic acid was extensively studied in the past 50 years [8], the mechanism by which it is biosynthesized and attached to protein was only recently elucidated [9]. In vivo, lipoic acid exists in very small proportion as free acid; instead, lipoic acid resides primarily as a cofactor bound to the ε-amino group of a specific Lys on a lipoyl-accepting protein domain. Many studies on lipoic acid biosynthesis have been performed using *Escherichia coli* (*E.* coli), which has

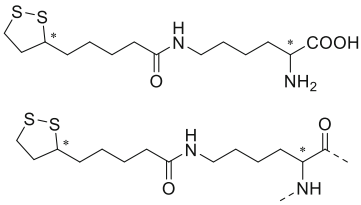

Fig. 3 Lipoyl-Lys (*top*) and representation of a protein-bound lipoic acid, a so-called lipoylated protein (*below*)

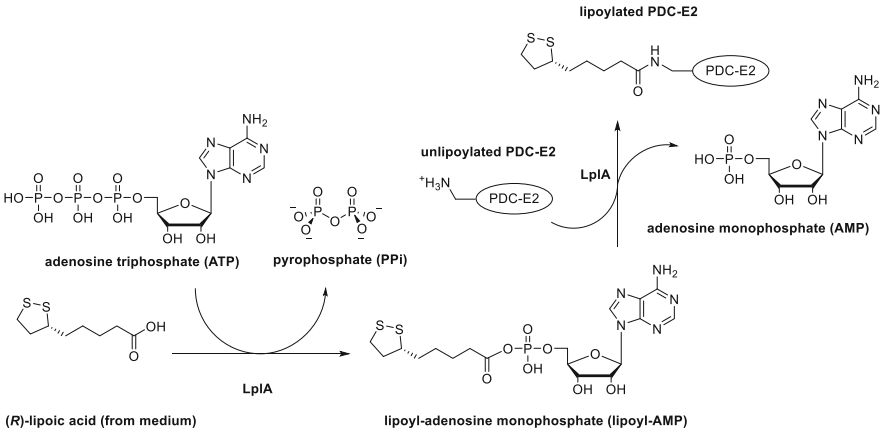

Scheme 2 PDC-E2 lipoylation using exogenous lipoic acid by the LplA pathway (adapted from Booker [12])

enabled identification of two different pathways, depending on different substrate sources. The first pathway is characterized by the use of exogenous lipoic acid, which is activated via ATP to form lipoyl-adenosine monophosphate by lipoate-protein ligase (LplA) [10], which, subsequently, transfers the lipoate-phosphate anhydride to the side chain of a Lys residue on the protein with release of AMP (Scheme 2) [11]. LplA is also able to use octanoic acid as substrate, but with reduced efficiency.

The second pathway involves endogenous lipoic acid synthesized from fatty acids. In this case, a lipoyl (octanoyl)-transferase called LipB transfers to lipoyl-accepting domains both lipoyl or octanoyl groups conjugated to an acyl carrier protein (ACP) [13]. Octanoyl-ACP is used as a lipoyl precursor. After transfer of the octanoyl group to the Lys residue of the target protein, the sulfur atoms are introduced with catalysis by a second enzyme, *N*-octanoyltransferase LipA, to obtain the lipoylated protein [14, 15] (Scheme 3).

The three pathways that employ respectively LipA, LipB, and LplA can be summarized as pictured in Scheme 4.

Among naturally occurring lipoylated proteins, lipoic acid is found as an essential cofactor of several key enzymes involved in oxidative metabolism: i.e.,

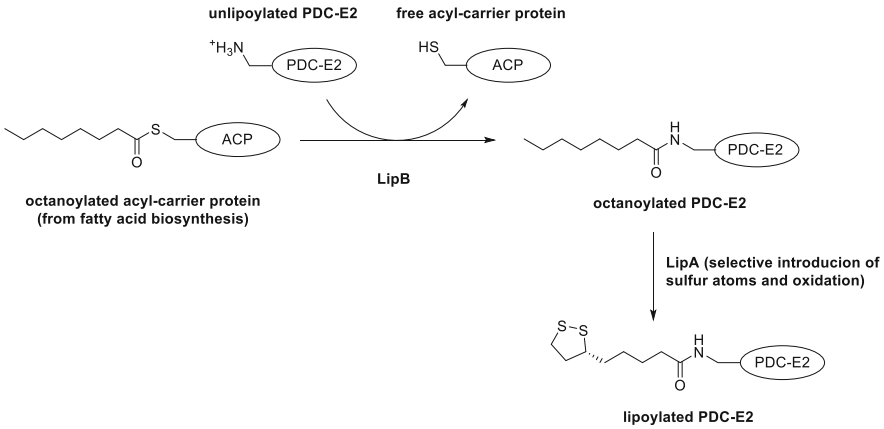

Scheme 3 Biosynthesis of lipoic acid from octanoyl-ACP, involving both LipB and LipA (adapted from Booker)

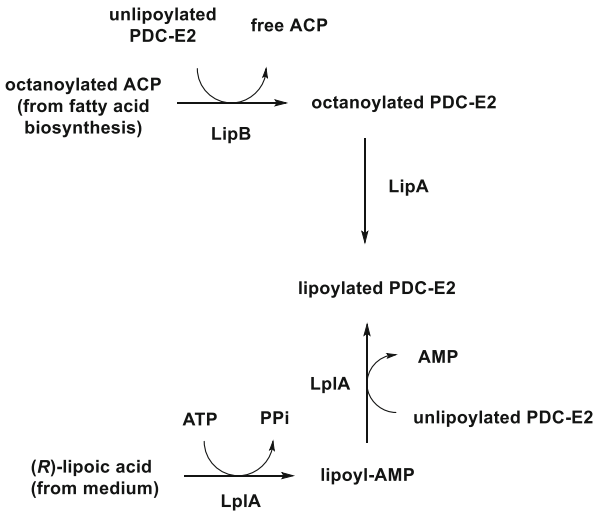

Scheme 4 Summary of PDC-E2 lipoylation pathways in vivo (for detailed molecular structures, refer to Schemes 2 and 3)

2-oxoacid dehydrogenase complex (2-OADC), pyruvate dehydrogenase complex (PDC), 2-oxoglutarate dehydrogenase (2-OGDH), and the glycine cleavage system [16–19]. The lipoyl moiety is covalently bound to these proteins and serves as a carrier of various reaction intermediates between the different enzyme active sites. Perham described these lipoyl-Lys residues as "swinging arms" [20] because of their high flexibility. Specifically, lipoylation is important for the cellular energetic cycle in mitochondria, because lipoic acid residues are essential cofactors of key enzymes involved in oxidative metabolism.

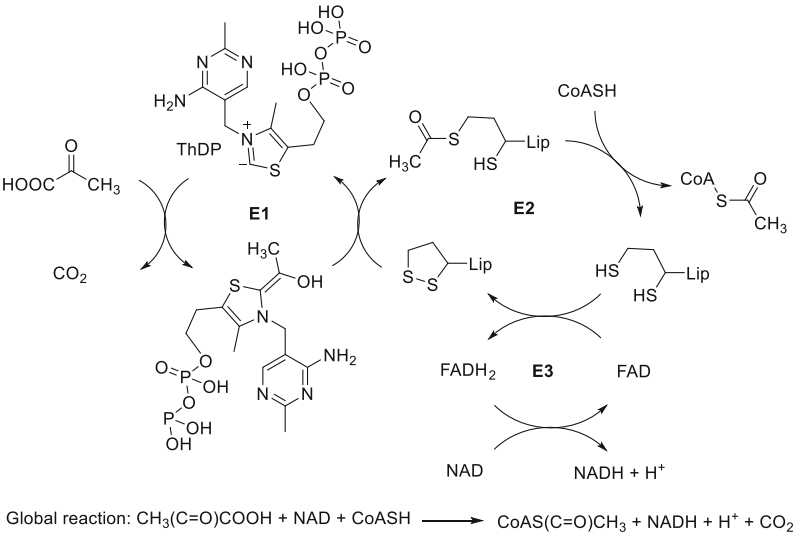

Scheme 5 The PDH reaction mechanism including E1, E2, and E3 subunits. *ThDP* thiamine diphosphate, *Lip* lipoyl-Lys moiety covalently bound to E2 subunit, *CoA* coenzyme A, *FAD* flavin adenine dinucleotide, *NAD* nicotine adenine dinucleotide

One of the most relevant lipoylated protein structures is the PDC enzymatic complex, essential for cell activity and energy production. Providing the link between the citric acid cycle and glycolysis, PDC is involved in pyruvate decarboxylation and reductive acetylation of coenzyme A (CoA) to form acetyl-CoA. PDC is composed of three subunits that work in concert (Scheme 5): E1 (thiamine diphosphate-dependent decarboxylase), E2 (dihydrolipoyl acetyltransferase), and E3 (dihydrolipoyl dehydrogenase). The E1 subunit catalyzes both oxidative decarboxylation of pyruvate and reductive acetylation of the lipoyl moiety. The E2 subunit transfers the acetyl group to coenzyme A. The E3 subunit regenerates the lipoyl moiety. Comparable mechanisms are found in the 2-OGDH and 2-OADC systems.

PDC is involved in primary biliary cirrhosis (PBC), an immune-mediated chronic inflammatory liver disease with slow progression, characterized by destruction of small interlobular bile ducts, gradual cholestasis, and portal inflammation. The serological hallmark of the pathology is characterized by high disease-specific anti-mitochondrial antibodies (AMA), which target primarily the E2 subunit of the PDC (PDC-E2). As the main immunogenic region of PDC-E2 was identified to contain the inner lipoyl domain of the protein, the involvement of lipoic acid as part of the epitope recognized by AMA has been investigated, albeit no final consensus has been attained.

Another example of lipoylated enzymes found in vivo is the glycine cleavage system, which is responsible for glycine decarboxylation. The glycine cleavage system comprises four proteins sharing similarities to the components of 2-OADC and catalyzing a coordinated set of reactions (Scheme 6): a pyridoxal phosphate-

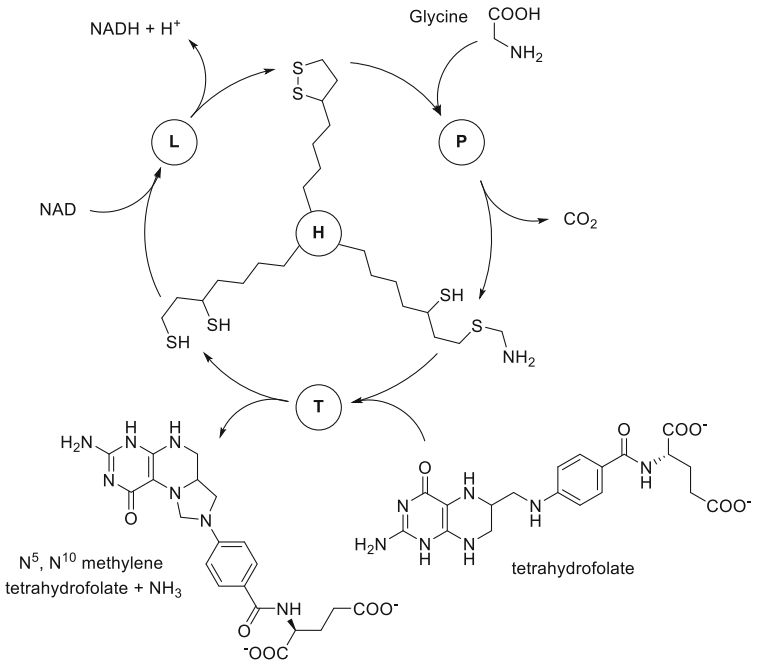

Scheme 6 The glycine cleavage system, including H, P (pyridoxal phosphate-dependent decarboxylase), T (aminomethyltransferase), and L (dihydrolipoyl dehydrogenase) proteins

dependent decarboxylase (P protein), a protein with a lipoyl-Lys residue that becomes reductively aminomethylated (H protein), an aminomethyltransferase T protein (requiring tetrahydrofolate as cofactor), and a dihydrolipoyl dehydrogenase (L protein), responsible for the reoxidation of the dihydrolipoyl group.

3 In Vitro Lipoylation: Synthetic Strategies to Obtain Lipoylated Peptides

Strategies for the synthesis of lipoylated peptides have involved both the attachment of lipoic acid to the lysine side chain of the target peptide and construction of an N^{ε}-lipoyl lysine suitable for introduction into the sequence through peptide synthesis. Both chemical and enzymatic methods were used for peptide lipoylation [21], the latter being accomplished by harnessing enzymes from the LpLA and LipB pathways.

Orthogonal protecting groups were critical for peptide lipoylation by chemical synthesis. For example, Tuaillon et al. [22] synthesized the N-terminal acetylated fragment (167–184) of PDC-E2 peptide. Lipoylation of position 173 was achieved by on-resin selective cleavage of Fmoc protection from the Lys side chain during

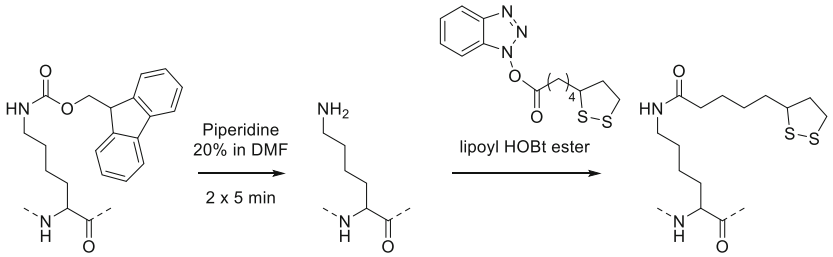

Scheme 7 On-resin selective deprotection of a Lys(Fmoc) residue in Boc/Bzl strategy, followed by on-resin lipoylation using lipoyl HOBt ester

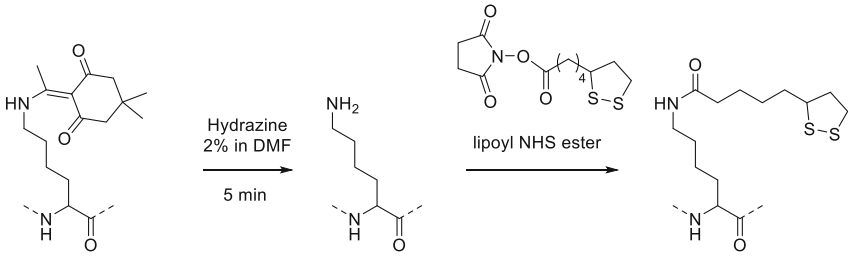

Scheme 8 On-resin Fmoc/tBu strategy featuring selective deprotection of a Lys(Dde) residue, followed by on-resin lipoylation using lipoyl NHS ester

Boc/Bzl solid-phase synthesis and acylation using the *N*-hydroxybenzotriazole ester of racemic lipoic acid (lipoyl HOBt ester, Scheme 7).

Similarly, using a Fmoc/tBu strategy, Long et al. [23] removed selectively the side-chain protection of Lys(Dde) with 2% hydrazine in DMF for 5 min and employed lipoyl *N*-hydroxysuccinimide ester (lipoyl NHS ester) for the acylation of the Lys side chain (Scheme 8). They synthesized several lipoylated peptides of various lengths (7-, 9-, 10-, and 12-mer) encompassing the inner lipoylated domain of the PDC-E2 protein.

Amano et al. applied a similar lipoyl NHS ester strategy to selectively lipoylate short unprotected peptides of the PDC-E2 sequence (15 amino acids) coupled to an agarose gel [24]. A specific peptide-spacer-linker combination was assembled by attachment of N^{α}-Fmoc-(N^{β}-Boc-amino-oxyacetyl)-L-diaminopropionic acid (Fmoc-Dpr(Boc-Aoa)) onto Rink amide resin, Fmoc removal, and coupling of *N*-Fmoc-2,2′-(ethylenedioxy)bis(ethylamine) monosuccinimide as a hydrophilic spacer, onto which the peptide sequence was elongated and capped by acetylation. The assembled peptide-spacer-linker unit was cleaved from the resin and coupled to a modified methyl-ketone agarose gel via an oxime bond. Lipoylation was performed at the last step using the lipoyl NHS ester (Scheme 9).

This convenient approach has become a popularly used method [25–28]. Drawbacks to peptide acylation include however incomplete lipoylation, which is typically monitored using the Kaiser test [29–31].

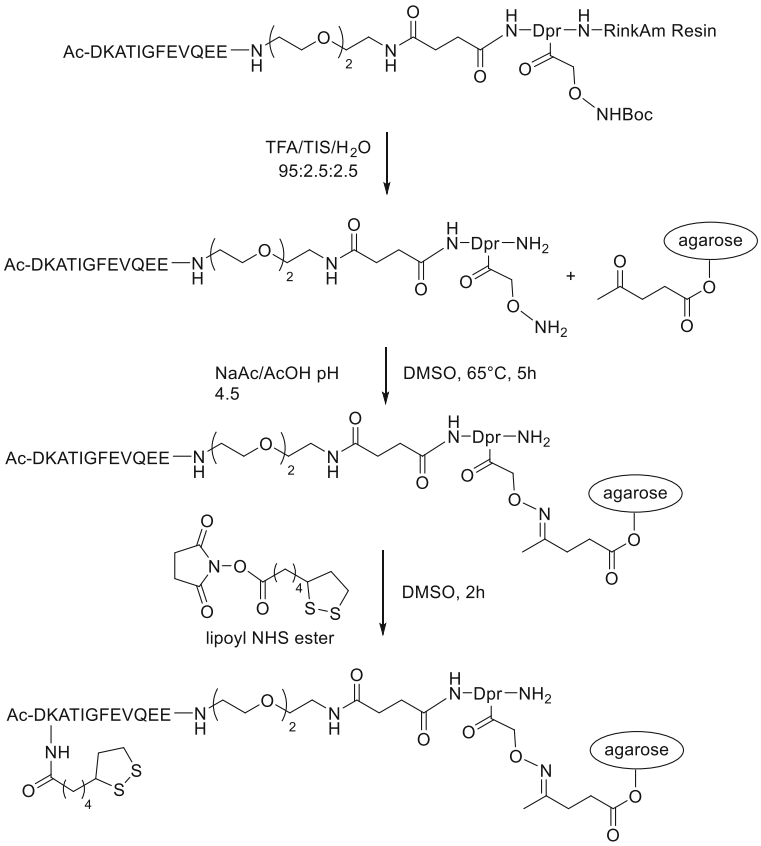

Scheme 9 Synthesis of agarose-conjugated lipoylated peptides via oxime bond formation and on-agarose lipoylation using lipoyl NHS ester (adapted from Amano et al.)

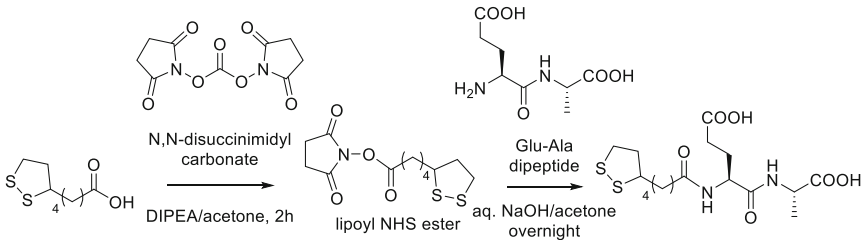

Scheme 10 Synthesis of an N-terminal lipoylated dipeptide Glu-Ala by Kates et al.

N-Terminal lipoylation of Glu-Ala dipeptide has also been performed without side chain or C-terminal carboxylate protection using lipoic acid activated with *N*, *N*-disuccinimidyl carbonate on >100 g scale [32] (Scheme 10).

The elucidation of in vivo lipoylation mechanisms led to discovery and partial purification of two enzymes from *E. coli* (LplA and LplB) that were subsequently employed in vitro for direct lipoylation of proteins [33]. For example, the inner lipoyl domain of human PDC-E2 was successfully obtained by using an in vitro lipoylation approach [34]. The ligases have been purified by heparin-agarose chromatography [35]. Employing expressed and purified lipoyl synthase (LipA) from *Sulfolobus solfataricus*, the octanoyl-Lys derivative of the tetrapeptide Thr-Glu-Lys-Ile was converted to the lipoyl-Lys containing peptide (Scheme 11) [36].

Various strategies were used to prepare suitably protected N^{ε}-lipoyl lysine [Lys (N^{ε}-lipoyl)] for subsequent peptide synthesis. For example, a lysine-copper complex was acylated with racemic lipoyl isobutyl carbonic anhydride [37–39], albeit in low yield due to polymerization of lipoic acid by a ring-opening mechanism featuring formation of intermolecular disulfide linkages to produce an insoluble polymer [40]. Matsugo et al. [41] coupled racemic lipoic acid to the side chain of N^{α}-Boc-Lys to obtain N^{ε}-lipoyl N^{α}-(Boc)Lys as a mixture of diastereomers (Scheme 12). Lipoic acid has also been coupled to alkylamines using 1-ethyl-3-(3-dimethylaminopropyl)carbodiimide (EDCI) [42].

Recently, novel lipoylated derivatives were described in which the amide bond has been replaced by bioisosteric groups, such as 1,2,4- and 1,3,4-oxadiazoles, 1,2,3-triazoles, thiazoles, or tetrazoles (Scheme 13) [43, 44]. Such methods offer

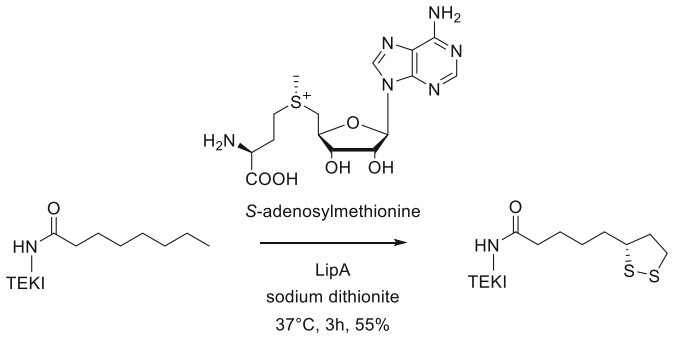

Scheme 11 Synthesis of a lipoyl derivative of an octanoylated tetrapeptide (adapted from Bryant et al.)

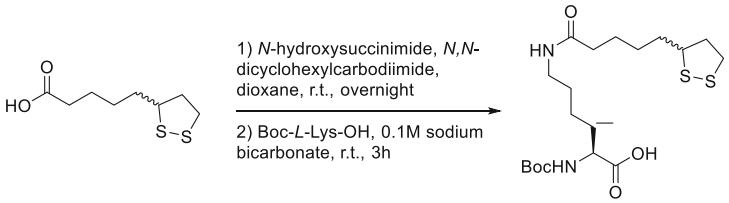

Scheme 12 Synthesis of an N^{ε}-lipoyl N^{α}-(Boc)Lys by Matsugo et al.

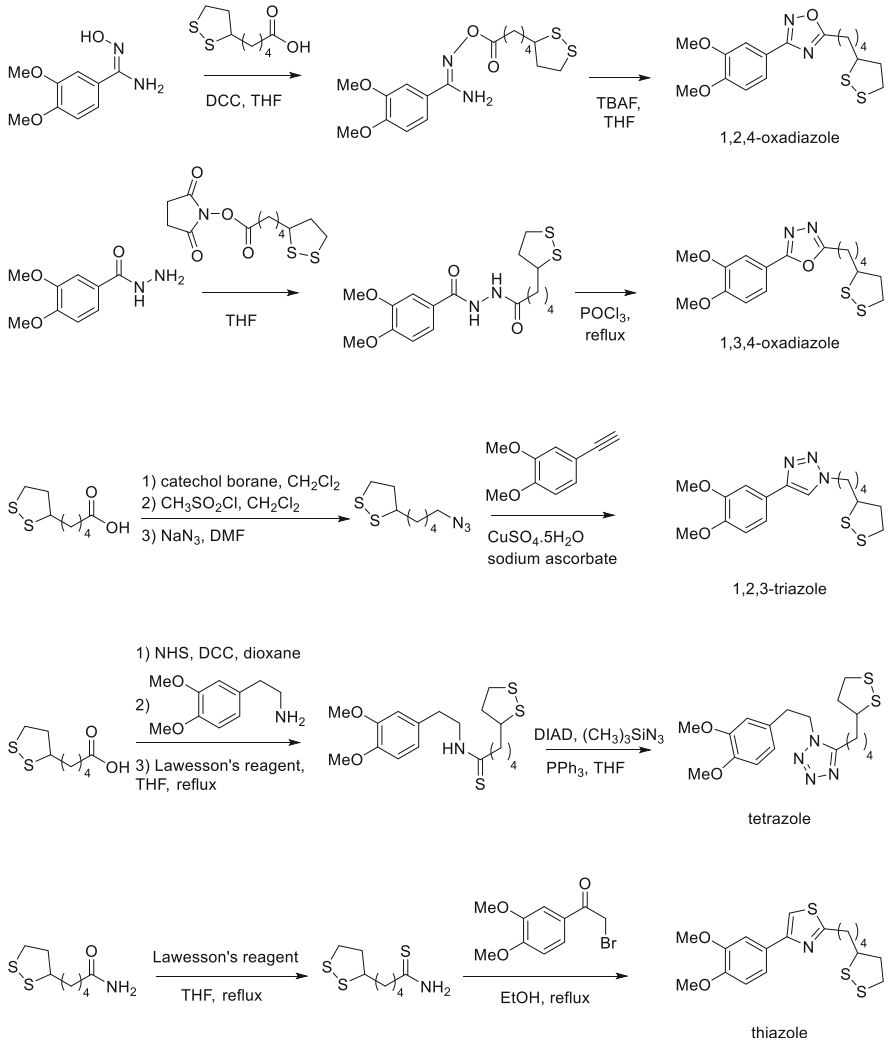

Scheme 13 Synthesis of lipoyl derivatives replacing the amide bond with bioisosteric groups (adapted from Koufaki et al.)

interesting potential for making lipoyl derivatives of peptides and proteins with increased protease stability.

Guillonneau et al. reported the synthesis of lipoylated *N*-alkyl morpholines, i.e., carbamate, thioamide, and thiocarbamate derivatives (Scheme 14) [45].

To facilitate the introduction of lipoyl moieties into peptide sequences, our laboratory has focused on the synthesis of enantiomerically pure lipoylated Lys derivatives for application as building blocks in the Fmoc/tBu strategy for solid-phase peptide synthesis [46]. Employing commercially available (*S*)-(–)- and (*R*)-

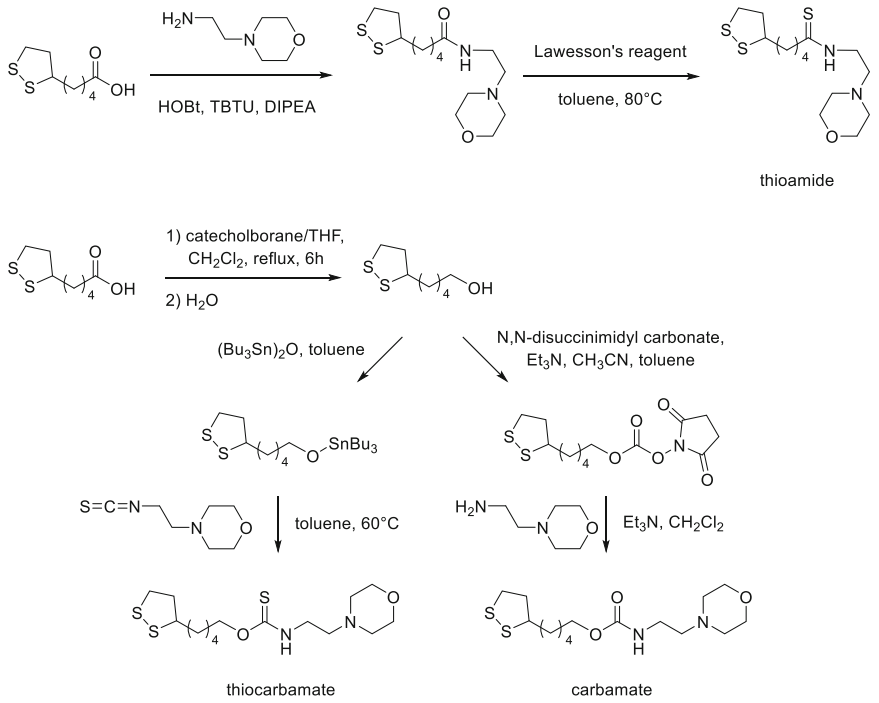

Scheme 14 Syntheses of thioamide, thiocarbamate, and carbamate derivatives of lipoyl-*N*-alkylmorpholine (adapted from Guillonneau et al.)

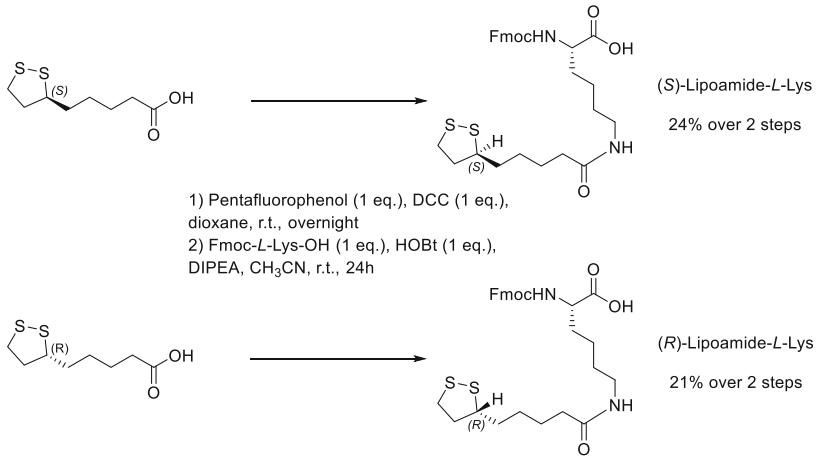

Scheme 15 Lipoylation of Fmoc-Lys by pentafluorophenyl ester strategy

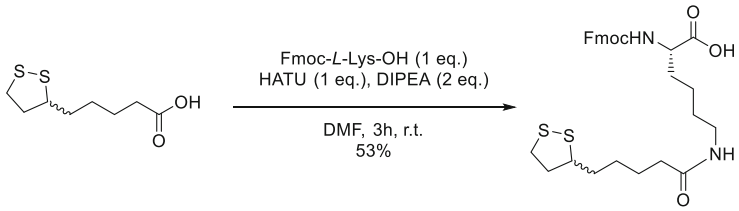

Scheme 16 Optimized protocol for N^{α}-Fmoc-N^{ε}-(lipoyl)Lys-OH synthesis

(+)-α-lipoic acids as enantiomerically pure, albeit expensive starting materials, the corresponding lipoyl pentafluorophenyl esters were synthesized from pentafluorophenol and *N*,*N*-dicyclohexylcarbodiimide [47]. The lipoyl pentafluorophenyl esters were coupled to the side chain of N^{α}-(Fmoc)Lys to yield building blocks for subsequent peptide synthesis (Scheme 15). Optimal activation conditions for the synthesis of N^{ε}-lipoyl N^{α}-(Fmoc)Lys were later developed by employing HATU (1-[bis(dimethylamino)methylene]-1H-1,2,3-triazolo[4,5-b] pyridinium 3-oxid hexafluorophosphate) and Hunig's base (*N*,*N*-diisopropylethylamine, DIPEA) for the coupling of lipoic acid to N^{α}-(Fmoc)Lys in DMF at room temperature for 3 h in 53% yield (Scheme 16).

4 Preparation of Dihydrolipoylated Peptides and Proteins

As mentioned, in vivo modification of lipoic acid derivatives to their dihydrolipoyl counterparts occurs during reductive acylation and aminomethylation of the 1,2-dithiolane ring. The mechanism for reductive acylation by PDC has been well studied [48, 49]. Application of the enzyme complex for the synthesis of dihydrolipoylated peptides and proteins is however not practical, because of the selectivity of PDC-E1 toward the lipoylated domain of the E2 component [50].

The first reduction of lipoic acid to dihydrolipoate in vitro was performed using sodium tetraborohydride [51]. This method has since proven useful in materials chemistry [52, 53], but may not be compatible with biomolecules, because the relatively strong reducing conditions could damage other functional groups of peptides and proteins. Moreover, the purification steps to remove the byproducts of reduction may be troublesome. More selective agents for reducing disulfide bridges were subsequently employed to make dihydrolipoyl residues, such as dithiothreitol (DTT) [54] and tris(2-carboxyethyl)phosphine (TCEP) [55, 56]. For example, our research group has developed an effective method for selective reduction of the 1,2-dithiolane ring of lipoylated peptides using DTT [64], which leaves other residues untouched (Scheme 17) [72]. Complete reduction is performed after one night of reaction, yielding the corresponding dihydrolipoamide peptide. Subsequent washes with diethyl ether, in which peptide is not soluble, enable removal of excess of DTT, as well as cyclic by-product resulting from

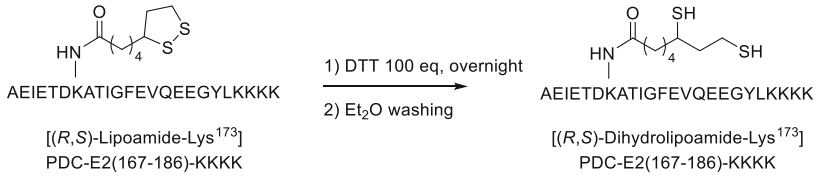

Scheme 17 Selective 1,2-dithiolane ring reduction of [(*R*,*S*)-lipoamide-Lys^{173}]PDC-E2 (167-186)-KKKK

DTT oxidation. This convenient method has been used to effectively obtain dihydrolipoamide-containing peptides without chromatographic purification.

Photo-induced reduction of lipoic acid derivatives to their dihydrolipoic acid counterparts was used to coat metallic surfaces [57]. In solution, photo-induced reduction should be performed with caution to avoid polymerization [58], which has been avoided by careful solvent selection. Using TLC monitoring during photo-induced reduction of lipoic acid, protic solvents were found to decrease polymerization, with best results employing propan-2-ol [59]. The –320 mV reduction potential of the lipoic acid-dihydrolipoic acid couple makes handling of the reduced dithiol challenging due to reoxidation back to the dithiolane necessitating inert conditions and in situ reduction [1].

5 Uses of Lipoic Acid and Lipoylated Molecules

Lipoic acid and dihydrolipoic acid moieties can chelate metals by way of the two sulfur atoms. Metals and their ions were coordinated by lipoic acid in vitro and in vivo. For example, lipoic acid-metal complexes were made with gold [60], mercury [61], copper [62], iron [63], as well as with ions such as Mn^{2+}, Pb^{2+}, Zn^{2+} [64, 65], and Cd^{2+} [66]. Dihydrolipoic acid was shown to form complexes with heavy metals such as As, Sb, and Bi [67]. Formation of metal complexes by lipoyl residues reduces oxidative damage, by diminishing reactive oxygen species (ROS) with potential to damage biological molecules, such as DNA, proteins, or lipids. Both lipoic acid and dihydrolipoic acid can scavenge physiologically relevant ROS in vitro [68]. The action of lipoic acid in vivo is less clear, because of its lower concentration in tissues relative to other intracellular antioxidants such as glutathione or vitamin C, albeit lipoic acid may have an important role as an indirect antioxidant regenerating other antioxidant species and chelating metals [69]. A recent study of the relative antioxidant properties of racemic and enantiomerically pure lipoic acid concluded that the natural (*R*)-enantiomer was more efficient [70].

The therapeutic utility of lipoic acid was examined to treat different diseases: e.g., diabetes mellitus, multiple sclerosis, and Alzheimer disease. In diabetes mellitus, lipoic acid administered intravenously was shown to improve impaired endothelial vasodilatation in neuropathy and vascular complications [71]. Multiple year treatment of diabetic neuropathy by intravenous administration of lipoic acid

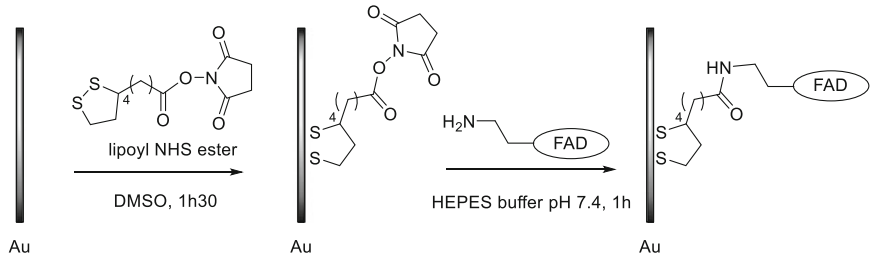

Scheme 18 Preparation of FAD-coated Au surfaces using lipoyl moiety as an anchor (adapted from Blonder et al.)

proved to be efficient for reducing significantly symptoms in diabetic patients [72]. Toward a treatment of multiple sclerosis (MS), lipoic acid was shown to be effective in prevention of experimental autoimmune encephalomyelitis (EAE), an animal model of MS [73]. The use of oral supplements of lipoic acid by patients suffering from MS has shown promise in clinical trials [74]. The use of lipoic acid has also shown promise for the treatment of Alzheimer disease [75, 76]. In particular, the antioxidant properties and metal chelation properties of lipoic acid may be beneficial to Alzheimer patients, who exhibited increased acetylcholine production.

The chemical properties of the 1,2-dithiolane ring were used to anchor lipoylated peptides and proteins to surfaces. In particular, self-assembled monolayers (SAM) were generated by the introduction of a lipoyl residue at the *N*-terminus or side chains of peptides and proteins to enable interactions with metals and adsorption to create thin layers on metallic surfaces such as gold [77–81] and silver [82]. Coupling of biomolecules to metallic surfaces is also possible using this technique, as reported for flavin adenine dinucleotide (FAD, Scheme 18) [83].

6 Summary

The in vivo and in vitro synthesis of the lipoic acid derivatives have been reviewed with focus on the implication of the heterocyclic 1,2-dithiolane ring in various fields: e.g., medicine as therapeutic agent, materials science as metal surface coating, and nutrition as antioxidant supplement. Moreover, lipoylated molecules offer potential as primary biliary cirrhosis synthetic antigens for studying autoimmune mechanisms. Lipoylation of peptides and proteins was performed by different pathways in vivo featuring coordinated enzymatic reactions, as well as in vitro by chemical and enzymatic methods. Considering novel methods for effective lipoylation of peptide and protein structures, as well as the relevance and utility of lipoic acid in biology and materials science, a wealth of future applications of this heterocyclic acid may be anticipated.

Acknowledgments ANR Chaire d'Excellence PeptKit 2009–2014 (grant n° ANR-09-CEXC-013-01), French-Italian University (Vinci Project grant n° C2-133), and Ente Cassa di Risparmio di Firenze are gratefully acknowledged for their financial support.

References

1. Reed LJ, DeBusk BG, Gunsalus IC, Hornberger CS Jr (1951) Science 114:93–94
2. Reed LJ (2001) J Biol Chem 276(42):38329–38336
3. Bullock MW, Brockman JA Jr, Patterson EL, Pierce JV, Von Saltza MH, Sanders F, Stoksad ELR (1954) J Am Chem Soc 76:1828–1832
4. Blaschke G, Scheidemantel U, Bethge H, Moller R, Beisswenger T, Huthmacher K (1994) Preparation and use of salts of pure enantiomers of alpha-lipoic acid. US Patent 5,281,722, 25 Jan 1994
5. Reche P, Perham RN (1999) EMBO J 18(10):2673–2682
6. Wallis NG, Perham RN (1994) J Mol Biol 236:209–216
7. Apweiler R, Hermjakob H, Sharon N (1999) Biochim Biophys Acta 1473:4–8
8. Parry RJ (1983) Tetrahedron 39(8):1215–1238
9. Cronan JE, Zhao X, Jiang Y (2005) Adv Microb Physiol 50:103–146
10. Fujiwara K, Takeuchi S, Okamura-Ikeda K, Motokawa Y (2001) J Biol Chem 276 (31):28819–28823
11. Fujiwara K, Okamura-Ikeda K, Motokawa Y (1994) J Biol Chem 269(24):16605–16609
12. Booker SJ (2004) Chem Biol 11:10–12
13. Zhao X, Miller JR, Jiang Y, Marletta MA, Cronan JE (2003) Chem Biol 10(12):1293–1302
14. Cicchillo RM, Booker SJ (2005) J Am Chem Soc 127(9):2860–2861
15. Miller JR, Busby RW, Jordan SW, Cheek J, Henshaw TF, Ashley GW, Broderick JB, Cronan JE Jr, Marletta MA (2000) Biochemistry 39(49):15166–15178
16. Reed LJ (1974) Acc Chem Res 7:40–46
17. De Kok A, Hengeveld AF, Martin A, Westphal AH (1998) Biochim Biophys Acta 1385:353–366
18. Perham RN (1991) Biochemistry 30:8501–8512
19. Motokawa Y, Fujiawara K, Okamura-Ikeda K (1995) In: Packer L, Cadenas E (eds) Bithiols in health and disease. Marcel Dekker, New York, pp 389–407
20. Perham RN (2000) Annu Rev Biochem 69:961–1004
21. Valeur E, Bradley M (2009) Chem Soc Rev 38:606–631
22. Tuaillon N, Andre C, Briand JP, Penner E, Muller S (1992) J Immunol 148(2):445–450
23. Long SA, Quan C, Van de Water J, Nantz MH, Kurth MJ, Barsky D, Colvin ME, Lam KS, Coppel RL, Ansari A, Gershwin ME (2001) J Immunol 167:2956–2963
24. Amano K, Leung PSC, Xu Q, Marik J, Quan C, Kurth MJ, Nantz MH, Ansari AA, Lam KS, Zeniya M, Coppel RL, Gershwin ME (2004) J Immunol 172:6444–6452
25. Amano K, Leung PSC, Rieger R, Quan C, Wang X, Marik J, Suen YF, Kurth MJ, Nantz MH, Ansari A, Lam KS, Zeniya M, Matsuura E, Coppel RL, Gershwin ME (2005) J Immunol 174:5874–5883
26. Rieger R, Leung PSC, Jeddeloh MR, Kurth MJ, Nantz MH, Lam KS, Barsky D, Ansari AA, Coppel L, Mackay IR, Gershwin ME (2006) J Autoimmun 27:7–16
27. Naiyanetr P, Butler JD, Meng L, Pfeiff J, Kenny TP, Guggenheim KG, Reiger R, Lam KS, Kurth MJ, Ansari AA, Coppel RL, Lopez-Hoyos M, Gershwin ME, Leung PSC (2011) J Autoimmun 37:209–216
28. Chen RCY, Naiyanetr P, Shu SA, Wang J, Yang GX, Kenny TP, Guggenheim KC, Butler JD, Bowlus C, Tao MH, Kurth MJ, Ansari AA, Kaplan M, Coppel RL, Lleo A, Gershwin ME, Leung PSC (2013) Hepatology 57(4):1498–1508

29. Kaiser E, Colescott RL, Bossiriger CD, Cook PI (1970) Anal Biochem 34:595–598
30. Hancock WS, Battersby JE (1976) Anal Biochem 71:260–264
31. Sarin VK, Kent SBH, Tarn JP, Merrifleld RB (1981) Anal Biochem 117:147–157
32. Kates SA, Casale RA, Baguisi A, Beeuwkes R III (2014) Bioorg Med Chem 22:505–512
33. Brookfield DC, Green J, Ali ST, Machado RS, Guest JR (1991) FEBS Lett 295:13–16
34. Quinn J, Diamond AG, Masters AK, Brookfield DE, Wallis NG, Yeaman SJ (1993) Biochem J 289:81–85
35. Green DE, Morris TW, Green J, Cronan JE Jr, Guest JR (1995) Biochem J 309:853–862
36. Bryant P, Kriek M, Wood RJ, Roach PL (2006) Anal Biochem 351:44–49
37. Nawa H, Brady WT, Koike M, Reed LJ (1960) J Am Chem Soc 82:896–903
38. Reed LJ, Koike M, Levitch ME, Leach FR (1958) J Biol Chem 232:143–158
39. Vaughan JR Jr (1952) J Am Chem Soc 74:6137–6139
40. Thomas RC, Reed LJ (1956) J Am Chem Soc 78:6148–6149
41. Matsugo S, Yasui F, Ozaki T (2003) ITE Lett Batteries New Technol Med 4(2):206–210
42. Brufani M, Medici I, Bettolo RM, Migneco LM, Marzella R, Figliola R, LaBella A (2011) Alpha lipoic acid derivatives and their use in drug preparation. US Patent 2011/0212954A1, 1 Sept 2011
43. Koufaki M, Kiziridi C, Alexi X, Alexis MN (2009) Bioorg Med Chem 17(17):6432–6441
44. Koufaki M, Kiziridi C, Nikoloudaki F, Alexis MN (2007) Bioorg Med Chem Lett 17 (15):4223–4227
45. Guillonneau C, Charton Y, Ginot YM, Fouquier-d'Herouel MV, Bertrand M, Lockhart B, Lestage P, Goldstein S (2003) Eur J Med Chem 38:1–11
46. Rentier C, Pacini G, Nuti F, Peroni E, Rovero P, Papini AM (2015) J Pept Sci 21:408–414
47. Kisfaludy L, Schon I (1983) Synthesis 4:325–327
48. Fries M, Jung HI, Perham RN (2003) Biochemistry 42(23):6996–7002
49. Sheng X, Liu Y (2013) Biochemistry 52(45):8079–8093
50. Graham LD, Packman LC, Perham RN (1989) Biochemistry 28(4):1574–1581
51. Gunsalus IC, Barton LS, Gruber W (1956) J Am Chem Soc 78(8):1763–1766
52. Susumu K, Uyeda T, Mednitz IL, Pons T, Delehanty JB, Mattoussi H (2007) J Am Chem Soc 129:13987–13996
53. Fang Z, Liu L, Xu L, Yin X, Zhong X (2008) Nanotechnology 19:235603–235609
54. Cleland WW (1964) Biochemistry 3(4):480–482
55. Burns JA, Butler JC, Moran J, Whitesides GM (1991) J Org Chem 56:2648–2650
56. Getz EB, Xiao M, Chakrabarty T, Cooke R, Selvin PR (1999) Anal Biochem 273:73–80
57. Palui G, Avellini T, Zhan N, Pan F, Gray D, Alabugin I, Mattoussi H (2012) J Am Chem Soc 134(39):16370–16378
58. Thomas RC, Reed LJ (1956) J Am Chem Soc 78(23):6148–6149
59. Brown PR, Edwards JO (1969) J Org Chem 34(10):3131–3135
60. Willey TM, Vance AL, Bostedt C, van Buuren T, Meulenberg RW, Terminello LJ, Fadley CS (2004) Langmuir 20:4939–4944
61. Su D, Yang X, Xia Q, Chai F, Wang C, Qu F (2013) RSC Adv 3:24618–24624
62. Nikolic RS, Krstic NS, Nikolic GM, Kocic GM, Cakic MD, Andelkovic DH (2014) Polyhedron 80:223–227
63. Suh JH, Moreau R, Heath SH, Hagen TM (2005) Redox Rep 10(1):52–60
64. Ou P, Tritschler HJ, Wolff SP (1995) Biochem Pharmacol 50:123–126
65. Sigel H, Prijs B, McCormick DB, Shih JCH (1978) Arch Biochem Biophys 187:208–214
66. Veljkovic AR, Nikolic RS, Kocic GM, Pavlovic DD, Cvetkovic TP, Sokolovic DT, Jevtovic TM, Basic JT, Laketic DM, Marinkovic MR, Stojanovic SR, Djordjevic BS, Krsmanovic MM (2012) Renal Failure 34(10):1281–1287
67. Ioannou PV, Tsivgoulis GM (2014) Monatsh Chem 145:897–909
68. Smith AR, Shenvi SV, Widlansky M, Suh JH, Hagen TM (2004) Curr Med Chem 11 (9):1135–1146
69. Packer L, Witt EH, Tritschler HJ (1995) Free Radical Biol Med 19:227–250

70. Tomassoni D, Amenta F, Amantini C, Farfariello V, Manelli LDC, Nwankwo IE, Marini C, Tayebati SK (2013) Int J Mol Sci 14:4580–4595
71. Heinisch BB, Francesconi M, Mittermayer F, Schaller G, Gouya G, Wolzt M, Pleiner J (2010) Eur J Clin Invest 40(2):148–154
72. Ziegler D, Nowak H, Kempler P, Vargha P, Low PA (2004) Diabet Med 21(2):114–121
73. Morini M, Roccatagliata L, Dell'Eva R, Pedemonte E, Furlan R, Minghelli S, Giunti D, Pfeffer U, Marchese M, Noonan D, Mancardi G, Albini A, Uccelli A (2004) J Neuroimmunol 148:146–153
74. Yadav Y, Marracci GH, Munar MY, Cherala G, Stuber LE, Alvarez L, Shinto L, Koop DR, Bourdette DN (2010) Mult Scler 16(4):387–397
75. Holmquist L, Stuchbury G, Berbaum K, Muscat S, Young S, Hager K, Engel J, Munch G (2007) Pharmacol Ther 113:154–164
76. Maczurek A, Hager K, Kenklies M, Sharman M, Martins R, Engel J, Carlson DA, Munch G (2008) Adv Drug Delivery Rev 60:1463–1470
77. Wang X, Nagata K, Higuchi M (2012) Thin Solid Films 520:2884–2891
78. Tappura K, Vikholm-Lundin I, Albers WM (2007) Biosens Bioelectron 22:912–919
79. Gatto E, Venanzi M (2013) Polym J 45:468–480
80. Xianhua L, Jiaofeng Y, Lin Z, Hongxi L, Yiren L (2013) Trans Tianjin Univ 19:248–254
81. Wen X, Linton RW, Formaggio F, Toniolo C, Samulski ET (2004) J Phys Chem A 108:9673–9681
82. Matulaitiene I, Kuodis Z, Eicher-Lorka O, Niaura G (2013) J Electroanal Chem 700:77–85
83. Blonder R, Willner I, Bückmann AF (1998) J Am Chem Soc 120:9335–9341

Index